2012

Real-time localization using received signal strength

Mohammed Rana Basheer

Department: Electrical and Computer Engineering

REAL-TIME LOCALIZATION USING RECEIVED SIGNAL STRENGTH

by

MOHAMMED RANA BASHEER

A DISSERTATION

Presented to the Faculty of the Graduate School of the

MISSOURI UNIVERSITY OF SCIENCE AND TECHNOLOGY

In Partial Fulfillment of the Requirements for the Degree

DOCTOR OF PHILOSOPHY

in

COMPUTER ENGINEERING

2012

Approved by

Jagannathan Sarangapani, Advisor
Sanjay Madria
Reza Zoughi
Daryl G. Beetner
R. Joe Stanley
Al Salour

PUBLICATION DISSERTATION OPTION

This dissertation would consist of the following five articles:

Paper 1, M.R. Basheer, and S. Jagannathan, "Enhancing Localization Accuracy in an RSSI Based RTLS Using R-Factor and Diversity Combination", has been submitted to the International Journal of Wireless Information Networks.

Paper 2, M.R. Basheer, and S. Jagannathan, "Receiver Placement Using Delaunay Refinement-based Triangulation in an RSSI Based Localization" has been revised and re-submitted to IEEE/ACM Transactions on Networking,

Paper 3, M.R. Basheer, and S. Jagannathan, "Localization of RFID Tags using Stochastic Tunneling", accepted in the IEEE Transactions on Mobile Computing

Paper 4, M.R. Basheer, and S. Jagannathan, "Localization and Tracking of Objects Using Cross-Correlation of Shadow Fading Noise", has been revised and resubmitted to the IEEE Transactions on Mobile Computing.

Paper 5, M.R. Basheer, and S. Jagannathan, "Placement of Receivers for Shadow Fading Cross-Correlation Based Localization", has been submitted to the IEEE Transactions on Mobile Computing.

ABSTRACT

Locating and tracking assets in an indoor environment is a fundamental requirement for several applications which include for instance network enabled manufacturing. However, translating time of flight-based GPS technique for indoor solutions has proven very costly and inaccurate primarily due to the need for high resolution clocks and the non-availability of reliable line of sight condition between the transmitter and receiver. In this dissertation, localization and tracking of wireless devices using radio signal strength (RSS) measurements in an indoor environment is undertaken. This dissertation is presented in the form of five papers.

The first two papers deal with localization and placement of receivers using a range-based method where the Friis transmission equation is used to relate the variation of the power with radial distance separation between the transmitter and receiver. The third paper introduces the cross correlation based localization methodology. Additionally, this paper also presents localization of passive RFID tags operating at 13.56MHz frequency or less by measuring the cross-correlation in multipath noise from the backscattered signals. The fourth paper extends the cross-correlation based localization algorithm to wireless devices operating at 2.4GHz by exploiting shadow fading cross-correlation. The final paper explores the placement of receivers in the target environment to ensure certain level of localization accuracy under cross-correlation based method. The effectiveness of our localization methodology is demonstrated experimentally by using IEEE 802.15.4 radios operating in fading noise rich environment such as an indoor mall and in a laboratory facility of Missouri University of Science and Technology. Analytical performance guarantees are also included for these methods in the dissertation.

ACKNOWLEDGEMENTS

I would like to thank my advisor Dr. Jagannathan Sarangapani for guiding me and providing me the motivation and vision to complete this dissertation. In addition, I would like to thank my parents Prof. E. Basheer and Asuma Beevi for installing in me the desire to seek out for knowledge how hard and far I have to struggle to get it.

TABLE OF CONTENTS

LIST OF ILLUSTRATIONS

PAPER III

PAPER IV

PAPER V

LIST OF TABLES

SECTION

1. INTRODUCTION

Wireless devices have permeated manufacturing environment with wide range of capabilities from monitoring solutions to real time command and control applications. In addition to data communication, these wireless devices may be leveraged to provide value added service such as an estimate of its location for applications such as asset flow management, physical security, robot tracking etc. There are several methods for wireless localization that rely on radio signal properties such as time of arrival [1], time difference of arrival [2], angle of arrival [3] or radio signal strength [4] to estimate the distance between a wireless transmitter and receiver. Time and angle-based location determination though can result in better accuracy but require special antennas or time synchronization hardware [5]. On the other hand, RSSI based solutions can only provide coarse-grained localization [6] whereas they are cost-effective and can be seamlessly added to any existing wireless device with just a software update. As a result, RSSI based localization schemes are preferred on IEEE 802.15.4 [4] and IEEE 802.11 [7] wireless networks.

Typically, Wireless communication devices provide an estimate of the received signal strength in the form of quantized values called Radio Signal Strength Indicator (RSSI) that is the logarithm of the received signal power in dBm. Manufacturers provide access to RSSI values stored in internal hardware registers of these communication devices through Application Programmer Interface (API). For IEEE 802.15.4 devices, RSSI values are reported as an 8-bit integer with the minimum value indicating received power less than 10 dB above the receiver sensitivity and the range of the RSSI spanning at least 40 dB with a linearity of ± 6 dB [8]. For XBEE radios, used in our experiments,

RSSI values maps the received signal power in dBM between -23 dBm to -92 dBM to an integer value between 23 to 92 [9].

Localization algorithms that use RSSI can be broadly classified into *Range-based* or *Range-free* algorithms depending on the mapping function $f: \mathbb{R}^{3d} \longmapsto \mathbb{R}$ that describes the mapping between the 3D Cartesian coordinates η_T of a transmitter and η_R of a receiver to the measured RSSI, R_{TR}, at the receiver written as $R_{TR} = f(\eta_T, \eta_R)$. If the mapping $f(\eta_T, \eta_R)$ is dependent upon the radial distance between η_T and η_R, then it is called *range-based* localization method. On the contrary, if the Cartesian coordinate of the transmitter is inferred using machine learning algorithms that directly maps the Cartesian coordinates to the measured RSSI values at various points within the localization area then it is called *range-free* localization.

Range-based methods typically rely on multilateration [10] or least square fitting [11] to map the range estimates to Cartesian coordinates whereas the range-free methods rely on pattern matching algorithms on a database of RSSI values collected at various points within the localization collected during an off-line time consuming process called radio profiling. However, both methodologies require periodic radio profiling/calibration, to account for common mode noises such as interference, humidity variations, open door or window or movement of objects in the target area, asymmetry in antenna radiation pattern etc., for consistent localization accuracy [4].

An indoor environment is a multipath rich environment where a single radio signal originating from a transmitter may split into multiple signals with varying phase, amplitude and time delay profile due to reflection, refraction and diffraction from windows, doors and other radio obstacles in the target area. These multiple signals will

combine at the receiver antenna either constructively or destructively resulting in large fluctuation in signal strength within a very short radial distance movement between a transmitter and receiver. This effect is called the fast fading or multipath fading.

In addition, mobility of people and machinery in the localization area can cause partial or complete blockage of radio signal path resulting in temporal variation of signal strength called slow fading or shadow fading. Accurate modeling of these fading noises has been difficult due to their dependency on line of sight (LoS) conditions between the transmitter and receiver. Generally, when a single LoS component dominates a Ricean distribution of the RSSI is more appropriate whereas, under no clear dominant LoS component called the Non LoS (NLoS) condition, Rayleigh distribution has been successful in predicting the RSSI fading.

In terms of estimation techniques used for RSSI-based localization, hidden Markov models were used in [12] to jointly track the position and LoS conditions between the transmitter and receiver. In this paper, the position and LoS conditions are treated as Markov chains whose state is hidden in the RSSI values collected at a receiver. A Bayesian particle filtering method that use a Gaussian movement profile as the prior distribution and the radio profile map as the likelihood to generate a posterior weights of possible transmitter location is provided in [13]. Manifold learning algorithms using Multi-Dimensional scaling [14], isomap [15] and Locally Linear Embedding (LLE) [16] were used to map pair-wise range estimates between transmitter and receivers to Cartesian coordinates. A zero configuration indoor localization algorithm was realized in [17] that used Singular Value Decomposition (SVD) to create a robust mapping function between the RSSI measurements and the Cartesian coordinates. The system adapts to the

changes in the indoor environment by periodically recalibrating the mapping function using the known position of the stationary receivers.

In comparison to the above localization techniques, our proposed localization methodology does not rely on mapping absolute RSSI values to geographic coordinates; instead we rely on first estimating pair-wise cross-correlation in RSSI between receiver pairs. Cross-correlation between any two random variables describes the extent to which perturbations in one random variable can be expressed by a linear function of the other random variable and hence are immune to common mode noises [18]. Consequently, if mobility of people or machinery causes the exact same perturbation in RSSI values at two adjacent receivers then they have to be exactly on top of each other. The further they are separated from each other, the perturbations dominates one receiver in comparison to the other depending on where the mobility is occurring and the position of the transmitter.

Common mode noises in RSSI caused by an open window, humidity or temperature changes that would have necessitated a re-profiling of the target area for range-free method or recalibration for range-based method is non-consequential in our localization method. Existing RSSI localization methods treat fading noise as sampling noises that is averaged out with a large RSSI sample sets, our localization scheme takes advantage of fading noise by measuring similarity between fading experienced by adjacent receivers to determine the position of a transmitter. However, cross-correlation in multipath fading noise rapidly falls to zero for radial-separation distance over one wavelength and consequently, localization using this method is relegated to wireless devices that operate at frequency 13.56MHz or below.

To extend the range of cross-correlation based localization method to frequency range of 2.4GHz, we propose a stochastic filtering process that extract shadow fading noise from RSSI values and measure the cross-correlation in shadow fading noise between adjacent receivers. It will be shown in Paper 4 that shadow fading correlation for an IEEE 802.15.4 receiver has much larger range than multipath fading noise correlation and is quite suited for localization.

1.1 ORGANIZATION OF THE DISSERTATION

In this dissertation, localization and tracking of wireless devices using signal strength measurement in an indoor environment is undertaken. The dissertation is presented in five papers, and their relation to one another is illustrated in Fig 1.1. The common theme of each paper is the localization of wireless transmitter from signal strength values measured by receivers placed around the localization area. The first two papers deal with localization using a range-based method where the Friis transmission equation is used to relate the variation of the power with radial separation between the transmitter and receiver. The third paper introduces our cross correlation based localization methodology. Additionally, this paper also presents localization of passive RFID tags operating at 13.56MHz frequency or less by measuring the cross-correlation of multipath noise in the backscattered signals.

The fourth paper extends the cross-correlation based localization algorithm to wireless devices operating at 2.4GHz by exploiting shadow fading cross-correlation. In addition, the paper also introduces a signal strength divergence based tracking method for localizing mobile transmitters. The final paper explores the placement of receivers in the target environment to ensure certain level of localization accuracy under cross-correlation

based localization method. The effectiveness of our cross-correlation based localization methodology is demonstrated using IEEE 802.15.4 radios operating in fading noise rich environment such as an indoor mall and ERL 114 of Missouri university of Science and Technology (Missouri S&T).

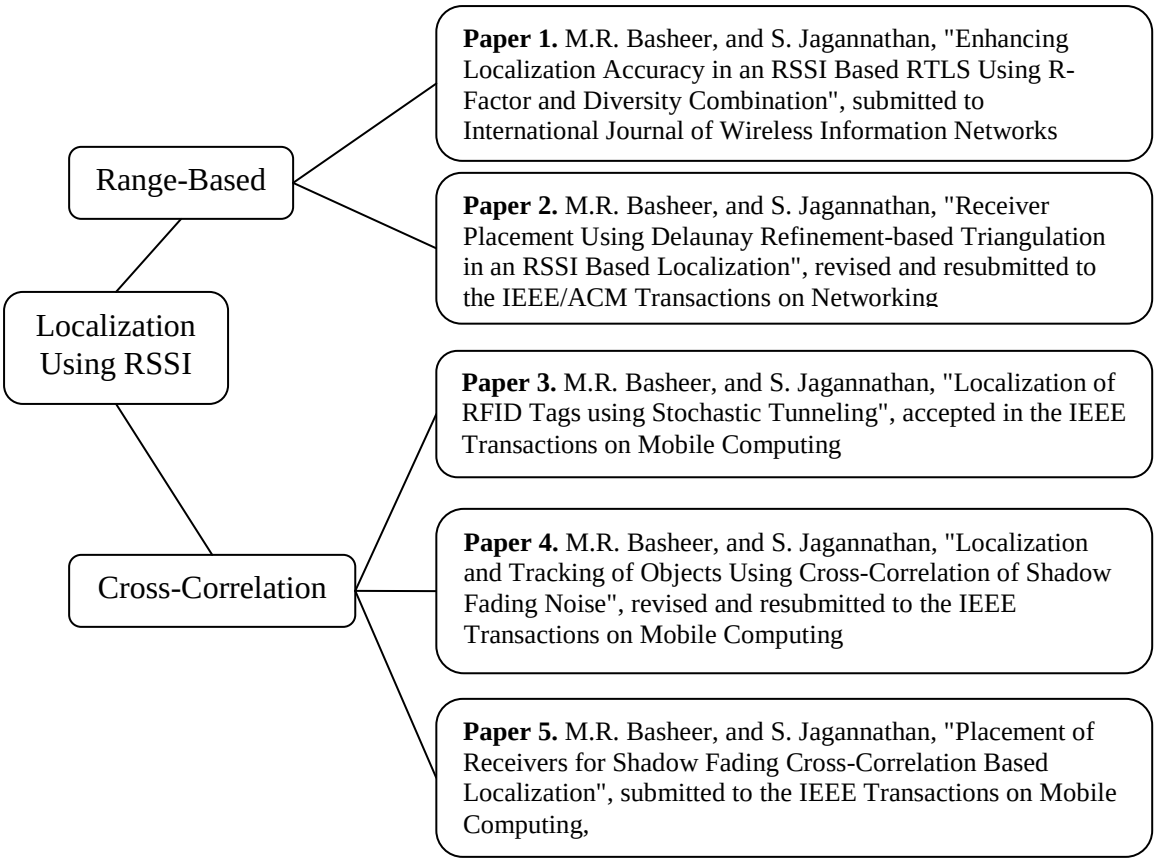

Fig 1.1 Dissertation outline

Paper 1 looks into the errors associated with range based localization method when a transmitter, whose position is unknown, is operating under either LoS or non-line of sight (NLoS) conditions with a group of receivers that are placed at known positions around the localization area. In this paper, Friis transmission equation is used as the mapping function between RSSI and radial separation between a transmitter and receiver

in the far field region. Using random variable transformation method on Ricean or Rayleigh distribution for LoS or NLoS condition respectively between the transmitter and receiver, the Probability Distribution Function (PDF) of radial distance estimate is derived under LoS and NLoS condtions. We introduce a localization quality metric for each receiver involved in range-based localization called the R-factor which is a measure of the mean square error (MSE) of the radial estimate by that receiver. This paper concludes by showing that the application of channel diversity at the receiver or transmitter such as antenna or frequency diversity, the R-factor at a receiver can be reduced thereby improving the accuracy of estimating the location of the transmitter.

Paper 2 deals with the issue of optimally placing the receivers around the localization area to ensure certain level of accuracy in locating the transmitter using a range based signal strength localization method. The proposed solution employs Constrained Delaunay Triangulation with Refinement and R-factor based localization quality metric to derive possible coordinates for receivers around the target area. Constrained Delaunay Triangulation with Refinement tessellates a 2D area into triangles, where each vertex in this triangle represents the Cartesian coordinate of a receiver that satisfies a quality criterion which for this paper is the localization error of the transmitter. However, Constrained Delaunay Triangulation with Refinement algorithm is sub-optimal in the number of triangular regions used to tessellate the localization area resulting in our placement algorithm being sub-optimal in the number of receivers required to achieve the user specified localization accuracy.

Paper 3 delves into passive localization of a cluster of Radio Frequency Identification (RFID) tags. This paper introduces a new range based localization method

where cross-correlation between multipath noises in the RSSI values, instead of the absolute RSSI value, is used to estimate the radial separation between a pair of RFID tags. The functional relationship that ties cross-correlation in multipath noise between a cluster of RFID tags and their relative radial separation is derived for both LoS and NLoS conditions. The localization problem considered in this paper is essentially estimating the Cartesian coordinates of a cluster of RFID tags when pair-wise RSSI correlation coefficient and the location of a subset of RFID tags called the anchor nodes are available. Due to the highly non-convex nature of the localization objective function used in this paper, a stochastic optimization algorithm called the simulated annealing with tunneling is used to solve for RFID locations. However, due to the rapid rate at which the multipath correlation coefficient falls to zero with radial separation over one wavelength between RFID tags, the practical applicability of this solution is relegated to RFID tags that operate at 13.56MHz (high frequency tags) and under.

Paper 4 extends the operating frequency range of cross-correlation based localization to IEEE 802.15.4 transceivers that operate at 2.4GHz by utilizing correlation among shadow fading noise instead of multipath fading noise. In this paper, shadow fading cross-correlation between receivers is used to estimate the position of a transmitter. To extract the shadow fading residuals from RSSI, a mean reverting stochastic process called Ornstein-Uhlenbeck process is employed. Subsequently, the extracted shadow fading residuals are used to build a semi-parametric Cumulative Density Function (CDF) for each receiver. These CDFs along with the correlation coefficient between receivers form the input to a student-t copula function which acts as the likelihood function for estimating the unknown position of the transmitter. Once

again stochastic optimization with tunneling is employed to solve this highly non-convex optimization function. Due to the large convergence time for stochastic optimization methods, we propose a dead-reckoning based tracking method that utilizes transmitter velocity estimates from α-divergence of shadow fading residuals and heading estimates from an on-board gyroscope for faster transmitter position estimates. To prevent the dead-reckoning errors from accumulating over time, we apply a particle Bayesian filter that generates several position estimates or particles around the current tracked position using the PDF of tracking error noise and then filter out erroneous ones using cross-correlation based student-t copula likelihood function.

Finally, Paper 5 deals with the issue of placing the receivers around the localization area to ensure certain level of accuracy in locating the transmitter using cross-correlation of shadow fading residuals. The proposed solution works in two stages. In the first stage, using the maximum communication range of a wireless transceiver and the layout of the localization workspace as inputs, the placement algorithm generates receiver position that will ensure complete localization coverage within this workspace. A location within the workspace is said to be under localization coverage when there are at least 3 receivers in communication range of a transmitter if it is located at that point. Subsequently, in stage two the dynamics of the cross-correlation based localization is introduced through the Cramer Rao Lower Bound (CRLB) in transmitter location estimation variance. CRLB is used as the localization accuracy metric to determine the number of shadow fading samples that each receiver should collect before computing the cross-correlation between receiver pairs such that the location estimates have accuracy better than a pre-specified error threshold. This is possible because the CRLB for

transmitter localization using shadow fading correlation, derived in this paper, is inversely proportional to the number of shadow fading samples used for computing cross-correlation between receiver pairs. The proposed placement solution was compared with Delaunay Refinement based placement strategy proposed in Paper 2 and was found to result in fewer number of receivers to achieve the pre-specified error threshold than the Delaunay refinement based placement algorithm in Paper 2.

1.2 CONTRIBUTIONS OF THE DISSERTATION

This dissertation provides contributions to the field of transmitter localization using signal strength measurements as well as to the optimal receiver placement strategy for guaranteed localization accuracy. The accuracy of the proposed cross-correlation of signal strength fading-based localization methodology is demonstrated in a multipath rich environment such as an indoor mall and in a typical laboratory environment using IEEE 802.15.4 radios. Paper 1 introduces a localization quality metric called the *R-factor* which is a measure of the mean square error of the radial distance estimate by a receiver. Base stations can exclude radial estimates from receivers with high R-factor values thereby improving the overall robustness of location estimates by avoiding outliers. Paper 2 provides a sub-optimal receiver placement strategy that will guarantee certain level of localization accuracy.

Paper 3 introduces the cross-correlation of signal fading based localization methodology. In addition, this paper derives the relationship between cross-correlation in backscattered multipath fading noise signals from a pair of passive RFID tags against the radial separation and LoS condition between them. Paper 4 provides a method to extract shadow fading residuals from signal strength values using a mean reverting stochastic process called the Ornstein-Uhlenbeck process. Additionally, this paper derives the joint

distribution of shadow fading residuals from receivers using copula function that forms the likelihood function for cross-correlation of signal strength based localization method. Finally, this paper also presents a velocity estimation technique that measures the rate at which Bayes error to a stationary transmitter hypothesis changes over time that is utilized for a tracking mobile transmitters.

Paper 5 present a receiver placement algorithm such that position estimates from cross-correlation of shadow fading noise measured by the receiver will locate a common transmitter with the location accuracy better than a pres-specified threshold. Cramer Rao Lower Bound for transmitter location estimate using shadow fading cross-correlation is derived and forms the metric that is used to control the number of samples collected at each receiver to attain the pre-specified error threshold.

1.3 REFERENCES

[1] Y. T. Chan, W. Y. Tsui, H. C. So, and P. C. Ching, B, "Time of arrival based localizatoin under NLOS conditions," IEEE Trans. Veh. Technol., vol. 55, pp. 17–24, Jan. 2006.

[2] M.D. Gillette, and H.F. Silverman, "A linear closed-form algorithm for source localization from time-differences of arrival," *IEEE Signal Processing Letters*, vol.15, no., pp.1-4, 2008.

[3] M. Cedervall and R. L. Moses, "Efficient maximum likelihood DOA estimation for signals with known waveforms in the presence of multipath," *IEEE Trans. Signal Processing*, vol. 45, pp.808 -811 1997.

[4] A. Ramachandran, and S. Jagannathan, "Spatial diversity in signal strength based WLAN location determination systems," *Proc. of the 32nd IEEE Conf. on Local Comp. Networks* , pp. 10-17, Oct. 2007.

[5] K. Pahlavan, X. Li, and J. P. Makela, "Indoor geolocation science and technology," *IEEE Communications Magazine*, vol. 40, no. 2, pp. 112–118, 2002.

[6] S. Krishnakumar and P. Krishnan, "On the accuracy of signal strength-based location estimation techniques," *Proc. of IEEE INFOCOM*, vol 1, pp. 642-650, 2005.

[7] M. Youssef, and A. Agrawala, “The Horus WLAN location determination system,” *Proc. of the 3rd inter. Conf. on Mobile Systems, Applications, and Service*, MobiSys '05. ACM Press, NY, pp. 205-218.

[8] IEEE 802.15.4-2006, Part 15.4: Wireless Medium Access Control (MAC) and physical layer (PHY) specifications for low-rate wireless personal area networks (WPANs), IEEE, Sept. 2006.

[9] XBee/XBee-PRO OEM RF Modules Datasheet, *Digi International Inc*, http://ftp1.digi.com/support/documentation/90000982_A.pdf, accessed Sept 2008.

[10] J. Koo, and H. Cha, “Localizing WiFi access points using signal strength,” *IEEE Communications Letters* , vol.15, no.2, pp.187-189, February 2011

[11] K. W. Cheung, H. C. So, W. Ma, and Y. T. Chan, “A constrained least squares approach to mobile positioning: algorithms and optimality,” *EURASIP J. Appl. Signal Process.*, pp. 150-150, Jan 2006.

[12] C. Morelli, M. Nicoli, V. Rampa, and U. Spagnolini, “Hidden Markov models for radio localization in mixed LOS/NLOS conditions,” *IEEE Transactions on Signal Processing*, vol.55, no.4, pp.1525-1542, April 2007

[13] V. Seshadri, G. V. Zaruba, and M. Huber, “A Bayesian sampling approach to in-door localization of wireless devices using received signal strength indication,” *in Proc. IEEE Int. Conf. Pervasive Comput. Commun. (PerCom 2005)*, Mar. 2005, pp. 75–84.

[14] X. Ji, and H. Zha, “Sensor positioning in wireless ad-hoc sensor networks using multidimensional scaling,” *23rd Annual Joint Conf. of the IEEE Computer and Commun. Soc.* , vol.4, pp. 2652- 2661, Mar. 2004.

[15] C. Wang, J. Chen, Y. Sun, and X. Shen, “Wireless sensor networks localization with Isomap,” *IEEE Int. Conf. on Commun.*, Jun. 2009.

[16] N. Patwari, and A. O. Hero, “Manifold learning algorithms for localization in wireless sensor networks,” *In Proc. of the IEEE Int. Conf. on Acoustics, Speech and Signal Processing*,vol.3,pp.857–860, May2004.

[17] H. Lim, L. Kung, J. Hou and H. Luo, “Zero-configuration robust indoor localization: Theory and experimentation,” *in Proceedings of IEEE INFOCOM*, pp.1-12, Apr. 2006.

[18] Nuttall, “Error probabilities for equicorrelated M-ary signals under phase-coherent and phase-incoherent reception,” *IRE Transactions on Information Theory*, vol.8, no.4, pp.305-314, July 1962.

I. ENHANCING LOCALIZATION ACCURACY IN AN RSSI BASED RTLS USING R-FACTOR AND DIVERSITY COMBINATION[1]

M. R. Basheer and S. Jagannathan

Abstract— *The fundamental cause of localization error in an indoor environment is fading and spreading of the radio signals due to scattering, diffraction, and reflection. These effects are predominant in regions where there is no-line-of-sight (NLoS) between the transmitter and the receiver. Efficient algorithms are needed to identify the subset of receivers that provide better localization accuracy since NLoS receivers can degrade location accuracy. This paper introduces a new parameter called the R-Factor to indicate the extent of radial distance estimation error introduced by a receiver and to select a subset of receivers that result in better accuracy in real-time location determination systems (RTLS). In addition, it was demonstrated that location accuracy improves with R-factor reduction which is achieved either by increasing the number of localization receivers or using channel diversity and combining RSSI values non-coherently using root mean square operation. Therefore, existing localization algorithms can utilize R-factor and diversity schemes to improve accuracy. Both analytical and experimental results are included to justify the theoretical results in terms of improvement in accuracy by using R-factor.*

Keywords*:* Diversity, Localization Error, Real-time Indoor Location System, R-factor, Ricean, Rayleigh

[1] Research Supported in part by GAANN Program through the Department of Education and Intelligent Systems Center. Authors are with the Department of Electrical and Computer Engineering, Missouri University of Science and Technology (formerly University of Missouri-Rolla), 1870 Miner Circle, Rolla, MO 65409. Contact author Email: mrbxcf@mail.mst.edu.

1. INTRODUCTION

Location information about an asset is a key requirement in the network-centric environment. In an outdoor environment, Global Positioning Systems (GPS) have been very successful, however, lack of satellite coverage and unit cost have severely restricted the use of GPS for indoor positioning. Consequently, a wide variety of technologies such as Time of Arrival (ToA), Time Difference of Arrival (TDoA), Angle of Arrival (AoA), and Received Signal Strength Indicator (RSSI) of radio [1] and acoustic [2] waves have been proposed for indoor localization. Several factors including large positioning errors, cost of synchronization hardware, and time consuming calibration issues, have limited the widespread adoption of these technologies.

Time and angle-based location determination though can result in better accuracy but require special antennas or time synchronization hardware. On the other hand, RSSI based solutions can only provide coarse-grained localization whereas they are cost-effective due to software-oriented nature. As a result, RSSI based localization schemes are preferred on IEEE 802.15.4 [1] and IEEE 802.11 [3] wireless networks.

The fundamental reason for localization error in an indoor environment is the result of scattered components which cause fading and spreading of the received signal. Fading results in variation of signal strength due to destructive or constructive addition of the signal and spreading leading to uncertainties in the measurement of signal arrival time. Consequently, indoor positioning algorithms perform unsatisfactorily under this condition. Several RSSI based solutions [4] [5] exist that employ stochastic wireless propagation models to predict the amplitude distribution of scattered components in NLoS regions. However, the added computational complexity of these solutions has

precluded better localization accuracy [6] [7]. Further, stochastic solutions for localization in NLoS regions require detailed radio-mapping of the target area referred to as *profiling* or *fingerprinting* which is normally tedious and time consuming.

Several statistical solutions have been proposed to detect receivers that are under NLoS condition and remove them from localization. The chi-square best-fit test was used in [8] to compare the probability density of received fading amplitudes to standard probability density function (PDF) such as Rayleigh, Ricean, and Log-normal distribution. Venkatraman *et al.* [9] assume a Gaussian distribution for the measured distance under LoS conditions and hence the problem of NLoS receiver detection is to look for non-Gaussian range measurements. However, hypothesis testing using chi-square test requires large sample size in order for the chi-square approximation to be valid [10 pp.215] while Gaussian distribution approximation for the received signal amplitude is only applicable under very strong LoS signal levels [11] which may classify receivers with moderate LoS component as NLoS.

Instead, in this paper, mean square error (MSE) of radial distance estimate is proposed as a metric for evaluating the quality of received signal used for localization. It is shown that the best case MSE of the radial distance estimate obtained from the Friis transmission equation [12] by using a point estimator for a receiver under NLoS condition is not suitable than the worst case MSE obtained for a receiver with LoS component. Unfortunately, there is no method available in the literature that uses this quality metric to identify in real-time a subset of receivers with LoS component and varying degree of NLoS component energy levels in order to attain better localization accuracy. Therefore, this work proposes a new parameter called the *R-Factor* to grade

the quality of a receiver used for localization under varying levels of NLoS energy. Next, it will shown that with an increase in the number of receivers that fall below a given R-factor threshold, or by increasing the diversity channels at a receiver, the location accuracy can be improved.

The R-Factor uses the generalized Ricean fading model since both empirical and theoretical studies from the past literature [13] [14] [15] of radio propagation in 2.4 GHz, 5 GHz and 60 GHz have shown that Ricean distribution accurately models fast fading in an indoor environment with dominant LoS while log-normal distribution can account for variation of signal strength over a larger area. Consequently, the proposed scheme could be applied for both indoor and outdoor localization by varying the Ricean K-factor. In addition, this work shows how receivers with multiple diversity channels can be combined using Root Mean Square (RMS) to further improve localization accuracy.

This paper begins by deriving the equation for MSE of the radial distance estimate obtained using a point estimator in a Ricean fading environment and shows that MSE degrades with R-factor and more importantly becomes unsatisfactory under NLoS conditions. Subsequently, R-factor is shown to be related to the localization error in the NLoS environment. Additionally it is demonstrated that the location accuracy improves with an increase in the number of receivers while keeping the R-factor below a threshold. Next, the use of diversity scheme and the appropriate combination of signals are shown to further reduce localization error. Finally, the theoretical conclusions are verified using experimental results.

Contributions of this paper include: (a) an analytical result which shows that for a radial distance estimator based on Friis transmission equation, the lower limit of the MSE

at a receiver under NLoS condition is higher than the upper limit of MSE for a receiver having LoS component but with equal energy in their NLoS components; (b) a new R-factor to quantify the radial distance estimation error introduced by a receiver; (c) an analytical result which demonstrates that localization accuracy improves either by increasing the number of receivers or with channel diversity and (d) finally, among diversity combination methods such as selection combination, averaging and root mean square (RMS), RMS result in the lowest R-factor and consequently the best localization accuracy in an RSSI based RTLS using Friis transmission equation for radial distance estimate.

2. MEAN SQUARE ERROR OF RADIAL DISTANCE ESTIMATE

The time varying signal measured at any receiver antenna is due to a combination of LoS and NLoS components. The amplitude and phase of the LoS component of the received signal are deterministic, whereas the NLoS component's amplitude and phase are represented as random variables. The probability density function (PDF) of the received signal amplitude random variable *X* is expressed by the Ricean distribution [16] as

$$f_X(x|A,\sigma_X) = \frac{x}{\sigma_X^2} exp\left(-\frac{A^2+x^2}{2\sigma_X^2}\right) I_0\left(\frac{Ax}{\sigma_X^2}\right) \quad (1)$$

where *x* is a possible value of *X*, $I_0(\cdot)$ represents the zero order modified Bessel function, $2\sigma_X^2$ is the local mean NLoS energy, and *A* is the amplitude of the LoS component. The term $K = \frac{A^2}{2\sigma_X^2}$ is referred to as the Ricean K-factor [16], which is defined as the ratio of the energy in the LoS component (A^2) to that of the NLoS components ($2\sigma_X^2$). Under NLoS condtions (*A=0*), Ricean distribution becomes Rayleigh distribution.

In this section, the mean and variance of the radial distance estimate for a receiver used for localization will be presented in Lemma 1 and subsequently will be used to derive the MSE for a receiver with LoS component in Lemma 2. Next, the lower bound MSE of the radial distance estimate for receivers under NLoS condition is compared with the best case MSE for a receiver with LoS component in Theorem 1.

Lemma 1: (*Mean and Variance of Radial Distance Estimate*): The mean and variance of the radial distance estimate by a receiver to a transmitter using Friis transmission equation based estimator under Ricean fading environment is given by

$$E(R|A,\sigma_X) = \left\{\frac{2l_0}{\sigma_x^2\pi\left[M\left(-\frac{1}{2},1,-K\right)\right]^2}\right\}^{\frac{1}{n}} + \frac{2\sigma_X^2(n+2)}{n^2 l_0}\left\{\frac{2l_0}{\sigma_x^2\pi\left[M\left(-\frac{1}{2},1,-K\right)\right]^2}\right\}^{\frac{1}{n}+1} \times\left\{1+K-\frac{\pi}{4}\left[M\left(-\frac{1}{2},1,-K\right)\right]^2\right\} \quad (2)$$

$$Var(R|A,\sigma_X) = \frac{8\sigma_X^2}{n^2 l_0}\left\{\frac{2l_0}{\sigma_x^2\pi\left[M\left(-\frac{1}{2},1,-K\right)\right]^2}\right\}^{\frac{2}{n}+1}\left\{1+K-\frac{\pi}{4}\left[M\left(-\frac{1}{2},1,-K\right)\right]^2\right\}. \quad (3)$$

where $K = \frac{A^2}{2\sigma_X^2}$ is the Ricean K factor, $M(\cdot,\cdot,\cdot)$ is the Confluent Hypergeometric Function (CHF) [17, p.503], l_0 is the Friis transmission equation factor that depend on the antenna geometry and transmission wavelength [12], and n is the path loss distance coefficient.

Proof: The radial distance (R) between the transmitter and a receiver is related to the received signal amplitude (X) at far field as

$$R = g(X) = \left(\frac{l_0}{X^2}\right)^{\frac{1}{n}}. \quad (4)$$

For small variation of signal strength around the mean$\mu = E(X|A,\sigma_X)$, (4) can be approximated by a second order Taylor series approximation as $R = g(X) \approx g'(\mu)(X-\mu) + \frac{1}{2}g''(\mu)(X-\mu)^2$ [18, p.77]. This results in the mean and variance of R as

$$E(R|A,\sigma_X) = E[g(x)] \approx g(\mu) + \frac{1}{2}\left[\frac{d^2}{dX^2}g(X)\right]_{X=\mu} Var(X|A,\sigma_X) \tag{5}$$

$$Var(R|A,\sigma_X) = Var[g(x)] \approx \left[\frac{d}{dX}g(X)\right]^2_{X=\mu} Var(X|A,\sigma_X). \tag{6}$$

Substituting the Ricean PDF's mean and variance for μ and $Var(X|A,\sigma_X)$ respectively in (5) and (6) renders the mean and variance of the radial distance estimate as (2) and (3).

Definition 1: (*Localization or Location Receiver*) A receiver for RSSI based RTLS, is called localization or location receiver if the estimated Ricean K-factor for the received signals at this receiver is greater than 9.6 dB $\left(\frac{A^2}{2\sigma_X^2} > 9\right)$. Utilizing only these receivers for RTLS avoids time consuming and costly pre-profiling of target area that is essential for localization with NLoS receivers.

Lemma 2: (*MSE for Localization Receiver*): The MSE of radial distance estimate using (4) for a receiver under Ricean environment is given by

$$MSE(R) = \frac{2l_0^{\frac{2}{n}}A^{-\frac{4}{n}}}{n^2K}\left[1 + \left(\frac{1}{2}+\frac{1}{n}\right)^2\frac{1}{K}\right]. \tag{7}$$

Proof: The MSE for the radial distance estimator can be calculated as

$$MSE(R) = Var(R|A,\sigma_X) + B_R^2. \tag{8}$$

where $B_R = E(R|A,\sigma_X) - d$ is the bias of the estimator and d is actual radial distance to the transmitter. Since, $K = \frac{A^2}{2\sigma_X^2} > 9$ the CHF terms in the mean and variance given by

lemma 1 can be approximated for a receiver as, $\lim_{K\to\infty}\left[M\left(-\frac{1}{2},1,-K\right)\right]^2=\frac{4}{\pi}K$ and $\lim_{K\to\infty}\left\{1+K-\frac{\pi}{4}\left[M\left(-\frac{1}{2},1,-K\right)\right]^2\right\}=\frac{1}{2}$ [17, p.508, §13.5.1]. This results in a simplified form for the bias and variance for the radial distance estimate as

$$B_R \approx \left(\frac{l_0}{A^2}\right)^{\frac{1}{n}}+\frac{(n+2)}{n^2 l_0}\left(\frac{l_0}{A^2}\right)^{\frac{1}{n}+1}\sigma_X^2-d \tag{9}$$

$$Var(R|A,\sigma_X)\approx\frac{2l_0^{\frac{2}{n}}A^{-\frac{4}{n}}}{n^2K}. \tag{10}$$

However, the actual radial distance *d* is related to the amplitude of the LoS component (*A*) by the Friis transmission equation as $d^n=\frac{l_0}{A^2}$. Hence applying (9) and (10) on (8) gives the mean square error in (7).

Remark 1: (*Accuracy of MSE for a Localization Receiver*): At $K=\frac{A^2}{2\sigma_X^2}>9$, the difference between the CHF approximation from the actual value is less than 1%. Hence (7) can be used for all practical purposes to estimate the MSE for localization receivers.

Remark 2: (*Upper Bound of MSE for a Localization Receiver*): For a receiver under Ricean environment, the upper bound of the MSE of (4) is given by

$$MSE(R)<\frac{(37n^2+4n+4)}{162n^4}\left(\frac{l_0}{A^2}\right)^{\frac{2}{n}}. \tag{11}$$

Proof: The upper bound of the NLoS component energy for a localization receiver is given by $\sigma_X^2<\frac{A^2}{18}$. Hence substituting this on (7) results in (11).

Remark 3: (*Lower Bound of MSE for a Receiver under NLoS*): For a receiver under NLoS condition, the lower bound of the MSE of (4) is given by

$$MSE(R)>\frac{2\sigma_X^2}{n^2 l_0}\left(\frac{2l_0}{\sigma_X^2\pi}\right)^{\frac{2}{n}+1}(4-\pi). \tag{12}$$

Proof: Setting Rayleigh distribution mean and variance for μ and $Var(X|\sigma_X)$ respectively in (5) and (6) and subtracting d from (5) gives the bias and variance for a receiver under NLoS condition as

$$B_R = \left(\frac{2l_0}{\sigma_X^2\pi}\right)^{\frac{1}{n}} + \frac{2\sigma_X^2(n+2)}{n^2 l_0}\left(\frac{2l_0}{\sigma_X^2\pi}\right)^{\frac{1}{n}+1}\left(\frac{4-\pi}{4}\right) - d \tag{13}$$

$$Var(R|A,\sigma_X) = \frac{2\sigma_X^2}{n^2 l_0}\left(\frac{2l_0}{\sigma_X^2\pi}\right)^{\frac{2}{n}+1}(4-\pi). \tag{14}$$

Applying (13) and (14) on (8) results in MSE for a receiver under NLoS condition as

$$MSE(R) = \frac{2\sigma_X^2}{n^2 l_0}\left(\frac{2l_0}{\sigma_X^2\pi}\right)^{\frac{2}{n}+1}(4-\pi) + \left[\left(\frac{2l_0}{\sigma_X^2\pi}\right)^{\frac{1}{n}} + \frac{2\sigma_X^2(n+2)}{n^2 l_0}\left(\frac{2l_0}{\sigma_X^2\pi}\right)^{\frac{1}{n}+1}\left(\frac{4-\pi}{4}\right) - d\right]^2. \tag{15}$$

For $\sigma_X > 0$ and setting $B_R = 0$ in (13) gives the lowest value of (15) for a receiver under NLoS as (12).

Theorem 1: (*Lower MSE for a Localization Receiver*): For the same amount of NLoS energy at a localization receiver and a receiver under NLoS conditions, the MSE of the radial distance estimate for the localization receiver is lower than that of the receiver under the NLoS condition.

Proof: Applying $\frac{A^2}{18\sigma_X^2} > 1$ for a localization receiver on (11) gives the upper limit of the MSE in terms of the NLoS energy as $\frac{(37n^2+4n+4)}{162n^4}\left(\frac{l_0}{18\sigma_X^2}\right)^{\frac{2}{n}}$. Assuming that a localization receiver and a receiver under NLoS condition were measured to have the same amount of energy in its NLoS components, then the localization receiver will have lower MSE if $\frac{(37n^2+4n+4)}{162n^4}\left(\frac{l_0}{18\sigma_X^2}\right)^{\frac{2}{n}} < \frac{2\sigma_X^2}{n^2 l_0}\left(\frac{2l_0}{18\sigma_X^2}\right)^{\frac{2}{n}+1}(4-\pi)$. This results in the following inequality $\left[\left(\frac{648}{\pi}\right)\left(\frac{36}{\pi}\right)^{\frac{2}{n}}(4-\pi) - 1\right]n^2 - 4n - 4 > 0$. Numerical analysis has shown

that, even at the lowest value for the left hand term of the inequality (occurring at $n = 2.442$), it was found to be satisfied.

3. R-FACTOR

In this section, R-factor is defined and subsequently related in Theorem 2 with location accuracy in a RSSI-based RTLS. Next in Theorem 3, it will be shown that with an increase in receiver count from w to $w+1$ where each receiver meeting the needed R-factor threshold, the location accuracy improves. For a localization receiver, the term $\left(\frac{1}{2}+\frac{1}{n}\right)^2 \frac{1}{K}$ in (7) is always less than 1 for $n > 0.4$, hence MSE can be reduced substantially by decreasing the term

$$\gamma = \frac{l_0^{\frac{2}{n}} A^{-\frac{4}{n}}}{n^2 K} = \frac{2 l_0^{\frac{2}{n}}}{n^2}\left(\frac{\sigma_X^2}{A^{\frac{4}{n}+2}}\right). \tag{16}$$

where γ is called the *R-factor* (Receiver Error Factor). For a localization receiver R-factor is related to the variance as

$$Var(R|A, \sigma_X) = 2\gamma. \tag{17}$$

The major significance of R-factor is that it not only includes the signal to noise ratio (K) as a factor in predicating the accuracy of radial distance estimates, but also path loss coefficient (n) and Friis transmission factor (l_0) thereby rendering a single localization quality metric for each receiver used for localization.

Theorem 2: (*R-factor and Upper Bound for Localization Error*): The upper bound of the localization error decreases with R-factor in a Ricean environment for a RSSI based RTLS.

Proof: Assume that w localization receivers, whose coordinates are given by (x_i, y_i), $i = 1, 2,..,w,$ are used to estimate the 2-D coordinates of an unknown transmitter. The

relationship between the estimated radial distance estimate R_i to the transmitter coordinate estimates *(X, Y)* is given as

$$R_i^2 = (X - x_i)^2 + (Y - y_i)^2; i = \{1,2,\cdots,w). \tag{18}$$

Subtracting R_i^2 from R_j^2 where $i \neq j$ and rearranging the terms in (18) results in

$$\frac{x_i^2+y_i^2}{2} - \frac{x_j^2+y_j^2}{2} - \frac{R_i^2-R_j^2}{2} = X\big(x_i - x_j\big) + Y\big(y_i - y_j\big). \tag{19}$$

Substitution of $c_{ij} = \frac{x_i^2+y_i^2}{2} - \frac{x_j^2+y_j^2}{2}, R_{ij}^2 = \big(r_i^2 - r_j^2\big), x_{ij} = \big(x_i - x_j\big)$ and $y_{ij} = \big(y_i - y_j\big)$ in (18) yields

$$c_{ij} - \frac{R_{ij}^2}{2} = x_{ij}X + y_{ij}Y. \tag{20}$$

For $w > 3$, the system is over determined and can be solved for *X* and *Y* using least squares as

$$X = \frac{\vec{X}_{ij}^T\vec{C}_{ij}}{[\vec{X}_{ij}\,\vec{Y}_{ij}]^T[\vec{X}_{ij}\,\vec{Y}_{ij}]} - \frac{\vec{X}_{ij}^T\vec{R}_{ij}^2}{2[\vec{X}_{ij}\,\vec{Y}_{ij}]^T[\vec{X}_{ij}\,\vec{Y}_{ij}]} \tag{21}$$

$$Y = \frac{\vec{Y}_{ij}^T\vec{C}_{ij}}{[\vec{X}_{ij}\,\vec{Y}_{ij}]^T[\vec{X}_{ij}\,\vec{Y}_{ij}]} - \frac{\vec{Y}_{ij}^T\vec{R}_{ij}^2}{2[\vec{X}_{ij}\,\vec{Y}_{ij}]^T[\vec{X}_{ij}\,\vec{Y}_{ij}]}. \tag{22}$$

where $\vec{R}_{ij}^2 = \big[R_{12}^2, R_{23}^2, \cdots, R_{ij}^2\big]^T$, $\vec{C}_{ij} = \big[c_{12}, c_{23}, \cdots, c_{ij}\big]^T$, $\vec{X}_{ij} = \big[x_{12}, x_{23}, \cdots, x_{ij}\big]^T$ and $\vec{Y}_{ij} = \big[y_{12}, y_{23}, \cdots, y_{ij}\big]^T$. Equations (21) and (22) are solvable provided the matrix $\big[\vec{X}_{ij}\,\vec{Y}_{ij}\big]^T\big[\vec{X}_{ij}\,\vec{Y}_{ij}\big]$ is not singular. Since (21) and (22) are similar, subsequent calculations will only consider the localization error in *X* coordinate. The mean of *X* is given by $E(X) = \frac{\vec{X}_{ij}^T\vec{C}_{ij}}{[\vec{X}_{ij}\,\vec{Y}_{ij}]^T[\vec{X}_{ij}\,\vec{Y}_{ij}]} - \frac{\vec{X}_{ij}^T E\big(\vec{R}_{ij}^2\big)}{2[\vec{X}_{ij}\,\vec{Y}_{ij}]^T[\vec{X}_{ij}\,\vec{Y}_{ij}]}$. Subtracting *E(X)* from (21) gives the absolute localization error in X axis as

$$|\Delta e_X| = |X - E(X)| = \left|\frac{\vec{X}_{ij}^T}{2[\vec{X}_{ij}\,\vec{Y}_{ij}]^T[\vec{X}_{ij}\,\vec{Y}_{ij}]}\big\{E\big(\vec{R}_{ij}^2\big) - \vec{R}_{ij}^2\big\}\right|. \tag{23}$$

Applying the triangle inequality on (23) and setting $\left|\vec{R}_{ij}^2\right| = \left|\vec{R}_i^2 - \vec{R}_j^2\right| \leq \vec{R}_i^2 + \vec{R}_j^2$ renders

$$|\Delta e_X| = |X - E(X)| \leq \left|\frac{\vec{X}_{ij}^T}{2[\vec{X}_{ij}\ \vec{Y}_{ij}]^T[\vec{X}_{ij}\ \vec{Y}_{ij}]}\right| \left|E\left(\vec{R}_{ij}^2\right) - \vec{R}_{ij}^2\right| \leq \left|\frac{\vec{X}_{ij}^T}{2[\vec{X}_{ij}\ \vec{Y}_{ij}]^T[\vec{X}_{ij}\ \vec{Y}_{ij}]}\right| \left|E\left(\vec{R}_{ij}^2\right) + \vec{R}_{ij}^2\right|$$

$$\leq \left|\frac{\vec{X}_{ij}^T}{2[\vec{X}_{ij}\ \vec{Y}_{ij}]^T[\vec{X}_{ij}\ \vec{Y}_{ij}]}\right| \left|E\left(\vec{R}_i^2\right) + E\left(\vec{R}_j^2\right) + \vec{R}_i^2 + \vec{R}_j^2\right|. \quad (24)$$

Hence the upper bound for the mean of absolute localization error can be computed from (24) as

$$E(|\Delta e_X|) \leq \left|\frac{\vec{X}_{ij}^T}{2[\vec{X}_{ij}\ \vec{Y}_{ij}]^T[\vec{X}_{ij}\ \vec{Y}_{ij}]}\right| \left|E\left(\vec{R}_i^2\right) + E\left(\vec{R}_j^2\right)\right|. \quad (25)$$

Substituting $E(R_i) \approx d_i$ and $Var(R_i)$ as in (17) results in $E(R_i^2) = Var(R_i) + E^2(R_i) = 2\gamma_i + d_i^2$. Hence

$$E(|\Delta e_X|) \leq \left|\frac{\vec{X}_{ij}^T}{2[\vec{X}_{ij}\ \vec{Y}_{ij}]^T[\vec{X}_{ij}\ \vec{Y}_{ij}]}\right| \left|2\gamma_i + d_i^2 + 2\gamma_j + d_j^2\right|. \quad (26)$$

Applying Markov's inequality gives the probability of the absolute localization error falling above a constant $\psi > 0$ as

$$P(|\Delta e_X| \geq \psi) \leq \frac{1}{2\psi}\left|\frac{\vec{X}_{ij}^T}{[\vec{X}_{ij}\ \vec{Y}_{ij}]^T[\vec{X}_{ij}\ \vec{Y}_{ij}]}\right| \left|2\gamma_i + d_i^2 + 2\gamma_j + d_j^2\right|. \quad (27)$$

Therefore a reduction in R-factor decreases the upper bound of the localization error. Next the localization accuracy with receiver count is explained through this theorem.

Theorem 3: (*Localization Accuracy with Localization Receiver Count*): Localization accuracy using *w+1* receivers is better in comparison with deploying *w* receivers in an RSSI based RTLS system when the maximum R-factor is kept the same in both cases.

Proof: An RTLS system with *w* localization receivers results in ${}^{w}C_2 = \frac{w(w-1)}{2}$ linear equations similar to (20). Having one more localization receiver increases the number of linear equations by $\Delta w = {}^{w+1}C_2 - {}^{w}C_2 = w$. The linear least square estimator has the asymptotic property that its variance tends to approach the Cramer-Rao lower bound on increasing the number of linear equations (sample size) [19 pp. 377]. Therefore the accuracy with $w + 1$ receivers is better than *w* receivers provided the maximum R-factor remains same.

Remark 5: (*Computing R-factor from Signal Strength*): By substituting $A = \frac{\sqrt{l_0}}{\frac{n}{d^2}}$ in (16), R-factor can be re-written in terms of *d* and the Ricean *K* factor as $\gamma = \frac{d^2}{n^2 K}$. Replace *d* by the sample mean of the estimated radial distance ($\bar{r}$), and compute the Ricean K-factor using the moment-method [20] to obtain

$$\gamma = \frac{\bar{r}^2(1-p)}{n^2\sqrt{p^2-s^2}}. \tag{28}$$

where s^2 and *p* are the sample variance and mean respectively of the signal strength measured by a receiver.

4. DIVERSITY AND R-FACTOR

Diversity is a method to improve certain aspects of the received signal by using two or more communication channels. Two commonly used diversity schemes for RTLS are spatial (multiple antennas single frequency) and frequency (single antenna multiple frequency). RTLS using the above diversity schemes were employed in [1] to mitigate signal fading. This is only possible if the selected diversity scheme ensures that the RSSI values from individual channels have minimal correlation among themselves, thereby minimizing the probability of simultaneous fading on all channels. Uncorrelated diversity

scheme channels result in identical but independent (i.i.d) signal distribution at each channel. Hence the resultant signal distribution resulting from a diversity scheme with *u* diversity channels is given by $X_{new} = g(X_1, X_2, \cdots, X_u)$. Where $g(\cdot)$ is the *diversity-combining* function, X_{new} is the resultant signal amplitude value, $X_i; i = \{1,2, \cdots, u\}$, is the signal amplitude value from i^{th} diversity channel. This section compares the three commonly used diversity combining schemes to reduce the R-factor and thus to improve localization accuracy in an RTLS setup. Since commercial receivers only provide the signal power (RSSI) without the phase information, the combination methods that are explored in this paper are non-coherent combinations i.e. the non-phase aligned RSSI values from the diversity channels are combined to generate the resultant RSSI value that is used for radial distance estimation to the transmitter.

Definition 2: (*Selection Combining*)**:** The channel with the highest signal amplitude value is selected as the X_{new} under selection combining or SC. Hence $X_{new} = \max(X_1, X_2, \cdots, X_u)$. The PDF of X_{new} can be derived from CDF and the i.i.d relation between the random variables as

$$f_{X_{new}}(x) = \frac{d}{dx}[F_X(x)]^u = u[F_X(x)]^{u-1} f_X(x). \tag{29}$$

where *x* is a possible value of X_{new}, $F_X(x)$ is the CDF and $f_X(x)$ is the PDF of the signal amplitude distribution of a channel in the diversity scheme.

Definition 3: **(***Averaging*) The resultant signal amplitude, X_{new}, is the average of the signal amplitudes from each channel in the diversity scheme $X_{new} = \frac{1}{u}\sum_{i=1}^{u} X_i$. The variance of X_{new} is given by

$$Var(X_{new}) = Var\left(\frac{1}{u}\sum_{i=1}^{u} X_i\right) = \frac{1}{u^2} Var(\sum_{i=1}^{u} X_i). \tag{30}$$

Definition 4: (*Root Mean Square*) The final signal amplitude value is the root mean square (RMS) of the amplitude values from each channel in the diversity scheme $X_{new} = \sqrt{\frac{1}{u}\sum_{i=1}^{u} X_i^2}$. The variance of X_{new} is given by

$$Var(X_{new}) = Var\left(\sqrt{\frac{1}{u}\sum_{i=1}^{u} X_i^2}\right) = \frac{1}{u} Var\left(\sqrt{\sum_{i=1}^{u} X_i^2}\right). \quad (31)$$

Since diversity receivers use the resultant combined RSSI value represented by X_{new} for estimating the radial distance to the transmitter, the MSE of radial distance estimate depends on $Var(X_{new})$ as the R-factor for this channel diversity receiver with u channels represented by $\gamma(u)$ can be written in terms of the signal variance $\sigma_{X_{new}}^2 = Var(X_{new})$ as

$$\gamma(u) = \frac{2l_0^{\frac{2}{n}}}{n^2}\frac{\sigma_{X_{new}}^2}{A^{\frac{4}{n}+2}} = \frac{2l_0^{\frac{2}{n}}}{n^2}\frac{\sigma_X^2}{A^{\frac{4}{n}+2}}\frac{\sigma_{X_{new}}^2}{\sigma_X^2} = \gamma\frac{Var(X_{new})}{\sigma_X^2}. \quad (32)$$

where $\gamma = \frac{2l_0^{\frac{2}{n}}}{n^2}\left(\frac{\sigma_X^2}{A^{\frac{4}{n}+2}}\right)$ is the R-factor given by (16).

Lemma 3: (*R-factor Variation with Diversity Channel Count in an LoS Environment*): In an RSSI based RTLS, the R-factor at a localization receiver with u diversity channels is greater than or equal to the R-factor obtained with $u+1$ diversity channels under diversity combination methods such as SC, Averaging, and RMS.

Proof: For a localization receiver, the modified zero order Bessel function of the first kind in (1) can be approximated as $I_0\left(\frac{Ax}{\sigma_X^2}\right) = \frac{\sigma_X}{\sqrt{2\pi Ax}} exp\left(\frac{Ax}{\sigma_X^2}\right)$ [17 p.377, §9.7.1]. This results in PDF of X at a localization receiver as $f_X(x|A,\sigma_X) = \sqrt{\frac{x}{A}}\frac{1}{\sqrt{2\pi}\,\sigma_X}\exp\left[-\frac{(x-A)^2}{2\sigma_X^2}\right]$. Since the signal amplitude random variable (X) is close to the mean (A) under LoS conditions, $\frac{x}{A} \approx 1$. Therefore the PDF of X can be approximated as $f_X(x|A,\sigma_X) =$

$\frac{1}{\sqrt{2\pi}\,\sigma_X}\exp\left[-\frac{(x-A)^2}{2\sigma_X^2}\right]$. Hence for a localization receiver, X is a Gaussian distributed random variable with mean A and variance σ_X^2.

The signal amplitude estimation error in diversity channel i for a localization receiver is given by $S_i = \Delta X_i = X_i - A$, where A is the mean of X_i. Since X_i has Gaussian distribution, S_i is also a Gaussian distributed random variable. The resultant signal estimation error due to diversity combination is given by $S_{new} = g(S_1, S_2, \cdots, S_u)$. Since $\sigma_{S_i}^2 = Var(S_i) = Var(X_i - A) - Var(X_i) = \sigma_{X_i}^2$, the R-factor (32) becomes

$$\gamma(u) = \gamma\frac{Var(X_{new})}{\sigma_X^2} = \gamma\frac{Var(S_{new})}{\sigma_S^2}. \tag{33}$$

The R-factor computation for SC, averaging and RMS diversity-combination functions is derived as shown below:

Selection Combining: Using this method, the resultant signal estimation error is given as

$$\begin{aligned} X_{new} &= \max(X_1, X_2, \cdots, X_u) = \max(S_1 + A, S_2 + A, \cdots, S_u + A) \\ &= \max(S_1, S_2, \cdots, S_u) + A \Rightarrow X_{new} - A = \max(S_1, S_2, \cdots, S_u). \end{aligned} \tag{34}$$

The PDF of the resultant signal estimation error can be derived from (29) along with the CDF and PDF of Gaussian distribution with zero mean as $f_{S_{new}}(s) = \frac{u\sqrt{2}}{2^u\sqrt{\pi}}\left[erfc\left(-\frac{s}{\sigma_X\sqrt{2}}\right)\right]^{u-1}\exp\left(-\frac{s^2}{2\sigma_X^2}\right)$ where *erfc* is the complimentary error function [17, p.297] and s is a possible value of S_{new}. To compute the R-factor for the receiver with the above signal strength distribution, the variance for this PDF must also be computed; however, a closed form equation for the variance does not exist. A numerical solution was therefore used to find the R-factor and plot the variation of R-factor with u for this receiver. Figure 1 displays the R-factor for this localization receiver against u diversity

channels combined using SC. The figure indicates that as the diversity channel count u increases, the R-factor drops rapidly, thus improving localization accuracy.

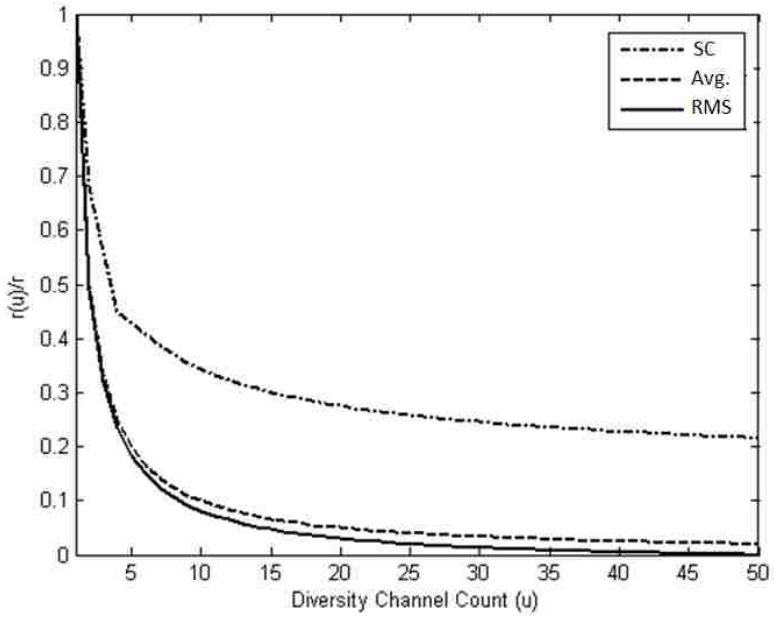

Fig 1. R-factor of a localization receiver's diversity combination using SC, Avg. & RMS

Averaging: The addition of u independent Gaussian distribution random variables with variance σ_S^2 result in a Gaussian distributed random variable whose variance equal to $u\sigma_S^2$ [21]. Therefore using (35), variance of S_{new} can be written as

$$Var(S_{new}) = \frac{1}{u^2} Var(\sum_{i=1}^{u} S_i) = \frac{\sigma_S^2}{u}. \quad (35)$$

The R-factor (33) for a localization receiver when diversity channels are combined using averaging becomes $\gamma(u) = \frac{\gamma}{u}$. Figure 1 shows the variation of R-factor with u for a localization receiver with diversity whose signals are combined using

averaging. These data indicate that R-factor decreases with diversity channel count when individual channels are combined using averaging for a localization receiver.

Root Mean Square: If u independent standard Gaussian distributed random variables are combined using RMS, this results in Chi-distribution with u degrees of freedom [21]. The variance for the resultant signal estimation error S_{new} can be derived from equation (31) and Chi-distribution variance as

$$Var(S_{new}) = \frac{1}{u} Var\left(\sqrt{\sum_{i=1}^{u} S_i^2}\right) = \left\{1 - \frac{2}{u}\left[\frac{\Gamma\left(\frac{u}{2}+\frac{1}{2}\right)}{\Gamma\left(\frac{u}{2}\right)}\right]^2\right\}\sigma_S^2. \quad (36)$$

where $\Gamma(.)$ is the Gamma function. Substituting (36) in R-factor (33) renders the R-factor for a Localization Receiver having u diversity channels combined using RMS as $\gamma(u) = \gamma\left\{1 - \frac{2}{u}\left[\frac{\Gamma\left(\frac{u}{2}+\frac{1}{2}\right)}{\Gamma\left(\frac{u}{2}\right)}\right]^2\right\}$. Figure 1 illustrates that under RMS, the R-factor is lower with diversity channels.

A comparison of the R-factor plots in Figure 1 clearly indicates that RMS has the lowest R-factor for a given value of diversity count u, and consequently renders the best location accuracy. Additionally, for all three combination methods, the R-factor value for a localization receiver with u diversity channels is greater than that of a localization receiver with $u+1$ diversity channels. Consequently, the localization error decreases with diversity channels. ■

Lemma 4: (*R-factor Variation with Diversity Channel Count in an NLoS Environment*) For a receiver-transmitter pair under NLoS conditions, the R-factor for a receiver with diversity channels is lower than without diversity when these channels are combined using RMS, averaging, or SC.

Proof: For a receiver under NLoS conditions (*A=0*), the PDF (1) can be written as $f_X(x|\sigma_X) = \frac{x}{\sigma_X^2}\exp\left(-\frac{x^2}{2\sigma_X^2}\right)$. Hence X is Rayleigh distributed under NLoS conditions. When Rayleigh distribution signal amplitude values from multiple diversity channels are combined using SC, averaging and RMS, the R-factor variation with diversity channel count must be analyzed for localization accuracy.

Selection Combining: The PDF of the resultant signal strength X_{new} can be derived by applying PDF and the CDF of Rayleigh distribution in (29) which gives

$$f_{X_{new}}(x) = \frac{ux}{\sigma_X^2}\left[1 - \exp\left(-\frac{x^2}{2\sigma_X^2}\right)\right]^{u-1}\exp\left(-\frac{x^2}{2\sigma_X^2}\right). \quad (37)$$

Since a closed form solution of the R-factor for (37) does not exist, numerical solution will be used to find the R-factor and plot the variation of R-factor with *u* for this receiver, as shown in figure 2. R-factor is reduced with diversity channel count *u* when channels are combined using SC under NLoS conditions.

Averaging: The variance of the sum of *u* Rayleigh distribution can be computed using Moment Generating Function (MGF) [18, p.78]. Let $Y = \sum_{i=1}^{u} Rayleigh(\sigma_X)$. The MGF of *Y* can be calculated as $M_Y(t) = E\{\exp[t\sum_{i=1}^{u} Rayleigh(\sigma_X)]\} = E\{\prod_{i=1}^{u}\exp[t \cdot$ *RayleighσX*. Since each diversity channel is assumed to be identical but independent, the expectation of the product of the random variables is equal to the product of the expectations. Therefore MGF is given as $M_Y(t) = \prod_{i=1}^{u} E\{\exp[t \cdot Rayleigh(\sigma_X)]\} = \left\{1 + \sqrt{\frac{\pi}{2}}\,\sigma_X t \exp\left(\frac{\sigma_X^2 t^2}{2}\right)\left[erfc\left(-\frac{\sigma_X t}{\sqrt{2}}\right)\right]\right\}^u$. The variance of Y can be computed from the first and second moment as

$$Var(Y) = \left(\frac{4-\pi}{2}\right)u\sigma_X^2. \quad (38)$$

Substituting (38) for *Var(Y)* in (30) gives variance of X_{new} as

$$Var(X_{new}) = \left(\frac{4-\pi}{2}\right)\sigma_X^2. \quad (39)$$

Applying (39) to (32) gives the R-factor for a receiver having u diversity channels combined using averaging under NLoS conditions with the transmitter as $\gamma(u) = \gamma\left(\frac{4-\pi}{2u}\right)$. Figure 2 illustrates the R-factor with diversity channel count u when individual channels are combined using averaging under NLoS conditions. Clearly, the R-factor, and hence the localization error, decreased as the diversity scheme was introduced.

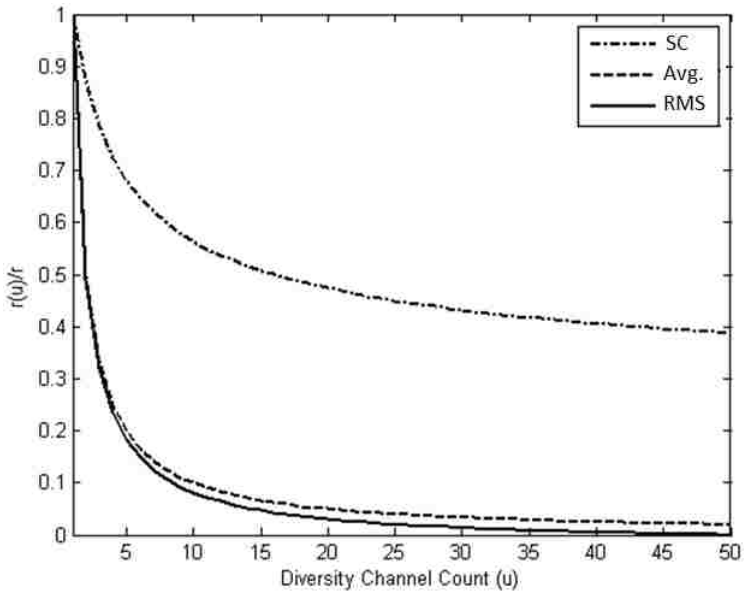

Fig 2. R-factor plot of diversity combination for a receiver under NLoS condition using SC, Avg. & RMS

Root Mean Square: For a Rayleigh distributed random variable X the PDF of the square operation ($G=X^2$, $X > 0$) can be found as

$$f_G(g) = f\left(\sqrt{G}\right)\frac{dX}{dG} = \frac{1}{\sigma_X^2}\exp\left(-\frac{g}{\sigma_X^2}\right) \quad (40)$$

where g is a possible value of G. Hence $X^2 \sim Exp(\sigma_X^2)$ is an exponential distribution with mean σ_X^2. The PDF of X_{new}^2, which is the sum of u exponential distributions, can be found using MGF. Let $Y = \sum_{i=1}^{u} X_I^2 = \sum_{i=1}^{u} Exp(\sigma_X^2)$. The MGF of Y can be calculated as $M_Y(t) = E\{\exp[t \sum_{i=1}^{u} Exp(\sigma_X^2)]\} = E\{\prod_{i=1}^{u} \exp[t \cdot Exp(\sigma_X^2)]\}$. Since the signal strength value from each diversity channel is independent, the independence criterion i.e., the expectation of the product of random variables is equal to the product of the expectations is applied resulting in $M_Y(t) = E\{\prod_{i=1}^{u} \exp[t \cdot Exp(\sigma_X^2)]\} = (1 + \sigma_X^2 t)^{-u}$. Hence the PDF of Y is a Gamma distribution given as $Y = X_{new}^2 \sim Gamma(u, \sigma_X^2)$. Finally, to get the RMS value, the square root is applied to Y resulting in Nakagami distribution [22]. The variance of X_{new} can be derived from the variance of Nakagami distribution and (31) as

$$Var(X_{new}) = \sigma_X^2 \left\{1 - \frac{1}{u}\left[\frac{\Gamma\left(u+\frac{1}{2}\right)}{\Gamma(u)}\right]\right\}. \tag{41}$$

Applying (41) on the R-factor (32) renders the R-factor for receiver with u diversity channels combined using RMS under NLoS conditions as $\gamma(u) = \gamma\left\{1 - \frac{1}{u}\left[\frac{\Gamma\left(u+\frac{1}{2}\right)}{\Gamma(2)}\right]^2\right\}$. Figure 2 shows R-Factor against diversity count u for a receiver under NLoS conditions where diversity channels are combined using RMS. As shown in Figure 2, the R-factor decreased as diversity count u is increased. One can conclude, therefore, that combining $u+1$ diversity channels using the RMS method at a receiver results in greater localization accuracy than that of a receiver where u diversity channels were combined using RMS. Comparison of the R-factor plots shows that RMS and SC schemes reduce the R-factor thereby improving accuracy. ■

Theorem 4*: (Improved Localization Accuracy with RMS Diversity Combination)* Localization accuracy of an RSSI based RTLS solution with *u* diversity channels that are combined using RMS is better than a receiver whose diversity channels are combined using averaging or SC.

Proof: From Lemma 1 and Lemma 2 it follows that the R-factor decreases with the RMS. Additionally, Figures 1 and 2 show that for a given value of diversity count *u*, the R-factor for RMS is the lowest of the three combination methods. Since R-factor is a measure of the localization error introduced by a receiver, a lower R-factor for a receiver results in better estimation of radial distance between the transmitter and the receiver, thus resulting in improved localization accuracy. ■

Remark 6 The localization error using RMS exceeding ψ can be computed by substituting R-factor $\gamma(u) = \gamma\left\{1 - \frac{1}{u}\left[\frac{\Gamma\left(u+\frac{1}{2}\right)}{\Gamma(u)}\right]^2\right\}$ into (27). Thus the accuracy can be adjusted by *w* and diversity channel count (u).

5. RESULTS AND ANALYSIS

In this section, experimental results are used to verify the theoretical contribution from previous sections.

5.1 RADIAL DISTANCE ESTIMATION ERROR WITH DISTANCE

To test the relationship between the actual radial distance and the estimation error, a transmitter-receiver pair was placed in a large indoor open environment. Since there were no immediate walls or other medium to reflect the RF waves, a uniform distribution of NLoS energy over the test environment was ensured. The radial distance between the transmitter and the receiver was varied from 1m to 5m and the RMS error of the estimated radial distance was computed for every 25cm. Figure 3 shows the plot of RMS

error of radial distance estimation against its actual value indicating that the radial estimation error increased approximately as the 2.25^{th} power of the actual distance.

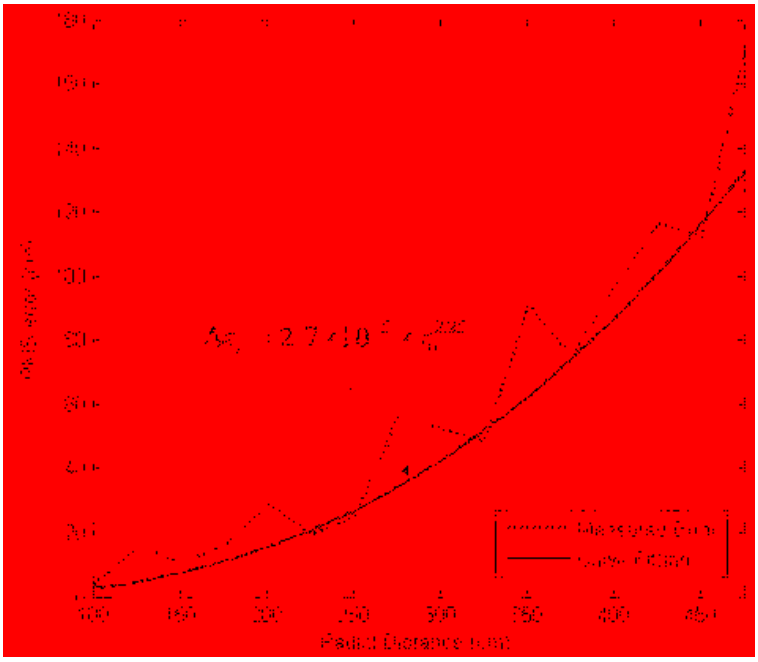

Fig 3. Estimation RMS error variation with actual radial distance

5.2 USING R-FACTOR TO DETECT NLOS

To verify Remark 4 that the R-Factor can be used to measure NLoS energy at a known radial distance between a transmitter and receiver, six wireless receivers (A, B, C, D, E and F) were placed at the circumference of a circle of radius 6 m as shown in Figure 4.1. The transmitter was held by a human operator who stood at the center of the circle. The operator initiated the RSSI measurements after orienting the transmitter at a certain angle θ with respect to the receiver F. The NLoS conditions were created by the human operator's body, which blocked the LoS to receivers behind him/her. The high operating

frequency of 2.45 GHz coupled with the short distance between the human operator's body and the transmitter ensured that the Fresnel radius at the operator's location was smaller than the operator's body.

The RSSI values which were collected every three seconds from all the receivers, for a total duration of five minutes, was computed and plotted in polar coordinates for various human orientations with respect to the receiver F, as shown in Figure 4.2. This figure indicates that the R-Factor peaked at receivers blocked by the operator's body indicating the ability of R-factor to identify NLoS conditions.

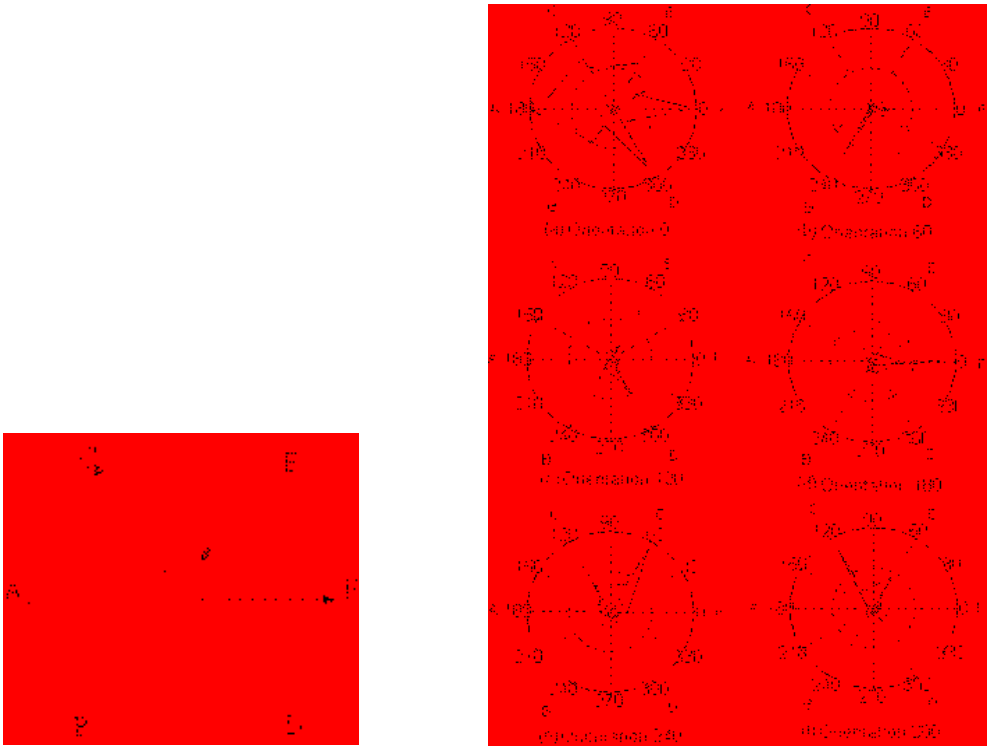

(1) Wireless receivers arranged in a circle around the transmitter

(2) Plot of R-factor for receivers placed at the circumference of a circle with the transmitter at the center

Fig 4. Variation of R-Factor at various angles

5.3 LOCALIZATION EXPERIMENTS

First, the RTLS test-bed is addressed before introducing the PSS/TIX localization algorithm [23].

5.3.1 TEST-BED AND IMPLEMENTATION All experiments were conducted using G4-SSN motes developed at Missouri University of Science and Technology (MST). G4-SSN motes use IEEE 802.15.4 wireless XBee transceivers from Maxstream. The MST RTLS receiver with spatial diversity is shown in Figure 5.

Fig 5. MST RTLS system

The receiver contains two independent wireless motes connected to quarter wave antennas. Each mote independently measured the RSSI on its antenna. To ensure identical but independent fading envelop PDF on the two antennas, they were spaced 25 cm (2λ) apart [1]. Each mote independently measured the RSSI on its antenna. The collected RSSI values were then sent wirelessly to a desktop machine acting as the RTLS

coordinator. The coordinator computed the R-factor for the receivers and then selected three receivers with lowest R-factor, which were then passed to the PSS/TIX algorithm to obtain the location of the transmitter.

The transmitter shown in Figure 5 is also a G4-SSN mote with a single quarter wave antenna. To prevent the receivers RSSI measurement circuitry from saturating when the received signal's RSSI value was greater than -40dBm, the maximum transmit power was set at 0dBm. The test-bed shown in Figure 6 spans 13m by 12m and covers the entire floor of LAB 114 on the Engineering Research Laboratory (ERL) building at MST. The target area was a typical lab environment filled with electronic equipment, chairs, tables, etc. A total of eight receivers marked R1 to R8 were placed on the target area as show in Figure 4. The positions of the receivers were selected to result in at least three localization receivers so that trilateration can be done.

5.3.2 LOCATION DETERMINATION ALGORITHM The PSS/TIX algorithm developed by Gwon and Jain [23] was used to locate the position of the transmitter. This algorithm uses a heuristic method called Proximity in Signal Space (PSS) to generate an RSSI versus distance mapping curve. The RSSI values measured by a wireless receiver are then translated to radial distances based on this table lookup. The radial distances to the transmitter are measured by multiple receivers and then passed to a modified version of triangulation called Triangular Interpolation and eXtrapolation (TIX). The Gwon and Jain version of the TIX algorithm selects the three receivers with the highest RSSI and uses their radial distance to the transmitter to compute the *x-y* coordinates.

5.3.3 LOCALIZATION RESULTS AND ANALYSIS To measure the advantage of using R-factor, three localization experiments were performed. In the first experiment,

the PSS/TIX by Gwon and Jain [23] was replicated. In this experiment, the three receivers needed for TIX were selected by the coordinator based on highest RSSI values. In the second experiment, the coordinator computed R-factor for each receiver and the three receivers with lowest R-factor were selected. TIX algorithm was then applied to locate the transmitter. The final experiment combined the spatial diversity, the R-Factor, and the TIX algorithm. The RSSI values of spatially diverse antennas were combined using RMS, and the R-Factor was computed for the combined RSSI. Once again, the three receivers for the TIX algorithm were selected based on the lowest R-Factor values.

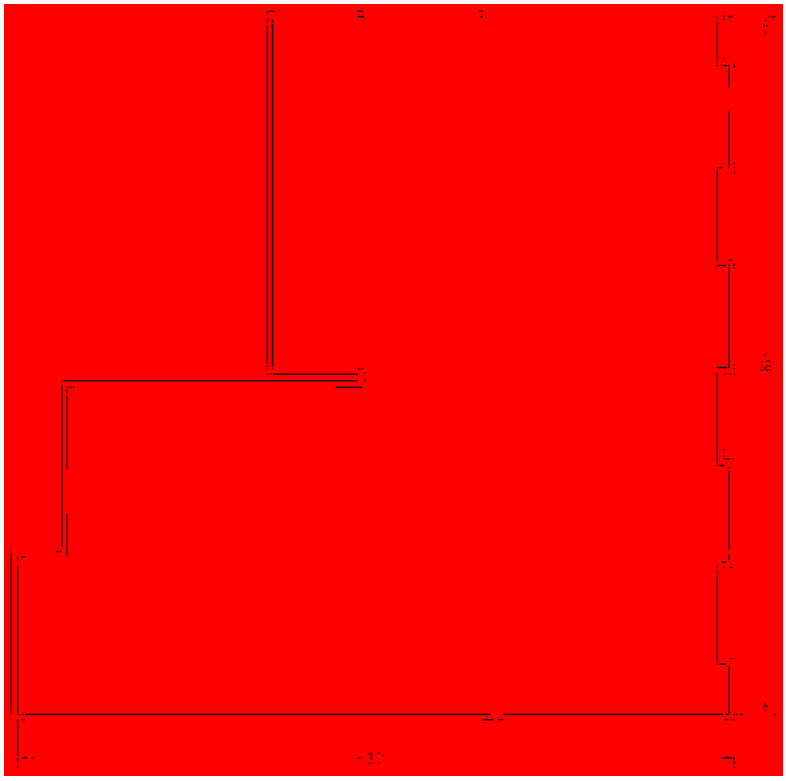

Fig 6. Floor Plan of ERL 114 with receivers numbered R1 to R8 marked with circles

Figure 7 was created from the CDF of the localization error values from eight locations on the target area. For each location, 50 localization measurements were collected, giving a total 400 localization error values to create the CDF plot.

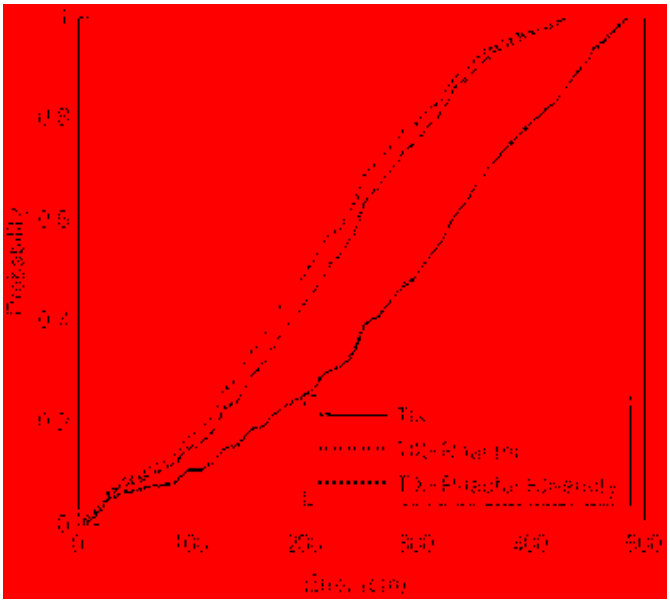

Fig 7. CDF of localization error

Table 1 presents the mean, the median, 90th percentile, and the standard deviation of the localization error. The mean error improved by 22%, the median error by 28%, and the 90th percentile by 22% from the PSS/TIX to the PSS/TIX with R-factor. Adding spatial diversity to the R-Factor improved the mean error by 27%, the median error by 32% and 90th percentile by 25% from the PSS/TIX. The standard deviation of the localization error decreased by 37%, when R-factor and spatial diversity was applied, to the PSS/TIX scheme which appears to the close to the theoretically predicted (55) reduction of 43% for $u=2$. Although PSS/TIX scheme is employed as an illustration,

other schemes can be deployed as well. Therefore proposed R-Factor improved the accuracy of the PSS/TIX localization scheme by selecting LoS receivers.

TABLE 1. SUMMARY OF LOCALIZATION ERROR LEVELS

Localization Method	**Localization Error (cm)**			
	Mean	***Median***	***90^{th} percentile***	***Std. dev***
PSS/TIX	342	298	432	62.81
PSS/TIX with R-factor	267	214	335	40.32
PSS/TIX with R-factor and Diversity	249	203	322	39.45

6. CONCLUSIONS

This paper presents a novel parameter called the R-Factor, and demonstrates its ability to identify receivers that exhibit low localization errors. It was shown that with an increase in localization receivers that fall under a given R-factor threshold, localization error can be improved. Additionally, diversity channels combined using RMS method was shown theoretically and experimentally to improve localization accuracy in an RSSI based RTLS. Experimental results demonstrate than an average 22% improvement in the mean localization accuracy when the R-factor was used in existing RTLS algorithms and 27% when diversity scheme with RMS was applied. Similarly, existing localization schemes that use time, angle or RSSI for positioning can therefore take advantage of the R-Factor to improve localization accuracy.

REFERENCES

[1] A. Ramachandran, and S. Jagannathan, “Spatial diversity in signal strength based WLAN location determination systems,” *Proc. of the 32nd IEEE Conf. on Local Comp. Networks*, pp. 10-17, Oct. 2007.

[2] N. B. Priyantha, A. Chakraborty, and H. Balakrishnan, “The Cricket location-support system,” *Proc. of ACM MOBICOM*, pp. 32-43, August 2000.

[3] M. Youssef, and A. Agrawala, “The Horus WLAN location determination system,” *Proc. of the 3rd inter. Conf. on Mobile Systems, Applications, and Service, MobiSys '05*. ACM Press, NY, pp. 205-218.

[4] D. Madigan, E. Elnahrawy, R. Martin, W. Ju, P. Krishnan, and A. Krishnakumar, “Bayesian indoor positioning systems,” *Proc. of the 24th IEEE Int. Conf. on Comp. Commun.*, pp. 324–331, March 2005.

[5] K. Pahlavan, X. Li, and J. P. Makela, “Indoor geolocation science and technology,” *IEEE Communications Magazine*, vol. 40, no. 2, pp. 112–118, 2002.

[6] S. Krishnakumar and P. Krishnan, “On the accuracy of signal strength-based location estimation techniques,” *Proc. of IEEE INFOCOM*, vol 1, pp. 642-650, 2005.

[7] E. Elnahrawy, X. Li, and R. P. Martin, “The limits of localization using signal strength: A comparative study,” *Proc. of the First IEEE Inte. Conf. on Sensor and Ad hoc Comm. and Networks*, pp. , 406-414, October, 2004.

[8] A. Lakhzouri, E. S. Lohan, R. Hamila, and M. Renfors, “Extended kalman filter channel estimation for line-of-sight detection in WCDMA mobile positioning,” *EURASIP Journal on Applied Signal Processing*, vol. 2003, no. 13, pp. 1268-1278, 2003.

[9] S. Venkatraman and J. Caffery Jr., “Statistical approach to nonline-of-sight BS identification,” *Proc. of the 5th International Symp. on Wireless Personal Multimedia Comm.*, vol. 1, pp. 296–300, Hawaii, USA, October 2002.

[10] M. M. Weiner, Adaptive Antennas and Receivers, *CRC Press*, 2005.

[11] M. H. Hashim and S. Stavrou, “Dynamic impact characterization of vegetation movements on radiowave propagation in controlled environment,” *IEEE Ant. Wireless Propagat. Letters*, vol. 2, pp. 316–318, 2003.

[12] H. T. Friis “A note on a simple transmission formula,” *Proc. IRE*, vol. 34, pp. 254-256, May 1946.

[13] H. Hashemi, “The indoor radio propagation channel,” *Proc. IEEE*, vol. 81, pp. 943-968, July 1993.

[14] M. Carroll, T. A. Wysocki, “Fading characteristics for indoor wireless channels at 5GHz unlicensed bands,” *in Proc. SympoTIC’03*, Bratislava, Slovakia, pp. 102-105, Oct. 2003.

[15] H. Y. Herben, M.H.A.J. Smulders, P.F.M., “Indoor radio channel fading analysis via deterministic simulations at 60 GHz,” *Wireless International Symposium on Communication Systems (ISWCS)*, pp. 144-148, Sept. 2006

[16] M. Patzold, Mobile Fading Channels, *John Wiley and Sons, Inc.*, West Sussex, U.K., 2002.

[17] M. Abramowitz and I. Stegun, Handbook of Mathematical Functions, *Dover*, New York, 1968.

[18] L. Bain and M. Engelhardt, Intro. to Probability and Mathematical Statistics, *Duxburry Press*, Pacific Grove, CA (1991).

[19] D. Kundu, and A. Basu, Stat. Comp: Existing Methods and Recent Developments, *Alpha Science Int'l Ltd.*, 2004.

[20] L. J. Greenstein, D. G. Michelson, and V. Erceg, “Moment-method estimation of the Ricean K-factor,” *IEEE Commun. Lett.*, vol. 3, pp. 175–176, 1999.

[21] Dyer, D.D., “Estimation of the scale parameter of the Chi distribution based on sample quantiles,” *Technometrics 15*, pp. 489-496 (1973).

[22] D. I. Laurenson. “Indoor Radio Channel Propagation Modeling by Ray Tracing Techniques,” *PhD thesis*, University of Edinburgh, 1994.

[23] Y. Gwon and R. Jain, “Error characteristics and calibration-free techniques for wireless LAN-based location estimation,” *Proc. of ACM MobiWac*, pp. 2-9, October 2004.

II. RECEIVER PLACEMENT USING DELAUNAY REFINEMENT BASED TRIANGULATION IN AN RSS BASED LOCALIZATION[1]

M. R. Basheer and S. Jagannathan

Abstract— *In this paper, a sub-optimal solution to the placement problem is introduced such that for a given workspace and a predefined location error threshold, the objective is to identify a minimum number of receivers while taking into account wireless fading and receiver layout effects so that no matter where the transmitter is located in the workspace, the error in estimating the position of the transmitter is less than a user specified threshold. To achieve this overall goal, first, localization error for received signal strength (RSS)-based M-receiver system localizing a transmitter is estimated. Subsequently, this estimator error along with the 2D-tessellation techniques such as Delaunay refinement are used to position candidate receivers not only to minimize their number needed to meet the location error threshold but also to reduce the dilution of localization accuracy due to the layout of receivers.*

Rigorous mathematical analysis indicates that the receiver count generated by our Delaunay refinement-based sub-optimal solution using triangular tiles is indeed bounded from the optimal count by a constant which in turn depends upon the workspace layout. However, by smoothing the layout and removing sharp edges in the workspace boundary, receiver count can be reduced. Finally, the sub-optimal scheme is demonstrated by using simulations and experimental data. The net result is a scheme to identify the number and

[1] Research Supported in part by GAANN Program through the Department of Education and Intelligent Systems Center. Authors are with the Department of Electrical and Computer Engineering, Missouri University of Science and Technology (formerly University of Missouri-Rolla), 1870 Miner Circle, Rolla, MO 65409. Contact author Email: mrbxcf@mail.mst.edu.

placement of receivers needed to meet a predefined threshold for locating a transmitter in a workspace.

Keywords: Delaunay refinement, Constrained Weighted Least Squares, Received Signal Strength, Optimal placement, Multipath, Fading

◆

NOMENCLATURE

Symbol	Description
M	Number of receivers deployed on a workspace
N	Number of RSS samples that each receiver collects to compute the mean before using the mean to estimate the radial distance to the transmitter
a	Path loss exponent
b, c	Radial distance variance parameters
P_i	Radio signal strength measured by i^{th} receiver
P_0	Signal strength measured by a receiver when the transmitter is at unit radial distance from it
d_i	True radial distance between a transmitter and i^{th} receiver in the workspace
r_i	Radial distance estimate from P_i
R	The maximum radial distance between the receiver and transmitter at which the packet loss experienced by the receiver $\leq 1\%$
$\eta_t = \{x_t, y_t\}$	2D Cartesian coordinates of the transmitter
$\eta_i = \{x_i, y_i\}$	2D Cartesian coordinates of the receiver
G	Planar straight line graph representing the localization workspace
ϵ_u	Pre-specified localization error threshold
$\epsilon(\eta)$	Localization error at location $\eta \in G$
η_t^*	Estimate of transmitter location using CWLS
n_i	Radial distance estimation variance at i^{th} receiver
$\Psi = diag\{n_1, n_2, \cdots, n_i\}$	Diagonal matrix of radial distance estimate variances
ϵ_{max}	Maximum localization error over the entire workspace G
$q = \frac{\max(lfs_G)}{\min(lfs_G)}$	A factor that determines the smoothness of the layout of a localization workspace.
T	Planar straight line graph after triangulation
λ_1,λ_2 *and* λ_3	Eigenvalues of matrix $X^T \Psi^{-1} \mathrm{X}$
σ^2	Variance of the RSS values measured by a receiver

1. INTRODUCTION

Location information of an asset is a key requirement in a Network Enabled Manufacturing (NEM) environment. New advancements in the fields of microelectronics and miniaturization have resulted in cheap, energy efficient, commercial, off-the-shelf hardware that uses Received Signal Strength (RSS) as a means for locating and tracking objects in real-time on a factory floor. RSS based localization has the advantage that any existing wireless hardware can seamlessly add the localization feature with just a software upgrade. As a result, RSS based localization schemes are preferred on wireless sensor networks using IEEE 802.15.4 [1] and WiFi infrastructures using IEEE 802.11 [2].

Localization error under a Ricean fading environment was studied in [3] by using RTLS motes operating at 2.4 GHz. Under this scheme [3], each receiver computes a quality factor called the R-factor, which is proportional to the radial distance variance, from the received signal strength. By collating multiple radial distance estimates from the receivers based on their R-factor and selecting a subset of radial distance values that satisfy a preset R-factor threshold, the base station provides a robust estimate of the 2D Cartesian coordinates of the transmitter on the workspace.

However, R-factor calculation is valid only under a Ricean fading environment where receivers have Line of Sight (LoS) conditions with the transmitter. For a typical workspace such as a factory floor with walls, machinery and personnel movement LoS conditions cannot be guaranteed uniformly at all points without an effective receiver placement strategy. Further, receiver count has to be minimized to reduce the cost of deployment while meeting the location error threshold which is the main goal of this paper.

In [4], Delaunay triangulation is used for solving the sensor coverage problem wherein the objective is to cover every point within the target area by the sensing region of a sensor. However, to minimize the number of receivers required to cover the target area, overlapping of sensing area is penalized in this scheme. By contrast for localization of objects and to determine the number of receivers, overlap of sensing area is necessary. This indicates that work in [4] is not directly suitable for localization. Additionally, Delaunay triangulation cannot generate new receiver positions based on a quality metric such as localization error of the transmitter unless Delaunay refinement-based tessellation scheme [5] is applied to determine the number and placement of receivers.

In [6], optimal sensor placement and motion coordination for target tracking problem is addressed while assuming a) Gaussian errors for radial distance measurements and b) the radial distance variance is assumed to be independent of the actual distance between the transmitter and receiver which is a stringent assumption. By using Fisher information determinant of the transmitter location estimator as the cost function, a receiver placement solution that maximizes this cost function was proposed. However, Gaussian distribution of range measurement arises only under very high signal (LoS) to noise (Non-LoS) ratio which limits the adaptability of this method in real environment. Further, our experiments [3] have shown a strong relationship between radial distance variance to the actual distance between the transmitter and receiver which clearly shows that the applicability of this method [6] is limited.

On the other hand, in [7], a sub optimal count algorithm for placing cameras on a workspace to localize mobile robots was presented. Angle of orientation measurements from two cameras was used to estimate the Cartesian coordinates of the robot. However,

this method cannot ensure all points on the workspace to have localization error less than a user specified error threshold. By contrast, in [8], the nonlinear Euclidean distance between M receivers and the transmitter is first linearized and then the unknown position of the transmitter is solved using linear least squares estimation technique. Receiver locations are selected such that the condition number, which is the ratio of the maximum to the minimum eigenvalue, of certain receiver position matrix is minimized.

However, the linearizing method used in [8] results in M linear equations with dependent errors rendering biased position estimates. Consequently, the receiver positions computed by [8] will render a non-uniform error throughout the workspace while it fails to minimize the localization error. In contrast, the adaptive beacon placement methodology in [9] addresses the problem of placing additional receivers (beacons) using an empirical approach to further improve localization accuracy given an initial set of receiver placement. Since the entire target area is not searched, this method does not yield a uniform location error while this solution can only generate new receiver positions that improve upon an initial receiver layout which itself is a major issue.

To mitigate the weaknesses of the above methods [4, 6-9], this paper proposes a sub-optimal solution for receiver placement in a target area where the objective is to minimize the number of receivers needed in order to ensure that any point on the target area will have a uniform localization error below a pre-specified threshold while taking into account wireless fading noise. The proposed solution involves dividing or tessellating the workspace into independent triangular domains or tiles using Jonathan Shewchuk's [5] variant of Rupert's Delaunay Refinement algorithm [10] where localization estimation error is used as the quality metric in deciding the triangle

dimensions. The location receivers are then placed at the vertices of these triangular tiles in order to meet the user specified threshold on location error while minimizing the cost of deployment.

Receiver layout with M receivers shown in Figure 1 can be viewed geometrically as a single polygonal tile with M vertices called M-sided polygon with localization receivers placed at its vertices. However, depending upon the size and geometry of the workspace and the communicate range R of the wireless devices, a single M-sided polygon tile may not be able to provide localization coverage over the entire workspace while keeping the localization error below a pre-specified threshold. Hence the localization workspace has to be subdivided into several such polygonal tiles using a process called *tessellation*. Therefore the total receiver count needed to ensure that any point on the workspace will have a localization error below a pre-specified threshold depends not only on the number of tiles but also on the vertex count (M) for each tile used to tessellate the workspace. Consequently, an M-sided polygon with the lowest vertex count and spans the largest area while respecting the localization error threshold is preferred for this placement problem.

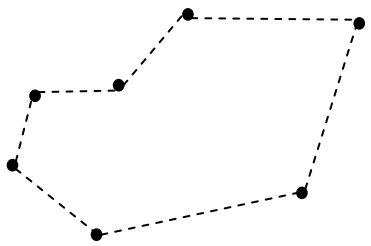

Fig 1. An $M = 7$ receiver layout arranged in the form of a polygon with receivers placed at its vertices

Therefore this paper begins by stating the receiver placement problem for an RSS-based RTLS with M receivers in section II. Section III (a) provides a brief background on the wireless propagation model used for this paper while section III (b) introduces the Constrained Weighted Least Squares (CWLS) method used for linearizing a non-linear least square problem. Subsequently, localization error is defined in section IV and the error in estimating the transmitter position with RSS values measured by M receivers deployed on a workspace is derived in Theorem 1. Section V defines the receiver layout quality metric as the maximum value of this localization error for all points within a workspace. It will be shown in Theorem 2 under section VI that for wireless receivers with a maximum communication range of R, arranging them in an equilateral triangular grid of side length R would result in the lowest number of receivers that are required to provide complete localization coverage. However, when receivers are constrained to be positioned within the workspace, arranging them in an equilateral triangular grid pattern near perimeter bounding walls may not be always feasible. Hence, section VII introduces a sub-optimal placement solution where the receivers are placed in equilateral triangular grids wherever possible except near boundary walls. However, in Theorem 3 of section VII, it will be shown that the number of receivers estimated by our solution is bounded by a constant from an optimal receiver count formed from an unconstrained equilateral triangular grid placement and this count can be adjusted through a design parameter. The net result is a receiver placement scheme that renders a suboptimal solution while meeting the pre-specified location error threshold while taking into account RSS noise arising due to fading, interference etc. In Section VIII, results and analysis of the

proposed approach is demonstrated in simulation and with hardware experiments. Subsequently, some concluding remarks are given.

2. PROBLEM STATEMENT

The placement problem considered in this paper is to find the number (M) and 2D Cartesian coordinates of wireless receivers $\eta_i; i \in \{1,2,\cdots,M\}$ within a localization workspace G that will result in the error in estimating the 2D Cartesian coordinates (η_t) of a wireless transmitter using RSS ranging through out the workspace to be less than a pre-specified threshold ϵ_u. i.e. $\epsilon_{max} = \max_{\eta \in G} \epsilon(\eta) \leq \epsilon_u$ where $\epsilon(\eta)$ is the localization error at location $\eta = \{x, y\} \in G$.

3. BACKGROUND

3.1 WIRELESS PROPAGATION MODEL

Radio signal power loss with increasing separation between the transmitter and receiver is a fundamental property of electromagnetic waves. Under far-field conditions between the transmitter and receivers Friis Transmisison Formula [11] is typically used as a large scale wireless propagation model that relates the measured radio signal power at a receiver to the radial distance to a transmitter. For an i^{th} receiver in a network of M receivers that is used for transmitter localization, the signal power P_i^* in dBm that this receiver should measure when the transmitter is radial separated by distance d_i is given by the Friis transmission formula as

$$P_i^* = P_0 - 10a \log_{10}(d_i)\,;\, i = 1,2,\ldots,M \qquad (1)$$

where P_0 is the signal power in dBm measured by receiver i when $d_i = 1$ unit and a is the path loss exponent. However, fading and other effects results in the measured signal strength having noise resulting in $P_i = P_i^* + e_i$ where P_i respresents the noisy measured

signal strength by the i^{th} receiver and e_i is the deviation of the measured signal strength in dBm from the log-linear relationship given by (1). For large scale propagation model, e_i is assumed to be log-normally distributed with zero mean and variance given by σ^2 [12].

If r_i represents the random variable corresponding to the estimated radial distance from the measured signal strength P_i then

$$r_i = 10^{-\frac{(P_i - P_0)}{10a}} \cong d_i\left(1 - e_i \frac{\ln 10}{10a}\right) \tag{2}$$

Applying the variance operator on (2) gives the variance of the radial distance estimate as

$$n_i \triangleq \mathrm{Var}(r_i) = d_i^2 \left(\frac{\ln 10}{10a}\right)^2 \mathrm{Var}(e_i) = c d_i^b \sigma^2 \tag{3}$$

where $\mathrm{Var}(\cdot)$ is the variance operator, $b = 2$, $c = \left(\frac{\ln 10}{10a}\right)^2$ and $\sigma^2 = \mathrm{Var}(e_i)$. Authors in [3] have derived the values for parameters b and c for non-Gaussian noise models for signal amplitude such as Ricean and Rayleigh.

The variance in radial distance (n_i) estimate at each receiver given by (3) can be reduced by averaging the measured RSS samples before using (2) to estimate r_i. This reduction in radial distance variance with RSS averaging at a receiver arises from central limit theorem [13] which states that if a receiver measures N RSS samples from a transmitter, represented by the set $P_i = \{P_{i1}, P_{i2}, \cdots, P_{iN}\}$, the sample average given by $\overline{P_i} = \frac{1}{N}\sum_{j=1}^{N} P_{ij}$ approaches in distribution to a normal distribution with mean given by P_i^* and signal strength variance given by $\mathrm{Var}(e_i) = \frac{\sigma^2}{N}$.

Now we will present the localization method that is used for estimating the 2D Cartesian coordinate of a transmitter.

3.2 CONSTRAINED WEIGHTED LEAST SQUARES

The problem of estimating the Cartesian coordinates of a transmitter from a series of radial distance estimates to it made by receivers deployed on a workspace may be expressed as a non-linear least squares problem as shown below.

If $\eta_t = \{x_t, y_t\}^T$ is the position of the transmitter that is to be estimated from RSS measurements made by M receivers within a workspace then from Euclidean distance equation for 2D space, the actual radial distance d_i between a common transmitter and an i^{th} receiver in this M receiver localization network is given by $d_i^2 = (x_t - x_i)^2 + (y_t - y_i)^2$ which may be rearranged as

$$x_t x_i + y_t y_i - \frac{(x_t^2 + y_t^2)}{2} = \frac{(x_i^2 + y_i^2 - d_i^2)}{2} \quad (4)$$

where $\eta_i = \{x_i, y_i\}^T$ is the Cartesian coordinate of the i^{th} receiver in this M receiver wireless network. If η_t is to be estimated from radial distance estimates obtained using (2), the non-linear term $(x_t^2 + y_t^2)$ in (4) will render the mean square error cost function used in least squares to be non-convex resulting in multiple local solutions for η_t. Therefore, to generate a convex cost function that renders a unique global solution for η_t, (3) has to be converted to a linear least squares problem. Constrained Weighted Least Squares (CWLS) is one such technique that will linearize a non-linear least square problem by introducing an intermediate parameter representing the non-linear parameters.

In (3) CWLS introduces an intermediate parameter R_s^2 that is related to the non-linear term in (4) as

$$\mathrm{R_s^2} = \mathrm{x_t^2} + \mathrm{y_t^2} \tag{5}$$

Therefore, the parameters to be estimated after CWLS linearization includes an intermediate variable resulting in $\eta_t^* = [x_t, y_t, R_s^2]^T$. Consequently the non-linear least squares problem of (4) can now be expressed in a linear least square formulation involving M linear equations in a matrix form as

$$\mathrm{X\eta_t^*} = \mathrm{Y} \tag{6}$$

where $X = \begin{bmatrix} x_1 & y_1 & -\frac{1}{2} \\ \vdots & \vdots & \vdots \\ x_N & y_N & -\frac{1}{2} \end{bmatrix}$, $Y = \frac{1}{2}\begin{bmatrix} x_1^2 + y_1^2 - r_1 \\ \vdots \\ x_N^2 + y_N^2 - r_N \end{bmatrix}$ and r_i is given by (2). Unlike the linearization method used in [8], CWLS has the advantage that the linearization technique does not result in measurement noise in (6) to be dependent resulting in biased estimates of η_t.

Now using (6) we will derive the transmitter location estimation error when CWLS is used to linearize (4).

4. LOCATION ESTIMATION ERROR

First the definition for a localization error in an RSS range based RTLS system is introduced before presenting a theorem on the localization error for an RSS-based RTLS system consisting of *N*-receivers.

Definition 1: (*Localization Error*) Given *M* line-of-sight (LoS) receivers that are deployed on a workspace *G* to estimate the position of a transmitter, the localization error in an RSS range based RTLS at location $\eta \in G$ is defined as the square root of the sum of the variances of estimated parameter and is given by

$$\epsilon(\eta) = \sqrt{T_r\big(Cov(\eta_t^*)\big)} \tag{6}$$

where $\eta_t^* = [x_t, y_t, R_s^2]^T$ is the estimated position of the transmitter and the intermediate variable given by (5) when the transmitter is at location $\eta \in G$, $Cov(\eta_t^*)$ is the covariance of the estimated parameters and $T_r(\cdot)$ is the trace operator on the covariance matrix. Since the trace of a square matrix is the sum of its eigenvalues [14], the square of the localization error $(\epsilon(\eta)^2)$ can be obtained as the sum of the eigenvalues of $Cov\ (\eta_t^*)$.

Now we are in a position to derive the localization error for an RSS range based RTLS.

Theorem 1 (*Localization Error for an RSS range based RTLS*): For an RTLS setup with M receivers placed at $[x_i, y_i]^T; i \in \{1,2, \dots, M\}$ in a workspace G, the localization error in estimating the position of the transmitter at $\eta \in G$ using CWLS is given by

$$\epsilon(\eta) = \sqrt{\frac{1}{\lambda_1} + \frac{\lambda_2}{(\lambda_2+\xi)^2} + \frac{\lambda_3}{(\lambda_3+\xi)^2}} \tag{8}$$

where $\epsilon(\eta)$ represents the localization estimation error at location $\eta \in G$, λ_1, λ_2 & $\lambda_3 \geq 0$ are the eigenvalues of the positive definite matrix $(X^T \Psi^{-1} X)$ with $X = \begin{bmatrix} x_1 - \bar{x} & y_1 - \bar{y} & -\frac{1}{2} \\ \vdots & \vdots & \vdots \\ x_M - \bar{x} & y_M - \bar{y} & -\frac{1}{2} \end{bmatrix}$, and $\bar{x} = \frac{\sum_{i=1}^{M} \frac{x_i}{n_i}}{\sum_{i=1}^{M} \frac{1}{n_i}}$, $\bar{y} = \frac{\sum_{i=1}^{M} \frac{y_i}{n_i}}{\sum_{i=1}^{M} \frac{1}{n_i}}$ are the variance centroid of the receiver layout where each receiver coordinate $(x_i, y_i); i \in \{1,2, \cdots, M\}$ is weighted by an estimate of the radial distance variance (n_i) given by (3), $\Psi = diag\{n_1, n_2, \dots, n_M\}$ is the diagonal radial distance variance matrix, and ξ is the Lagrange multiplier defined as the cost of having an η_t^* that deviates from the quadratic constraint (5)**.**

Proof: Let the transmitter be positioned at location $\eta \in G$ with η_t^* representing its estimate using linear least squares method on (6). The CWLS technique for linearization

poses the original non-linear problem as a constrained minimization problem of the following cost function $(X\eta - Y)^T\Psi^{-1}(X\eta - Y)$ subject to constraint $Q^T\eta + \eta^T S\eta = 0$ where $S = diag\{1,1,0\}$ and $Q = [0 \quad 0 \quad -1]^T$. The solution for this minimization problem is provided in [15] as

$$\eta_t^* = (X^T\Psi^{-1}X + \xi S)^{-1}\left(X^T\Psi^{-1}Y - \frac{\xi}{2}Q\right) \tag{9}$$

where ξ is the Lagrange multiplier that defines the cost of an R_s^2 estimate deviating from the quadratic equation (5). However, the unconstrained solution for the above cost function, represented as $\hat{\eta}_t$, is given by $\hat{\eta}_t = (X^T\Psi^{-1}\mathrm{X})^{-1}(X^T\Psi^{-1}Y)$ which is related to the constrained solution given by (9) as

$$\eta_t^* = Z\hat{\eta}_t - \frac{\xi}{2}H \tag{10}$$

where $Z = [I + \xi(X^T\Psi^{-1}X)^{-1}S]^{-1}$ and $H = \left[0 \quad 0 \quad -\frac{1}{t}\right]^T$.

From (10), the covariance of η_t^* may be expressed in terms of the covariance of $\hat{\eta}_t$ as $Cov(\eta_t^*) = ZCov(\hat{\eta}_t)Z^T$ and the square of the localization error from (7) for the CWLS estimate η_t^* is given by $\epsilon(\eta)^2 = Tr\left(Cov(\eta_t^*)\right) = Tr(ZCov(\hat{\eta}_t)Z^T)$. Lets define $W = (X^T\Psi^{-1}X + \xi S)^{-1}$ then $\epsilon(\eta)^2$ can be written in terms of W as

$$\epsilon(\eta)^2 = T_r[Z(X^T\Psi^{-1}X)^{-1}Z^T] = T_r[W(X^T\Psi^{-1}X)W^T]. \tag{11}$$

To derive (11) the trace of the matrix $W(X^T\Psi^{-1}X)W^T$ has to be computed which involves finding the eigenvalues of $W(X^T\Psi^{-1}X)W^T$. But first, we will derive the eigenvalues of $X^T\Psi^{-1}X$ and then use those values to derive the eigenvalues of $W(X^T\Psi^{-1}X)W^T$. Since $\sum_{i=1}^{M}\left(\frac{x_i - \bar{x}}{n_i}\right) = 0$ and $\sum_{i=1}^{M}\left(\frac{y_i - \bar{y}}{n_i}\right) = 0$ the matrix $X^T\Psi^{-1}X$ can be expressed in the following form

$$X^T\Psi^{-1}X = \begin{bmatrix} u & v & 0 \\ v & w & 0 \\ 0 & 0 & t \end{bmatrix} \tag{12}$$

where $u = \sum_{i=1}^{M} \frac{(x_i-\bar{x})^2}{n_i}$, $v = \sum_{i=1}^{M} \frac{(x_i-\bar{x})(y_i-\bar{y})}{n_i}$, $w = \sum_{i=1}^{M} \frac{(y_i-\bar{y})^2}{n_i}$, and $t = \frac{1}{4}\sum_{i=1}^{M} \frac{1}{n_i}$. In addition, the eigenvalue decomposition of $X^T\Psi^{-1}X$ has the form $X^T\Psi^{-1}X = V\Lambda V^T$ where V is the unitary eigenvector and Λ is the diagonal matrix given by $\Lambda = diag\{\lambda_1, \lambda_2, \lambda_3\}$ where $\lambda_1 = t$ and $\lambda_2, \lambda_3 = \frac{u+w\pm\sqrt{(u-w)^2+4v^2}}{2}$.

Now we will use λ_1, λ_2 and λ_3 to derive the eigenvalues of $W(X^T\Psi^{-1}X)W^T$ needed in (11). Since, $W = (X^T\Psi^{-1}X + \xi S)^{-1} = V(\Lambda + \xi S)^{-1}V^T$. Therefore, $W(X^T\Psi^{-1}X)W^T = V(\Lambda + \xi S)^{-1}V^TV\Lambda V^TV(\Lambda + \xi S)^{-1}V^T$ which can be written in eigenvalue decomposition form as $V(\Lambda + \xi S)^{-1}\Lambda(\Lambda + \xi S)^{-1}V^T = V\Omega V^T$ where $\Omega = diag\left\{\frac{1}{\lambda_1}, \frac{\lambda_2}{(\lambda_2+\xi)^2}, \frac{\lambda_3}{(\lambda_3+\xi)^2}\right\}$. Therefore, the eigenvalues of $W(X^T\Psi^{-1}X)W^T$ are $\frac{1}{\lambda_1}, \frac{\lambda_2}{(\lambda_2+\xi)^2}$ and $\frac{\lambda_3}{(\lambda_3+\xi)^2}$ resulting in localization error for an RSS based RTLS using CWLS as (8). ■

5. RECEIVER PLACEMENT QUALITY METRIC

The localization error for CWLS given by (8) can be explained by examining the individual terms $\frac{1}{\lambda_1}, \frac{\lambda_2}{(\lambda_2+\xi)^2}$ and $\frac{\lambda_3}{(\lambda_3+\xi)^2}$ in (8). For instance, the localization error term $\frac{1}{\lambda_1} = \frac{4}{\sum_{i=1}^{M}\frac{1}{n_i}}$ is the result of the radial distance estimation noise n_i caused by fading effects. This error can be reduced by special antenna designs or by increasing the number of RSS samples that are used for averaging at each receiver before estimating the radial distance using (2) whereas the terms $\frac{\lambda_2}{(\lambda_2+\xi)^2}$ and $\frac{\lambda_3}{(\lambda_3+\xi)^2}$ include not only the effects of radial distance estimation noise but also the geometry of the receiver layout. However the Lagrange multiplier term ξ is an artifact of our linearization of (4) using CWLS and its

value is dictated by the cost of violating the quadratic constraint (5) by the solution given by (9). When $\xi = 0$, i.e. the quadratic constraint (5) is not binding or in other words the least square cost function incur no additional cost in violating the quadratic constraint, the localization error would be the maximum and is given by

$$\epsilon_{max}(\eta) = \sqrt{\frac{1}{\lambda_1} + \frac{1}{\lambda_2} + \frac{1}{\lambda_3}} = 2\sqrt{\frac{1}{\sum_{i=1}^{M} \frac{1}{n_i}} + \frac{u+w}{uw-v^2}} \tag{13}$$

whereas when the quadratic constraint is not to be violated at under any situation then $\xi = \infty$, resulting in the localization error given by $\epsilon_{min}(\eta) = \sqrt{\frac{1}{\lambda_1}}$. The placement problem considered in this paper is to ensure that no matter where the transmitter is positioned within the workspace G, the localization error in this workspace is less than a pre-specified localization error threshold ϵ_u i.e. $\epsilon(\eta) < \epsilon_u; \forall \eta \in G$ or $\epsilon_{max}(\eta) < \epsilon_u; \forall \eta \in G$. Therefore, the metric that is of interest in this paper to evaluate the localization error under a particular receiver placement scenario is defined as

$$\epsilon_{max} \triangleq max_{\forall \eta \in G}\{\epsilon_{max}(\eta)\} \tag{14}$$

The above receiver placement quality metric is the worst case localization error of a transmitter in workspace G and can be reduced by decreasing the radial estimation variance n_i at each receiver or by adjusting the placement of receivers so as to reduce the term $\frac{u+w}{uw-v^2}$ in (13).

6. UNCONSTRAINED RECEIVER PLACEMENT GEOMETRY

We will now derive the optimal receiver placement pattern that will result in complete localization coverage. But first we will define localization coverage within the workspace.

Definition 2: (*Localization Coverage*) A location η within the workspace G is said to be under localization coverage if there are at least 3 receivers in communication range of a transmitter when it is placed at that position i.e. $\eta_t = \eta$.

$$C(\eta) \triangleq \sum_{i=1}^{M} I_{\{0,R\}}(\|\eta - \eta_i\|) \geq 3 \tag{15}$$

where $C(\eta)$ is the localization coverage of location $\eta \in G$, R is the maximum communication range of transmitter/receiver pair, $\eta_i; i \in \{1,2,\cdots,M\}$ are the location of the M receivers and $I_{\{0,R\}}(\|\eta - \eta_i\|) = \begin{cases} 1, & 0 \leq \|\eta - \eta_i\| \leq R \\ 0, & elsewhere \end{cases}$ is the indicator function.

Typically, wireless receivers define the communication range as the distance to the transmitter at which the input signal strength to a receiver falls below its receiver sensitivity [16]. However, this distance is not isotropic and varies depending on multitude of factors such as fading, interference etc. However, for this paper we define the communication range R as the maximum distance between the transmitter and receiver where the percentage packet loss experienced by the receiver is above a pre-specified threshold.

Definition 3: (*Neighbors of a receiver*) For a set of M receivers deployed in workspace G, a subset of receivers $\mathbb{N}_i$ is said to be the neighbors of a receiver i that is located at η_i if and only if $\|\eta_i - \eta_j\| \leq R$ where η_j is the location of receiver $j \in \mathbb{N}_i$.

Theorem 2: (*Equilateral Triangular Grid for Optimal Receiver Placement*) A receiver placement strategy whose objective is to span the largest area under localization coverage with least number of receiver while ensuring no coverage holes exists within the placement grid, will have all its receivers placed in an equilateral triangular grid.

Proof: Let $H_i = \{\eta_{i1}, \eta_{i2}, \cdots, \eta_{i\mathrm{K}}\}$ represents the position of K receivers that are the neighbors of a receiver i in this placement algorithm. Under the assumption that the

placement of a receiver is not restricted by the boundaries of a workspace, this placement algorithm will attempt to place receivers maximally separated from each other while maintaining complete localization coverage. If R represents the maximum communication range of the wireless receivers in this network, the maximum radial distance a receiver i can be separated from its immediate neighboring receiver without creating localization coverage holes is R i.e. $\|\eta_i - \eta_{il}\| = R; l \in \{1,2,\cdots,\mathrm{K}\}$.

Figure 2 shows the localization coverage formed around receiver i and its two neighboring receivers j and k that are separated by radial length R from i and spanning an interior angle θ. The total localization coverage region due to receivers i, j and k , represented as A_L depends on θ and for $0 < \theta \leq \frac{2\pi}{3}$ it is the region of overlap of three circles as in Figure 2.1 and 2.2 whereas for $\frac{2\pi}{3} < \theta \leq \pi$ A_L is the region of overlap of two circles as in Figure 2.3. The area of region A_L is given by

$$|A_L| = \begin{cases} [\pi - \theta - sin\,\theta]R^2 & ,\frac{2\pi}{3} < \theta \leq \pi \\ \left[\frac{4\pi}{3} - \sqrt{3} - \theta\right]\frac{R^2}{2} & ,0 < \theta \leq \frac{2\pi}{3}. \end{cases} \quad (16)$$

To span the entire communication range of receiver i under localization coverage, other neighbors of receiver i will be placed around it leading to overlap in localization coverage which is undesirable. However, the region that falls within a triangle defined by the edges connecting receivers i, j and k has the potential for being only covered by receivers i, j and k. Therefore, the localization coverage region A_L can be divided into two distinct regions depending on whether it falls within or outside this triangular region. Region A_O that overflows this triangular region could potentially overlap with the coverage provided by other receivers in workspace G whereas, region A_C is uniquely covered by i, j and k provided the area of overlapping is zero i.e. $|A_O| = 0$ in Figure 2.

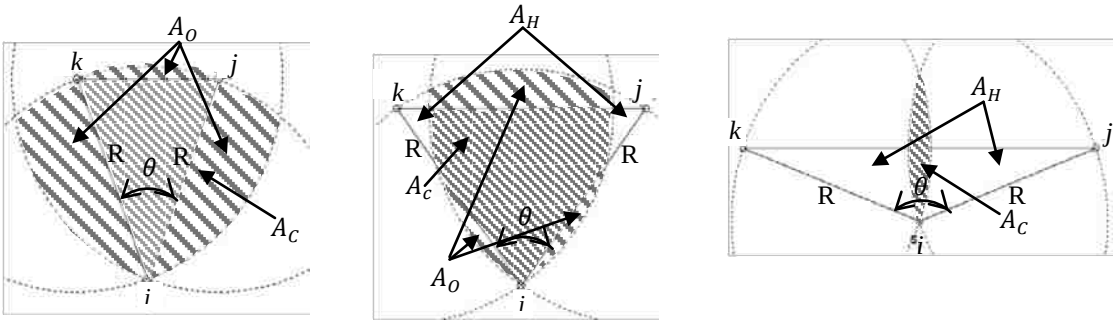

(1) $0 < \theta \leq \frac{\pi}{3}$ (2) $\frac{\pi}{3} < \theta \leq \frac{2\pi}{3}$ (3) $\frac{2\pi}{3} < \theta \leq \pi$

Fig 2. Location coverage at a receiver

From Figure 2.2 and 2.3, when $\theta > \frac{\pi}{3}$, the triangular region formed from i, j and k now includes a coverage hole represented by A_H. Therefore, to span the communication range of i under localization coverage without any coverage holes, the range of θ is restricted between $0 < \theta \leq \frac{\pi}{3}$. Consequently, to have the least number of receivers needed to span the communication range of i under localization coverage for $0 < \theta \leq \frac{\pi}{3}$ the area of triangular region ($|A_C|$) has to be maximized while the area of localization coverage overlapping region ($|A_O|$) has to be minimized. In other words the ratio $\frac{|A_C|}{|A_O|} = \frac{|A_C|}{|A_L|-|A_C|} = \frac{1}{\frac{|A_L|}{|A_C|}-1}$ has to be maximized or maximize the ratio $\frac{|A_C|}{|A_L|}$. For $0 < \theta \leq \frac{\pi}{3}$, $|A_C| = \frac{1}{2}R^2 \sin\theta$ and $|A_L| = \left[\frac{4\pi}{3} - \sqrt{3} - \theta\right]\frac{R^2}{2}$ resulting in $\frac{|A_C|}{|A_L|}$ given by

$$\frac{|A_C|}{|A_L|} = \frac{\sin\theta}{\frac{4\pi}{3}-\sqrt{3}-\theta}; 0 < \theta \leq \frac{\pi}{3} \quad (17)$$

which attains maximum when $\theta = 60$ degrees. ■

Therefore, when the receiver placement are not restricted by a bounding wall, an equilateral grid placement of receivers within a workspace where the receivers are

separated by the communication range R will result in complete localization coverage with least number of receivers. However, when receivers are restricted to be located within a bounding wall, equilateral triangular placement is not always possible. Now we will present a method that will attempt to place receivers in triangular grids that are close to equilateral triangles wherever possible except on regions that are close to bounding walls.

7. TESSELLATING THE WORKSPACE USING TRIANGLES

A typical 2D localization workspace G such as a room or a lab may be represented as a Planar Straight Line Graph (PSLG) which can be sub-divided into polygonal regions using a process called *tessellation*. For our optimal receiver count localization coverage, workspace will be tessellated into equilateral triangle of side length equal to the communication range R. However, tessellation of workspace into equilateral triangles may not be always possible due to perimeter walls of the workspace. Consequently, we will apply a sub-optimal placement algorithm that will place receivers in triangular grid that are as close to an equilateral triangular grid as possible constrained by the perimeter wall.

It has been mathematically proved that any workspace can be subdivided into non intersecting triangles for a 2D workspace [17]. A triangulation (tessellation of a region into triangles) T of a workspace G, represented as a PSLG, is called a valid localization receiver placement for G if, for all points within the convex hull of G, excluding holes, there exists a triangle such that the maximum localization error given by (14) is lower than the localization error threshold ϵ_u.

First, relevant computational geometry terms are defined before we proceed.

Definition 4: (*Delaunay Triangulation*) A triangulation *T* of a set *G* of points is defined as Delaunay triangulation (DT) if no points in *G* lies inside the circumcircle of any triangle in *T*.

This above property is called the *empty circumcircle* property of DT. Another important property of DT is that it maximizes the minimum angle among all possible triangulation of *G*. Hence the triangles generated by DT are as close to equilateral triangle as possible.

Definition 5 (*Constrained Delaunay Triangulation*): A triangulation *T* is a Constrained Delaunay Triangulation (CDT) of an input PSLG, *G*, if each edge of *G* is an edge in *T* and is close to DT as possible [18].

CDT is required for our receiver placement algorithm to ensure that the perimeter walls of our localization workspace are respected when generating the triangles in T. CDT achieves this by relaxing the empty circumcircle property of DT near the bounding walls of *G*.

Definition 6 (*Delaunay Refinement*): A triangulation *T* is defined as a Delaunay Refinement (DR) triangulation of an input PSLG, *G*, if the generated triangles are either CDT or DT and in addition satisfy a user specified quality metric [5].

Unlike DT and CDT, DR triangulation adds new vertices called *Steiner points.* Steiner points are added to ensure that the user quality metric, which in our case is the localization error given by (14) being less than the pre-specified error threshold ϵ_u, for each triangle in T, is satisfied. Steiner points are typically added at the circumcenter of a triangle.

Definition 7 (*Cardinality of Triangulation*): The cardinality of a triangulation T represented as $|T|$ is the number of vertices in this triangulation.

For DR the total number of vertices is the sum total of Steiner points and the vertices in the input PSLG. Since the receivers are placed at the vertices, $|T|$ equals the number of receivers in a placement algorithm.

Definition 8 (*Local Feature Size*): Given a PSLG, G, the local feature size at an arbitrary point v relative to G, denoted by $lfs_G(v)$ is the radius of the smallest disk centered at v that intersects two non-incident segments or vertices of G.

Figure 3.1 illustrates the local feature size for points A, B and C in the plane relative to the PSLG. The local feature size for point A is the radius of the circular disc centered at A and is bounded by two vertices. Local feature size for the point B is bounded by two non-intersecting segments while for point C is determined by vertices. Local feature size is a continuous function that varies uniformly over the workspace as shown in Figure 3.2 and is nowhere zero. In a DR triangulation, satisfying the quality metric while ensuring that the generated triangles are as close to the equilateral triangle for workspace with low local feature size will result in large number of receivers that are placed close to each other. This would be quite inefficient use of receivers for a placement algorithm.

Since receivers are placed at the vertices of the triangles in T, the *receiver placement methodology* that this paper proposes can be formulated as follows: Given an input workspace G, and a localization error threshold ϵ_u, the objective is to minimize the cost function defined in terms of cardinality as $J = |T|$ subject to the following constraint $\epsilon_{\max} \leq \epsilon_u$ where $\epsilon_{\max}$ is the localization error given by (14) for every triangle $t \in T$.

Delaunay refinement is the technique that our paper uses to search through the input workspace G in linear time to solve for receiver placements that result in minimizing the final receiver count ($|T|$).

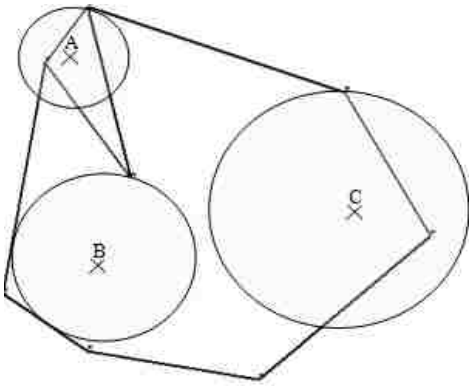

(1) LFS at A,B & C represented as radius of circular disc

(2) Continuous LFS plot of a PSLG with regions in dark having low LFS

Fig 3. Local feature size

In the following theorem it will be shown that the proposed methodology indeed results in sub-optimal receiver count.

Theorem 3 (*Upper Bound for Receiver Count*): For a given workspace *G*, and a localization error threshold (ϵ_u), the receiver count ($|T|$) generated using Delaunay refinement triangulation on *G* is suboptimal and is upper bounded by the receiver count $(|T_{opt}|)$ for an optimal triangulation of the above receiver placement problem as,

$$|T| < (1 + p)|T_{opt}| \tag{18}$$

where $p \propto \left[\frac{\max(lfs_G)}{\min(lfs_G)}\right]^2$ and $\min(lfs_G) = \min_{\forall \eta \in G}\left(lfs_G(\eta)\right)$ and $\max(lfs_G) = \max_{\forall \eta \in G}\left(lfs_G(\eta)\right)$ are the minimum and maximum local feature size respectively for all locations $\eta \in G$ before applying Delaunay refinement triangulation T.

Proof: Assume that the input workspace G had n vertices and assume that H additional vertices (Steiner points) had to be added due to Delaunay refinement triangulation on G to satisfy the localization error quality constraint, then the final receiver count which is equal to the number of vertices in the final triangulation T is given by the sum of newly added vertices (H) and the original vertices in G as $|T| = H + n$. However, as explained in [19], the local feature size integral, $\int_{\eta \in G} \frac{d\eta}{lfs_T^2(\eta)}$, where $lfs_T(\eta)$ represents the local feature size at location $\eta \in G$ after application of Delaunay refinement triangulation T on G, is at least a constant factor $\pi\left(\ln\frac{3}{2} - \frac{1}{3}\right)$ times the number of Steiner points, H, resulting in the following lower bound as

$$\int_{\eta \in G} \frac{d\eta}{lfs_T^2(\eta)} > \pi\left(ln\frac{3}{2} - \frac{1}{3}\right)(|T| - n) \tag{19}$$

From theorem 2, lowest receiver count occurs when all triangles in T are equilateral. However, depending on workspace geometry, tessellation with only equilateral triangles may not always be feasible. Nevertheless, an optimal triangulation T_{opt} on G will have angles that are very close to 60^0 (equilateral triangle). Let α be the minimum angle in T_{opt} then from [19], the local feature size integral over G, $\int_{\eta \in G} \frac{d\eta}{lfs_G^2(\eta)}$, where $lfs_G(\eta)$ represents the local feature size at location $\eta \in G$ before DR triangulation T, is at most a factor that is depended on α, $\left\{\frac{\mu}{\alpha} + \pi[1 - 4\ln(\cos\alpha)]\right\}$, times the total vertices in T_{opt} resulting in the following upper bound as

$$\int_{\eta \in G} \frac{d\eta}{lfs_G^2(\eta)} < \left\{\frac{\mu}{\alpha} + \pi[1 - 4\, ln(cos\, \alpha)]\right\} \left|T_{opt}\right| \tag{20}$$

where μ is a constant that depends on whether G has holes (permanent obstructions within the boundary of workspace) or not.

For any location $\eta \in G$, $lfs_G(\eta) \leq \max(lfs_G)$ and $lfs_T(\eta) \geq \min(lfs_T)$. Combining these inequalities result in

$$lfs_G(\eta) \leq \left\{\frac{max(lfs_G)}{min(lfs_T)}\right\} lfs_T(\eta); \forall \eta \in G \tag{21}$$

For a location $\eta \in G$, $lfs_T(\eta)$ is a measure of the largest possible size of a triangle (measured by the circumradius of the triangle) containing the location η [19]. Therefore, if $\min(lfs_T) < \min(lfs_G)$ then the triangulation T has created triangles that are smaller than that determined by the sharpest corner in the input PSLG G which is undesirable. Therefore our placement algorithm will ensure that $\min(lfs_T) \geq \min(lfs_G)$ resulting in (21) being re-written as

$$lfs_G(\eta) \leq q lfs_T(\eta); \forall \eta \in G \tag{22}$$

where $q = \frac{\max(lfs_G)}{\min(lfs_G)}$. Using (22) the feature size integral before and after triangulation T now satisfies the following inequality

$$q^2 \int_{\eta \in G} \frac{d\eta}{lfs_G^2(\eta)} \geq \int_{\eta \in G} \frac{d\eta}{lfs_T^2(\eta)} \tag{23}$$

From (19), (20) and (23) the following constraint

$$q^2 \left\{\frac{\mu}{\alpha} + \pi[1 - 4\, ln(cos\, \alpha)]\right\} \left|T_{opt}\right| > \pi \left(ln\frac{3}{2} - \frac{1}{3}\right) (|T| - n) \tag{24}$$

is derived. By rearranging the terms in (24), the final receiver count $(|T|)$ is upper bounded by the optimal receiver count $\left(\left|T_{opt}\right|\right)$ as

$$|T| < \left\{\frac{n}{|T_{opt}|} + q^2 \frac{\left\{\frac{\mu}{\alpha} + \pi[1 - 4\, ln(cos\, \alpha)]\right\}}{\pi\left(ln\frac{3}{2} - \frac{1}{3}\right)}\right\} \left|T_{opt}\right| \tag{25}$$

Since $\frac{n}{|T_{opt}|} \leq 1$ and setting $p = q^2 \frac{\left\{\frac{\mu}{\alpha}+\pi[1-4\ln(\cos\alpha)]\right\}}{\pi\left(\ln\frac{3}{2}-\frac{1}{3}\right)} \Rightarrow p \propto q^2 = \left\{\frac{\max(lfs_G)}{\min(lfs_G)}\right\}^2$ in (25) gives (18). ■

Remark 2: Receiver count generated using DR can be reduced by increasing the local feature size of workspace G which can be explained as follows: From Theorem 3, $p \propto \left\{\frac{\max(lfs_G)}{\min(lfs_G)}\right\}^2$ therefore, increasing $\min(lfs_G)$ will result in $\frac{\max(lfs_G)}{\min(lfs_G)} \to 1$. Hence a workspace G with uniform local feature size such as a regular polygon will result in lower localization receiver count. For workspace with small segments and sharp angles, the local feature size has low values and hence should be avoided or smoothed out. This may be accomplished during a preprocessing stage where the input PSLG, G, is passed through a local feature size enhancement phase that removes small angles and small segments from G. A segment in G is considered small if for the length of that segment, the fading noise is highly correlated (segment length less than a twice the wavelength [1]) or those that are smaller than ϵ_u.

8. RESULTS AND ANALYSIS

In this section, feasibility of the proposed receiver placement algorithm will be demonstrated to localize a transmitter on a workspace that spans 12m x 12m with a maximum localization error (ϵ_u) of 1m. Additionally, through simulations the effect of number of RSS samples that each receiver should collect compute the mean before applying (2) to estimate radial distance on RSS variance (σ^2) and localization error threshold (ϵ_u) will be analyzed. The indoor workspace used for this experiment is a typical laboratory space with moderate clutter from workbenches, desks and occasional human traffic.

8.1 RECEIVER PLACEMENT USING DELAUNAY REFINEMENT

The flowchart for the proposed receiver placement algorithm using Delaunay refinement is shown in Figure 4. Essentially, the method consists of the following five steps.

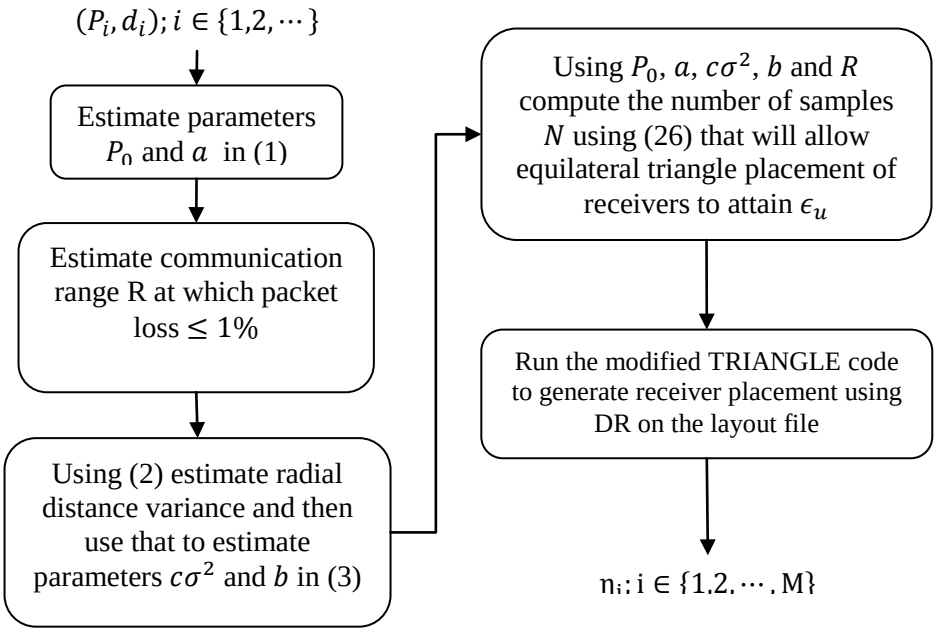

Fig 4. Flow chart of the receiver placement algorithm

Step 1: (*Estimating P_0 and a*) For increasing radial separation d_i between the receiver and transmitter, collect the measured RSS P_i values at the receiver. Using (1) estimate the parameters P_0 and path loss exponent a in the least square sense.

For our experiment the transmitter-receiver pair used is an XBee radio operating at frequency 2.45GHz and maximum transmitter output power of 0dBm and receiver sensitivity of -90dBm. Figure 5.1, shows the measured and least square estimated variation of the received signal strength in dBm with radial distance in meters.

Parameters P_0 and a obtained using least square are $P_0 = -38.9177\ dBm$ and $a = 2.5702$.

Step 2: (*Communication Range*) Using P_0 and a on (1), the radial distance at which the input signal strength at a receiver should fall below its receiver sensitivity of -90dbM is 120m. However, our experiments with communication range of the XBee radio has shown that the maximum radial distance the transmitter and receiver before the packet loss exceeded 1% of broadcast message from transmitter was at 6m. Therefore, for our localization experiment the parameter R representing the maximum communication range between wireless devices was set at 6m.

Step 3 (*Estimating $c\sigma^2$ and b*) Using the values for parameters P_0 and a estimated in previous step, derive the relationship between the radial distance variance against actual radial distance as in (3).

Figure 5.2 shows the measured and computed values for radial distance variance with actual radial distance between the transmitter and receiver for $c\sigma^2 = 0.0391$ and $b=2.1862$. Clearly the estimated radial distance variance increases with the actual radial distance as opposed to the assumption in [6]. This dependency between the radial distance variance to the actual radial distance could be attributed to the decreasing signal to noise ratio with increased radial distance causing large fluctuation in radial distance estimation for small change in RSS noise.

Step 4: (*RSS sample count*) The number of RSS samples that each receiver will have to collect for averaging before the radial distance is estimated during actual localization runs is estimated as follows:

As explained in section 6 the optimal placement is an equilateral triangular grid with side length R. For a single equilateral triangular tile in this triangulation, the maximum localization error occurs at its centroid can be computed from (13) and is given by $\epsilon_{\max} = \sqrt{\frac{c\sigma^2}{N}\left(\frac{R}{\sqrt{3}}\right)^b\left(\frac{1}{3}+\frac{1}{R^2}\right)}$ where $c\sigma^2$, b are from step 2 and N is the number of RSS samples to be collected by each receiver. To allow this equilateral tile to be a valid placement tile, $\epsilon_{\max}$ should be less than or equal to the pre-specified error threshold ϵ_u resulting in the RSS sample count at each receiver satisfying the following inequality

$$N \geq \left\lceil \frac{1}{\epsilon_u^2}\left(\frac{R}{\sqrt{3}}\right)^b\left(\frac{1}{3}+\frac{1}{R^2}\right)c\sigma^2 \right\rceil \tag{26}$$

where $\lceil\cdot\rceil$ is the ceil operator. Using the values for b and $c\sigma^2$ from step 3 and $R = 6m$ from step 2 for our localization workspace only one RSS sample has to be collected at the receiver to result in $\epsilon_u = 1m$.

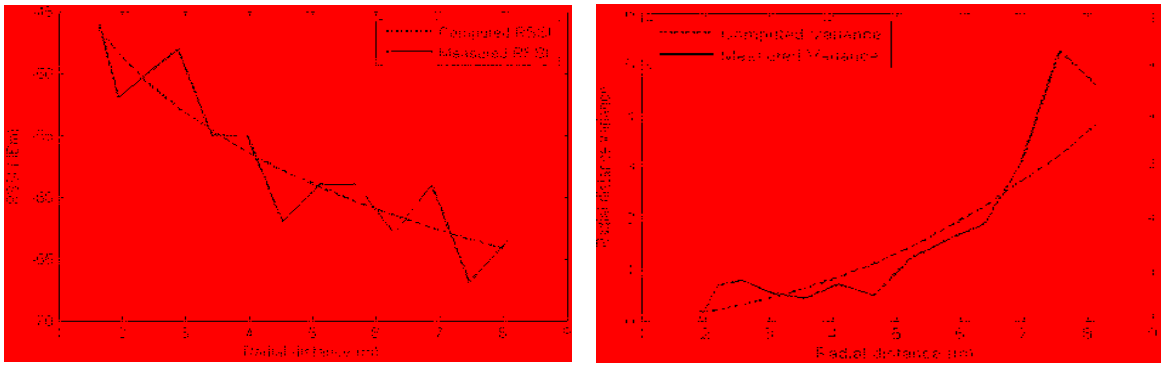

(1) RSS vs. actual radial distance

(2) Radial distance variance vs. actual radial distance

Fig 5. RSS and radial distance variance with actual radial distance

Step 5: (*Receiver placement generation*) The localization workspace is now fed to the TRIANGLE [20] application in the form of vertices, boundaries and obstructions as specified by application. The output is the coordinates of the receiver and the triangles to which they are associated

The TRIANGLE application source code was recompiled with our triangle division quality metric such that if the maximum value of localization error given by (14) computed with parameters (P_0, a, R, $c\sigma^2$ and b) from previous steps for a triangle exceeds ϵ_u= 1m then that triangle is sub-divided based on the rules of Delaunay refinement triangulation [5].

8.2 LOCALIZATION EXPERIMENT

The efficacy of the receiver layout generated by our Delaunay Refinement based (DR) algorithm was compared against the Delaunay Triangulation (DT) based method used in [4]. The *Srange* and *Prange* parameter values needed for [4] were set at 4m and 1m respectively. These values were selected from Figure 6.2 and correspond to the radial distance (*Srange* - *Prange*) value at which the estimation error was close to 1m. As mentioned previously, for the proposed Delaunay refinement based algorithm, the output from the quality mesh generator program TRIANGLE [20] was used position the localization receiver. Figure 6.1 and 6.2 shows the generated receiver layout for DR and DT based algorithms. The triangular localization domains generated by the tessellation of the input workspace is shown in dashed lines and the receivers are positioned at their vertices.

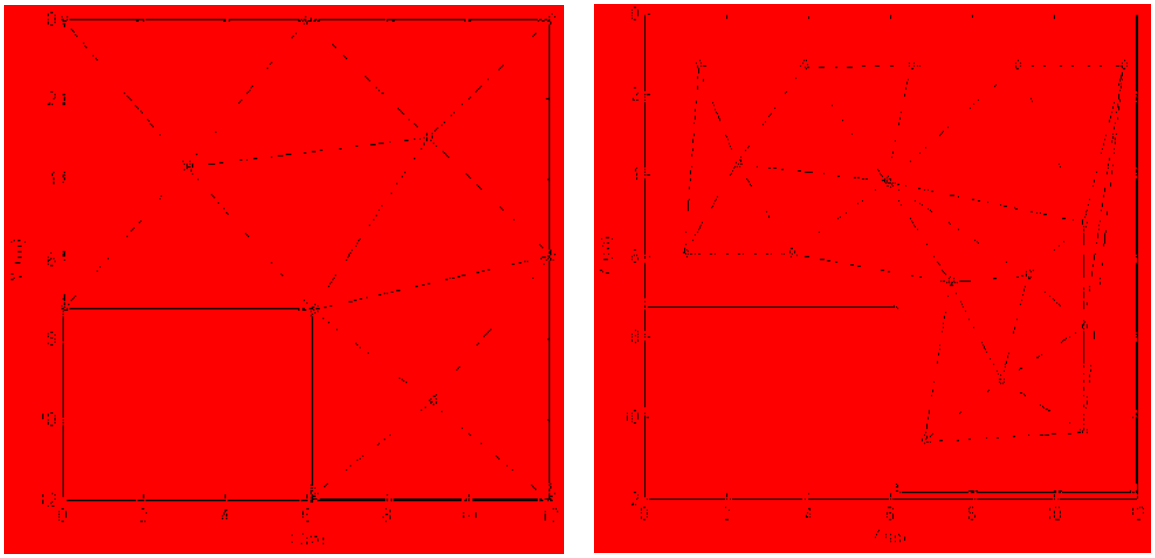

(1) Layout using DR method (11 receivers) (2) Layout using DT (16 receivers)

Fig 6. Comparison of the receiver layout using DR and DT

The localization error was estimated from thirty data packets broadcasted by the transmitter at eight randomly chosen sample locations on the workspace. The receivers collected the broadcast packets, and their signal strength measurements were used to estimate the radial distance to the transmitter using (25). The radial distance values are then used to estimate the possible triangles on which the transmitter might be located and finally CWLS is then used to estimate the 2D-Cartesian coordinates for the triangular tile which resulted in the lowest estimation variance.

The localization error was estimated from thirty data packets broadcasted by the transmitter at eighteen randomly chosen sample locations as shown in Figure 7. The receivers collected the broadcast packets, and their signal strength measurements were used to estimate the radial distance to the transmitter using (2). The radial distance values are then used to estimate the possible triangles on which the transmitter might be located and finally CWLS is then used to estimate the 2D-Cartesian coordinates of the

transmitter. The transmitter localization error at any sample location is the radial distance between the estimated coordinates and the candidate test locations $(T_1, T_2, \cdots, T_{18})$.

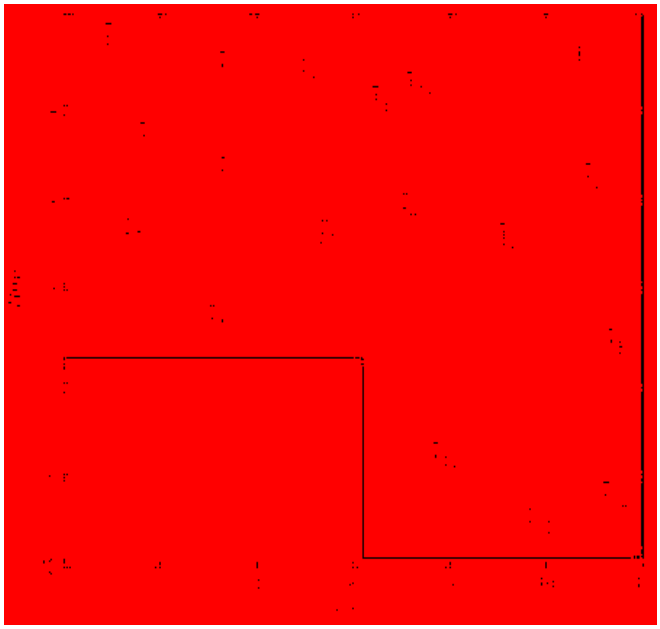

Fig 7. Test points for localization accuracy

At each sample location, the transmitter was localized thirty times resulting in a net total of 540 localization error measurements to generate the Cumulative Distribution Function (CDF) plot as shown in Figure 8.

Table 1, lists the mean, median, 75th percentile and standard deviation of the localization error. From this table, 75% of all transmitter localization error estimates for the DR method fell close to $\epsilon_u = 1m$. Since our standard total error equation (7) is the square root of the mean square error and from table 1 the mean error is less than pre-specified error threshold of $\epsilon_u = 1m$ thereby validating the efficacy of our placement algorithm. Additionally, DR method achieved better accuracy with just 11 receivers in

comparison to 16 receivers required by the DT method. This could be attributed to the near equilateral triangular tiles generated for the DR method in comparison to the DT method.

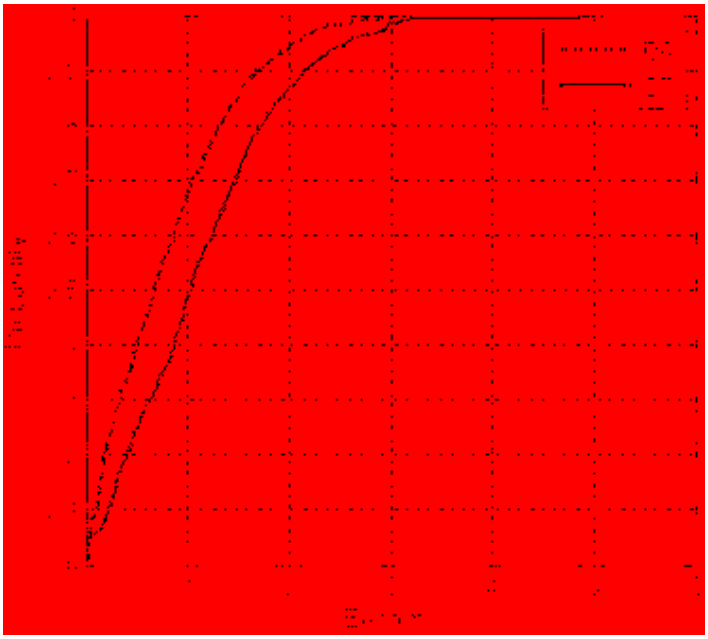

Fig 8. CDF of localization error

The 25% of measurements that had above 1m error could be due to unaccounted factors such as WiFi networks interference, path loss parameter variations, azimuth antenna radiation pattern etc. Interference from other networks in the localization workspace can result in temporary packet loss at a receiver which would affect radial distance variance, similarly variation in path loss exponent can manifest as large radial distance estimation variance. Typically, when receivers experience higher than designed radial distance variance, they may increase the number of RSS samples collected at each receiver as in (26) to reduce the radial distance variance.

TABLE 1. SUMMARY OF LOCALIZATION ERROR LEVELS

	Localization Error (m)			
Layout Generation Algorithm	***Mean***	***Median***	***75^{th} percentile***	***Std. dev***
Delaunay Refinement (DR)	0.808	0.678	1.189	0.657
Delaunay Triangulation (DT)	1.137	1.038	1.589	0.786

8.3 SIMULATIONS

To understand the impact of RSS noise and localization error threshold on the generated receiver count the following.

8.3.1 RSS SAMPLE COUNT VS. ϵ_u The multipath noise was set at $c\sigma^2 = 0.0391$ and then the RSS sample count was plotted as given by (26) for varying localization error threshold ϵ_u. Figure 9 shows the plot of RSS sample count vs. localization error threshold.

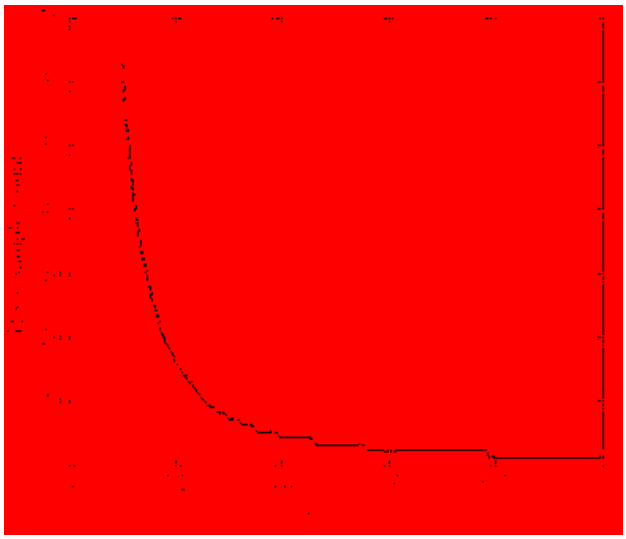

Fig 9. RSS sample count vs. localization error threshold ϵ_u

Clearly from (26) the RSS sample count should increase exponentially with reduced error threshold. However, from our experimental runs, attaining localization accuracy better than 0.5m using RSS ranging has proven to be a challenge which as pointed out in section 8.2 may be attributed to a host of unaccounted factors in our wireless propagation model. Additionally, from (26) each receiver could monitor the radial distance variance and adjust the RSS sample count accordingly to keep the localization error below the pre-specified threshold ϵ_u.

8.3.2 RECEIVER COUNT FROM DR AND OPTIMAL PLACEMENT

Equation (18) gives the upper bound for the ratio of receivers under DR placement and an optimal placement involving equilateral triangles. In this simulation, our attempt is to find how tight the receiver count bound given by (18) is for two typical floor plans with respect to a receiver count for an optimal placement. The first layout under consideration is a shopping mall that measures 705 units x 657 units whereas the second layout is that of an airport which measures 1541 units x 1191 unit. For our simulation, the communication range for the wireless devices was assumed to be at $R = 100\ units$. The values for parameters in (1) and (2) such as a, b, $c\sigma^2$ and P_0 were assumed to be same as that measured during our localization experiment i.e. $P_0 = -38.9177\ dBm$, $a = 2.5702$, $c\sigma^2 = 0.0391$ and $b = 2.1862$.

From section 6, an optimal placement where the receivers are not constrained by the perimeter wall would be an equilateral grid with grid spacing R. Therefore, the optimal placement for our simulation involved a brute force search where the orientation, x and y offset of the start of the equilateral grid is varied to find that placement which

resulted in the lowest number of receivers to span the entire workspace under localization coverage. Figure 10 shows the optimal and DR placement for the two layouts.

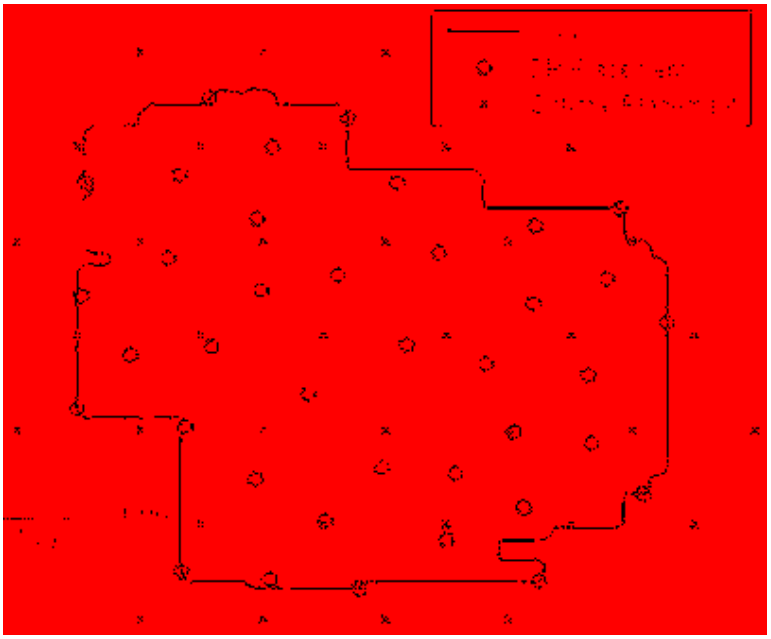

(1) Layout of a mall

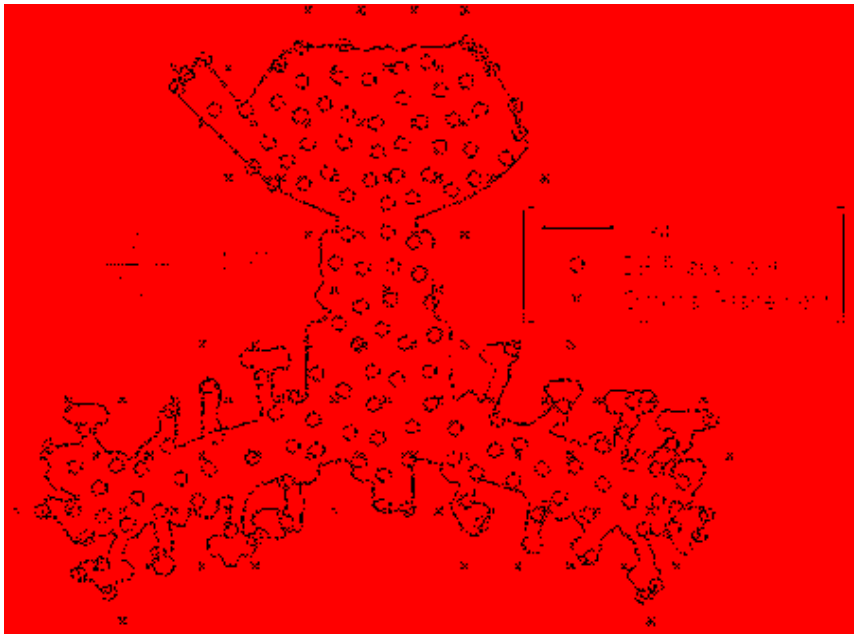

(2) Layout of an airport.

Fig 10. DR and optimal placement of receivers

The value for p in (18), that sets the upper bound for the receiver count, for shopping mall layout was computed to be 11.3 while that for the airport layout was found to 9.78. However, from simulation, the receiver count generated by DR placement was much closer to the receiver count for an optimal placement as is visible from the values 1.06 and 1.62 for shopping mall and airport layout respectively. This large discrepancy could be explained due to the factor $q = \frac{\max(lfs_G)}{\min(lfs_G)}$ in (22) that was used as a multiplication factor to ensure that the product of this factor times the local feature size after triangulation is always greater than the local feature size of the input PSLG. A much tighter bound may be derived if a lower value of this multiplicative factor can be found.

9. CONCLUSIONS

In this paper, a novel placement algorithm that uses Delaunay refinement algorithm to tessellate an input workspace into triangular tiles was presented. The feasibility of the proposed receiver placement algorithm was demonstrated using simulations and an experimental setup with eight receivers that localized a transmitter 75% of the time with a maximum localization error of 1m. The receiver count generated by our algorithm while sub-optimal, was shown mathematically bounded by a constant to an optimal placement algorithm. From simulations it was shown that for a shopping mall and an airport layout this bound was much tighter than the one derived in (18). In addition, analytically, it was shown that this bound can be tightened by smoothing the input layout to our receiver placement algorithm which may involve removing segments that are shorter than twice the wavelength of the wireless devices used for localization.

REFERENCES

[1] A. Ramachandran, and S. Jagannathan, "Spatial diversity in signal strength based WLAN location determination systems," *Proc. of the 32nd IEEE Conf. on Local Comp. Networks* , pp. 10-17, Oct. 2007.

[2] M. Youssef, and A. Agrawala, "The Horus WLAN location determination system," *Proc. of the 3rd inter. Conf. on Mobile Systems, Applications, and Service*, MobiSys '05. ACM Press, NY, pp. 205-218.

[3] M. R. Basheer, S. Jagannathan, "R-Factor: A New Parameter to Enhance Location Accuracy in RSSI Based Real-time Location Systems," *Sensor, Mesh and Ad Hoc Communications and Networks, SECON '09. 6th Annual IEEE Communications Society Conference on* , pp. 1-9, 22-26 June 2009.

[4] C. Wu, K. Lee, and Y. Chung, "A Delaunay Triangulation based method for wireless sensor network deployment," *Computer Communications*. Volume 30, Issue 14-15, pp. 2744-2752, Oct 2007.

[5] J.R. Shewchuk, "Delaunay Refinement Algorithms for Triangular Mesh Generation," *Computational Geometry: Theory and Applications*, 22(1-3): pp. 21-74, May 2002.

[6] S. Martínez, and F. Bullo, "Optimal sensor placement and motion coordination for target tracking," *Proc. of the inter. Conf. on Robotics and Automation*, Barcelona, Spain, pp. 4544-4549, April 2005.

[7] V. Isler, "Placement and distributed deployment of sensor teams for triangulation based localization," *In Proc. IEEE ICRA*, pp. 3095-3100, May, 2006.

[8] Yousi Zheng, Han Wang, Lei Wan, Xiaofeng Zhong, "A Placement Strategy for Accurate TOA Localization Algorithm," *Annual Conference on Communication Networks and Services Research*, pp. 166-170, 2009.

[9] N. Bulusu, J. Heidemann and D. Estrin, "Adaptive beacon placement," *Distributed Computing Systems, 2001. 21st International Conference on.* , pp. 489-498, Apr 2001.

[10] J. Rupert, "A Delaunay refinement algorithm for quality 2-dimensional mesh generation," *Journal of Algorithms*, Vol. 18, Issue. 3, pp. 548-585, May 1995.

[11] H. T. Friis "A note on a simple transmission formula," *Proc. IRE*, vol. 34, pp. 254-256, May 1946.

[12] B. M. Donlan, D. R. McKinstry and R. M. Buehrer , “The UWB indoor channel: large and small scale modeling,” *Wireless Communications, IEEE Transactions on* , vol.5, No.10, pp.2863-2873, Oct. 2006.

[13] L. Bain and M. Engelhardt, Intro. to Probability and Mathematical Statistics, *Duxburry Press*, Pacific Grove, CA (1991).

[14] J.N. Franklin, Matrix Theory, Prientice Hall, New Jersey, 1968.

[15] K. W. Cheung, H. C. So, W. Ma, and Y. T. Chan, “A constrained least squares approach to mobile positioning: algorithms and optimality,” *EURASIP J. Appl. Signal Process.*, pp. 150-150, Jan 2006.

[16] XBEE/XBEE-PRO RF Modules: Product Manual v1. x E x - 802.15.4 Protocol, Digi International Inc, http://ftp1.digi.com/support/documentation/90000982_G.pdf, accessed on Jul 9, 2012.

[17] G. K. Francis, and J. R. Weeks, “Conway's ZIP Proof,” *Amer. Math. Monthly* 106, pp. 393-399, 1999

[18] L. P. Chew, “Constrained Delaunay Triangulations,” *Proc. of the Third Annual Symposium on Computational Geometry (SoCG)*, pp 215-222, 1987

[19] S. A. Mitchell, “Cardinality bounds for triangulations with bounded minimum angle,” *Proc. of the 6th Canadian Conf. Computational Geometry*, pp. 326–331, 1994.

[20] J.R. Shewchuk, Triangle, A Two-Dimensional Quality Mesh Generator and Delaunay Triangulator, http://www.cs.cmu.edu/~quake/triangle.html, accessed on Jul. 9, 2012

III. LOCALIZATION OF RFID TAGS USING STOCHASTIC TUNNELING[1]

M. R. Basheer and S. Jagannathan

Abstract— *This paper presents a novel localization scheme in the three dimensional wireless domain that employs cross-correlation in backscattered signal power from a cluster of Radio Frequency Identification (RFID) tags to estimate their location. Spatially co-located RFID tags, energized by a common tag reader, exhibit correlation in their Received Signal Strength Indicator (RSSI) values. Hence for a cluster of RFID tags, the posterior distribution of their unknown radial separation is derived as a function of the measured RSSI correlations between them. The global maxima of this posterior distribution represent the actual radial separation between the RFID tags. The radial separations are then utilized to obtain location estimates of the tags. However, due to the non-convex nature of the posterior distribution, deterministic optimization methods that are used to solve true radial separations between tags provide inaccurate results due to local maxima, unless the initial radial separation estimates are within the region of attraction of its global maximum. The proposed RFID localization algorithm called LOCalization Using Stochastic Tunneling (LOCUST) utilizes constrained simulated annealing with tunneling transformation to solve this non-convex posterior distribution. The tunneling transformation allows the optimization search operation to circumvent or "tunnel" through ill-shaped regions in the posterior distribution resulting in faster*

[1] Research Supported in part by GAANN Program through the Department of Education and Intelligent Systems Center. Authors are with the Department of Electrical and Computer Engineering, Missouri University of Science and Technology (formerly University of Missouri-Rolla), 1870 Miner Circle, Rolla, MO 65409. Contact author Email: mrbxcf@mail.mst.edu.

convergence to the global maximum. Finally, simulation results of our localization method are presented to demonstrate the theoretical conclusions.

***Keywords**:* Antenna Correlation, Rayleigh Channel, Fading, Spatial Diversity, maximum a posteriori, Markov Chain Monte Carlo, Composite Likelihood, Multi-Dimensional Scaling, Stochastic Tunneling.

Nomenclature

Symbol	*Description*	*Symbol*	*Description*
M	Number of RFID tags	λ	RFID tag operation frequency
$\eta_i = \{\eta_{ix}, \eta_{iy}, \eta_{iz}\}^T$	x, y, and z coordinates of i^{th} RFID tag	P_i	Random variable corresponding to the backscattered power from RFID tag *i*
		μ_i	Average power from RFID tag *i*
Θ_{ij}	Azimuth angle of tag reader orientation with respect to RFID tags *i* and *j*	ρ_{ij}	Cross-correlation in backscattered signal power between RFID tags *i* and *j*
Φ_{ij}	Elevation angle of tag reader orientation with respect to RFID tags *i* and *j*	$\gimel_{ij}$	Square of the correlation between quadrature amplitude components of backscattered signals from RFID tags *i* and *j*
		$\sigma_{\rho_{ij}}$	Variance in estimating ρ_{ij} from backscattered RSSI values from RFID tags *i* and *j*
δ_{ij}^{θ}	Concentration of backscattered signals from tags *i* and *j* around Θ_{ij}	$\hat{\rho}_{ij}^{*}$	Method of Moment estimate of ρ_{ij} from backscattered power from RFID tags *i* and *j*
δ_{ij}^{ϕ}	Concentration of backscattered signals from tags *i* and *j* around Φ_{ij}	N_p	Number of backscattered power samples from RFID tags *i* and *j* used to estimate ρ_{ij}
r_{ij}	Radial separation between RFID tags *i* and *j*		

1. INTRODUCTION

Accurate identification and location of an asset using radio frequency identification (RFID) tags is a key requirement for several logistical applications including supply chain management, shop floor assembly and so on. RFID tags operating

at low (125–134.2 kHz and 140–148.5 kHz), high (13.56 MHz) and ultra-high (868–928 MHz) frequencies are currently employed in variety of applications such as asset tracking, toll road metering, retail sales, public transit ticketing etc [1]. Typically, RFID tags are passive devices that are energized by radio waves transmitted by a tag reader in its vicinity. This energy from the incoming radio waves is used to send back its unique identity information to the tag reader by switching the radar cross-section (RCS) of tag's antenna between multiple states [2]. Though existing applications primarily employ RFID tags for identification purpose, adding location information can provide important value addition especially for logistics industry [3], if passive tags can be utilized. For example, RFID tags attached to items in a freight container can not only uniquely identify them but also provide a map of their physical location within the freight container when they pass by a tag reader as shown in Figure 1.

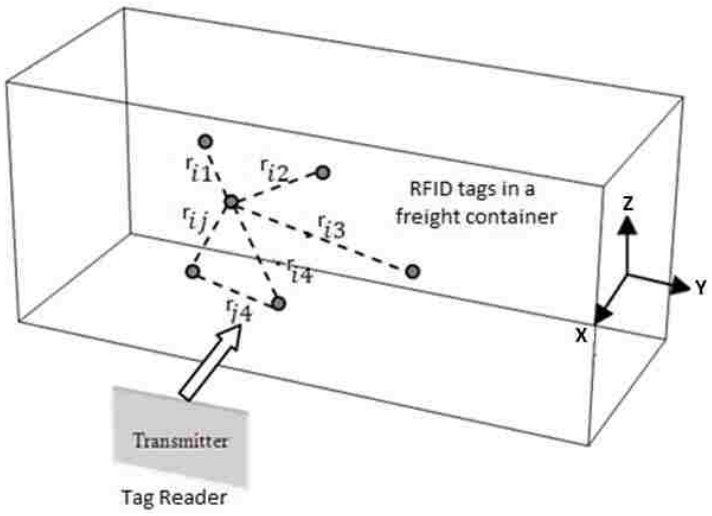

Fig 1. RFID tags in a frieght container

There are several approaches for RFID localization using phase difference of signals [4], angle of arrival [5] or adjusting transmission power [6] of radio waves. Compared to these [4-6] methods, localization by measuring backscattered RSSI from tags has the advantage that any existing tag reader can implement the localization feature with just a software upgrade. However, RSSI is affected by the line of sight (LoS) conditions between a transmitter and a receiver with localization accuracy guarantees achievable only under excellent LoS conditions [7]. Whereas, under non-line of sight (NLoS) conditions, periodic radio signal strength profiling of localization workspace, which is a bottleneck, is essential to ensure minimal localization error.

One of the main reasons for large localization error in RSSI based methodology is the multipath fading effects [7] which are caused by scattering of radio signals due to obstacles in the workspace. These scattered signals reach the receiver antenna at different amplitudes, angles and phase. These signals are then superimposed at the antenna resulting in constructive or destructive fading in its radio signal strength.

While fading is destructive in general, however, it may be exploited to improve localization accuracy. Co-located RFID tags have similar scattering environment and hence exhibit similar fading statistics. Therefore, by computing the correlation in RSSI values measured by the tag reader, radial distance between co-located tags may be inferred. This paper presents a novel localization scheme for RFID tags where pair-wise RSSI correlation measurement obtained from backscattered signals is used to estimate the radial separation among co-located tags.

Localization from correlation measurement between time varying-isotropic data embedded with random noise field has been addressed in the recent literature [8-12]. In

[8-10], localization was treated as a dimensionality reduction problem where data measurement sampled over time generates a data point in a high dimensional space. This data is then reduced to a low dimensional (2D or 3D) Cartesian coordinates using multi-dimensional scaling (MDS). However, a linear relationship assumption between correlation coefficient and radial separation of transmitters in MDS severely restricts its applicability in wireless environment since RSSI correlation is a highly nonlinear function of radial distance.

In [11, 12], centralized manifold learning (non-linear dimensionality reduction) techniques such as Isomap, Local Linear Embedding (LLE) and Hessian LLE are used for localization. In this approach the linearity between the correlation measurement and radial distance is restricted to a small area containing a tag and its K nearest neighbors. However, from our analysis, the linearity between RSSI and radial distance becomes invalid even in the immediate vicinity at operating frequencies greater than 10MHz.

To mitigate the weakness of the above methods [8-12], the proposed localization method uses a parametric estimation approach where it first attempts to infer the true radial separation between tags from observed pair wise RSSI correlation values generated from backscattered signals using stochastic search methods. Subsequently, Cartesian coordinates are derived from these radial separation estimates using MDS or LLE. The major contribution of this paper are (a) the derivation of a joint PDF of backscattered power measurements at the tag reader from a pair of RFID tags, (b) the development of functional relationship between the RSSI correlation parameters and the radial separation between tags, and (c) the derivation of the posterior distribution of radial separation between a cluster of RFID tags as a function of the measured pair-wise RSSI correlation.

Next a global maximum of this posterior distribution is obtained via the Maximum a Posteriori (MAP) estimator for the radial separation between RFID tags.

Therefore, this paper begins in Section 2 by defining the tag localization problem as estimating the true radial separation among passive RFID tags from RSSI values measured at the tag reader. Section 3.1 provides a brief background on von Mises distribution that is used to model the angle of arrival of backscattered signals at the tag reader. Section 3.2 introduces the composite likelihood (CL) method that presents a computationally less intensive approach for generating likelihood functions for MAP estimators. The CL method helps to model complicated interdependencies arising between backscattered signals due to fading. To understand these signal interdependencies, Section 4 begins by deriving the joint probability density function (PDF) of signal power from a pair of co-located RFID tags in Theorem 1. The functional relationship between the dependency parameters, called the RSSI correlation parameters, and the radial separation between a pair of co-located RFID tags under LoS and NLoS conditions in the presence of the tag reader is derived in Corollary 1.

Next, Lemma 2 provides a Method of Moment (MoM) estimator for obtaining RSSI correlation parameters from RSSI values measured by the tag reader since commercial receivers only provide backscattered signal strength information in the form of RSSI values. To estimate the radial distance from RSSI correlation parameters, the likelihood or the probability of observing a particular RSSI correlation parameter value between a pair of co-located RFID tags when the radial separation between them is known is presented in Theorem 2.

Subsequently, Corollary 4 extends this likelihood to a larger workspace with $M \geq 3$ passive RFID tags using CL method. Any radial separation vector that maximizes this CL function has the highest probability of being the true radial separation between RFID tags. However, due to the non-injective nature of the relationship between the RSSI correlation parameters and radial separation there will be multiple local maxima for CL. Therefore, Lemmas 3 and 4 add robustness to our radial estimates by imposing radial separation prior distributions and triangle inequality constraints.

This results in Theorem 3 where the objective function for the MAP estimator for RFID localization is presented. Due to the non-convex, slow converging nature of this objective function, stochastic optimization with tunneling transformation is used to solve this constrained optimization problem in Section 4.3. Section 5 presents the flowchart of the proposed localization algorithm which is referred here as LOCUST. Results and analysis are presented in Section 6. Finally, Section 7 concludes the paper with a discussion about the proposed method, improvements and future work.

2. PROBLEM STATEMENT

Consider a workspace with M RFID tags where the 3D coordinate of the i^{th} $;i \in [1,2,\cdots,M]$ RFID tag is denoted by $\eta_i = \{\eta_{ix}, \eta_{iy}, \eta_{iz}\}^T$. It is assumed that the location information of a subset of RFID tags in the workspace called the anchor nodes are perfectly known and placed around the perimeter of the workspace while the locations of all other tags are unknown. In addition, a RFID tag reader placed along the x-axis with y and z coordinates zeros, is able to simultaneously measure the backscattered RSSI information from all the tags. Then, the localization problem considered here is to

infer the true radial separation between RFID tags in this workspace from pair-wise RSSI correlation measurements made at the tag reader.

The primary purpose of anchor nodes is to disambiguate the infinite number of RFID tag coordinates arising from translation and rotation of the localization workspace to a unique global coordinate system defined by the anchor nodes. It was shown in [13] that positioning anchor nodes around the periphery improves the chance of obtaining a unique solution. However, the minimum number of anchor nodes and their placement within the workspace to obtain the best localization accuracy is beyond the scope of this paper. Nevertheless, for typical applications that we envisage for our solution involve localizing the position of RFID tags within an enclosure such as industrial refrigerator or freight containers where the anchor nodes can be easily placed outside the enclosure.

In the next section, background information on the distribution used to model angle of arrival of backscattered signals and the CL method is given before moving onto the methodology.

3. BACKGROUND

3.1 VON-MISES DISTRIBUTION

The von Mises distribution or the circular normal distribution was introduced by von Mises to study the deviation of measured atomic weights from integral values [14]. The PDF of a von Mises distribution is given by

$$f\left(\theta|\Theta,\delta^{\theta}\right)=\frac{\exp\{\delta^{\theta}\,cos(\theta-\Theta)\}}{2\pi I_0\left(\delta^{\theta}\right)} \tag{1}$$

where δ^{θ} is the concentration parameter that denotes the density of random variable θ around mean Θ and $I_0(\cdot)$ is the modified Bessel function of the first kind and order zero

[15 pp.374]. This distribution may be thought of as a wrapped normal distribution with an interval of 2π.

In this paper, von Mises distribution is used to model the PDF of the angle of arrival (θ) of backscattered signals around the tag reader orientation Θ with concentration controlled by a parameter δ^{θ}. Concentration parameter δ^{θ} in LOCUST is estimated offline during profiling phase where RFID tags at preset locations are localized and δ^{θ} is adjusted to reduce the mean square error of localization.

3.2 COMPOSITE LIKELIHOOD

Estimating parameters for a complicated system with intricate dependency between observations involves the derivation of a full likelihood function that encapsulates all its complexities. For a large number of interdependent observations, full likelihood derivation may be infeasible or computationally burdensome. However, the full likelihood function may be approximated by a weighted product of pair-wise likelihood function forming a pseudo-likelihood function as in Composite Likelihood (CL) method [16] given by

$$CL(\theta) = \prod_{i=1}^{M} \prod_{j>i}^{M} L_{ij}\left(\nu \middle| x_i, x_j\right)^{w_{ij}} \tag{2}$$

where $\mathrm{CL}(\cdot)$ is the composite likelihood function that is used to approximate the full likelihood, ν is the parameter vector that is being estimated from M observations of random variable X whose samples observed over time i are given by $x_i; i \in \{1,2,\cdots,M\}$, $L_{ij}\left(\theta \middle| x_i, x_j\right)$, $L_{ij}\left(\cdot \middle| x_i, x_j\right)$ is the pair-wise likelihood function between samples x_i and $x_j; j \in \{1,2,\cdots,M\}$ and w_{ij} is the weight function that determines the influence of the pair-wise likelihood $L_{ij}(\cdot \mid \cdots)$ on the overall likelihood function. It was shown in [17] that CL

based estimators can be consistent, asymptotic normal and provide a valid compromise between computational burden and robustness in estimating high dimensional parameters.

For radial distance estimation from RSSI measurement using the MAP estimator, the likelihood function has to encapsulate the complicated interdependency arising between RSSI values due to multipath fading. Derivation of this likelihood function in a workspace with large number of RFID tags is a non-trivial problem. Therefore this paper approximates the actual likelihood function pair-wise by combining joint PDF of RSSI values from co-located RFID tags to form a pseudo-likelihood function using CL method. Next, the localization of RFID tags from power measurements will be described.

4. LOCALIZATION FROM BACKSCATTERED RSSI

In this paper, the tag localization problem is presented as estimating the true radial separation between passive RFID tags from joint probability distribution of RSSI values measured at the tag reader. Initially, the approach is introduced when a pair of RFID tags is present and then it is extended to the case for over two tags.

4.1 RSSI CORRELATION PARAMETERS

Now we will derive the joint PDF of backscattered RSSI values from a pair of co-located RFID tags.

Theorem 1: (*Joint Distribution of Backscattered RSSI*) Joint PDF of backscattered RSSI values measured by a tag reader from any two RFID tags separated by radial distance r_{12} is given by

$$f_{P_1P_2}(p_1,p_2) = \frac{(1-\rho_{12})}{\mu_1\mu_2(1-\rho_{12}+\gamma_{12})^2} \exp\left\{-\frac{\frac{p_1}{\mu_1}+\frac{p_2}{\mu_2}}{(1-\rho_{12}+\gamma_{12})}\right\} I_0\left(\sqrt{\frac{4p_1\,p_2\rho_{12}}{(1-\rho_{12}+\gamma_{12})^2\mu_1\mu_2}}\right) \quad (3)$$

where $P_1$and P_2 are the backscattered RSSI random variables from tag 1 and 2 respectively with p_1 and p_2 being their realizations, $\mu_1 > 0$ and $\mu_2 > 0$ are their average

values, $0 \leq \rho_{12} \leq 1$ and $0 \leq \daleth_{12} \leq 1$ are the RSSI correlation parameters and $\mathrm{I}_0(\cdot)$ is the zero[th] order modified Bessel function of the first kind [15 pp. 374].

Proof: Please refer to the appendix. ■

For our localization method, RSSI correlation parameters ρ_{12} and $\daleth_{12}$ in (3) for a pair of passive RFID tags are the primary parameters of interest and hence their functional relationship to tag radial distance separation and tag reader orientation will now be derived in the Corollary

Corollary 1: (*RSSI Correlation Parameters*) The functional relationship between the RSSI correlation parameters $(\rho_{12}, \daleth_{12})$, the radial separation (r_{12}), the tag reader azimuth orientation (Θ_{12}) and the concentration parameter $\left(\delta_{12}^{\theta}\right)$ for a pair of co-located RFID tags 1 and 2 is given by

$$\rho_{12} = \left\{ J_0(\hat{r}_{12}) + \frac{2}{I_0(\delta_{12}^{\theta})} \sum_{n=1}^{\infty} F_n\left(\hat{r}_{12}, \Theta_{12}, \delta_{12}^{\theta}\right) \right\}^2 \tag{4}$$

$$\daleth_{12} = \left\{ \frac{2}{I_0(\delta_{12}^{\theta})} \sum_{n=0}^{\infty} G_n\left(\hat{r}_{12}, \Theta_{12}, \delta_{12}^{\theta}\right) \right\}^2 \tag{5}$$

where λ is the operating wave length, $\hat{r}_{12} = \frac{2\pi}{\lambda} r_{12}$, $F_n\left(\hat{r}_{12}, \Theta_{12}, \delta_{12}^{\theta}\right) = I_{2n}\left(\delta_{12}^{\theta}\right) J_{2n}(\hat{r}_{12})\, cos(2n\Theta_{12}) \cos(n\pi)$, $G_n\left(\hat{r}_{12}, \Theta_{12}, \delta_{12}^{\theta}\right) = I_{2n+1}\left(\delta_{12}^{\theta}\right) J_{2n+1}(\hat{r}_{12})\, sin\left[(2n+1)\left(\frac{\pi}{2} - \Theta_{12}\right)\right]$, $I_n(\cdot)$ and $J_n(\cdot)$ are the modified and ordinary Bessel functions respectively of the first kind and order *n*.

Proof: See appendix. ■

Next, we will evaluate the RSSI correlation parameters under special condition when NLoS dominate between the tag reader and the RFID tags.

Corollary 2: (*RSSI Correlation Parameters under NLoS*) Under NLoS conditions with a tag reader, the RSSI correlation parameters for co-located passive RFID tags are given by

$$\rho_{12} = [J_0(\hat{r}_{12})]^2 \tag{6}$$

$$\gamma_{12} = 0 \tag{7}$$

Proof: Under NLoS condition, the signal is highly dispersed i.e. $\delta_{12}^{\theta} = 0$. Hence $\mathrm{I}_{2n}\left(\delta_{12}^{\theta}\right) = 0$ for $n \geq 1$ and $\mathrm{I}_{2n+1}\left(\delta_{12}^{\theta}\right) = 0$ for n ≥ 0 resulting in $G_n\left(\hat{r}_{12}, \Theta_{12}, \delta_{12}^{\theta}\right) = 0$ and $F_n\left(\hat{r}_{12}, \Theta_{12}, \delta_{12}^{\theta}\right) = 0$ in (4) and(5). Therefore ρ_{12} is given by (6) and $\gamma_{12} = 0$ as in (7). ■

Corollary 3: (*Joint* PDF *of RSSI under NLoS*) Joint PDF of RSSI values measured by a tag reader from a pair of RFID tags that are separated by radial distance r_{12} under NLoS conditions is given by the Downton's bivariate exponential (DBVE) distribution [19] as

$$\mathrm{f}_{\mathrm{P}_1\mathrm{P}_2}(\mathrm{p}_1, \mathrm{p}_2) = \frac{1}{\mu_1\mu_2(1-\rho_{12})} \exp\left(-\frac{\frac{\mathrm{p}_1}{\mu_1}+\frac{\mathrm{p}_2}{\mu_2}}{(1-\rho_{12})}\right) \mathrm{I}_0\left(\sqrt{\frac{4\mathrm{p}_1\,\mathrm{p}_2\rho_{12}}{(1-\rho_{12})^2\mu_1\mu_2}}\right) \tag{8}$$

Proof: Applying (6) and (7) in (3) results in the joint RSSI distribution under NLoS for co-located tags as (8). ■

Equations (4) and (5) relates RSSI correlation parameters ρ_{12} and γ_{12} respectively to unknown radial separation (r_{12}), tag reader orientation (Θ_{12}) and backscattered concentration $\left(\delta_{12}^{\theta}\right)$. Hence, either of these RSSI correlation parameters could be used for radial distance estimation. However, from Corollary 2, ρ_{12} is the only term that is non-zero under both LoS and NLoS conditions and consequently the only RSSI correlation

parameter that is used for localization in this paper. Henceforth, any reference to RSSI correlation parameter in this paper implies using the parameter ρ_{12}.

From appendix (A11), ρ_{12} is defined as the square of the received signal amplitude covariance normalized by the average backscattered power for tag 1 and 2. However, most commercial off-the-shelf tag readers do not provide direct access to quadrature signal amplitude components of incoming backscattered signals. Hence, ρ_{12} has to be estimated from the more readily available RSSI measurements at the tag reader. Now we will derive the computationally simpler method of moment (MoM) estimators for RSSI correlation parameter ρ_{12} from RSSI values measured at the tag reader. First we will derive the general joint moment for a pair of backscattered signals in Lemma 1 and then in Lemma 2 we will use the joint moment to derive the MoM estimator for ρ_{12}.

Lemma 1: (*Moments of RSSI Product*) If P_1 and P_2 are the backscattered RSSI measured by a tag reader from co-located RFID tags then the joint m^{th} moment of P_1 and n^{th} moment of P_2 is given by

$$E(P_1^m P_2^n) = m!\, n!\, \mu_1^m \mu_2^n \left[\frac{(1-\rho_{12}+\gamma_{12})^{m+n}}{(1-\rho_{12})^m}\right] \mathcal{P}_n^{(0,m-n)}\left(\frac{1+\rho_{12}}{1-\rho_{12}}\right) \qquad (9)$$

where $\mathcal{P}_n^{(\alpha,\beta)}(\cdot)$ is the Jacobi polynomial [15 pp. 774].

Proof: Refer to the appendix. ■

Now from the joint moment, we will derive the MoM estimator for the RSSI correlation ρ_{12}.

Lemma 2: (*MoM Estimator for RSSI Correlation*) Method of moment estimator for the RSSI correlation ρ_{12} from N_p backscattered RSSI value measurements from two co-located RFID tags 1 and 2 is given by

$$\hat{\rho}_{12}^{*}=\begin{cases}1 & \hat{\rho}_{12}>1\\ \hat{\rho}_{12} & 0\le\hat{\rho}_{12}\le 1.\\ 0 & \hat{\rho}_{12}<0\end{cases} \tag{10}$$

where

$$\hat{\rho}_{12}=\frac{N_p\sum_{\mathrm{i}=1}^{N_p}(\mathrm{p}_{1\mathrm{i}}\mathrm{p}_{2\mathrm{i}})}{\sum_{\mathrm{i}=1}^{N_p}(\mathrm{p}_{2\mathrm{i}})\sum_{\mathrm{i}=1}^{N_p}(\mathrm{p}_{2\mathrm{i}})}-1 \tag{11}$$

Proof: Refer to the appendix. ■

Now we will derive the likelihood of observing a particular RSSI correlation value at the tag reader when the radial distance, tag reader orientation and backscattered concentration of two co-located RFID tags are available.

Theorem 2: (*Approximate PDF of RSSI Correlation*) The large sample approximate conditional PDF of the RSSI correlation estimate obtained from N_p pair-wise RSSI values measured by the tag reader from two co-located RFID tags that are separated by radial distance r_{12}, oriented at azimuth angle Θ_{12} with a tag reader and under backscattered signal concentration of δ_{12}^{θ} is given by

$$f\left(\hat{\rho}_{12}^{*}|r_{12},\Theta_{12},\delta_{12}^{\theta}\right)=\frac{1}{\sigma_{\rho_{12}}}\frac{\phi_N\left(\frac{[\hat{\rho}_{12}^{*}-\rho_{12}]}{\sigma_{\rho_{12}}}\right)}{\Phi_{\mathrm{N}}\left(\frac{1-\rho_{12}}{\sigma_{\rho_{12}}}\right)}I_{[0,1]}(\hat{\rho}_{12}^{*}) \tag{12}$$

where $I_{[0,1]}(\hat{\rho}_{12}^{*})$ is the indicator function that restricts the support of this PDF between [0, 1], ρ_{12} is the correlation parameter given by (4), $\sigma_{\rho_{12}}^{2}=\frac{2\rho_{12}}{N_p}$ and $\phi_N(\cdot)$ and $\Phi_{\mathrm{N}}(\cdot)$ are the PDF and CDF respectively of a standard normal distribution.

Proof: See appendix. ■

4.2 LIKELIHOOD FUNCTION FOR RADIAL DISTANCE ESTIMATION

So far, the pair wise joint PDF for two tags has been introduced and the correlation parameter is estimated from the backscattered signals. Next we will combine

multiple pair-wise joint PDF in a workspace with $M \geq 3$ RFID tags using CL method to generate the pseudo-likelihood function that forms the objective function for our radial distance estimation problem.

Corollary 4: (*Pseudo-likelihood of Radial Separations and Tag Reader Orientations*) The pseudo-likelihood function of the RFID tag radial separations and tag reader orientation in a workspace with $M \geq 3$ RFID tags when the sample pair-wise RSSI correlation values are available is given by

$$CL(R,\Theta) = \prod_{i=1}^{M}\prod_{j>i}^{M} \frac{1}{\left[\Phi_{\mathrm{N}}\left(\frac{1-\rho_{ij}}{\sigma_{\rho_{ij}}}\right)\sigma_{\rho_{ij}}\right]^{w_{ij}}} \exp\left\{-\frac{w_{ij}\left[\hat{\rho}_{ij}^{*}-\rho_{ij}\right]^{2}}{2\sigma_{\rho_{ij}}^{2}}\right\} \tag{13}$$

where $\hat{\rho}_{ij}^{*}$ is the sample RSSI correlation value estimated from N_p pair-wise RSSI samples values using (10), ρ_{ij} is the RSSI correlation value given by (4), r_{ij} is the radial separation, w_{ij} is a likelihood weighting function between tag $i; i \in \{1,2,\cdots,M\}$ and tag $j; j \in \{1,2,\cdots,M\}$, $\sigma_{\rho_{ij}}^{2} = \frac{2\rho_{ij}}{N_p}$, $R = \left\{r_{ij}; j > i; i,j \in 1,2,\cdots,M\right\}$ is the vector of unknown radial separation parameters and $\Theta = \left\{\Theta_{ij}; j > i; i,j \in 1,2,\cdots,M\right\}$ is the vector of unknown tag reader orientation parameters.

Proof: The CL based pseudo-likelihood function for estimating radial distances and tag reader orientation is given by

$$CL(R,\Theta) = \prod_{i=1}^{M}\prod_{j>i}^{M} f\left(\hat{\rho}_{ij}^{*}|r_{ij},\Theta_{ij},\delta_{ij}^{\theta}\right)^{w_{ij}} . \tag{14}$$

The simplistic weighting function

$$w_{ij} = \begin{cases} 1, & r_{ij} \leq 2\lambda \\ 0, & x > 2\lambda \end{cases} \tag{15}$$

was chosen to reduce the computational burden of estimating R and Θ by removing radial separation values that are far enough to have any significant contribution to the likelihood

(13). In [22], it was shown that RSSI values from wireless tags that are more than 2λ separated are statistically independent rendering (4) and (5) to be zero. Therefore, substituting (12) for $f\left(\hat{\rho}_{ij}^{*}|r_{ij},\Theta_{ij}\right)$ in (14) gives (13). ■

Any radial separation vector R that maximizes (13) has the highest probability of being the true radial separation between tags. However, due to the non-injective nature of (4) that gives same RSSI correlation value for multiple values of radial separation between RFID tags, there will be multiple local maxima for (13). Therefore, to improve the chance of our localization algorithm converging to the global maxima of (13), we will constrain the range of the estimated parameters by assigning prior distributions.

The χ-distribution with three degrees of freedom called the Maxwell-Boltzmann distribution [23 pp.434] is a natural choice for the prior distribution of radial separations when RFID tags are assumed to be positioned normally distributed around the localization coordinate system origin. Therefore, $f\left(r_{ij}\right)\sim\chi_3(\sigma_r)$ where r_{ij} is the radial distance estimate between tag i and j, σ_r is the unknown mode parameter the controls the spread of RFID tags around the coordinate system origin. Further, to simplify the estimation, we will assume that the localization workspace is small enough to result in backscattered signals from all the tags to have more or less similar backscattered concentration i.e. $\delta_{\mathrm{ij}}^{\theta}=\delta^{\theta}=\mathrm{constant}$ where δ_{ij}^{θ} is the concentration of backscattered signals from tags i and j. Finally, for tag orientation, a non-informative uniform prior distribution is assumed. These prior distributions increases the chance of (13) converging to a global maxima while transforming the likelihood function in to a posterior distribution of the unknown radial separations and tag reader orientation as shown in the next Lemma.

Lemma 3: (*Posterior Distribution of Radial Separations and Tag Reader Orientations*) Given the vector of sample pair-wise RSSI correlation values (Ω) and backscattered concentration $\left(\delta^{\theta}\right)$ at a workspace, the posterior distribution of the RFID tag radial separations (R) and tag reader orientation (Θ) in a workspace with $M \geq 3$ RFID tags is given by

$$f\left(R,\Theta|\Omega,\delta^{\theta}\right) \propto \frac{\exp\left\{-\frac{b}{2\sigma_r^2}\right\}}{\sigma_r^{(2a+1)}} \prod_{i=1}^{M}\prod_{j>i}^{M}\left\{\left[\frac{\mathrm{r}_{\mathrm{ij}}^2}{\Phi_{\mathrm{N}}\left(\frac{1-\rho_{ij}}{\sigma_{\rho_{ij}}}\right)\sigma_{\rho_{ij}}\sigma_r^3}\right]^{w_{ij}} \exp\left(-w_{ij}\left[\frac{\left(\hat{\rho}_{ij}^{*}-\rho_{ij}\right)^2}{2\sigma_{\rho_{ij}}^2}+\frac{r_{ij}^2}{2\sigma_r^2}\right]\right)\right\} \quad (16)$$

where $\hat{\rho}_{ij}^{*}$ is the sample RSSI correlation value estimated by the tag reader from N_p backscattered RSSI values of tag i and j as in (10), ρ_{ij} is the RSSI correlation value given by (4), $\Omega = \left\{\hat{\rho}_{ij}^{*}; j > i; i,j \in 1,2,\cdots,M\right\}$ is the vector of sample RSSI correlation values, $R = \left\{r_{ij}; j > i; i,j \in 1,2,\cdots,M\right\}$ is the vector of radial separations between RFID tags, $\Theta = \left\{\Theta_{ij}; j > i; i,j \in 1,2,\cdots,M\right\}$ is the vector of tag reader orientations for RFID tag pairs and δ^{θ} is the backscattered concentration at the workspace.

Proof: Refer to the appendix. ■

To evaluate (16), sample values for mode parameter σ_r have to be generated from its full conditional distribution. From (16), the full conditional distribution of σ_r is given by $f\left(\sigma_r|r_{ij}\right) \propto \frac{\exp\left\{-\frac{b+\sum_{i=1}^{M}\sum_{j>i}^{M} w_{ij}r_{ij}^2}{2\sigma_r^2}\right\}}{\sigma_r^{(2a+1)+3\sum_{i=1}^{M}\sum_{j>i}^{M} w_{ij}}}$ which is a square root inverted gamma distribution as $SIG\left(a+\frac{3}{2}\sum_{i=1}^{M}\sum_{j>i}^{M} w_{ij}, b+\sum_{i=1}^{M}\sum_{j>i}^{M} w_{ij}r_{ij}^2\right)$. Since SIG is related to the Gamma distribution, Gibbs sampling [25] using $Gamma\left(a+\frac{3}{2}\sum_{i=1}^{M}\sum_{j>i}^{M} w_{ij}, \frac{2}{b+\sum_{i=1}^{M}\sum_{j>i}^{M} w_{ij}r_{ij}^2}\right)$ is used to generate sample values for the mode parameter. When there is very little

information available beforehand, a small a (> 0.5) is used while b is selected such that mean of $SIG(a,b)$ matches the sample radial separation standard deviation i.e.

$$b = \frac{2}{M(M-1)}\left[\frac{\Gamma(a)}{\Gamma\left(a-\frac{1}{2}\right)}\right]^2 \sum_{i=1}^{M}\sum_{j>i}^{M} r_{ij}^2 \tag{17}$$

where $\Gamma(\cdot)$ is the Gamma function [15 pp.255].

We will now apply triangle inequality to ensure that the radial separation generated by solving (16) in a workspace with $M \geq 3$ passive RFID tags lead to valid Cartesian coordinates $\eta_i = \{\eta_{ix}, \eta_{iy}, \eta_{iz}\}^T; i \in \{1,2,\cdots,M\}$ for the RFID tags.

Lemma 4: (*Radial Separation and Triangle Inequality*): In a workspace with $M \geq 3$ RFID tags, any three valid radial separation estimates between tags should satisfy the triangle inequality.

Proof: Assume a workspace with *M* RFID tags as in Figure 2. Let η_i, η_j and η_k be the Cartesian coordinates of any three tags in this workspace such that $r_{ij} = \|\eta_i - \eta_j\|$, $r_{ik} = \|\eta_i - \eta_k\|$and $r_{jk} = \|\eta_j - \eta_k\|$ are the true radial separation between the tags and $r_{jk} \geq r_{ik}, r_{ij}$.

As long as $\eta_i \neq \eta_j \neq \eta_k$ then η_i, η_j and η_k define a 2D plane and form the vertices of a triangle with sides r_{ij}, r_{ik} and r_{jk}. In Euclidean space, the sides of a triangle satisfy the following triangle inequality

$$r_{ij} + r_{ik} - r_{jk} > 0 \tag{18}$$

Hence any three radial separation estimates by the tags that violate (18) cannot be part of an Euclidean space. ■

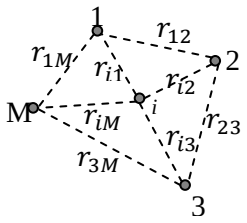

Fig 2. Tags in a workspace with radial distance shown in dotted lines

The metric for evaluating violations of triangular inequality for radial separation r_{ij}, r_{ik} and r_{jk} between tags *i*, *j* and *k* is given by

$$\beth_{ijk} = \left(\frac{r_{jk}}{r_{ij}+r_{ik}}\right)\left(1 + r_{jk} - r_{ij} - r_{ik}\right): r_{jk} \geq r_{ik}, r_{ij}. \quad (19)$$

This metric was first proposed in [26] for validating round trip delays measured between networked PCs. Valid triangles in Euclidean space have $\beth_{ijk} \leq 1$ while a value greater than 1 imply invalid triangle since the radial distances do not satisfy triangle inequality. Higher the value of $\beth_{ijk}$, the worse is the triangle inequality violation.

Now from Lemmas 1 and 2, the objective function for localization can be derived in Theorem 3.

Theorem 3: (*Objective Function for Localization*) The objective function for the purpose of estimating radial separation (R), tag orientation (Θ) between RFID tags from pair wise RSSI correlation measured at a tag reader is given by

$$L\left(R, \Theta, \Xi\,|\Omega, \delta^{\theta}\right) = \log_{\mathrm{e}} f\left(R, \Theta|\Omega, \delta^{\theta}\right) - \sum_{i=1}^{M}\sum_{j>i}^{M}\sum_{\substack{k>i \\ j\neq k}}^{M} \xi_{ijk}\left(\beth_{ijk} - 1\right). \quad (20)$$

where $\Omega = \left\{\hat{\rho}_{ij}^{*}; i > j\right\}; i, j \in \{1,2,\cdots,M\}$ is the vector of sample RSSI correlation values, $\hat{\rho}_{ij}^{*}$ is the sample RSSI correlation value estimated by the tag reader from N_p backscattered RSSI values of tag i and j and δ^{θ} is the backscattered concentration at the

workspace, $\xi_{ijk} \geq 0$ are the individual Lagrange multipliers and $\Xi = \{\xi_{ijk}; j > i, k > i, j \neq k\}$ is the vector of Lagrange multipliers that are to be estimated to satisfy triangle inequality constraint.

Proof: The MLE of unknown radial separation from pair wise RSSI correlation values from a workspace with *M* RFID tags is the radial separation values that maximize log-posterior distribution in Lemma 3 provided the triangular inequality in Lemma 4 is satisfied. Hence this constrained optimization problem is converted to an unconstrained optimization problem using the Lagrange multiplier as (20). ■

For M tags in a workspace there are $N_r = \frac{M(M-1)}{2}$ radial separation and tag orientation parameters to be estimated. In addition, there are $N_\xi = {}^{M}C_3 = \frac{M(M-1)(M-2)}{6}$ triangle inequality constraints, formed by selecting any 3 tags from *M* tags, that need to be satisfied. Even for moderate values of *M*, the total number of parameters that are to be optimized for (20) increases as $O(M^3)$ which could be prohibitively time consuming to converge. However, most of the triangles formed by selecting radial distances between any 3 tags from *M* tags overlap or intersect with one another as shown in Figure 3.1.

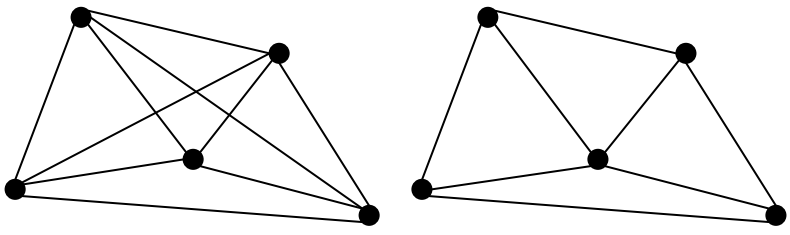

(1) 10 Triangles (2) 4 Triangles

Fig 3. Possible set of triangles used as constraints for (16)

Overlapping triangles are duplicating the same constraint and consequently there is no additional information being gleaned from satisfying these triangle inequality constraints. A unique set of constraints can be ensured by selecting non-overlapping/non-intersecting triangles as in Figure 3.2. One technique to achieve this is to divide the polyhedron formed by *M* tags into tetrahedrons using 3D Delaunay triangulation resulting in at the most $O\left(M^{\lceil 1.5 \rceil}\right)$ tetrahedrons [27]. Subsequently, group the 4 triangular faces of each tetrahedron into a list that contains only unique list of triangles. This changes the parameter count increase as $O(M^2)$ thereby improving the convergence speed of (20).

Next the constrained optimization algorithm that maximizes (20) is introduced

4.3 STOCHASTIC CONSTRAINED OPTIMIZATION

To compute the maximum for a non-convex function as in (20) using nonlinear optimization techniques such as Newton-Raphson require an initial value to be located within the region of attraction of global maximum. Under these initial conditions, the movement in the direction of steepest gradient will result in a local maximum, while occasional movement away from local maxima is needed. Hence, stochastic optimization using Markov Chain Monte Carlo (MCMC) method called Constrained Simulated Annealing (CSA) is used. Primary reason for choosing simulated annealing over other stochastic optimization techniques is its guaranteed convergence in asymptotic time [28]. Details about CSA and steps for initialization are specified in [29]. CSA is a variant of the popular Simulated Annealing (SA) optimization. For optimizing (20), CSA looks for saddle points (local maxima) that occur at the local maxima in radial distance space and local minima in Lagrange multiplier space. Hence there are separate acceptance functions for radial separation and Lagrange multiplier space to account for their different optimization objectives.

From localization simulation runs, a large amount of iterations of CSA were spent in traversing from one local maximum to another even though there is no better solution between these two maxima. This is due to highly uneven terrain of the cost function which includes several closely spaced local maxima separated by deep trenches as in Figure 4.

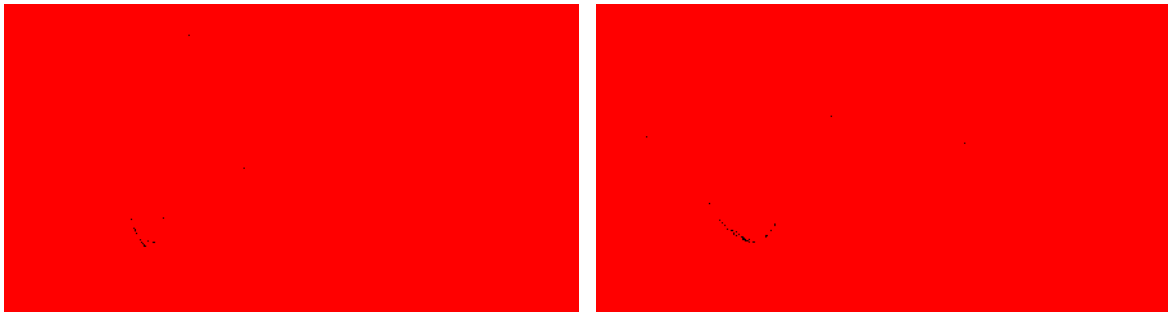

(1) Frequency = 20MHz (2) Frequency = 10MHz

Fig 4. Terrain of (16) at various frequencies under NLoS conditions

In [30], this was solved using tunneling function given by

$$f_{STUN}(R, \Theta, \Xi) = \exp\{\gamma(L(R, \Theta, \Xi|\Omega, \delta^{\theta}) - L_{max})\} \quad (21)$$

where $L(R, \Theta, \Xi|\Omega, \delta^{\theta})$ is given by (20), L_{max} is the highest value of (20) encountered so far and $\gamma > 0$ is the amplifying factor. By continuously adjusting L_{max} (21) maps the entire region up to L_{max} onto the interval [0, 1] while amplifying regions above L_{max} using γ as shown in Figure 5.

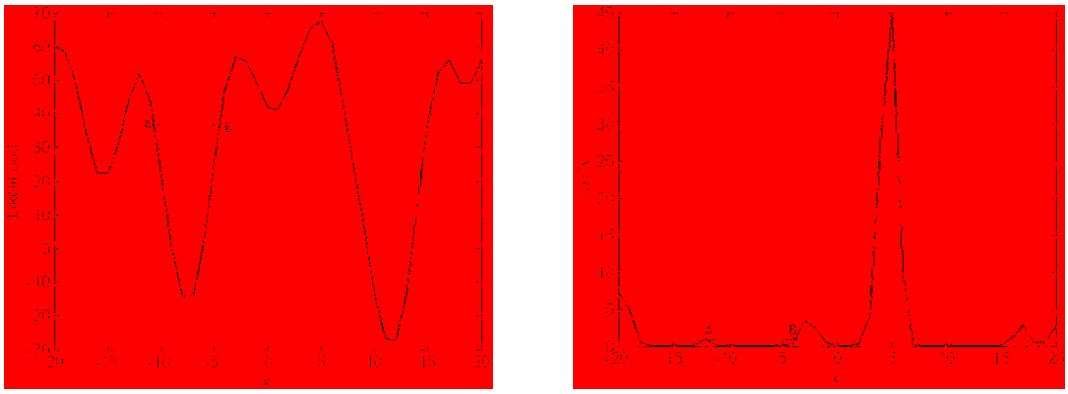

(1) Before tunneling transformation (2) After tunneling transformation

Fig 5. Tunneling effect on cost function

Finally, the output from CSA is converted to Cartesian coordinates using dimensionality reduction algorithms such as classical MDS or LLE which are then re-oriented to a global reference using known locations of anchor nodes as explained in next section.

4.4 ANCHOR NODE PLACEMENT

Anchor nodes are used to re-orient the RFID tag locations obtained during the stochastic optimization search process to a global coordinate system defined by the known locations of the anchor nodes. This translation is required as the radial distances between tags are invariant to translation and rotation of the localization workspace. Therefore, to perform this re-orientation, 6 parameters (the 3 Euler rotation angles that define rotation around x, y and z axis and three element translation vector that defines translation in x, y and z axis) has to be inferred. In [31], this problem was solved by formulating a least-square form of relationship between anchor node locations in the two coordinate systems as

$$\eta_i = \hat{\eta}_i R + T + N_i. \quad (22)$$

where $\hat{\eta}_i$ and η_i are the location of the i^{th} anchor node in global coordinate system and the stochastic search process output respectively, R is the 3D-rotation matrix defined by Euler angles, T is the translation vector and N_i are the noise terms. Since there are six parameters to be inferred, the least-square problem will be an undetermined system if the number of anchor nodes is less than six. This essentially defines the lower limit for the number of anchor nodes in a 3D localization problem. In addition, the variance of the estimated parameters is dependent on the stability of the following matrix inverse $(\hat{\eta}\hat{\eta}^T)^{-1}$ where $\hat{\eta} = [\hat{\eta}_1, \hat{\eta}_2, \cdots, \hat{\eta}_M]$ represent the global Cartesian coordinates of the anchor nodes and M is the number of anchor nodes. Therefore, to reduce the variance of the estimated rotation/translation parameters the options available are to increase the number of anchor nodes (M) or increase the spread of the location of anchor nodes $\hat{\eta}$ so that the determinant $\det(\hat{\eta}\hat{\eta}^T)$ is as large as possible. However, increasing the number of RFID tags (both anchor nodes and unknown tags) increases the computation overhead during the stochastic search step since this increases the number of parameters for radial separation to be estimated, which in turn results in more time to converge to a global solution.

Now we will present flow chat of the proposed LOCUST algorithm

5. LOCUST ALGORITHM

For a workspace with M RFID tags, the LOCUST algorithm can be described by the flow chart in Figure 6.

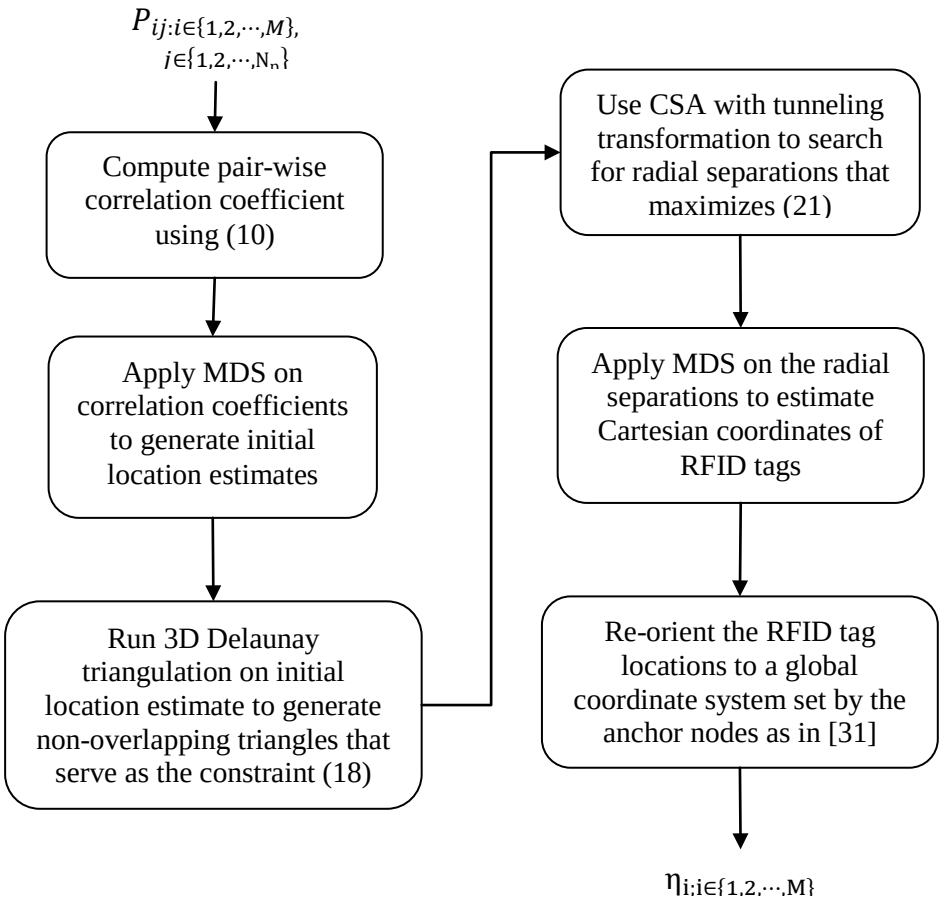

Fig 6. Flow chart of the proposed localization scheme

The LOCUST algorithm starts with the measurement step where the tag reader collects N_p RSSI measurements from each of the M RFID tags in the localization workspace. The $M \times N_p$ power measurement matrix P_{ij} forms the input to the initialization step where pair-wise correlation coefficients are computed using (12) resulting in an $M \times M$ matrix of backscattered correlation coefficients $\hat{\rho}^*_{ij}; i, j \in \{1,2,\cdots,M\}$. Subsequently, MDS algorithm is applied on $\hat{\rho}^*_{ij}$ matrix and the 3D tag locations resulting from MDS are re-oriented to a global coordinate system defined by the known location of anchor nodes. These initial RFID location points forms the input to

a 3D Delaunay triangulation algorithm that generates a list of non-overlapping triangles which are used to generate the triangular inequality constraints (18). Now the LOCUST performs the stochastic search step where CSA and tunneling transformation algorithm are used to search through the domain of radial distance values between RFID tags that will maximizes (21). Finally, the radial distance estimates from stochastic search step forms the input to the MDS algorithm that generates 3D Cartesian coordinates for the RFID tags which are once again re-oriented to a global reference system.

Now we will present the localization results from MDS [8], LLE [11] and LOCUST for multiple frequencies.

6. RESULTS AND ANALYSIS

This section compares the performance of LOCUST with MDS [8] and LLE [11] based localization through simulations for m=8 tags and n=8 anchor nodes in a 20m x 20m x 20m workspace. The anchor nodes were placed at the vertices of this cubical workspace whereas the RFID tags were positioned randomly using uniform distribution within this cubical workspace. The tag reader was positioned outside the cubical workspace along the X axis at (25m, 0, 0). The true radial separation and azimuth angles for each RFID tag pair are then used to calculate the true value of ρ_{12} between them using (4). For NLoS conditions the true values for ρ_{12} were obtained using the simplified form (5) that only requires radial separation between the tags.

The 16×16 RSSI correlation matrix with estimation noise was simulated by generating double truncated normal random variables with mean (ρ) given by (4) and variance given by $\sigma_{\rho}^{2} = \frac{2\rho}{N_p}$ for $N_p = 100$ RSSI samples. This correlation matrix is then passed to the CSA algorithm which output a 16×16 radial separation matrix that

maximizes (21). Finally, this radial separation estimate matrix forms the input to MDS algorithm which generates 3D Cartesian coordinates that are then re-oriented to a global reference using anchor nodes as in [31]. Total of 50 Monte Carlo simulation trials were performed for each method under LoS and NLoS conditions to determine the mean, median, std. dev and 90th percentile of localization errors. Figure 7.1 shows the CDF plot of localization errors when tags are operating at 20MHz under NLoS condition $(\delta^{\theta} = 0)$ while Figure 7.2 shows the same localization error under moderate LoS conditions $(\delta^{\theta} = 4)$.

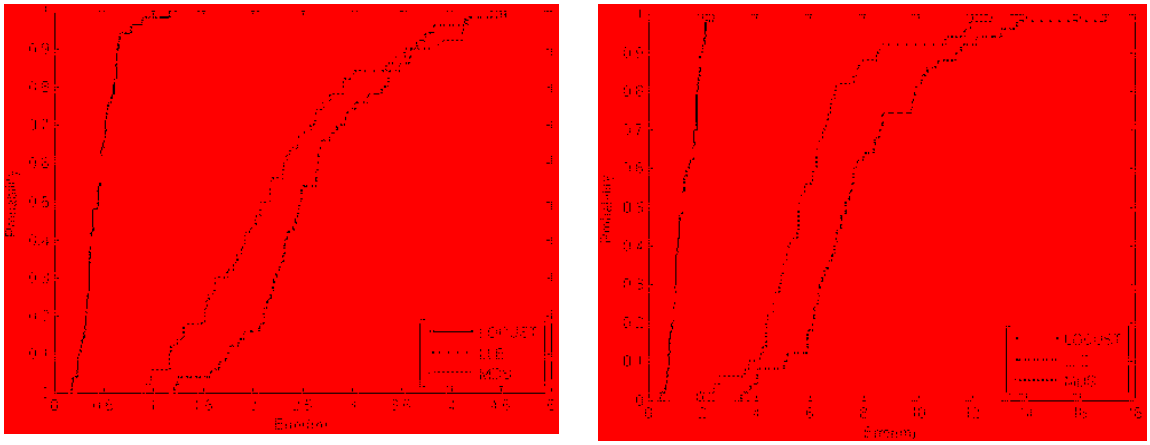

(1) $\delta^{\theta} = 0$ (2) $\delta^{\theta} = 4$

Fig 7. CDF of localization error at 20MHz

Simulations were repeated for 60 KHz, 1 MHz, 2.5 MHz, 5 MHz, 10 MHz and 15 MHz to study the effect of operating frequency on localization error. Table I lists localization error statistics for MDS, LLE and LOCUST under NLoS while Table II lists the localization errors under LoS conditions. From the results, at frequencies ($f \leq 5$MHz)

the performance of all three localization methodologies were similar. This was expected since the radio wavelength at these frequencies were larger than the largest radial separation between tags resulting in ρ_{ij} being almost linear with r_{ij}. However at frequencies above 5 MHz, LOCUST performed better than MDS and LLE. In particular at 20MHz, MDS and LLE have very large localization errors. This could be attributed to the highly non-linear terrain of the posterior log-likelihood function (16) at higher frequencies thereby rendering linearity assumptions made by LLE and MDS inaccurate whereas LOCUST makes no such linearity assumptions and uses numerical optimization methods to find the radial separations that maximizes (21).

TABLE 1. SUMMARY OF NLOS LOCALIZATION ERROR LEVELS $\left(\delta^{\theta} = 0\right)$

Method	F (MHz)	Localization Error (m)			
		Mean	Median	90th percentile	Std. dev.
LOCUST	20.0	0.454	0.429	0.676	0.172
LLE		2.764	2.67	4.095	0.949
MDS		2.272	2.136	3.378	0.778
LOCUST	15.0	0.343	0.331	0.518	0.127
LLE		1.009	0.969	1.507	0.351
MDS		0.935	0.889	1.429	0.375
LOCUST	10.0	0.233	0.230	0.307	0.056
LLE		0.248	0.245	0.326	0.06
MDS		0.194	0.192	0.263	0.05
LOCUST	5.00	0.201	0.189	0.322	0.09
LLE		0.270	0.260	0.396	0.10
MDS		0.194	0.186	0.308	0.086
LOCUST	2.50	0.195	0.191	0.283	0.066
LLE		0.187	0.180	0.272	0.063
MDS		0.202	0.195	0.286	0.062
LOCUST	1.00	0.111	0.103	0.177	0.048
LLE		0.198	0.191	0.291	0.07
MDS		0.127	0.117	0.197	0.062
LOCUST	0.06	0.105	0.099	0.164	0.048
LLE		0.202	0.197	0.289	0.066
MDS		0.177	0.165	0.281	0.072

TABLE 2. SUMMARY OF LOS LOCALIZATION ERROR LEVELS $(\delta^{\theta} = 4)$

Method	F (MHz)	Localization Error (m)			
		Mean	Median	90^{th} percentile	Std. dev.
LOCUST	20.0	1.359	1.259	1.943	0.485
LLE		7.90	7.318	11.382	2.652
MDS		6.019	5.609	8.486	2.238
LOCUST	15.0	0.850	0.804	1.179	0.268
LLE		2.866	2.831	3.818	0.874
MDS		2.92	2.566	4.923	1.490
LOCUST	10.0	0.696	0.702	1.067	0.286
LLE		1.684	1.657	2.509	0.599
MDS		1.722	1.652	2.383	0.513
LOCUST	5.00	0.274	0.243	0.469	0.135
LLE		0.542	0.500	0.791	0.201
MDS		0.477	0.434	0.786	0.207
LOCUST	2.50	0.236	0.227	0.323	0.066
LLE		0.198	0.179	0.287	0.061
MDS		0.192	0.192	0.256	0.059
LOCUST	1.00	0.131	0.114	0.278	0.060
LLE		0.189	0.185	0.177	0.059
MDS		0.118	0.112	0.159	0.041
LOCUST	0.06	0.154	0.170	0.216	0.057
LLE		0.213	0.189	0.327	0.081
MDS		0.178	0.173	0.261	0.062

Another interesting observation is that the accuracy of LOCUST degraded with frequency. This is more observable under LoS conditions. At higher frequencies, the ratio of radial separation to operating wavelength is larger resulting RSSI correlation (4) having values close to zero. This results in large estimation noise at the truncation boundaries leading to larger localization error. Additionally under increasing LoS condition and at higher frequencies, the terrain of (16) becomes highly uneven resulting in LOCUST spending considerable time navigating through local maxima and finally terminating prematurely after preset iterations at a local maximum. However, MCMC based stochastic optimization such as CSA is statistically guaranteed to converge to

global maximum with computation time [28]. Hence, theoretically, localization error of LOCUST can be improved at the expense of increased computation time.

Table III lists the change in localization accuracy when the number of anchor nodes is varied from 6 to 12 while keeping the number of unknown tags constant at 8.

TABLE 3. SUMMARY OF LOCALIZATION ERROR LEVELS FOR VARYING ANCHOR NODE COUNT AT F=5MHZ AND $\delta^{\theta} = 4$

Anchor Node Count	Localization Error (m)			
	Mean	Median	90th percentile	Std. dev.
6	0.486	0.432	0.713	0.253
7	0.354	0.378	0.693	0.173
8	0.293	0.278	0.492	0.142
9	0.223	0.244	0.454	0.119
10	0.215	0.210	0.431	0.113
11	0.220	0.216	0.441	0.121
12	0.236	0.225	0.469	0.136

The localization accuracy improved when anchor node count was increased from six to ten whereas it started decreasing for anchor node counts eleven and twelve. This may be explained due to the final condition used for LOCUST. The current implementation of LOCUST employs a heuristic rule in [29] that terminates this algorithm after preset iterations. This could result in premature termination of LOCUST when the number of radial distances to be estimated is quite large. For the simulation run with twelve anchor nodes, there are 200 radial separations to be estimated which would result in LOCUST algorithm not being able to explore (21) thoroughly for optimal radial separations resulting in the observed degradation in localization accuracy.

Essentially, LOCUST algorithm converts the non-convex terrain of likelihood function of correlation coefficients between RFID tags to a convex likelihood function of radial separations between RFID tags. Hence the added computation complexity of LOCUST comes from navigating through local maxima of the (21) and as such is much slower than greedy convex search algorithms used by MDS and LLE. In addition, LOCUST employs MDS or LLE to perform the initial translation from correlation coefficients to location estimates and in the final phase the translation from radial distance estimates to the RFID tag location estimates. Hence the computational complexity of LOCUST has to be at least twice that of MDS or LLE.

7. CONCLUSIONS

This paper proposes a novel stochastic localization algorithm called LOCUST where functional dependency between pair wise RSSI cross-correlation measured by a tag reader is used to infer the unknown location of the RFID tags. It was shown through simulations to exhibit lower localization errors than linear algorithms such as MDS and non-linear manifold learning algorithms such as LLE. Due to statistical guarantees of finding global maximum, the localization accuracy of LOCUST could be further improved at the expense of increased computation time.

REFERENCES

[1] R. Want, “An introduction to RFID technology,” *IEEE Pervasive Computing*, vol. 5, no. 1, pp. 25-33, Jan.-Mar. 2006.

[2] P. V. Nikitin, and K. V. S. Rao, “Theory and measurement of backscattering from RFID tags,” *IEEE Antennas and Propagation Magazine*, vol. 48, no. 6, pp. 212-218, Dec, 2006.

[3] C. Hillbrand, and S. Robert, “Shipment Localization Kit: An automated approach for tracking and tracing general cargo,” *Int. Conf. on the Management of Mobile Business*, pp.46, 9-11 July 2007.

[4] P.V. Nikitin, R. Martinez, S. Ramamurthy, H. Leland, G. Spiess, and K.V.S Rao, "Phase based spatial identification of UHF RFID tags," *IEEE Int. Conf. on RFID*, pp.102-109, 14-16, April 2010.

[5] M. Kim, and N. Chong, "Direction sensing RFID reader for mobile robot navigation," *IEEE Trans. on Automation Science and Engineering*, vol. 6, no. 1, Jan. 2009, pp. 44 – 54.

[6] Y. Park, J. W. Lee, and S. W. Kim, "Improving position estimation on RFID tag floor localization using RFID reader transmission power control," *IEEE Int. Conf. on Robotics and Biomimetics*, pp.1716-1721, Feb. 2009.

[7] M. R. Basheer, and S. Jagannathan, "R-Factor: A new parameter to enhance location accuracy in RSSI based real-time location systems," *Proc. of 6th Annual IEEE Commun. Soc. Conf. on Sensor, Mesh and Ad Hoc Commun. and Networks*, pp. 1-9, Jun. 2009.

[8] X. Ji, and H. Zha, "Sensor positioning in wireless ad-hoc sensor networks using multidimensional scaling," *23rd Annual Joint Conf. of IEEE Comp. and Commun. Soc.* , vol.4, pp. 2652- 2661, Mar. 2004.

[9] J. A. Costa , N. Patwari, and A. O. Hero, "Distributed weighted-multidimensional scaling for node localization in sensor networks," *ACM Trans. on Sensor Networks*, vol.2, No.1, pp.39-64, Feb. 2006.

[10] Y. Shang, W. Ruml, Y. Zhang, and M. P. Fromherz, "Localization from mere connectivity," *In Proc. of the 4th ACM int. Symposium on Mobile Ad Hoc Networking & Computing*, pp. 201-212, Jun. 2003.

[11] N. Patwari, and A. O. Hero, "Manifold learning algorithms for localization in wireless sensor networks," *Proc. of IEEE Int. Conf. on Acoustics, Speech and Signal Proc.*,vol.3,pp.857–860, May 2004.

[12] C. Wang, J. Chen, Y. Sun, and X. Shen, "Wireless sensor networks localization with Isomap," *IEEE Int. Conf. on Commun.*, Jun. 2009.

[13] J.N. Ash and R.L Moses, "On optimal anchor node placement in sensor localization by optimization of subspace principal angles," *Proc. of the IEEE Int. Conf. on Acoustics, Speech and Signal Processing*, pp. 2289 – 2292, April 2008.

[14] K. V. Mardia, and P. E. Jupp, Directional statistics, John Wiley and Sons, New York, 2000.

[15] M. Abramowitz, and I. Stegun, Handbook of mathematical functions, Dover, New York, 1968.

[16] C. Varin, and P. Vidoni, "Pairwise likelihood inference for general state space models," *Econometrics Reviews*, vol. 28, no. (1-2), pp. 170-185, September, 2009.

[17] C. Varin, N. Reid, and D. Firth, "An overview on composite likelihood methods," Statistica Sinica, 21, in press., 2011.

[18] G. L. Stuber, "*Principles of mobile communication*," Kluwer Academic Publishers, Boston, 1996.

[19] F. Downton, "Bivariate exponential distributions in reliability theory," *J. of The Royal Stat. Society*, vol. 32, pp. 408-417, 1970.

[20] S. Nadarajah, and S. Kotz, "Sums, products, and ratios for downton's bivariate exponential distribution,". *Stoch. Environ. Res. Risk Assessment*, vol. 20, no. 3, pp. 164–170, 2006.

[21] R. Fisher, "The truncated normal distribution," *British Association for the Adv. of Science, Mathematical Tables*, vol.5, pp.33-34, 1931.

[22] A. Ramachandran, and S. Jagannathan, "Spatial diversity in signal strength based WLAN location determination systems," *Proc. of the 32nd IEEE Conf. on Local Comp. Networks* , pp. 10-17, Oct. 2007.

[23] N. M. Laurendeau, Statistical Thermodynamics: Fundamentals and Applications, Cambridge Unversity Press, Cambridge, 2005.

[24] S. J. Wu, D. H. Chen, and S. T. Chen, "Bayesian inference for Rayleigh distribution under progressive censored sample," *Applied Stochastic Models in Business and Industry*, vol.22, no. 3, pp. 269-279, May 2006.

[25] A. E. Gelfand, A. F. M Smith, "Sampling-based approaches to calculating marginal densities," *Journal of the American Statistical Association*, vol. 85, no. 410 pp. 398-409, June 1990.

[26] S. Banerjee, T. G. Griffin, and M. Pias, "The interdomain connectivity of PlanetLab nodes," *In Passive and Active Measur. Workshop*, 2004.

[27] R. Seidel, "The upper bound theorem for polytopes: an easy proof of its asymptotic version," *Computational Geometry*, vol. 5, no. 2, pp. 115-116, September 1995.

[28] B. Gidas, "Non stationary markov chains and convergence of simulated annealing algorithms," *J. Stat. Physics*, vol.39, pp.73-131, Apr. 1985.

[29] B. W. Wah, Y. Chen, and T. Wang, "Simulated annealing with asymptotic convergence for nonlinear constrained optimization," *J. of Global Optimization*, vol. 39, no. 1, pp. 1-37, Sep. 2007.

[30] W. Wenzel, and K. Hamacher, "Stochastic tunneling approach for global minimization of complex potential energy landscapes," *American Physical Society*, vol. 82, no. 5, pp. 3003-3007, Apr. 1999.

[31] K. S. Arun, T. S. Huang, and S. D. Bolstein, "Least square fitting of two 3-d point sets," *IEEE Trans. Pattern Anal. Machine Intell.*, vol. PAMI-9, no. 5, pp. 698-700, Sep. 1987.

APPENDIX

Proof of Theorem 1 (*Joint Distribution of Backscattered RSSI*) Assume a tag reader is measuring backscattered RF signals from two RFID tags 1 and 2 that are separated by radial distance r_{12} as in Figure 8. In addition, let there be N radio obstacles such as walls or partitions in their environment which are scattering the radio signals. The complex form of the backscattered radio signals reaching the tag reader from tags 1 and 2 can be expressed as $Z_1 = X_1 + iY_1$ and $Z_2 = X_2 + iY_2$ respectively.

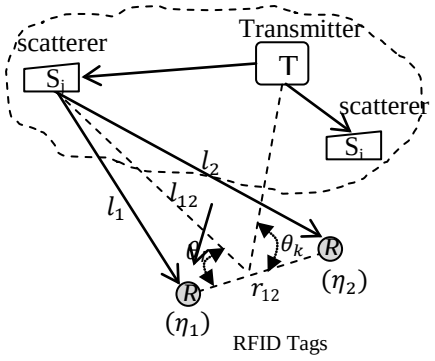

Fig 8. Scattering of radio waves by objects in the workspace before reaching the RFID tags 1 and 2

Assume that the relative velocity between the tag reader and RFID tags are small enough to render any Doppler frequency shifts to be negligible in comparison to the operating frequency (f), then the quadrature components (X_i, Y_i) of the incoming radio signals at the RFID tags can be represented as the sum of N multipath signals as

$$X_i = A_{ri} \sum_{j=1}^{N} \alpha_j \cos\left[2\pi f\left(t - T_j^i\right) + \varphi_j\right] \quad \text{(A1)}$$

$$Y_i = A_{ri} \sum_{j=1}^{N} \alpha_j \sin\left[2\pi f\left(t - T_j^i\right) + \varphi_j\right] \quad \text{(A2)}$$

where $A_{ri}: i \in \{1,2\}$ is the amplitude of the backscattered signal from ith tag, $\alpha_j: j \in \{1,2,\dots,N\}$ are IID (Independent and Identically Distributed) attenuation of the jth scattered signal, T_j^i is the backscattered signal arrival delay for the jth scattered signal from ith RFID tag and φ_j are the phase of the when it leaves the jth scatterer.

Since X_i and Y_i in (A1) and (A2) are the final composite sum of N IID random variables, therefore, central limit theorem dictates that X_i and Y_i converge in distribution to normal distributions [18] for large values of N (typically $N > 30$). Let $\mathbb{Q} = [X_1, Y_1, X_2, Y_2]^T$ represents the vector that contains this normal distributed signal components then the PDF of $\mathbb{Q}$ is multivariate normal distribution given by

$$f_{\mathbb{Q}}(q) = \frac{C_{\mathbb{Q}}}{|\Lambda|^{\frac{1}{2}}} \exp\left(-\frac{1}{2}(q^T \Lambda^{-1} q)\right) \quad \text{(A3)}$$

where $C_{\mathbb{Q}}$ is the normalization constant, $q = [x_1, y_1, x_2, y_2]^T$ is a value of $\mathbb{Q}$ and $\Lambda = E[\mathbb{Q}\mathbb{Q}^T]$ is given by

$$\Lambda = \begin{bmatrix} E[X_1X_1^T] & E[X_1Y_1^T] & E[X_1X_2^T] & E[X_1Y_2^T] \\ E[Y_1X_1^T] & E[Y_1Y_1^T] & E[Y_1X_2^T] & E[Y_1Y_2^T] \\ E[X_2X_1^T] & E[X_2Y_1^T] & E[X_2X_2^T] & E[X_2Y_2^T] \\ E[Y_2X_1^T] & E[Y_2Y_1^T] & E[Y_2X_2^T] & E[Y_2Y_2^T] \end{bmatrix}. \quad \text{(A4)}$$

Now $\mathrm{E}[\mathrm{X}_1\mathrm{Y}_1^{\mathrm{T}}] = \mathrm{E}[\mathrm{X}_2\mathrm{Y}_2^{\mathrm{T}}] = \mathrm{E}[\mathrm{Y}_1\mathrm{X}_1^{\mathrm{T}}] = \mathrm{E}[\mathrm{Y}_2\mathrm{X}_2^{\mathrm{T}}] = 0$ since the real and complex parts of the incoming signals are orthogonal to each other. In addition, let the average received energy be represented by μ_1 and μ_2 as $\frac{1}{2}\mu_1 \triangleq \mathrm{E}[\mathrm{X}_1\mathrm{X}_1^{\mathrm{T}}] = \mathrm{E}[\mathrm{Y}_1\mathrm{Y}_1^{\mathrm{T}}]$ and $\frac{1}{2}\mu_2 \triangleq \mathrm{E}[\mathrm{X}_2\mathrm{X}_2^{\mathrm{T}}] = \mathrm{E}[\mathrm{Y}_2\mathrm{Y}_2^{\mathrm{T}}]$. The covariance terms between the incoming signal amplitude components be represented by ϱ_{12} and ξ_{12} as $\frac{1}{2}\varrho_{12} \triangleq \mathrm{E}[\mathrm{X}_1\mathrm{X}_2^{\mathrm{T}}] = \mathrm{E}[\mathrm{X}_2\mathrm{X}_1^{\mathrm{T}}] = \mathrm{E}[\mathrm{Y}_1\mathrm{Y}_2^{\mathrm{T}}] = \mathrm{E}[\mathrm{Y}_2\mathrm{Y}_1^{\mathrm{T}}]$and $\frac{1}{2}\xi_{12} \triangleq \mathrm{E}[\mathrm{X}_1\mathrm{Y}_2^{\mathrm{T}}] = \mathrm{E}[\mathrm{Y}_1\mathrm{X}_2^{\mathrm{T}}] = -\mathrm{E}[\mathrm{X}_2\mathrm{Y}_1^{\mathrm{T}}] = -\mathrm{E}[\mathrm{Y}_2\mathrm{X}_1^{\mathrm{T}}]$ resulting in (A4) being simplified as

$$\Lambda = \frac{1}{2}\begin{bmatrix} \mu_1 & 0 & \varrho_{12} & \xi_{12} \\ 0 & \mu_1 & \xi_{12} & \varrho_{12} \\ \varrho_{12} & -\xi_{12} & \mu_2 & 0 \\ -\xi_{12} & \varrho_{12} & 0 & \mu_2 \end{bmatrix}. \quad \text{(A5)}$$

Inverse of matrix Λ is given by

$$\Lambda^{-1} = \frac{1}{2|\Lambda|^{\frac{1}{2}}}\begin{bmatrix} \mu_2 & 0 & -\varrho_{12} & -\xi_{12} \\ 0 & \mu_2 & -\xi_{12} & -\varrho_{12} \\ -\varrho_{12} & \xi_{12} & \mu_1 & 0 \\ \xi_{12} & -\varrho_{12} & 0 & \mu_1 \end{bmatrix} \quad \text{(A6)}$$

where $|\Lambda|$ is the determinant of matrix Λ. Square-root of the determinant of matrix Λ is given by

$$|\Lambda|^{\frac{1}{2}} = \frac{\mu_1\mu_2}{4}[1 - \rho_{12} + \tau_{12}], \quad \text{(A7)}$$

where ρ_{12} and τ_{12} denote the square of the signal amplitude correlation parameters, henceforth called the RSSI correlation parameters, which are given by

$$\rho_{12} = \frac{\varrho_{12}^2}{\mu_1\mu_2}, \quad \text{(A8)}$$

$$\gamma_{12} = \frac{\xi_{12}^2}{\mu_1 \mu_2}. \tag{A9}$$

Transforming the PDF of $\mathbb{Q}$ in (A7) to random vector $\mathcal{B} = [\mathrm{P}_1, \mathrm{P}_2, \Psi_1, \Psi_2]^{\mathrm{T}}$ where $\mathrm{P_i} = \mathrm{X_i X_i^T} + \mathrm{Y_i Y_i^T} : \mathrm{i} \in \{1,2\}$ and $\Psi_\mathrm{i} = \tan^{-1}\left(\frac{\mathrm{Y_i}}{\mathrm{X_i}}\right) : \mathrm{i} \in \{1,2\}$ are the instantaneous power and phase of the backscattered signals from tags, gives the PDF of $\mathcal{B}$ as

$$f_{\mathcal{B}}(b) = f_{\mathbb{Q}}\left(\sqrt{p_1}\cos\psi_1,\ \sqrt{p_1}\sin\psi_1, \sqrt{p_2}\cos\psi_2, \sqrt{p_2}\sin\psi_2\right) |J(b)| \tag{A10}$$

with $\mathrm{b} = [\mathrm{p}_1, \mathrm{p}_2, \psi_1, \psi_2]^{\mathrm{T}}$ denoting a realization of $\mathcal{B}$, while the Jacobian is given by

$$|J(b)| = \begin{vmatrix} \frac{\cos\psi_1}{2\sqrt{p_1}} & \frac{\sin\psi_1}{2\sqrt{p_1}} & 0 & 0 \\ 0 & 0 & \frac{\cos\psi_2}{2\sqrt{p_2}} & \frac{\sin\psi_2}{2\sqrt{p_2}} \\ -\sqrt{p_1}\sin\psi_1 & \sqrt{p_1}\cos\psi_1 & 0 & 0 \\ 0 & 0 & -\sqrt{p_2}\sin\psi_2 & \sqrt{p_2}\cos\psi_2 \end{vmatrix} = \frac{1}{4}. \tag{A11}$$

Setting (A6) for Λ^{-1} and (A7) for $|\Lambda|^{\frac{1}{2}}$ in (A3) and applying the result on (A10) renders the distribution for $\mathcal{B}$ as

$$f_{\mathcal{B}}(b) = \mathrm{C}_{\mathcal{B}} \exp\left\{-\frac{\frac{p_1}{\mu_1}+\frac{p_2}{\mu_2}}{(1-\rho_{12}+\gamma_{12})} + \sqrt{\frac{4p_1 p_2 \rho_{12}}{(1-\rho_{12}+\gamma_{12})^2 \mu_1 \mu_2}}\cos(\psi_1 - \psi_2)\right\} \tag{A12}$$

where $\mathrm{C}_{\mathcal{B}}$ is the normalization constant. Since the random vector $\mathcal{B}$ involves both instantaneous power and phase, the marginal joint distribution of power, $\mathrm{f_P}(\mathrm{p}_1, \mathrm{p}_2)$, can be obtained from $\mathcal{B}$ by integrating (A12) over the entire domain, $[0, 2\pi]$, of instantaneous phase random variables Ψ_1 and Ψ_2 as

$$f_P(p_1, p_2) = C_{\mathcal{B}} \exp\left(-\frac{\frac{p_1}{\mu_1}+\frac{p_2}{\mu_2}}{(1-\rho_{12}+\gamma_{12})}\right) \times \int_0^{2\pi}\int_0^{2\pi} \exp\left\{\sqrt{\frac{4p_1 p_2 \rho_{12}}{(1-\rho_{12}+\gamma_{12})^2 \mu_1 \mu_2}}\cos(\psi_1 - \psi_2)\right\} d\psi_1\, d\psi_2 \tag{A13}$$

Setting $\frac{1}{4\pi^2}\int_0^{2\pi}\int_0^{2\pi}\exp\{x\cos(\psi_1-\psi_2)\}\,d\psi_1\,d\psi_2 = I_0(x)$ as the zeroth order modified Bessel function of the first kind in (A13) results in the marginal joint distribution of RSSI values from co-located RFID tags as

$$f_P(p_1,p_2) = C_{\mathcal{B}}\exp\left(-\frac{\frac{p_1}{\mu_1}+\frac{p_2}{\mu_2}}{(1-\rho_{12}+\gamma_{12})}\right)I_0\left(\sqrt{\frac{4p_1\,p_2\rho_{12}}{(1-\rho_{12}+\gamma_{12})^2\mu_1\mu_2}}\right). \qquad (A14)$$

The normalization constant $C_{\mathcal{B}}$ can be found by integrating (A14) over the entire domain of P_1 and P_2 since $\int_0^\infty\int_0^\infty f_P(p_1,p_2)dp_1\,dp_2 = 1$. To find $C_{\mathcal{B}}$ let $A(p_2) = \int_0^\infty \exp\left(-\frac{p_1}{\mu_1(1-\rho_{12}+\gamma_{12})}\right)I_0\left(\sqrt{\frac{4p_1\,p_2\rho_{12}}{(1-\rho_{12}+\gamma_{12})^2\mu_1\mu_2}}\right)dp_1$ so that $\int_0^\infty\int_0^\infty f_P(p_1,p_2)dp_1\,dp_2 = C_{\mathcal{B}}\int_0^\infty \exp\left(-\frac{\frac{p_2}{\mu_2}}{(1-\rho_{12}+\gamma_{12})}\right)A(p_2)dp_2$. Applying a change of variables as $p_1 = x^2$ and setting $p = \frac{1}{\mu_1(1-\rho_{12}+\gamma_{12})}$ and $c = \sqrt{\frac{4p_2\rho_{12}}{(1-\rho_{12}+\gamma_{12})^2\mu_1\mu_2}}$ gives $A(p_2) = 2\int_0^\infty x\exp(-px^2)\,I_0(cx)dx$. From [20 Lemma 4], $A(p_2)$ can be computed as $\int_0^\infty x\exp(-px^2)\,I_0(cx)dx = \frac{1}{2p}\exp\left(\frac{c^2}{4p}\right)$ resulting in $A(p_2) = \mu_1(1-\rho_{12}+$ 712exppμ12ρ12μ21−ρ12+712. Therefore, $\int_0^\infty\int_0^\infty f_P(p_1,p_2)dp_1\,dp_2 = C_{\mathcal{B}}\mu_1(1-\rho_{12}+\gamma_{12})\int_0^\infty \exp\left\{-\frac{(1-\rho_{12})p_2}{\mu_2(1-\rho_{12}+\gamma_{12})}\right\}dp_2 =$ $C_{\mathcal{B}}\frac{\mu_1\mu_2(1-\rho_{12}+\gamma_{12})^2}{1-\rho_{12}} = 1$ resulting in $C_{\mathcal{B}}$ given by

$$C_{\mathcal{B}} = \frac{(1-\rho_{12})}{\mu_1\mu_2(1-\rho_{12}+\gamma_{12})^2} \qquad (A15)$$

Therefore setting (A15) for $C_{\mathcal{B}}$ in (A1) results in (3). ■

Proof of Corollary 1 (*RSSI Correlation Parameters*) Assume a local spherical coordinate system with its origin halfway between the RFID tags as shown in Figure 1. In

this coordinate system, assume that the j^{th} multipath component reflecting from a scatterer is oriented at an azimuth angle of θ_j and elevation angle of ϕ_j. The extra time the scattered radio signal from the j^{th} scatterer takes to reach the RFID tag 2 in comparison to tag 1 is given by $\Delta T_j^{12} = T_j^1 - T_j^2 = \frac{l_1 - l_2}{c}$ where $l_1 = \sqrt{l_{12}^2 \cos^2\phi_j + \frac{r_{12}^2}{4} + l_{12} r_{12} \cos\phi_j \cos\theta_j}$ and $l_2 = \sqrt{l_{12}^2 \cos^2\phi_j + \frac{r_{12}^2}{4} - l_{12} r_{12} \cos\phi_j \cos\theta_j}$. Assuming that the radial separation between tags is small enough to render $l_{12}\cos\phi_j \gg \frac{r_{12}}{2}$ then ΔT_j^{12} can be approximated as $\Delta T_j^{12} \approx \frac{r_{12}}{c}\cos\theta_j = \frac{\hat{r}_{12}}{2\pi f}\cos(\theta_j)$ where $c = f\lambda$ is the speed of radio waves. Hence from (A1) and (A2) the parameters $\mu_1, \mu_2, \varrho_{12}$ and ξ_{12} can be written as

$$\mu_1 = \mathrm{Var}(Z_1) = A_{r1}^2 E\left[\sum_{j=1}^{N}(\alpha_j)^2\right], \tag{A16a}$$

$$\mu_2 = \mathrm{Var}(Z_2) = A_{r2}^2 E\left[\sum_{j=1}^{N}(\alpha_j)^2\right], \tag{A16b}$$

$$\varrho_{12} = \{E[X_1 X_2^T] + E[Y_1 Y_2^T]\} = A_{r1}A_{r2}E\left\{\sum_{j=1}^{N}(\alpha_j)^2 cos(\hat{r}_{12}\, cos\,\theta_j)\right\}, \tag{A16c}$$

$$\xi_{12} = \{E[X_1 Y_2^T] - E[X_2 Y_1^T]\} = A_{r1}A_{r2}E\left\{\sum_{j=1}^{N}(\alpha_j)^2 sin(\hat{r}_{12}\, cos\,\theta_j)\right\}. \tag{A16d}$$

Assume that the tag reader is oriented at azimuth and elevation angle Θ_{12} and Φ_{12} respectively in the local spherical coordinate system formed between tags 1 and 2 as shown in Figure 1. In addition, the azimuth θ_j and elevation ϕ_j of the angle of arrival of jth backscattered signal PDF are given by (1) resulting in

$$f_\Theta(\theta|\Theta_{12}, \delta_{12}^\theta) = \frac{\exp\{\delta_{12}^\theta cos(\theta - \Theta_{12})\}}{2\pi I_0(\delta_{12}^\theta)}, \tag{A17}$$

$$f_{\Phi}\left(\phi|\Phi_{12},\delta_{12}^{\phi}\right)=\frac{\exp\left\{\delta_{12}^{\phi}\,cos(\phi-\Phi_{12})\right\}}{2\pi I_0\left(\delta_{12}^{\phi}\right)}. \tag{A18}$$

where $\delta_{12}^{\theta}\geq 0$ and $\delta_{12}^{\phi}\geq 0$ represents the concentration of backscattered signals around the tag reader azimuth and elevation orientation Θ_{12} and Φ_{12} respectively. The von Mises PDF used for (A17) and (A18) can handle both LoS and NLoS conditions between the tag reader and RFID tags by adjusting the value of concentration parameters δ_{12}^{θ} and δ_{12}^{ϕ}. Under NLoS conditions, a signal can reach the tags with equal probability from any angle i.e. the signals are highly dispersed $\left(\delta_{12}^{\theta}=\delta_{12}^{\phi}=0\right)$ resulting in Θ and Φ having uniform distributions whereas under good LoS conditions, signals are highly concentrated $\left(\delta_{12}^{\theta}\gg 1\text{ and }\delta_{12}^{\phi}\gg 1\right)$ around Θ_{12} and Φ_{12} resulting in Θ and Φ being normally distributed.

The fractional signal strength carried by the j^{th} backscattered signal reaching the tag at azimuth angle θ_j and elevation ϕ_j is given by $\left(\alpha_j\right)^2=f_{\Theta}\left(\theta_j|\Theta_{12},\delta_{12}^{\theta}\right)f_{\Phi}\left(\phi_j|\Phi_k,\delta_{12}^{\phi}\right)d\theta_j d\phi_j$ where $\alpha_j: j\in\{1,2,\dots,N\}$ are the IID attenuation factors as in (A1) and (A2). For large number of scatterers i.e. $N\rightarrow\infty$ in the workspace, the summation terms in (A16a) and (A16b) becomes $\sum_{j=1}^{N}\alpha_j^2=\int_0^{2\pi}f_{\Theta}\left(\theta_j|\Theta_{12},\delta_{12}^{\theta}\right)d\theta_j\int_0^{2\pi}f_{\Phi}\left(\phi_j|\Phi_k,\delta_{12}^{\phi}\right)d\phi_j=1$. Hence μ_1 and μ_2 can be simplified as

$$\mu_1=A_{r1}^2 \tag{A19a}$$

$$\mu_2=A_{r2}^2. \tag{A19b}$$

Similarly for large N, the summation terms in (A16c) can be written as $\sum_{j=1}^{N}\left(\alpha_j\right)^2\cos\left(\hat{r}_{12}\cos\theta_j\right)=$

$\int_0^{2\pi} f_\Theta(\theta_j|\Theta_{12},\delta_{12}^\theta)\cos(\hat{r}_{12}\cos\theta_j)\,d\theta_j \int_0^{2\pi} f_\Phi(\phi_j|\Phi_k,\delta_{12}^\phi)d\phi_j =$

$\int_0^{2\pi} f_\Theta(\theta_j|\Theta_{12},\delta_{12}^\theta)\cos(\hat{r}_{12}\cos\theta_j)\,d\theta$ and that of (A16d) can be written as

$\sum_{j=1}^{N}(\alpha_j)^2\sin(\hat{r}_{12}\cos\theta_j) =$

$\int_0^{2\pi} f_\Theta(\theta_j|\Theta_{12},\delta_{12}^\theta)\sin(\hat{r}_{12}\cos\theta_j)\,d\theta_j \int_0^{2\pi} f_\Phi(\phi_j|\Phi_k,\delta_{12}^\phi)d\phi_j =$

$\int_0^{2\pi} f_\Theta(\theta_j|\Theta_{12},\delta_{12}^\theta)\sin(\hat{r}_{12}\cos\theta_j)\,d\theta_j$. Therefore, the cross-correlated terms ϱ_{12} and ξ_{12} under von Mises distribution becomes

$$\varrho_{12} = \frac{\sqrt{\mu_1\mu_2}}{2\pi I_0(\delta_{12}^\theta)}\int_0^{2\pi}\exp\{\delta_{12}^\theta cos(\theta_j-\Theta_{12})\}cos[\hat{r}_{12}\,cos\,\theta_j]\,d\theta_j \quad \text{(A19c)}$$

$$\xi_{12} = \frac{\sqrt{\mu_1\mu_2}}{2\pi I_0(\delta_{12}^\theta)}\int_0^{2\pi}\exp\{\delta_{12}^\theta cos(\theta_j-\Theta_{12})\}sin[\hat{r}_{12}\,cos\,\theta_j]\,d\theta_j \quad \text{(A19d)}$$

Applying change of variable $\theta_j = \frac{\pi}{2}+\vartheta_j$ in (A19c, d) to make it pliable for integration results in

$$\varrho_{12} = \frac{\sqrt{\mu_1\mu_2}}{2\pi I_0(\delta_{12}^\theta)}\int_0^{2\pi}\exp\left\{\delta_{12}^\theta cos\left(\frac{\pi}{2}+\vartheta_j-\Theta_{12}\right)\right\}cos[\hat{r}_{12}\,sin\,\vartheta_j]\,d\vartheta_j \quad \text{(A20a)}$$

$$\xi_{12} = \frac{\sqrt{\mu_1\mu_2}}{2\pi I_0(\delta_{12}^\theta)}\int_0^{2\pi}\exp\left\{\delta_{12}^\theta cos\left(\frac{\pi}{2}+\vartheta_j-\Theta_{12}\right)\right\}sin[\hat{r}_{12}\,sin\,\vartheta_j]\,d\vartheta_j \quad \text{(A20b)}$$

The Jacobi-Anger expansion [15 pp.361] for $\exp\left\{\delta_{12}^\theta\cos\left(\frac{\pi}{2}+\vartheta_j-\Theta_{12}\right)\right\}$ is given by

$$exp\left\{\delta_{12}^\theta\,cos\left(\frac{\pi}{2}+\vartheta_j-\Theta_{12}\right)\right\} = \sum_{n=-\infty}^{\infty} I_n(\delta_{12}^\theta)\,exp\left[in\left(\frac{\pi}{2}+\vartheta_j-\Theta_{12}\right)\right]. \quad \text{(A21)}$$

Hence applying (A21) on (A20a) results in

$$\varrho_{12} = \frac{\sqrt{\mu_1\mu_2}}{2\pi I_0(\delta_{12}^\theta)}\sum_{n=-\infty}^{\infty} I_n(\delta_{12}^\theta)\,exp\left[in\left(\frac{\pi}{2}-\Theta_{12}\right)\right]\int_0^{2\pi}\exp(in\vartheta_j)\,cos[\hat{r}_{12}\,sin\,\vartheta_j]\,d\vartheta_j$$

$$= \frac{\sqrt{\mu_1\mu_2}}{4\pi I_0(\delta_{12}^\theta)}\sum_{n=-\infty}^{\infty} I_n(\delta_{12}^\theta)\,exp\left[in\left(\frac{\pi}{2}-\Theta_{12}\right)\right]$$

$$\times\left\{\int_0^{2\pi} exp(in\vartheta_j + i\hat{r}_{12}sin\vartheta_j)\,d\vartheta + \int_0^{2\pi} exp(in\vartheta_j - i\hat{r}_{12}sin\vartheta_j)\,d\vartheta_j\right\}$$

$$= \frac{\sqrt{\mu_1\mu_2}}{2I_0(\delta_{12}^{\theta})} \sum_{n=-\infty}^{\infty} I_n(\delta_{12}^{\theta})\, exp\left[in\left(\frac{\pi}{2} - \Theta_{12}\right)\right] J_n(\hat{r}_{12})\{i^{2n} + 1\}. \quad \text{(A22)}$$

Setting (A22) on (A8) results in $\rho_{12} = \left\{\sum_{n=-\infty}^{\infty} \frac{I_n(\delta_{12}^{\theta}) J_n(\hat{r}_{12}) \exp\left[in\left(\frac{\pi}{2} - \Theta_{12}\right)\right][i^{2n}+1]}{2I_0(\delta_{12}^{\theta})}\right\}^2 =$

$\left\{J_0(\hat{r}_{12}) + \frac{2}{I_0(\delta_{12}^{\theta})} \sum_{n=1}^{\infty} I_{2n}(\delta_{12}^{\theta})\, J_{2n}(\hat{r}_{12}) \cos(2n\Theta_{12}) \cos(n\pi)\right\}^2$ as in (4). Similarly, applying (A21) on (A20b) results in

$$\xi_{12} = \frac{\sqrt{\mu_1\mu_2}}{2\pi I_0(\delta_{12}^{\theta})} \sum_{n=-\infty}^{\infty} I_n(\delta_{12}^{\theta})\, exp\left[in\left(\frac{\pi}{2} - \Theta_{12}\right)\right] \int_0^{2\pi} \exp(in\vartheta_j)\, sin\left[\hat{r}_{12}\, sin\, \vartheta_j\right] d\vartheta_j$$

$$= \frac{-i\sqrt{\mu_1\mu_2}}{4\pi I_0(\delta_{12}^{\theta})} \sum_{n=-\infty}^{\infty} I_n(\delta_{12}^{\theta})\, exp\left[in\left(\frac{\pi}{2} - \Theta_{12}\right)\right]$$

$$\times \left\{\int_0^{2\pi} exp(in\vartheta_j + i\hat{r}_{12} sin\vartheta_j)\, d\vartheta_j - \int_0^{2\pi} exp(in\vartheta_j - i\hat{r}_{12} sin\vartheta_j)\, d\vartheta_j\right\}$$

$$= \frac{-i\sqrt{\mu_1\mu_2}}{2I_0(\delta_{12}^{\theta})} \sum_{n=-\infty}^{\infty} I_n(\delta_{12}^{\theta})\, exp\left[in\left(\frac{\pi}{2} - \Theta_{12}\right)\right] J_n(\hat{r}_{12})\{i^{2n} - 1\}. \quad \text{(A23)}$$

Setting (A23) on (A9) gives

$$\gamma_{12} = -\left\{\frac{1}{2I_0(\delta_{12}^{\theta})} \sum_{n=-\infty}^{\infty} I_n(\delta_{12}^{\theta}) \exp\left[in\left(\frac{\pi}{2} - \Theta_{12}\right)\right] J_n(\hat{r}_{12})[i^{2n} - 1]\right\}^2$$

$$= \left\{\frac{2}{I_0(\delta_{12}^{\theta})} \sum_{n=0}^{\infty} I_{2n+1}(\delta_{12}^{\theta}) J_{2n+1}(\hat{r}_{12}) \sin\left[(2n+1)\left(\frac{\pi}{2} - \Theta_{12}\right)\right]\right\}^2 \text{as in (5).} \quad \blacksquare$$

Proof of Lemma 1 (*Moments of RSSI product*) One can express

$$E(P_1^m P_2^n) = \frac{(1-\rho_{12})}{\mu_1\mu_2(1-\rho_{12}+\gamma_{12})^2} \int_0^{\infty} p_1^m \exp\left(-\frac{p_1}{\mu_1(1-\rho_{12}+\gamma_{12})}\right)$$

$$\times \int_0^{\infty} p_2^n \exp\left(-\frac{p_2}{\mu_2(1-\rho_{12}+\gamma_{12})}\right) I_0\left(\sqrt{\frac{4p_1\, p_2\rho_{12}}{(1-\rho_{12}+\gamma_{12})^2\mu_1\mu_2}}\right) dp_2\, dp_1. \quad \text{(A24)}$$

Setting $w^2 = p_2$ on (A24) results in

$$E(P_1^m P_2^n) = \frac{2(1-\rho_{12})}{\mu_1\mu_2(1-\rho_{12}+\gamma_{12})^2} \int_0^{\infty} p_1^m \exp\left(-\frac{p_1}{\mu_1(1-\rho_{12}+\gamma_{12})}\right)$$

$$\times \int_0^{\infty} w^{2n+1} \exp\left(-\frac{w^2}{\mu_2(1-\rho_{12}+\gamma_{12})}\right) I_0\left(\sqrt{\frac{4\, p_1\rho_{12}}{(1-\rho_{12}+\gamma_{12})^2\mu_1\mu_2}}\, w\right) dw\, dp_1 \quad \text{(A25)}$$

From [20] set $\int_0^\infty \mathrm{w}^{2\mathrm{n}+1} \exp\left(-\frac{\mathrm{w}^2}{\mu_2(1-\rho_{12}+\gamma_{12})}\right) \mathrm{I}_0\left(\sqrt{\frac{4\,\mathrm{p}_1\rho_{12}}{(1-\rho_{12}+\gamma_{12})^2\mu_1\mu_2}}\,\mathrm{w}\right)\mathrm{dw} = \frac{\mathrm{n}!}{2^1\mathrm{p}^{\mathrm{n}+1}} \exp\left(\frac{\mathrm{p}_1\rho_{12}}{\mu_1(1-\rho_{12}+\gamma_{12})}\right) \mathrm{L}_\mathrm{n}^0\left(-\frac{\mathrm{p}_1\rho_{12}}{\mu_1(1-\rho_{12}+\gamma_{12})}\right)$, where $\mathrm{L}_\mathrm{n}^\mathrm{v}(\cdot)$ is the Generalized Laguerre polynomial [15 pp.775], on (A24) resulting in

$$E(P_1^m P_2^n) = \frac{n!\mu_2^n(1-\rho_{12})}{\mu_1(1-\rho_{12}+\gamma_{12})^{1-n}} \times \int_0^\infty p_1^m \exp\left(-\frac{1-\rho_{12}}{\mu_1(1-\rho_{12}+\gamma_{12})}\mathrm{p}_1\right) L_n^0\left(-\frac{\rho_{12}}{\mu_1(1-\rho_{12}+\gamma_{12})}p_1\right) dP_1 \quad \text{(A26)}$$

From [20]

$$\int_0^\infty x^{\alpha-1}\, exp(-px)\, L_n^\zeta(cx)dx = \frac{\Gamma(\alpha)}{p^\alpha}\mathcal{P}_n^{(\zeta,\alpha-\zeta-n-1)}\left(1-\frac{2c}{p}\right) \quad \text{(A27)}$$

where $\Gamma(\cdot)$ is the gamma function [15 pp.255]. Hence setting $\mathrm{x} = \mathrm{p}_1$, $\alpha = \mathrm{m} + 1$, $\zeta = 0$, $\mathrm{p} = \frac{(1-\rho_{12})}{\mu_1(1-\rho_{12}+\gamma_{12})}$ and $\mathrm{c} = \frac{\rho_{12}}{\mu_1(1-\rho_{12}+\gamma_{12})}$ in (A27) and applying the result on (A26) results in (9). ■

Proof of Lemma 2 (*MoM Estimator for RSSI Correlation*): The first few population moments computed from (32) in Lemma 1 are

$$E(P_1) = \mu_1\left[1+\frac{\gamma_{12}}{1-\rho_{12}}\right]\mathcal{P}_0^{(0,1)}\left(\frac{1+\rho_{12}}{1-\rho_{12}}\right) = \mu_1\left[1+\frac{\gamma_{12}}{1-\rho_{12}}\right] \quad \text{(A28a)}$$

$$E(P_2) = \mu_2[1-\rho_{12}+\gamma_{12}]\mathcal{P}_1^{(0,-1)}\left(\frac{1+\rho_{12}}{1-\rho_{12}}\right) = \mu_2\left[1+\frac{\gamma_{12}}{1-\rho_{12}}\right] \quad \text{(A28b)}$$

$$E(P_1P_2) = \mu_1\mu_2\left[\frac{(1-\rho_{12}+\gamma_{12})^2}{(1-\rho_{12})}\right]\mathcal{P}_1^{(0,0)}\left(\frac{1+\rho_{12}}{1-\rho_{12}}\right) = \mu_1\mu_2\left[1+\frac{\gamma_{12}}{1-\rho_{12}}\right]^2(1+\rho_{12}) \quad \text{(A28c)}$$

$$E(P_1^2P_2^2) = 4(\mu_1\mu_2)^2\left[\frac{(1-\rho_{12}+\gamma_{12})^4}{(1-\rho_{12})^2}\right]\mathcal{P}_2^{(0,0)}\left(\frac{1+\rho_{12}}{1-\rho_{12}}\right)$$

$$= (\mu_1\mu_2)^2\left[1+\frac{\gamma_{12}}{1-\rho_{12}}\right]^4(1+4\rho_{12}+\rho_{12}^2). \quad \text{(A28d)}$$

From (A28a-c) it can be shown that $\rho_{12} = \frac{E(P_1P_2)}{E(P_1)E(P_2)} - 1$. Substituting the population moments with sample moments in $\rho_{12} = \frac{E(P_1P_2)}{E(P_1)E(P_2)} - 1$ results in the method of moments estimator for $\hat{\rho}_{12}$ from Np backscattered RSSI values measured at the tag reader as in (11). Since the range for $\hat{\rho}_{12}$ has to be between [0, 1], the estimator (11) has to be truncated resulting in correlation ρ_{12} estimate given by (10). ■

Proof of Theorem 2 (*Approximate PDF of RSSI Correlation*) For large values of N_p, the sample RSSI averages $\frac{1}{N_p}\sum_{i=1}^{N_p}(p_{1i})$ and $\frac{1}{N_p}\sum_{i=1}^{N_p}(p_{2i})$ from tags 1 and 2 can be assumed to be constants that equals the population average $E(P_1)$ and $E(P_2)$ respectively. Hence (11) can be approximated as $\hat{\rho}_{12} = \frac{\frac{1}{N_p}\sum_{i=1}^{N_p}(p_{1i}p_{2i})}{E(P_1)E(P_2)} - 1$. Let P_i represents the random variable corresponding to signal strength value for tag $i; i \in \{1,2\}$ with p_{ij} representing its realization at sample measurement instance $j; j \in \{1,2, \dots, N_p\}$. In addition, let $X = P_1P_2$ with $x_j = p_{1j}p_{2j}$ as its jth sample realization and $y = \frac{1}{N_p}\sum_{j=1}^{N_p} x_j$ the sample realization of random variable Y. From central limit theorem, the distribution of Y for large values of N_p is a normal distribution given by $f_Y(y) = \frac{\sqrt{N_p}}{\sigma_x}\phi\left(\frac{y-\mu_x}{\frac{\sigma_x}{\sqrt{N_p}}}\right)$ where $\mu_x = E(X) = E(P_1P_2) = E(P_1)E(P_2)(1 + \rho_{12})$ and $\sigma_x^2 = Var(X) = [E(P_1^2P_2^2) - E^2(P_1P_2)] = 2[E(P_1)E(P_2)]^2\rho_{12}$. Since $\hat{\rho}_{12} = \frac{\frac{1}{N_p}\sum_{i=1}^{N_p}(p_{1i}p_{2i})}{E(P_1)E(P_2)} - 1 = \frac{Y}{E(P_1)E(P_2)} - 1$, the distribution of $\hat{\rho}_{12}$ is normal with mean and variance given by $E(\hat{\rho}_{12}) = \frac{E(Y)}{E(P_1)E(P_2)} - 1 = \rho_{12}$ and $Var(\hat{\rho}_{12}) = \frac{Var(Y)}{[E(P_1)E(P_2)]^2} = \frac{2\rho_{12}}{N_p} = \sigma_{\rho_{12}}^2$. Therefore, the PDF of estimator $\hat{\rho}_{12}^*$ is a double truncated normal distribution [21] obtained by restricting the support of the PDF of $\hat{\rho}_{12}$

between [0, 1] resulting in $\left(\hat{\rho}_{12}^{*}|\mathrm{r}_{12},\Theta_{12},\delta_{12}^{\theta}\right)=\frac{1}{\sigma_{\rho_{12}}}\frac{\phi_{\mathrm{N}}\left(\frac{\left[\hat{\rho}_{12}^{*}-\rho_{12}\right]}{\sigma_{\rho_{12}}}\right)}{\left[\Phi_{\mathrm{N}}\left(\frac{1-\rho_{12}}{\sigma_{\rho_{12}}}\right)+\Phi\left(\frac{\rho_{12}}{\sigma_{\rho_{12}}}\right)-1\right]}\mathrm{I}_{[0,1]}(\hat{\rho}_{12}^{*})$.

However, $\Phi_{\mathrm{N}}\left(\frac{\rho_{12}}{\sigma_{\rho_{12}}}\right)=\Phi_{\mathrm{N}}\left(\frac{\mathrm{N_p}}{2}\right)\approx 1$ thereby simplifying the PDF of $\hat{\rho}_{12}^{*}$ as in (12). ■

Proof of Lemma 3 (*Posterior Distribution of Radial Separations and Tag Reader Orientations*) Likelihood function (13) can be transformed into posterior distribution using Bayes theorem by multiplying the likelihood function (13) with priors for the estimated parameters. As explained previously, $\delta_{\mathrm{ij}}^{\theta}=\delta^{\theta}=\text{constant}$, a non-information uniform prior distribution is used for tag orientation and for radial separation $\mathrm{f}\left(\mathrm{r_{ij}}\right)\sim\chi_3(\sigma_{\mathrm{r}})$.

The unknown mode parameter σ_{r} will be estimated during localization optimization runs using intermediate radial distance estimates. To account for error in estimating σ_{r} from intermediate radial distance values, Square-root Inverted Gamma distribution ($\mathrm{SIG(a,b)}$: $\mathrm{a}>0.5, b>0$) [24] conjugate prior distribution is assigned to σ_{r} i.e. $\sigma_{\mathrm{r}}^{-2}\sim\mathrm{Gamma}\left(\mathrm{a},\frac{2}{\mathrm{b}}\right)$. To ease the computation burden, radial distance prior distributions will be weighted as in (14) resulting in the posterior distribution function obtained by multiplying the likelihood (14) and the prior distribution of the radial separation as

$$\mathrm{f(R,\Theta|\Omega)}=\mathrm{f}(\sigma_{\mathrm{r}})\prod_{\mathrm{i=1}}^{\mathrm{M}}\prod_{\mathrm{j}>i}^{\mathrm{M}}\left[\mathrm{f}\left(\hat{\rho}_{\mathrm{ij}}^{*}|\mathrm{r_{ij}},\Theta_{\mathrm{ij}},\delta_{\mathrm{ij}}^{\theta}\right)\mathrm{f}\left(\mathrm{r_{ij}}\right)\right]^{\mathrm{w_{ij}}}. \qquad \text{(A29)}$$

In (A29) set $\mathrm{f}\left(\hat{\rho}_{\mathrm{ij}}^{*}|\mathrm{r_{ij}},\Theta_{\mathrm{ij}},\delta_{\mathrm{ij}}^{\theta}\right)$ as in (12), the equation for Maxwell-Boltzmann distribution in $\mathrm{f}\left(\mathrm{r_{ij}}\right)$ and the equation for square root inverted gamma distribution in $\mathrm{f}(\sigma_{\mathrm{r}})$ resulting in posterior distribution as (16). ■

IV. LOCALIZATION AND TRACKING OF OBJECTS USING CROSS-CORRELATION OF SHADOW FADING NOISE[1]

M. R. Basheer and S. Jagannathan

Abstract**—** *Multipath and shadow fading are the primary cause for positioning errors in a Received Signal Strength Indicator (RSSI) based localization scheme. While fading, in general, is detrimental to localization accuracy, cross-correlation and divergence properties of shadow fading residuals may be utilized to improve localization and tracking accuracy of mobile IEEE 802.15.4 transmitters. Therefore, this paper begins by presenting a stochastic filter that models the fast changing multipath fading as a mean reverting Ornstein-Uhlenbeck (OU) process followed by a Generalized Auto Regressive Conditional Heteroskedasticity (GARCH) filtering to isolate the slow changing shadow fading residuals from measured RSSI values. Subsequently, a novel wireless transmitter localization scheme that combines the measured cross-correlation in shadow fading residuals between adjacent receivers using a Student-t Copula likelihood function is proposed. However, the long convergence time for this highly non-convex copula function might render our method unsuitable for tracking applications. Therefore, we present a faster tracking method where the velocity and heading of a mobile transmitter are estimated from α −Divergence between shadow fading signals and an onboard gyroscope respectively. To bind the localization error in this tracking method, the transmitter location estimates are smoothed by a Bayesian particle filter. The performance of our proposed localization and tracking method is validated over simulations and hardware experiments.*

Keywords*: Bayes Filter, Copula Function, Divergence , GARCH , Maximum Likelihood , Ornstein-Uhlenbeck, Spatial Correlation, Shadow Fading.*

[1] Research Supported in part by GAANN Program through the Department of Education and Intelligent Systems Center. Authors are with the Department of Electrical and Computer Engineering, Missouri University of Science and Technology (formerly University of Missouri-Rolla), 1870 Miner Circle, Rolla, MO 65409. Contact author Email: mrbxcf@mail.mst.edu.

Nomenclature

Symbol	Description	Symbol	Description
M	Number of wireless receivers	ב	Dependency matrix between shadow fading residuals
$\eta_i = \{x_i, y_i\}^T$	x and y coordinates of i^{th} wireless receiver	$C(u_1, u_2, \dots, u_M, ב)$	Copula function acting on uniform random variables $u_i; i \in \{1,2,\cdots,M\}$ with dependency ב
$\eta_T = \{x_T, y_T\}^T$	x and y coordinates of wireless transmitter	$\mathcal{L}(z_s^1, z_s^2, \cdots, z_s^M \mid ב)$	Likelihood function of shadow fading residuals $z_s^i; i \in \{1,2\cdots,M\}$ with dependency ב
τ_m	Maximum path delay of scattered radio signals arriving at a receiver (For an IEEE 802.15.4 receiver this is the RSSI integration time)	ρ_{ij}	Cross-correlation in shadow fading residual between wireless receivers i and j
Z_s^i	Random variable representing the shadow fading residual at the i^{th} receiver	S_i	Elliptical scattering region surrounding receiver i and the transmitter
σ_s^2	Shadow fading variance	r_{ij}	Radial distance between receivers i and j
$M(S)$	Random variable representing the scatterer count within a region S in the localization workspace	r_i	Radial distance between transmitter and receiver i
ω	Scatterer such as pedestrian density per unit area	$c_{ς,ב}(\cdot)$	M-variate student-t copula density with $ς$ degree of freedom
N	Number of shadow fading residuals collected at a receiver to compute CDF	$D_\alpha(C_1 \| C_2)$	α-divergence of classifying a random variable X into groups C_1 or C_2
$\tilde{F}_i^N(z)$	Semi-parametric CDF of shadow fading residuals at i^{th} receiver	v_n	Velocity of mobile transmitter at n^{th} RSSI sampling instance
U_i, L_i	Upper and lower tail location parameters for shadow fading residuals at receiver i above/below which the Pareto distribution is used	ϕ_n	Heading of the mobile transmitter at n^{th} RSSI sampling instance
ζ_i	Pareto distribution shape parameter at receiver i	α_i^j	Attenuation introduced by i^{th} obstacle in the workspace on the radio wave that is reaching receiver j
ϑ_i	Pareto Distribution scale parameter at receiver i	$t_ς^{-1}(\cdot)$	Inverse CDF of a student-t distribution with degree of freedom $ς$

1. INTRODUCTION

Accurate estimation of an asset location is an important requirement for monitoring and control applications in a manufacturing environment. There are several methods for indoor localization but compared to angle or time-based methodologies, RSSI based localization algorithms have the advantage that any existing wireless hardware can seamlessly add the localization feature with just a software update [1]. However, periodic radio profiling of the target application area is a pre-requisite for achieving the desired localization accuracy [1].

The primary cause of localization error in RSSI-based algorithms is channel fading [2]. Fading can be either fast changing due to constructive/destructive interference caused by multipath radio signals or slow changing due to relevant radio obstructions in the path of the incoming radio signals called shadowing. Localization under multipath fading is particularly difficult due to the dependency of multipath fading statistics on Line of Sight (LoS) conditions between the receiver and the transmitter [3].

However, the authors in [4] have shown that by spatial averaging with a window of size 10λ, where λ is the wavelength of the radio signals, multipath effects can be removed from RSSI without degrading the underlying shadow fading effects. Therefore, this paper proposes a mean-reverting stochastic scheme called Ornstein-Uhlenbeck (OU) to model the RSSI values measured by each receiver so that the underlying shadow fading noise may be extracted as the long-term mean of the this process. Subsequently, the similarity in shadow fading noise observed by adjacent receivers is used to locate the position of the common transmitter.

Transmitter localization obtained from correlated noise measurements observed at adjacent receivers was investigated in [5]. However, the method relied on correlation between multipath fading noise which, as pointed out in [5], falls rapidly to zero within one wavelength of radial separation between the receiver and transmitter thereby limiting its applicability to frequencies less than $10MHz$.

In [6], shadow fading loss over a workspace was modeled as isotropic and wide-sense stationary Gaussian random field with zero mean and exponentially decaying spatial correlation. In this model, the net shadow fading loss between a transmitter and receiver is defined as the normalized line integral of this random loss field over the radial

distance separating the receiver and transmitter. However, wireless devices such as IEEE 802.15.4 transceiver, commonly used for indoor localization applications, computes RSSI as the squared sum of incoming signal amplitude over a window of time called the RSSI integration time [7]. This results in an elliptical scattering region surrounding the transmitter and receiver where any pedestrians or machinery traffic can affect the RSSI measured by the receiver. Therefore, the shadow fading loss for an IEEE 802.15.4 devices are more accurately measured by an area integral of the spatial loss field over this elliptical scattering region as opposed to the line integral proposed in [6]. Consequently, the shadow fading model used in [6] would result in underestimating the cross-correlation thereby causing a large localization error.

In [8-10], localization was treated as a dimensionality reduction problem where data sampled over time generates a point in a high dimensional space. Multi-Dimensional Scaling (MDS) scheme was used for dimensionality reduction to estimate location in [8]. However, linear relationship requirement between correlation coefficient and radial-distance in MDS severely restricts its applicability in a wireless environment where RSSI correlation is a highly nonlinear function of the radial distance [5] between receivers.

In [9, 10], centralized manifold learning (nonlinear dimensionality reduction) algorithms such as Isomap, Local Linear Embedding (LLE) and Hessian LLE are used for localization. In these approaches the linearity between the correlation measurement and radial distance is restricted to a small area containing K nearest neighbors. However, from [5], the linearity between RSSI and radial distance breaks downs even in the immediate vicinity for operating frequencies greater than 10MHz.

In an indoor environment, the slow changing shadow fading is caused by the presence of pedestrians or other relevant radio obstructions which partially or completely block the radio signal paths between the receiver and transmitter. While shadow fading can result in non-trivial localization errors, traditionally, it has been treated as sampling noise that is averaged out with large RSSI sample sets. On the contrary, the proposed localization scheme takes advantage of the shadow fading noise by measuring similarity in fading statistics experienced by adjacent receivers.

However, to derive an efficient and statistically consistent transmitter location using Maximum Likelihood Estimate (MLE) requires the realization of a likelihood function which incorporates all interdependencies between shadow fading loss and radial separation with a common transmitter at each receiver, which is a non-trivial task. Therefore, this paper borrows the Copula technique commonly used in financial statistics to approximate this likelihood function when only the marginal distributions (shadow fading noise distribution at each receiver) and their pair-wise inter-dependency (correlation coefficients) are available. The Cartesian location of the common transmitter in this scheme is found when this copula based likelihood function attains its maximum. However, due to the non-convex nature of this function, gradient descent algorithms such as Newton-Raphson will stop at a local maximum rather than the global maximum. Consequently, we have used a stochastic optimization technique called Simulated annealing with stochastic tunneling [5] to search through this uneven terrain for a transmitter location that will maximize this copula function.

Simulated annealing based stochastic optimization techniques are statistically guaranteed to converge to a solution at the expense of computation time [11]. However,

for continuous tracking of a mobile transmitter, this technique may not be practically realizable due to the slow position updates. Therefore, this paper proposes a faster tracking system in the second part of the paper that continuously estimates the speed of the mobile transmitter by measuring the α-divergence of RSSI values over time. An on-board heading sensor realized using gyroscope or antenna arrays in addition to the proposed α-divergence based speed estimation can result in a fully functional dead-reckoning based tracking system. Since dead-reckoning systems suffer from accumulation of position errors over time [12], a Bayesian particle filter is used to correct this drift by generating a series of possible location estimates, called particles, around the initial location estimate obtained from dead reckoning system. Subsequently, the filtered position is generated by taking a weighted average of the particles where the weights are provided by the copula likelihood function.

Our proposed tracking method can handle both mobile and stationary transmitters as it reverts to simulated annealing based localization algorithm when transmitter velocity estimates are zero. In addition, our method is particularly suited for transmitter localization in fading rich environment such as an indoor mall, laboratories or factory floors etc. since it takes into account the effect of pedestrian and machinery traffic near the vicinity of wireless devices.

The contributions of this paper include: a technique for extracting shadow fading residuals from RSSI values, derivation of the shadow fading cross-correlation in IEEE 802.15.4 receivers due to pedestrian traffic or obstacles, a localization technique that utilize this cross-correlation in shadow fading between adjacent wireless receivers to locate a transmitter, derivation of the relationship between α-divergence in shadow

fading residuals and transmitter velocity and finally a Bayesian particle filter that uses copula based cross-correlation likelihood function to limit accumulation of localization error over time.

The paper is organized as follows. Section 2 starts by presenting the localization problem as estimating the position of a transmitter from RSSI values measured by a set of receivers placed at known positions around the localization area. Subsequently, the shadow fading wireless channel model called the Geometrically Based Single Bounce Elliptical Model (GSBEM) is introduced. Next, background information of the Copula function used to create the cross-correlation likelihood function from shadow fading residuals at receivers is presented. Thereafter, the α-divergence method used for velocity estimation of a mobile transmitter is briefly discussed.

Section 3 introduces the proposed transmitter localization using shadow fading cross-correlation. The Subsection 3.1 starts with the Ornstein-Uhlenbeck (OU) stochastic filter that is used to extract shadow fading residuals from RSSI. Subsequently, the semi-parametric approach that uses a combination of empirical Cumulative Distribution Function (CDF) and Generalized Pareto Distribution (GPD) to model shadow fading distribution in an indoor environment is discussed. Subsection 3.2 derives the theoretical relation between shadow fading cross-correlation arising between a pair of IEEE 802.15.4 receivers and their radial separation from a common transmitter in Theorem 1. Subsection 3.3, combines the semi-parametric shadow fading distributions from subsection 3.1 and the cross-correlation between receivers derived in Subsection 3.2 using a student-t copula function to create the likelihood function which in turn is used to estimate transmitter position in Theorem 2.

Copula based likelihood function helps to overcome the linearity requirement between cross-correlation and radial distance as imposed in [8-10] by allowing non-Gaussian distributions of shadow fading residuals at the receivers. However, this improved accuracy comes at the cost of longer convergence time due to the stochastic optimization algorithm used in solving this highly non-convex copula based likelihood function which may not unsuitable for mobile transmitters. Therefore, Section 4 presents a tracking method for mobile transmitters where faster position updates are required. This section starts with dead reckoning based tracking methods that use the novel mobile transmitter velocity estimation from α-divergence of RSSI values which is given in Theorem 3. To prevent the accumulation of localization error over time, a Bayesian particle filter is proposed where the dead reckoning based position estimates are smoothed by the student-t copula based cross-correlation likelihood function derived in Section 3.3. Section 5 lists the steps involved in our proposed localization and tracking algorithm. Results and analysis are presented in Section 6 whereas Section 7 concludes the paper with a discussion about the proposed method, improvements and future work.

2. LOCALIZATION PROBLEM AND RELEVANT BACKGROUND INFORMATION

2.1 PROBLEM STATEMENT

Consider a network of M wireless receivers whose coordinates $\eta_i = \{x_i, y_i\}^T; i \in \{1,2,\dots,M\}$ are a priori known. These receivers are periodically receiving broadcast signals from a transmitter within the localization area whose coordinates $\eta_T = \{x_T, y_T\}^T$ are unknown. The localization problem considered in this paper is to infer the true location of a transmitter (η_T) from shadow fading correlation arising between adjacent receivers. The tracking problem considered in this paper is to continuously predict the

position and heading (ϕ) of the mobile transmitter over time from α-divergence and fading correlation.

Now we will present a brief background about shadow fading wireless model, Copula functions and α-divergence.

2.2 INDOOR WIRELESS PROPAGATION MODEL

This paper builds on a wireless propagation model called the Geometrically Based Single Bounce Elliptical Model (GBSBEM) [13] to derive the shadow fading correlation arising between adjacent receivers due to pedestrian traffic/obstacles in the area. The GBSBEM was originally proposed for modeling the angle of arrival (AoA) and time of arrival (ToA) of radio signals at a receiver with LoS conditions to the transmitter. However, GBSBEM has a useful ToA property that makes it particularly suited for modeling RSSI measured by an IEEE 802.15.4 transceiver.

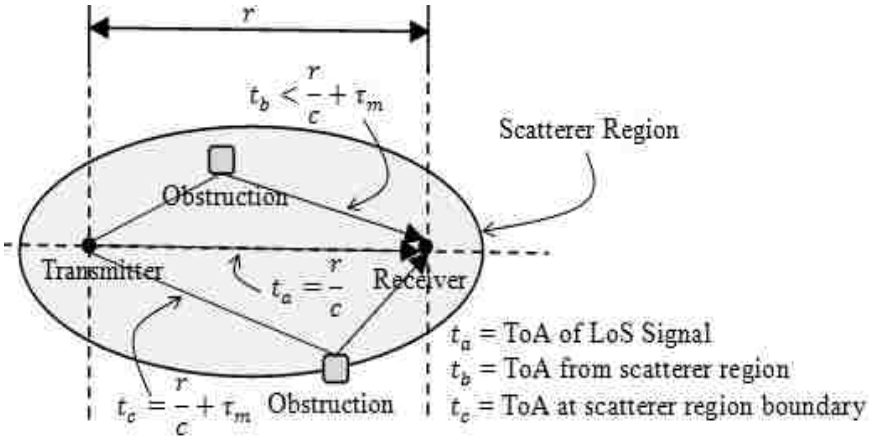

Fig 1. GBSBEM wireless channel model

In GBSBEM, any radio signal that reaches the wireless receiver after bouncing off of a scatterer in the localization region can affect signal fading if and only if its ToA (t) satisfies the following upper bound in t given by $t \leq \frac{r}{c} + \tau_m$ where r is the radial separation between the transmitter and receiver, c is the speed of radio waves, $\frac{r}{c}$ is the ToA of LoS signal and τ_m is the receiver specific maximum path delay for scattered signals. This upper bound in ToA for signals reaching the receiver defines an elliptical scattering region surrounding the transmitter and receiver, as shown in Figure 1, with the transmitter and receiver forming the foci and the major and minor axis of this ellipse are given by $r + r_m$ and $\sqrt{r_m^2 + 2r_m r}$ respectively where $r_m = c\tau_m$. Any traffic movement in this elliptical region could potentially influence the RSSI measured at the receiver.

An IEEE 802.15.4 receiver computes RSSI as the squared sum of incoming signal amplitude arriving within a window of time called RSSI integration time [7]. Therefore, any radio signal that reaches this receiver after bouncing off of a scatterer within the elliptical scattering region defined by the RSSI integration time will influence the RSSI measured by the receiver. At any RSSI sampling instance by an IEEE 802.15.4 receiver, if there are k radio obstacles within its elliptical scattering region, then we propose to model the net shadow fading loss Z_s^i measured by this i^{th} IEEE 802.15.4 transceiver in a network of M wireless receivers as a compound Poisson process given by

$$Z_s^i = \sum_{j=1}^{k} \alpha_j^i \quad (1)$$

where $\alpha_j^i; j \in \{1,2,\cdots,k\}, i \in \{1,2,\cdots,M\}$ are realization from a stationary Gaussian random variable with mean μ_s and variance σ_s^2 that represents the attenuation caused by i^{th} radio obstacle within the scattering region and k is the number of radio signal scatterers within this elliptical scattering region that is assumed to be Poisson distributed.

Poisson distribution has been successfully used in the past to model human traffic within an area [14]. Hence by modeling the pedestrian traffic as a homogeneous Poisson process where the scatterers are moving independently of each other, (1) can account for shadow fading noise in a workspace with pedestrian and machinery traffic. Therefore, for a localization area with an average density of ω scatterers per unit area, if $M(S)$ represents the number of scatterers within an elliptical scattering region S, then the probability that $M(S) = k$ is given by the Poisson distribution as

$$P[M(S) = k] = Poisson(\omega|S|) = \frac{exp\{-\omega|S|\}(\omega|S|)^k}{k!} \quad (2)$$

where $P[M(S) = k]$ is the probability that $M(S) = k$, $|S| = \pi ab$ is the area of the elliptical scatterer region S, $a = \frac{1}{2}(r_m + r)$ and $b = \frac{1}{2}\sqrt{r_m^2 + 2r_m r}$ are the semi-major and semi-minor axis respectively of S, r is the radial separation between the transmitter and receiver and r_m is related to the maximum path delay variable τ_m of GBSBEM as $r_m = c\tau_m$ with c being the speed of radio waves.

Unlike the log-normal shadow fading models [3] where realizations from random variableZ_s^i, represented as $Z_s^i(t); t \in \mathbb{N}$, are assumed to be independent, our shadow fading model treats $Z_s^i(t)$ realizations measured by adjacent receivers at the same instance t as dependent random variables. This dependency in shadow fading loss arises from the presence of similar radio obstacles in their scattering regions. Dependent shadow fading loss has been the basis for a recent correlated shadow fading model called Network Shadowing (NeSh) [6]. In this model, shadowing fading loss between a transmitter and a receiver is formulated as the line integral of a stationary Gaussian path loss function along the radial distance between them. However, due to the RSSI integration window employed by IEEE 802.15.4 transceivers, any radio obstacles that are

within the elliptical scattering region of a transmitter/receiver pair, but not necessarily blocking their LoS conditions, can influence the RSSI measured by the receiver. The line integral in [6] fails to account for these scatterers and consequently underestimates the correlation in shadow fading between adjacent receivers.

Now we will introduce the copula method used in financial statistics to generate the likelihood function for MLE when only the marginal distributions of random variables and their pair-wise interdependency are only available.

2.3 COPULA FUNCTIONS

Copula is a joint cumulative distribution function (CDF) of standard uniform random variables such that $C(u_1, u_2, \dots, u_M, \beth) = P(U_1 \leq u_1, U_2 \leq u_2, \dots, U_M \leq u_M | \beth)$ where $C(u_1, u_2, \dots, u_M, \beth)$ is the copula function, $U_i \sim U(0,1); i \in \{1,2, \dots, M\}$ are the standard uniform distributions with u_i being their realizations, $P(U_1 \leq u_1, U_2 \leq u_2, \dots, U_M \leq u_M | \beth)$ is the joint CDF of random variables $U_i; i \in \{1,2, \cdots, M\}$ and $\beth$ is the $M \times M$ dependency matrix between the random variables $\{U_1, U_2, \cdots U_M\}$ [15].

For a set of random variables $X_i; i \in \{1,2, \dots, M\}$ that are not uniformly distributed, Copula technique for generating the likelihood function involves the following steps.

The realization x_i of a random variable X_i is translated to a standard uniform random variable by applying the CDF, $F_i(x_i)$, of X_i as $u_i = F_i(x_i) = P[X_i \leq x_i]; i \in \{1,2, \cdots, M\}$.

The dependency matrix $\beth$ and the copula function $C(F_1(x_1), \dots, F_M(x_M), \beth)$ are then used to generate the joint CDF $P(U_1 \leq u_1, U_2 \leq u_2, \dots, U_M \leq u_M | \beth)$.

Finally, the likelihood function, $\mathcal{L}(x_1, x_2, \cdots, x_M|ב)$, of $x_i; i \in \{1,2, \dots, M\}$ is derived by taking the partial derivative of the joint CDF with respect to the random variables $X_i; i \in \{1,2, \cdots, M\}$ as

$$\mathcal{L}(x_1, x_2, \cdots, x_M|ב) = \frac{\partial}{\partial X_1 \partial X_2 \cdots \partial X_M} C(F_1(x_1), \dots, F_M(x_M), ב). \quad (3)$$

There are several families of copula functions to choose from, such as, the Gaussian and Student-t copula that falls under the elliptical copula family; Gumbel, Frank and Clayton copulas that fall under the Archimedean family etc. The particular choice of copula function depends on the type of dependency (linear dependency, tail dependency etc.) that is of interest [16]. Since the objective of this paper is to estimate the transmitter location from cross-correlation of shadow fading noise, which is a linear dependency between shadow fading noise, elliptical family of copulas are better suited for our application. In particular, this paper will employ student-t copula since the t-copulas capture the linear dependency between extreme values of the random variable [17]. In an indoor localization scenario, adjacent receivers more often experience simultaneous peaks or troughs in RSSI due to pedestrians or other radio obstacles crossing their line of sight path to the transmitter.

Now we will introduce the statistical technique that will be used to measure the velocity of a mobile transmitter

2.4 α - DIVERGENCE

In statistics, divergence arises in classification problems where a measurement x has to be categorized into either belonging to one of two possible groups C_1 or C_2. Miss-classification occurs when x is assigned to C_1 while it should have been in C_2 or vice versa. The average probability of such misclassification is measured by the Bayes error

and α-divergence or specifically Chernoff α-divergence is the upper bound of this Bayes error [18]. The α-divergence of classifying a random variable X into groups C_1 or C_2 is defined as

$$D_\alpha(C_1 \parallel C_2) = -log \int f(x|C_1)^\alpha f(x|C_2)^{1-\alpha} dx \quad (4)$$

where $C_1 \parallel C_2$ implies divergence operation between groups C_1 and C_2, $f(x|C_i)$ is the PDF of the random variable X given that it belongs to group $C_i; i \in \{1,2\}$, x is a single realization of this random variable X and the integration in (4) is performed over the entire range of random variable X. By varying the value of α in (4), divergence measures commonly used in classification such as Kullback-Leibler $(\alpha \to 1)$ divergence and Bhattacharyya coefficient $(\alpha = 0.5)$ can be obtained. Later it will be shown that for a wireless transmitter, its velocity is proportional to the measured α-divergence between RSSI samples.

Now we will present the cross-correlation of shadow fading residuals used to locate a transmitter.

3. LOCALIZATION FROM SHADOW FADING RESIDUALS

This section will start by presenting the stochastic filter that is used to isolate shadow fading residuals from the measured RSSI values. An RSSI value measured by a receiver is the net effect of several processes such as path loss, polarization, multipath and shadow fading etc. Therefore, we will present a mean reverting OU filter in conjunction with GARCH filtering to isolate shadow fading residuals from measured RSSI values.

3.1 SHADOW FADING NOISE EXTRACTION FROM RSSI

In [4], the underlying shadow fading process was extracted from wireless signal strength at 2GHz in an indoor environment using spatial averaging window of size 10λ. Therefore, RSSI signal $X(t)$ at sampling instance t will be modeled as a mean reverting OU process [19] given by

$$dX(t) = v_t[X_s(t) - X(t)]dt + \sigma_f dW(t) \quad (5)$$

where $dX(t)$ is a small change in RSSI for a small increment in time dt, v_t is the relative speed with which the transmitter is moving away from the receiver as measured between sampling instance $t-1$ and t, $X_s(t)$ is the local mean of RSSI which is a combination of deterministic power loss such as path loss given by Friis transmission equation, antenna gain variations, polarization losses etc and slow changing shadow fading noise due to pedestrian traffic, σ_f^2 is the variance of fast fading or multipath noise and $dW(t)$ is a delta increment of a standard Brownian motion.

If ΔT is the period between broadcast message and the v_t is available by measuring the α-divergence of RSSI as explained later in section 4, then $X_s(t)$ and σ_f in (5) can be estimated from least square regression by rewriting (5) as

$$Y(t) = a(t) + \epsilon_w(t) \quad (6)$$

where $Y(t) = [X(t) - X(t-\Delta T)] + X(t)v_t\Delta T$, $a(t) = v_t X_s(t)\Delta T$, and $\epsilon_w(t) = \sigma_f[W(t) - W(t-\Delta T)]$. Since $dW(t)$ is a stationary standard normal distribution, $Y(t)$ follows a normal distribution with mean $a(t)$ and variance σ_f^2. Therefore, the local mean $X_s(t)$ and σ_f^2 in (5) can be easily estimated from sample mean and sample variance of $Y(t)$ in (6) respectively.

Since the local mean $X_s(t)$ includes the deterministic path loss component, a first order auto-regressive (AR) process approximation for $X_s(t)$ as in [20] will be applied to extract the zero mean shadow fading residuals as

$$X_s(t) = \mu_r(t) + \beta X_s(t-1) + \epsilon_s(t) \quad (7)$$

where $\mu_r(t)$ accounts for all the deterministic power loses, β is the auto-correlation between successive samples of $X_s(t)$ and $\epsilon_s(t) = \sigma_s(t)Z_s(t)$ is the deviation of $X_s(t)$ from the first order AR process assumption, $\sigma_s^2(t)$ is the shadow fading variance and $Z_s(t)$ is the realization from $Z_s$which is a stationary zero mean shadow fading residual with normalized variance. Shadow fading noise Z_s is caused by the movement of pedestrians or machinery in the scattering area, therefore the statistics of Z_s is the random variable of interest in this paper for measuring similarity in shadow fading noise between receivers.

Finally, to account for variation in pedestrian traffic, the shadow fading variance is assumed to change over time and is modeled as a first order GARCH process as

$$\sigma_s^2(t) = b_0 + b_1\sigma_s^2(t-1) + b_2\epsilon_s^2(t-1) \quad (8)$$

where b_0, b_1 and b_2 are GARCH coefficients to be determined. A maximum likelihood based solution for the GARCH process is provided in [21] which is used in this paper to estimate b_0, b_1 and b_2 in (8) and then filter out the shadow fading residuals $Z_s(t)$ from $X_s(t)$.

Therefore, the steps involved in extracting the shadow fading residuals for an IEEE 802.15.4 transceiver are:

(a) The transmitter periodically broadcasts its current heading message

(b) Using (15) estimate the transmitter velocity v_t.

(c) Estimate $X_s(t)$ in (5) from the sample mean of $Y(t)$

(d) Estimate the GARCH residuals $Z_s(t)$ from $X_s(t)$ using MLE as in [21]. (MATLAB has an easy to use function called *garchfit* which performs this operation.)

Now we will derive the theoretical expression that relates the cross-correlation in shadow fading residuals measured by a receiver pair and their radial separation from a transmitter in the localization area.

3.2 SHADOW FADING CORRELATION COEFFICIENT

Since shadow fading is caused by relevant radio obstructions within the scattering region surrounding the transmitter and receiver, neighboring receivers will have similar radio obstacles in their vicinity and consequently will experience similar shadow fading statistics. Figure 2 shows the elliptical scattering regions S_1 and S_2 surrounding receivers R_1 and R_2 respectively.

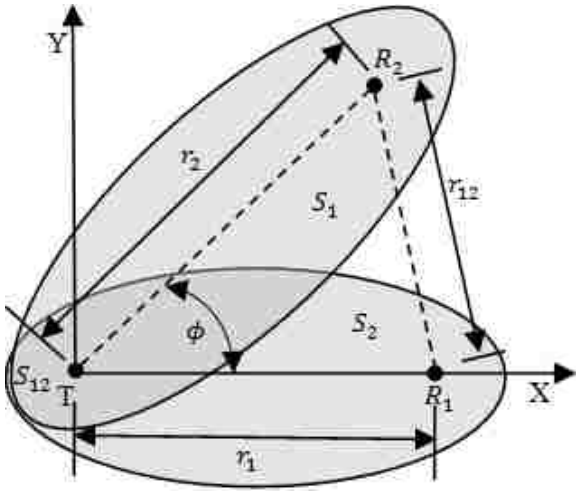

Fig 2. Overlapping of scattering regions causing cross-correlation in shadow fading

Any pedestrians or movement of machinery in these elliptical regions S_1 or S_2 will result in shadow fading in corresponding receiver. For the region S_{12} which overlaps both S_1 and S_2, pedestrian or machinery traffic will affect the shadow fading at both the receivers simultaneously resulting in shadow fading noise dependency between them. Details about the derivation of the area of intersection between two ellipse using Gauss-Green theorem is in the appendix.

Theorem 1 will now derives the shadow fading dependency between a pair of IEEE 802.15.4 receivers caused by pedestrian or machinery traffic in its vicinity.

Theorem 1: (*Shadow Fading Correlation Coefficient*) Shadow fading noise correlation coefficient (ρ) between two IEEE 802.15.4 receivers R_1 and R_2 separated by radial distances r_1 and r_2 respectively from a common transmitter is given by

$$\rho = \frac{|S_{12}|}{\sqrt{|S_1||S_2|}} \tag{9}$$

where S_1 and S_2 are the elliptical scatterer regions surrounding receivers R_1 and R_2 respectively, S_{12} is overlapping region between scattering regions S_1 and S_2 and $|\cdot|$ is the area operator.

Proof: Please refer to appendix. ■

To derive the Copula based likelihood function for transmitter localization, the CDF of Z_s has to be determined. In [22], it was observed that the residuals obtained after GARCH filtering were non-Gaussian with fat-tails. Since derivation of an exact closed-form parametric expression for the CDF of Z_s is quite difficult, a semi-parametric approach will be used to model the CDF of shadow fading residuals such that for regions around the mode of the residuals will be modeled using non-parametric empirical CDF whereas for the upper and lower tails of the residual distribution, where sample points are

sparse by definition, a parametric Generalized Pareto Distribution (GPD) will be applied. The empirical CDF for the i^{th} receiver from N shadow fading residuals is given by

$$\hat{F}_i^N(z) = \frac{1}{N}\sum_{k=1}^{N} I\left(z_s^i(k) \le z\right); i\epsilon\{1,2,\dots,M\} \tag{10}$$

where $I(\cdot)$ is the indicator function and $z_s^i(1), z_s^i(2), \dots, z_s^i(N)$ are N shadow fading residuals measured by the i^{th} receiver in the localization area. The GPD parameterizes shadow fading residual distribution tails using three parameters η, ζ and ϑ where $\eta \in \mathbb{R}$ is the location parameter that sets the upper/lower percentile threshold above/below which GPD is applicable, $\zeta \in \mathbb{R}$ is the shape parameter that controls the rate at which the tail of the distribution goes to zero and $\vartheta \in \mathbb{R}^+$ is the scale parameter that accounts for variance in tail data. Therefore, semi-parametric CDF, $\tilde{F}_i^N(z)$, obtained by combining (10) and CDF of GPD is given by

$$\tilde{F}_i^N(z) = \begin{cases} \hat{F}_i^N(z), & L_i < z < U_i \\ \frac{1}{\vartheta_i}\left[1 + \zeta_i\left(\frac{z-U_i}{\vartheta_i}\right)\right], & z \ge U_i \\ \frac{1}{\vartheta_i}\left[1 - \zeta_i\left(\frac{z-L_i}{\vartheta_i}\right)\right], & z \le L_i \end{cases} \tag{11}$$

where U_i and L_i are the upper and lower tail location parameters respectively. For transmitter localization, U_i and L_i are control variables that determines the extent of tail dependency between shadow fading residuals, whereas, parameters ζ_i and ϑ_i are estimated using MLE as in [23]. Now we will combine (10) and (11) to derive the likelihood of observing a particular sequence of cross-correlation in shadow fading residuals between receivers to localize a transmitter.

3.3 STUDENT-T COPULA BASED SHADOW FADING CROSS-CORRELATION LIKELIHOOD FUNCTION

In the following theorem, we will derive the student-t copula based likelihood function for estimating the position of a transmitter.

Theorem 2: (*Shadow Fading Cross-Correlation Likelihood Function*) The likelihood of observing the following sequence $\{z_s^i\}; i \in \{1,2,\cdots,M\}$ of shadow fading residuals from a network of M receivers used for estimating the position of a common transmitter is given by the following likelihood function as

$$\mathcal{L}(z_s^1, z_s^2, \cdots, z_s^M|\beth) = c_{\varsigma,\beth}\{t_\varsigma^{-1}[\tilde{F}_1^N(z_s^1)], \ldots, t_\varsigma^{-1}[\tilde{F}_K^N(z_s^M)]\} \quad (12)$$

where $t_\varsigma^{-1}(\cdot)$is the inverse CDF or quantile function of a student-t distribution with degree of freedom ς, $\tilde{F}_i^N(z_s^i); i \in \{1,2,\ldots,M\}$ is semi-parametric shadow fading residual CDF for the i^{th} receiver, $c_{\varsigma,\beth}(\cdot)$ is an M-variate student-t copula density with ς degree of freedom [17], $\beth$ is an $M \times M$ correlation coefficient matrix given by $\beth = \{\rho_{kl}\}; k, l \in \{1,2,\ldots,M\}$ and ρ_{kl} is the correlation coefficient between receiver k and l given by (9).

Proof: Please refer to appendix. ■

To compute the maximum for a non-convex function given in (12) using nonlinear optimization techniques such as Newton-Raphson scheme require an initial value to be located within the region of attraction of global maximum. Under these initial conditions, the movement in the direction of steepest gradient will result in a local maximum. However, for initial conditions that are far from the global maxima, there is a very high probability the solution can get stuck in a local maximum unless the optimization algorithm occasionally moves away from it. Hence, stochastic optimization using Simulated Annealing with Stochastic Tunneling as in [5] is used to solve (12). Primary reason for choosing this method over other stochastic optimization techniques are (a) guaranteed convergence of simulated annealing in asymptotic time [11], and (b) tunneling helps to move from one local maxima to another faster thereby improving convergence time [5]. Even with tunneling, convergence time required for sub-meter

localization accuracy in an indoor mall was close to 30 seconds. Therefore, we will now present a faster tracking algorithm that use velocity estimates from α-divergence of shadow fading residuals smoothed by Bayesian filters to localize a mobile transmitter.

4. MOBILE TRANSMITTER TRACKING

This section begins by introducing the mobile transmitter velocity estimation from α-divergence of shadow fading residuals.

4.1 SPEED ESTIMATION USING α - DIVERGENCE

As explained in Section 2.4, α-divergence is a measure of the Bayesian error in a hypothesis testing. Hence by continuously estimating α-divergence of RSSI values, the system is measuring the Bayesian error for the hypothesis that all RSSI values observed at the receivers are originating from a stationary transmitter. The following theorem will derive this Bayesian error for a mobile IEEE 802.15.4 transmitter.

Theorem 3: *(α-divergence of a mobile IEEE 802.15.4 transmitter)* For a mobile transmitter operating under GBSBEM wireless channel model, α-divergence of received signal strength measured between two time instances $(n-1)$ and n in an indoor localization area is given by

$$D_{\alpha}(n-1 \parallel n) = \omega|S_{n-1}|\left\{1+(1-\alpha)\gamma_{n-1}-(1+\gamma_{n-1})^{(1-\alpha)}\right\} \qquad (13)$$

where $\gamma_{n-1} = \left(1+\frac{\beta_{n-1}r_{n-1}}{r_m+r_{n-1}}\right)\sqrt{1+\frac{2\beta_{n-1}r_{n-1}}{r_m+2r_{n-1}}}-1$, $\beta_{n-1} = \sqrt{1-\frac{2\Delta r_n \cos\theta_{n-1}}{r_{n-1}}+\left[\frac{\Delta r_n}{r_{n-1}}\right]^2}-1$, θ_{n-1} is the azimuth angle of arrival of LoS radio signal at the receiver with respect to the direction of motion of the transmitter while r_{n-1} is the radial separation between the transmitter and receiver respectively at time instance $n-1$, Δr_n is the distance the transmitter travelled between time instances $n-1$ and n and $r_m = c\tau_m$ with c as the

speed of radio waves and τ_m is the maximum multipath delay for an IEEE 802.15.4 receiver.

Proof: Please refer to appendix. ■

Corollary 1: (*Velocity estimation under small displacements*) For a mobile transmitter, under small displacements between α-divergence computation instances, the transmitter velocity v_n at start of time instance n can be approximated as

$$v_n = -\frac{2}{\pi\omega\alpha(1-\alpha)b_{n-1}\cos\theta_{n-1}\Delta T_v} D_\alpha(n-1 \parallel n) \quad (14)$$

where $D_\alpha(n-1 \parallel n)$ is the α-divergence measurement between time instances $n-1$ and n, θ_{n-1} is the relative bearing of the mobile transmitter with respect to the stationary receiver at time instance $n-1$, ΔT_v is the time interval between α-divergence computation instance $n-1$ and n.

Proof: For $r_m + r_{n-1} \gg \Delta r_n \Rightarrow \gamma_{n-1} \ll 1$ resulting in $\gamma_{n-1} \approx -\frac{2\Delta r_n \cos\theta_{n-1}}{r_m + r_{n-1}}$. Hence the α-divergence in (11) can be approximated as $D_\alpha(n-1 \parallel n) = \omega|S_{n-1}|\left\{\frac{\alpha(1-\alpha)}{4}\gamma_{n-1}^2 + O(\gamma_{n-1}^3)\right\} \approx \frac{\alpha(1-\alpha)}{4}\omega|S_{n-1}|\gamma_{n-1}^2 =$ $\alpha(1-\alpha)\frac{\pi}{2}\omega b_{n-1}\cos\theta_{n-1}\Delta T v_{n-1}$ where $b_{n-1} = \frac{1}{2}\sqrt{r_m^2 + 2r_m r_{n-1}}$ and $v_n = \frac{\Delta r_n}{\Delta T_v}$. ■

Corollary 2: (*Velocity estimation using α-divergence for IEEE 802.15.4 transceiver*) For a mobile IEEE 802.15.4 transceivers, the transmitter velocity can be approximated as

$$v_n = \frac{4}{\pi\omega\alpha(1-\alpha)r_m\cos\theta_{n-1}\Delta T_v} D_\alpha(n-1 \parallel n) \quad (15)$$

where $D_\alpha(n-1 \parallel n)$ is the α- divergence measurement between RSSI sampling instances $n-1$ and n, θ_{n-1} is the azimuth angle of arrival of LoS component at the receiver with respect to the direction of motion of the transmitter at sampling instance

$n-1$ and $D_\alpha(n \parallel n+1)$ is the α-divergence measurement between time sampling instances n and $n+1$.

Proof: An IEEE 802.15.4 device measures RSSI by averaging the square of the signal amplitude over 128μs [24] which results in a very large value for r_m. Hence for indoor environment where $r_{n-1} \ll r_m$ results in $b_{n-1} \approx \frac{r_m}{2}$. Therefore, by substituting $b_{n-1} = \frac{r_m}{2}$ in (12) gives the speed of the mobile transmitter as in (13). ■

From (13) speed estimation with $\alpha = \{0,1\}$ is indeterminate. Hence Bhattacharyya Coefficient with $\alpha = 0.5$ was used in this paper for IEEE 802.15.4 transmitter speed estimation. Now we will present the mobile transmitter location update equation and the Bayesian filter that is used to bind the accumulation of localization error over time.

4.2 BAYESIAN FILTERING OF A MOBILE TRANSMITTER USING STUDENT-T COPULA LIKELIHOOD

To track a mobile IEEE 802.15.4 transmitter, the speed estimate (v_n) obtained from α-divergence of RSSI values is combined with the heading (ϕ_n) information obtained from a gyroscope or an antenna array [25] attached to the mobile transmitter. The 2D coordinates and ϕ_n of the mobile transmitter at time instance n represented by the vector $\eta_n = [x_n, y_n, \phi_n]^T$, is recursively updated as

$$\begin{bmatrix} x_n \\ y_n \\ \phi_n \end{bmatrix} = \begin{bmatrix} x_{n-1} \\ y_{n-1} \\ \phi_{n-1} \end{bmatrix} + \begin{bmatrix} v_n \Delta T_v \cos \phi_{n-1} \\ v_n \Delta T_v \sin \phi_{n-1} \\ \dot{\phi}_n \Delta T_v \end{bmatrix} \tag{16}$$

where $\dot{\phi}_n$ and v_n are the control inputs to the state update equation with $\dot{\phi}_n$ being the azimuth angular velocity and $v_n = \frac{4D_\alpha(n-1\|n)}{\pi\omega\alpha(1-\alpha)r_m\Delta T_v \sin(\varphi_{n-1}-\phi_{n-1})}$ is the speed of the mobile transmitter obtained by setting $\theta_{n-1} = 90 - \varphi_{n-1} + \phi_{n-1}$ in (13), ΔT_v is the state

update period, ϕ_{n-1} is the heading of the mobile transmitter at RSSI sampling instance $n-1$ and $\varphi_{n-1} = tan^{-1}\left(\frac{y_{n-1}}{x_{n-1}}\right)$ is the absolute bearing of the mobile transmitter with respect to the x-axis. From Figure 3, $\theta_{n-1} = 90 - \varphi_{n-1} + \phi_{n-1}$.

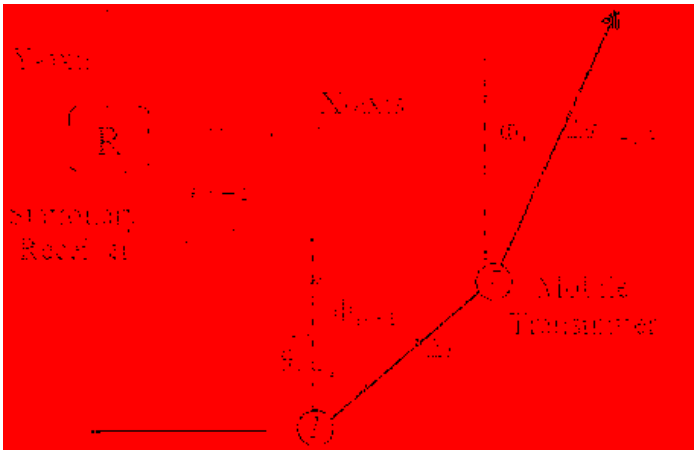

Fig 3. Tracking of a mobile transmittter

Since dead reckoning based tracking results in incremental position error [7] over time, a Bayesian particle filtering method is proposed to bind the localization error. In this filtering method, a series of position estimates (η_n^i), called particles, are generated around the dead reckoning based position estimate (η_n) at time instance n as $\eta_n^i = \eta_n + N_i; i \in \{1,2,\cdots,K\}$ where K is the number of particles, N_i is the process noise in the dead reckoning system. Assuming a dead reckoning system with Gaussian process noise with co-variance matrix given by V_S then the K Gaussian particles can be generated from (16) as

$$\eta_n^i = \eta_n + N([\Delta x, \Delta y, \Delta\phi]^T, V_s \Delta T_v^2); i \in \{1,2,\cdots,K\} \qquad (17)$$

where $\eta_n^i = \left[x_n^i, y_n^i, \phi_n^i\right]$, $\eta_n = [x_{n-1}, y_{n-1}, \phi_{n-1}]^T$, K represents the number of particles and $N([\Delta x, \Delta y, \Delta\phi]^T, V_s \Delta T_v^2)$ is the multivariate Gaussian process noise with $\Delta x = v_n \Delta T_v \cos\phi_{n-1}$, $\Delta y = v_n \Delta T_v \sin\phi_{n-1}$ and $\Delta\phi = \dot{\phi}_n \Delta T_v$. At any position update instance n, the base station collects the shadow fading residuals $z_s^1, z_s^2, \cdots, z_s^M$ at each receiver as the measurement M_n to build the semi-parametric CDF for (11). If $P\left(\eta_n^i | \eta_{1:n-1}, M_{1:n-1}\right)$ is the prior probability of the transmitter being at location η_n^i given all previous measurements $(M_{1:n-1})$ and previous states $(\eta_{1:n-1})$ leading up to sampling instance $n-1$ then on receiving the measurement M_n at the base station, the posterior probability, $P\left(\eta_n^i | \eta_{1:n-1}, M_{1:n}\right)$, of each particle η_n^i can be computed from the Bayes Theorem as

$$P\left(\eta_n^i | \eta_{1:n-1}, M_{1:n}\right) \propto P\left(\eta_n^i | \eta_{1:n-1}, M_{1:n-1}\right) P\left(M_n | \eta_{1:n-1}, \eta_n^i, M_{1:n-1}\right) \quad (18)$$

where $P\left(M_n | \eta_{1:n-1}, \eta_n^i, M_{1:n-1}\right)$ is the likelihood function which is the probability of observing measurement M_n at time instance n if all previous transmitter states $(\eta_{1:n-1})$, previous measurements $(M_{1:n-1})$ and the current transmitter location η_n^i are available.

Since shadow fading residual measurement M_n at time instance n is only dependent on the current transmitter position η_n^i, $P\left(M_n | \eta_{1:n-1}, \eta_n^i, M_{1:n-1}\right) = P\left(M_n | \eta_n^i\right)$ which is the likelihood function given by (12). From (16), if the state of the tracked mobile transmitter is available at time instance $n-1$ then η_n^i is independent of all previous measurements $M_{1:n-1}$ and previous states $\eta_{1:n-2}$ resulting in $P\left(\eta_n^i | \eta_{1:n-1}, M_{1:n-1}\right) = P\left(\eta_n^i | \eta_{n-1}\right)$. For the dead reckoning system (16) with Gaussian process noise, $P\left(\eta_n^i | \eta_{n-1}\right) = f\left(\eta_n^i - \eta_{n-1}\right)$ which is the PDF a Gaussian distribution

with mean $\left[v_n \Delta T_v \cos \phi_{n-1}, v_n \Delta T_V \sin \phi_{n-1}, \dot{\phi}_n \Delta T_V\right]^T$ and co-variance matrix $V_s \Delta T_v^2$ computed at $\eta_n^i - \eta_{n-1}$. Therefore, (18) becomes

$$P\left(\eta_n^i | \eta_{1:n-1}, M_{1:n}\right) \propto f\left(\eta_n^i - \eta_{n-1}\right) \mathcal{L}(z_s^1, z_s^2, \cdots, z_s^M | \beth_i) \quad (19)$$

where $\beth_i$ is the $M \times M$ correlation coefficient matrix given by $\beth_i = \{\rho_{kl}^i\}; k, l \in \{1,2, \ldots, M\}; i \in \{1,2, \cdots, N\}$ and ρ_{kl}^i is the cross-correlation computed for i^{th} particle η_n^i using (9). Finally, the Bayesian smoothed location estimate at time instance n from K particles, $\eta_n^i; i \in \{1,2, \cdots, K\}$, is the expected value given by

$$\eta_n = \sum_{i=1}^{N} \eta_n^i P\left(\eta_n^i | \eta_{1:n-1}, M_{1:n}\right) \quad (20)$$

Now we will present the entire localization and tracking algorithm of a mobile transmitter by measuring cross-correlation of shadow fading noise at receivers placed within a localization workspace.

5. LOCALIZATION AND TRACKING ALGORITHM

Localization of a mobile transmitter from RSSI values measured at the receiver can be expressed in a flow chart as in Figure 4.

The steps involved in tracking a mobile transmitter are:

(a) Initialization: The initial position and heading of the mobile transmitter $\eta_1 = [x_1, y_1, \phi_1]^T$ is assumed to be known to the receiver. For stationary transmitters, the heading information is not required. In addition, the positions of the M stationary receivers are also assumed to be known. Of the M receivers, one of them will be placed at the origin of Cartesian coordinate. This receiver acts as the base station for tracking the mobile transmitter.

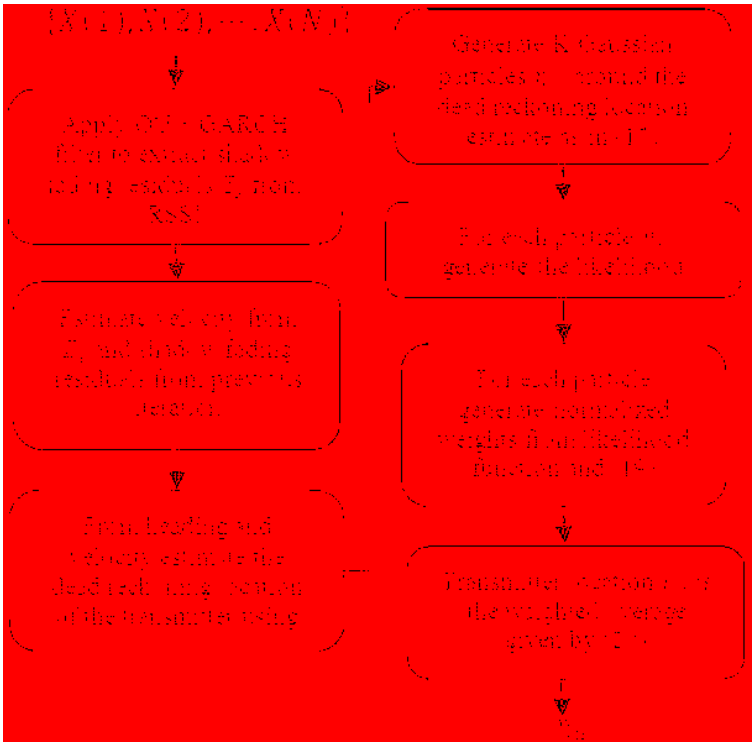

Fig 4. Flow chart of mobile transmitter tracking

(b) Periodic Heading Broadcast: At each sampling instant, the mobile transmitter broadcasts N packets that contain the current azimuth angular velocity $\dot{\phi}_n$ measured by an on-board gyroscope or compass as one of its field.

(c) Shadow Fading Extraction: The N RSSI values collected by each receiver at sampling instant n is passed through an OU filter to extract N shadow fading residuals as explained in Section 3.1. These shadow fading residuals are then used to build the semi-parametric CDF as in (11).

(d) Velocity estimation: Compute α-divergence, $D_\alpha(n-1 \parallel n)$, from shadow fading residuals collected at time instant $n-1$ and n using [18]. Use the state information η_{n-1}

at sampling instance $n-1$ along with $D_\alpha(n-1 \parallel n)$ to compute mobile transmitter velocity v_n using (15).

(e) Particle Generation: Generate K Gaussian particles $\eta_n^i; i \in \{1,2,\cdots,K\}$ from η_{n-1}, v_n and $\dot{\phi}_n$ using (17) and compute their prior probability from the PDF of a Gaussian distribution as $P(\eta_n^i - \eta_{n-1})$.

(f) Bayes Filtering: For each particle position η_n^i compute the $M \times M$ cross-correlation matrix ב between M receivers in the localization area using (9). Using the shadow fading residual measurement at time instance n and ב, compute the likelihood function given by (12).

(g) Posterior Probability: Let the product of the likelihood function computed in step 6 and the prior probability computed in step 5 be called the weight (w_n^i) or relevance of each particle. These weights can be easily normalized to the posterior distribution using the law of total probability as $P(\eta_n^i|\eta_{1:n-1}, M_{1:n}) = \frac{w_n^i}{\sum_{i=1}^n w_n^i}$.

(h) Position Estimation: Finally, applying (20) on the posterior probability, $P(\eta_n^i|\eta_{1:n-1}, M_{1:n})$, computed in step 7 for each particle η_n^i gives the Bayes smoothed mobile transmitter location (η_n) for time instance n.

(i) Repeat Steps **b** to **h**.

Now results will be presented to verify our theoretical assertions

6. RESULTS AND ANALYSIS

The localization and tracking algorithm was implemented on an IEEE 802.15.4 wireless mote called Z1 mote. Both the transmitter and receivers are Z1 motes that run on a 16-bit MSP430 microcontroller with CC2420 as the radio. Details about the CC2420

radio can be found here [24]. The RSSI collection process is coordinated by a base station/receivers which is a Z1 mote connected to a PC through the USB port. According to [26], a whip antenna on CC2420 should provide a gain of 1.9dB resulting in a maximum communication range of up to 212m before the signal strength falls below the receiver sensitivity of around -83dBm. However, our range experiments using Z1 mote with a whip antenna showed that the maximum communication range under pedestrian traffic was around 40m.

First a MATLAB simulation will be performed to understand the effect of following parameters: a. Radial separation between receivers(r_{12}), b. Radial separation between transmitter and receiver 2 (r_2), c. RSSI integration time (τ_m), and d. Radio obstacle density (ω) on shadow fading cross correlation (9). Subsequently, feasibility of the proposed localization and tracking algorithm will be evaluated in an indoor food court area of a local mall.

6.1 SHADOW FADING ρ SIMULATION

Correlated shadow fading residuals were simulated by first generating independent Poisson distributed interferer count for disjoint regions $S_1 \cap S_{12}^c$, $S_2 \cap S_{12}^c$ and S_{12} within S_1 and S_2. Subsequently, independent standard normal random variables corresponding to attenuation of each interferer were generated. Finally, the net attenuation at receiver R_i is the sum of attenuations for interferers in regions $S_i \cap S_{12}^c, i \in \{1,2\}$ and S_{12}.

Figure 5.1 plots estimated and computed correlation coefficient from a sample size of 100 shadow fading residuals from receiver R_1 and R_2 such that $r_1 = 10m$ and $r_2 = 10m$ while r_{12} was varied from 1m to 15m. The RSSI integration time was set at

$\tau_m = 128\mu s$ and the radio obstacle density was set at $\omega = 1$ interferer/sq.m. Figure 5.2 plots the standard deviation of correlation coefficient estimate.

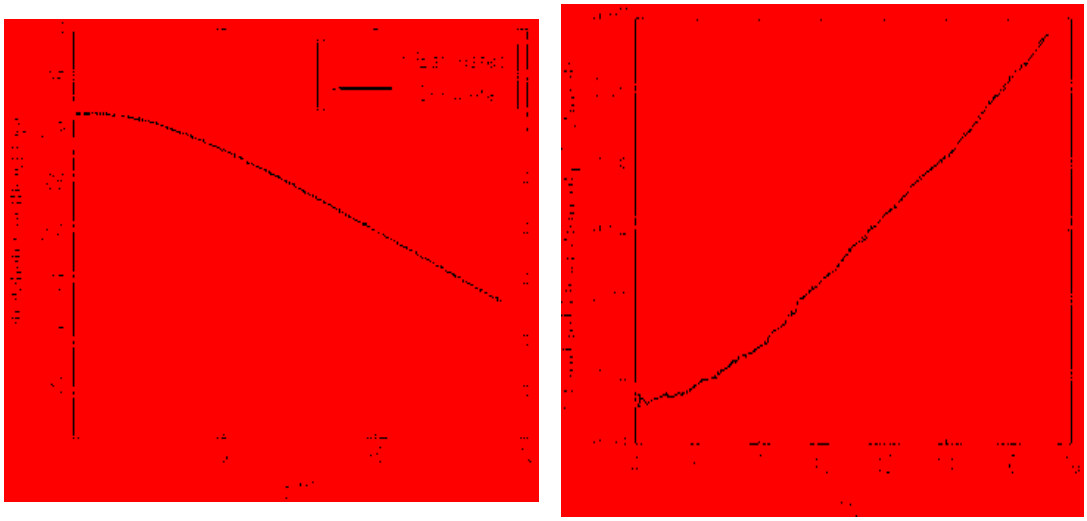

(1) r_{12} vs. ρ (2) Standard deviation of r_{12} vs. ρ

Fig 5. Correlation coefficient vs. radial separation between receivers

Increasing r_{12} while keeping r_1 and r_2 constant results in the overlapping area S_{12} being reduced while the elliptical area S_1 and S_2 remains fixed. Consequently, the correlation coefficient given by (9) will reduce with increased r_{12} as in Figure 5.1. The monotonic increase in standard deviation of the correlation coefficient estimate with increasing $r_{12}$is also an artifact of reduced $|S_{12}|$ area with increasing r_{12}. Smaller $|S_{12}|$ results in a fewer number of interferers between R_1 and R_2 thereby effectively reducing the sample size for correlation coefficient estimation. This results in increased estimation error as observed in Figure 5.2.

Figure 6.1 plots the estimated and computed correlation coefficient when $r_1 = 10m$ and $r_{12} = 10m$ while r_2 was varied from 1m to 15m. RSSI integration time and radio obstacle density were set at $\tau_m = 128\mu s$ and $\omega = 1$ interferer/sq.m respectively. In this scenario, area of S_1 remains constant, while the area of both S_2 and S_{12} are increasing with r_2. Apparently, the area of S_{12} seems to increase faster than that of S_2 as is evident by the increase in correlation coefficient with increasing r_2. However, the standard deviation for correlation coefficient estimation shown in Figure 6.2 does not seem to follow monotonic path as in previous Figure 6.2 due to the change in both S_{12} and S_2 area.

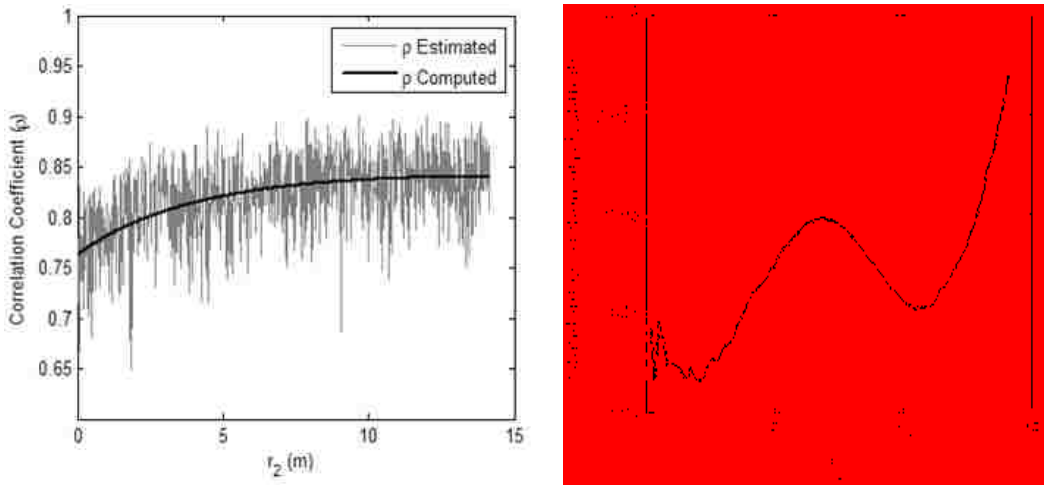

(1) r_2 vs. ρ (2) Standard deviation of r_2 vs. ρ

Fig 6. Correlation coefficient vs. radial separation between transmitter-receiver

Figure 7.1 plots RSSI integration time (τ_m) vs ρ when radial separations r_1, r_2 and r_{12} remains the same and the interferer density is $\omega = 1$ interferer/sq.m. As the integration time increases, the $S_1$and S_2 can be approximated by circular regions with

radii r_m and their centers separated by distance r_{12}. The correlation coefficient (9) can be approximated as $\rho \approx \frac{2}{\pi} cos^{-1}\left(\frac{r_{12}}{2r_m}\right) - \frac{r_{12}}{\pi r_m}\sqrt{1-\frac{r_{12}^2}{4r_m^2}} \to 1$ when $\frac{r_{12}}{r_m} \to 0$ as in Figure 7.1. Figure 7.2 plots standard deviation for ρ vs. ω. Increasing ω results in large number of interferers in the overlapping area, S_{12}, thereby increasing the sample size for correlation coefficient estimation and thus reducing the estimation error.

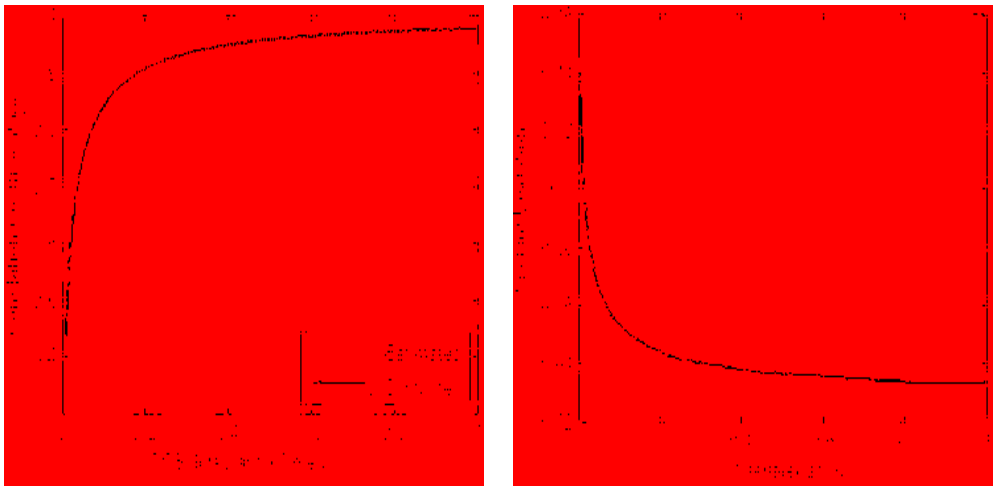

(1) τ_m vs. ρ (2) ω vs. standard deviation of ρ

Fig 7. Effect of τ_m and ω on ρ

6.2 TRANSMITTER LOCALIZATION IN A FOOD COURT

The food court area of a local mall, whose layout shown in Figure 8 was specifically chosen for our localization experiments due to high pedestrian traffic resulting in large ω. From simulations, large ω should result in better correlation coefficient estimates and consequently better localization accuracy. The localization area

measured 1250 sq. m with an average of 1000 people moving within this area during peak lunch hour traffic on a weekend between 10 AM and 1 PM.

Total of 8 wireless receivers (marked R_1 to R_8 in Figure 8) were placed evenly around the periphery of the localization area. To calibrate the localization algorithm, the RSSI integration time τ_m has to be estimated by maximizing (12) at 8 known transmitter locations and then averaging their results resulting in $\tau_m = 129\mu s$ for Z1 motes.

Layout of the food court area used for localization experiment with dark lines showing the boundary walls

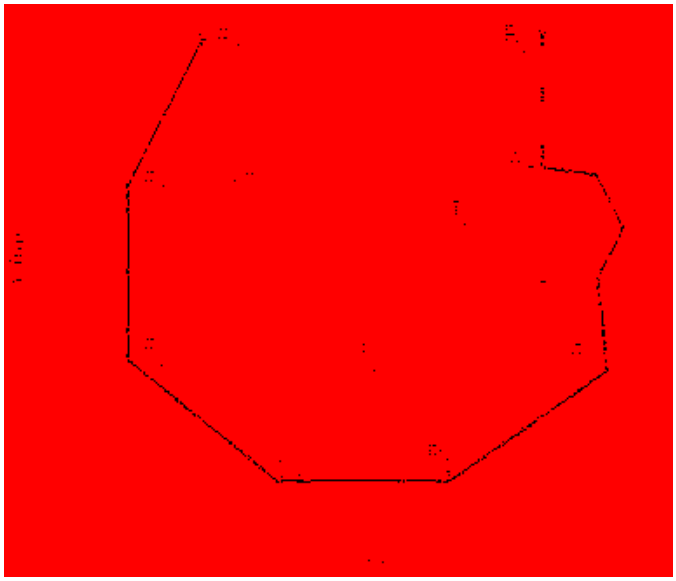

Fig 8. Layout of the food court area used for localization experiment with dark lines showing the physical boundary walls

Localization iteration begins with the base station instructing the transmitter to broadcast 10 packets back to back. At the end of this broadcast session, the base station

collects the transmitter's RSSI values measured by each receiver. If any receiver failed to receive any of the broadcast packets in this session, then the base station restarts the session again by requesting the transmitter to resend another 10 packets. Upon completion of 10 such sessions, the base station has now 100 RSSI measurements from each receiver on which the base station runs the OU MLE estimator [19] to estimate the slow varying local mean value. Subsequently, AR/GARCH filtration removes the serial correlation and heteroskedasticity from this local mean using [21] to extract the zero mean shadow fading residuals. These shadow fading residuals form the input to the semi-parametric CDF estimator (11) where the shape and scale parameter are estimated as in [23]. The tail control parameters such as η, U_i and L_i for GPD in (11) were heuristically set at 4, 90th percentile and 10th percentile respectively. Finally, simulated annealing with tunneling transformation as in [5] was used to find transmitter location that maximizes (12).

TABLE 1. LOCALIZATION ERROR LEVELS AT VARIOUS LOCATIONS

Transmitter Location	**Localization Error (m)**			
	Mean	**Median**	**90th Perc.**	**Std. Dev**
T_1	2.458	2.329	3.962	1.727
T_2	2.378	2.267	3.628	1.221
T_3	3.537	3.496	5.234	2.377
T_4	2.739	2.912	4.138	1.839

Performance of our localization algorithm at four randomly chosen points marked T_1 through T_4 in the localization area is summarized in Table 1. The large localization

error at T_3 could be attributed to it being in a corner resulting in larger radial separation from receivers. The performance of using (12) to estimate the transmitter location was compared with using MDS to estimate transmitter location from pair-wise correlation coefficient. The results are given in Table II.

Large localization error for MDS is due to the linear assumption between the correlation coefficient and radial separation.

TABLE 2. SUMMARY OF LOCALIZATION ERROR

Method	**Localization Error (m)**			
	Mean	**Median**	**90th Perc.**	**Std. Dev**
Proposed Method	2.778	2.751	4.2405	1.791
MDS	12.343	15.925	25.358	6.464

6.3 TRACKING EXPERIMENT

The tracking experiment was conducted within building ERL 114 of Missouri University of Science and Technology (MST). The area of interest is a typical laboratory environment measuring 12m x 13m containing test equipments, pumps, shelves etc as shown in Figure 9. The mobile transmitter was tracked by 8 wireless receivers marked R_1 through R_8 with receiver R_1 acting as the base station receiver. The mobile IEEE 802.15.4 transmitter is held by a human walking at a constant pace along the solid white line shown in Figure 9. The transmitter heading measurements is provided by 3DM-GX2 Attitude Heading Reference System (AHRS) built by Microstrain that is attached to the transmitter. This AHRS has accelerometers, electronic compass and gyroscopes making it

a fully functional Inertial Navigation System (INS). The transmitter broadcasts the heading information at 50 times a second.

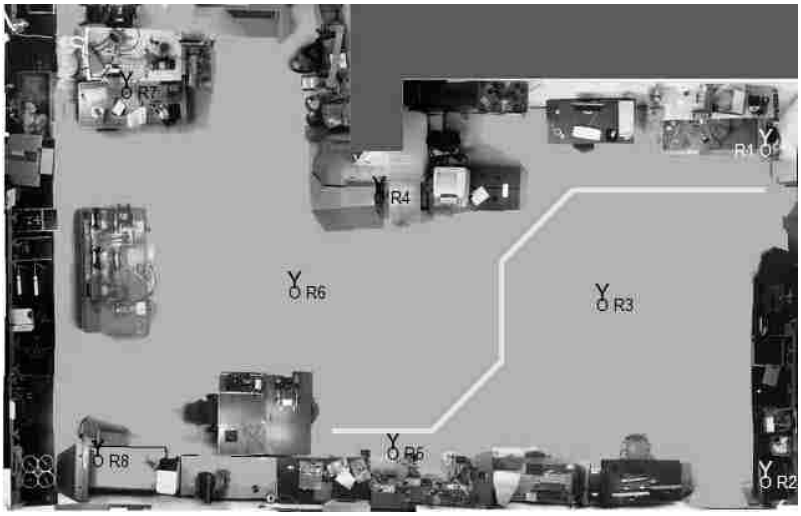

Fig 9. Top view of ERL 114 with receiver positions shown

The number of RSSI samples collected (N) by the receivers before applying the OU and GARCH filtering to extract the shadow fading residuals in a mobile scenario is determined by the operating wavelength $\lambda = 12.5cm$, RSSI broadcast period $\Delta T = 20ms$ and the last best transmitter velocity estimate v_n resulting in N given by $N = \frac{10\lambda}{v_n \Delta T}$. Unlike the localization experiment in section 6.1, each receiver runs the shadow fading extraction algorithm locally and the extracted residuals are sent to the base station. This helps to reduce the processing overhead at the base station. The base station then builds the empirical CDF from shadow fading residuals for copula based likelihood function (12). As in previous experiment the GPD tail control parameters η, U_i and L_i were set heuristically at 4, 90th percentile and 10th percentile respectively.

The accuracy of tracking the mobile transmitter using our copula smoothing algorithm is compared against dead-reckoning based tracking using α-divergence and heading information from AHRS and the Inertial Navigation System (INS) realized using accelerometers and gyroscopes on AHRS. Figure 10 shows the tracked positions of the mobile transmitter after 5 runs of each of the three tracking methodologies considered here.

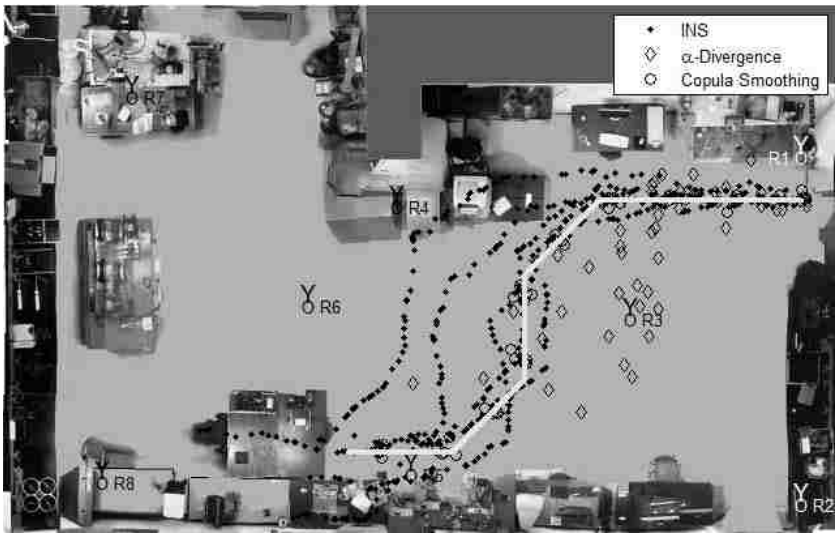

Fig 10. Tracked points from INS, α-divergence and copula smoothing methods

For copula based tracking, $M = 10{,}000$ particles where generated at step 5. Increasing the particle count beyond 10,000 did not improve the tracking accuracy but resulted in significant time lag between position updates. Figure 11 shows the Root Mean Square Error (RMSE) metric used for comparing the error in three tracking methodologies over time. RMSE for a single tracking run is computed by taking the shortest distance between a localized point and the white track shown in Figure 10.

As expected, RMSE of dead-reckoning based tracking methods (α-divergence & INS) increased over time. This is due to the accumulation of input errors caused by the integration of inputs velocity or acceleration to the state equation (16) to realize the transmitter location. For α-divergence based tracking the communication and processing overhead arising due to broadcast from the transmitter and shadow fading residual extraction resulted in large time gap between position updates in comparison to INS based tracking. The effect of this large time gap is reflected in the higher RMSE for α-divergence based tracking in Figure 11.

Fig 11. RMSE from INS, α-divergence and copula smoothing methods

Figure 12 shows the velocity estimates from α-divergence of RSSI measured at the base station and integration of accelerometer output in AHRS. The accelerometers in AHRS has a resolution of $\pm 0.005g$ and a range of $\pm$5g Since the measured velocity

(0.05m/s ~ 0.30m/s) is very close to the lower limit of the accelerometer, the velocity measurements seems to be dominated by short spikes caused by the walking motion of the human carrying the transmitter. Application of Bayesian particle smoothing technique on α-divergence based tracking helped reduce its RMSE thereby making this tracking methodology comparable or slightly better than INS with the major advantage that, unlike INS, RMSE for copula smoothing does not seem to increase over time.

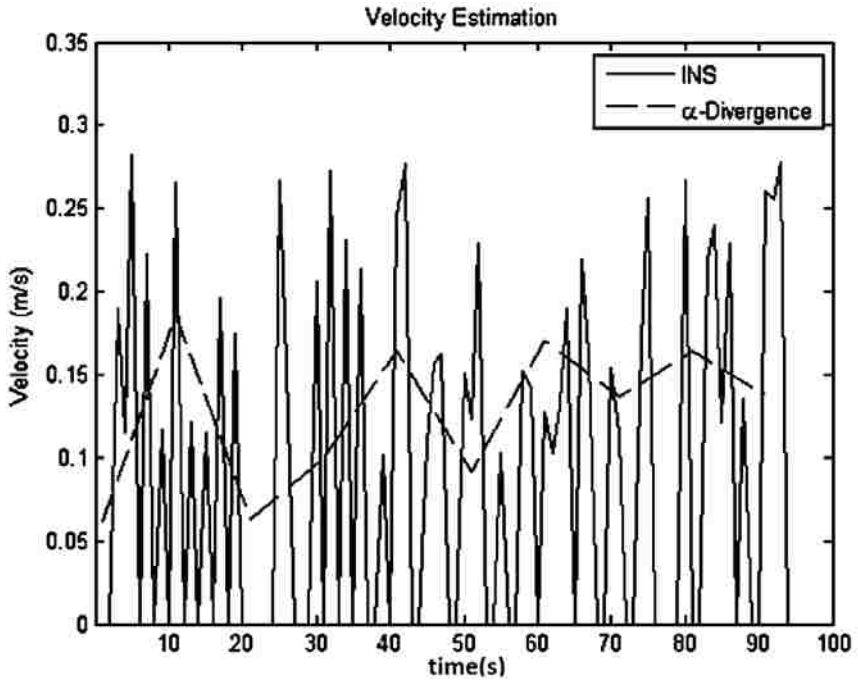

Fig 12. Velocity estimates from INS and α-divergence

Table 3 lists the statistics of RMSE computed for the three tracking methodologies considered in this paper. Clearly, copula smoothing technique seems to provide significant advantage over dead-reckoning based tracking systems.

TABLE 3. SUMMARY OF TRACKING ERROR LEVELS

Method	Tracking RMSE (m)			
	Mean	**Min**	**Max**	**Std. Dev**
α-divergence	0.3859	0.0464	0.8652	0.2944
Copula Smoothing	0.1777	0.0105	0.4379	0.1505
INS	0.2466	0.0025	0.6719	0.1972

In comparison to localization experiment in Section 6.1, Bayesian particle filter based tracking method was able to achieve sub-meter accuracy primarily due to the generated particles in step 5 of copula smoothing algorithms were very close to the global maxima of the likelihood function (12) thereby converging faster to the global solution. When transmitter is stationary, velocity estimates will be close to zero and the time to converge to a global solution will still be large.

7. CONCLUSIONS

This paper proposes a novel localization algorithm that uses Copula technique to derive the MLE for transmitter localization. It was shown through an experiment in a local food court of a shopping mall that our proposed solution localizes targets under pedestrian traffic with an average accuracy of 2.78m. In addition, optimizing (12) to find MLE of transmitter location was shown experimentally to have better accuracy than applying MDS after pair-wise estimation of RSSI correlation coefficients.

Due to statistical guarantees of finding global maximum using simulated annealing based stochastic optimization technique, localization accuracy of our proposed algorithm could be further improved at the expense of increased computation time. In addition, our proposed tracking algorithm using α-divergence, specifically Bhattacharyya Coefficient, for velocity estimation followed by Copula smoothing was able to achieve sub-meter accuracy. Test results from a laboratory environment have clearly demonstrated that our

copula based tracking method is a feasible alternative to inertial navigational systems on mobile robots or human tracking systems.

REFERENCES

[1] A. Ramachandran, and S. Jagannathan, "Spatial diversity in signal strength based WLAN location determination systems," *Proc. of the 32nd IEEE Conf. on Local Comp. Networks* , pp. 10-17, Oct. 2007.

[2] N. R. Yousef, A. Sayed, and L. Jalloul, "Robust wireless location over fading channels," *IEEE Trans. Veh. Technol.*, vol. 52, no. 1, pp. 117–126, 2003.

[3] H. Hashemi, H, "The indoor radio propagation channel," *Proc. of the IEEE* , vol.81, no.7, pp.943-968, Jul 1993.

[4] R.A. Valenzuela, O. Landron, and D.L. Jacobs, "Estimating local mean signal strength of indoor multipath propagation," *IEEE Trans. on Veh. Technol*., vol.46, no.1, pp. 203-212, Feb 1997.

[5] M. R. Basheer, and S. Jagannathan, "Localization of objects using stochastic tunneling," *IEEE Wireless Commun. Networking Conf. (WCNC)*, pp.587-592, 28-31 Mar. 2011.

[6] P. Agrawal, and N. Patwari, "Correlated link shadow fading in multi-hop wireless networks," *IEEE Trans. on Wireless Communications*, vol. 8, no. 8, pp. 4024-4036, Aug. 2009.

[7] Hyeon-Jin Jeon, T. Demeechai, Woo-Geun Lee, Dong-Hwan Kim and Tae-Gyu Chang, "IEEE 802.15.4 BPSK Receiver Architecture Based on a New Efficient Detection Scheme," *IEEE Trans. on Signal Processing*, vol.58, no.9, pp.4711-4719, Sept. 2010.

[8] X. Ji, and H. Zha, "Sensor positioning in wireless ad-hoc sensor networks using multidimensional scaling," *23rd Annual Joint Conf. of the IEEE Comp. and Commun. Soc.* , vol.4, pp. 2652- 2661, Mar. 2004.

[9] N. Patwari, and A. O. Hero, "Manifold learning algorithms for localization in wireless sensor networks," *In Proc. IEEE Int. Conf. on Acoustics, Speech and Signal Proc.*, vol. 3, pp.857–860, May 2004.

[10] C. Wang, J. Chen, Y. Sun, and X. Shen, "Wireless sensor networks localization with Isomap," *IEEE Int. Conf. on Commun.*, Jun. 2009.

[11] B. Gidas, "Non stationary markov chains and convergence of simulated annealing algorithms," *J. Stat. Physics*, vol.39, pp.73-131, Apr. 1985.

[12] J. Borenstein, H. Everett, L. Feng, and D. Wehe, "Mobile robot positioning: Sensors and techniques," *Journal of Robotic Systems*, vol. 14, no. 4, pp.231-249, 1997.

[13] J.C. Liberti, and T.S. Rappaport, "A geometrically based model for line-of-sight multipath radio channels," *Vehicular Tech. Conf., 1996. 'Mobile Tech. for the Human Race'., IEEE 46th* , vol.2, pp.844-848, May 1996.

[14] A. B. Chan, and N. Vasconcelos, "Counting People with Low-Level Features and Bayesian Regression," *IEEE Transactions on Image Processing*, vol.21, no.4, pp.2160-2177, Apr. 2012.

[15] R. B. Nelsen, "An Introduction to Copulas, Lectures Notes in Statistics," Springer Verlag, New York, 1998.

[16] P. Embrechts, F. Lindskog, and A. McNeil, "Modeling dependence with Copulas and applications to risk management," *in Handbook of Heavy Tailed Distributions in Finance*, ed. S. Rachev, Rotterdam, NL: Elsevier, Chapter 8, pp. 329-384, 2003.

[17] S. Demarta, and A. McNeil, "The t-Copula and Related Copulas," *Int. Statistics Review*, vol. 73, no. 1, pp. 111-129, April 2005.

[18] A.O. Hero, B. Ma, O. Michel, and J. Gorman. "Alpha-divergence for classification, indexing and retrieval," *Technical Report CSPL-328, University of Michigan Ann Arbor, Communications and Signal Processing Laboratory*, May 2001.

[19] L. Valdivieso, W. Schoutens and F. Tuerlinckx, "Maximum likelihood estimation in processes of Ornstein-Uhlenbeck type," *Statistical Inference for Stochastic Processes*, Vol. 12, No. 1, pp. 1-19, 2009.

[20] K. E. Baddour, and N. C. Beaulieu, "Autoregressive modeling for fading channel simulation," *IEEE Trans. on Wireless Communications*, vol.4, no.4, pp. 1650-1662, July 2005.

[21] T. Bollerslev, "Generalized Autoregressive Conditional Heteroskedasticity," *J. of Econometrics*, vol. 31, no. 3, pp. 307-327, 1986.

[22] T. Bollerslev, R. Y. Chou, K. F. Kroner. "ARCH modeling in finance. A review of the theory and empirical evidence," *Journal of Econometrics,* Vol. 52, No. 1, pp. 5-59, April 1992.

[23] J. R. M. Hosking and J. R. Wallis, "Parameter and quantile estimation for the Generalized Pareto Distribution," *Technometrics*, Vol. 29, No. 3, pp. 339-349j, Aug 1987.

[24] Texas Instruments, 2.4GHz IEEE 802.15.4/ZigBee-ready RF Transceiver, *http://www.ti.com/lit/ds/symlink/cc2420.pdf*, accessed Sep 26, 2011.

[25] B. N. Hood, and P. Barooah, "Estimating DoA From Radio-Frequency RSSI Measurements Using an Actuated Reflector," *IEEE Sensors Journal*, vol.11, no.2, pp.413-417, Feb. 2011.

[26] G. E. Jonsrud, Folded dipole antenna for CC2400, CC2420, CC2430, CC2431, and CC2480, Texas Instruments, *http://www.ti.com/lit/an/swra093d/swra093d.pdf*, accessed Sep 26, 2011.

APPENDIX

Computing Area of Overlap between Ellipses

The overlapping area $|S_{12}|$ in (9) can be calculated by first computing the point of intersection $p_l = (x_{pl}, y_{pl}); l \in \{1,2,3,4\}$ between elliptical regions S_1 and S_2. Since the maximum RSSI path detection delay τ_m is same for both receivers, and the ellipses $S_1$and S_2 share a common focus at the transmitter, it can be easily shown that the number of intersection points is only two. Let $p_1 = (x_{p1}, y_{p1})$ and $p_2 = (x_{p2}, y_{p2})$ be the point of intersection between S_1 and S_2 then to find p_1 and p_2 , simultaneously solve the implicit polynomial equations of ellipse $S_1$and S_2 by eliminating one variable, for e.g. x, leading to a quartic equation in y. The intersection points are then the real solutions of this quartic equation. The generalized implicit equation of an ellipse with semi-major and

semi-minor axis given by a_i and b_i, oriented at an angle ϕ_i w.r.t x-axis with center at (cx_i, cy_i) is given by $\frac{[(x-cx_i)\cos\phi_i+(y-cy_i)\sin\phi_i]^2}{a_i^2}+\frac{[-(x-cx_i)\sin\phi_i+(y-cy_i)\cos\phi_i]^2}{b_i^2}=1$. For S_1, $\phi_1=0$ and $(cx_1,cy_1)=(0,0)$ while for ellipse S_2, $\phi_2=\phi=cos^{-1}\left(\frac{r_1^2+r_2^2-r_{12}^2}{2r_1r_2}\right)$and $(cx_2,cy_2)=\left(\frac{r_2}{2}cos\,\phi-\frac{r_1}{2},\frac{r_2}{2}sin\,\phi\right)$. Subsequently, the area can be computed from p_l using Gauss-Green theorem as $|S_{12}|=|S_1|+|S_2|-\frac{1}{2}\int_0^{\pi}\left[x_1(\theta_1)\frac{dy_1(\theta_1)}{d\theta}-y_1(\theta_1)\frac{dx_1(\theta_1)}{d\theta}\right]d\theta-\frac{1}{2}\int_{\pi}^{2\pi}\left[x_2(\theta_2)\frac{dy_2(\theta_2)}{d\theta}-y_2(\theta_2)\frac{dx_2(\theta_2)}{d\theta}\right]d\theta$

where $\theta_1=\frac{(\psi_{12}-\psi_{11})}{\pi}\theta+\psi_{11}$, $\theta_2=\frac{(\psi_{22}-\psi_{21})}{\pi}\theta+2\psi_{21}-\psi_{22}$, $\psi_{11}=\cos^{-1}\left(\frac{x_{p1}}{a_1}\right)$, $\psi_{12}=cos^{-1}\left(\frac{x_{p1}}{a_1}\right)$, $\psi_{21}=tan^{-1}\left(\frac{a_2[(y_{pl}-cy_2)cos(\phi)-(x_{pl}-cx_2)sin(\phi)]}{b_2[(y_{pl}-cy_2)sin(\phi)+(x_{pl}-cx_2)cos(\phi)]}\right)$ $\psi_{22}=tan^{-1}\left(\frac{a_2[(y_{p2}-cy_2)cos(\phi)-(x_{p2}-cx_2)sin(\phi)]}{b_2[(y_{p2}-cy_2)sin(\phi)+(x_{p2}-cx_2)cos(\phi)]}\right)$, $x_1(\theta_1)=a_1\,cos(\theta_1)-\frac{(x_{p1}+x_{p2})}{2}$, $y_1(\theta_1)=b_1\,sin(\theta_1)-\frac{(y_{p1}+y_{p2})}{2}$, $x_2(\theta_2)=a_2\,cos(\phi)\,cos(\theta_2)-b_2\,sin(\phi)\,sin(\theta_2)+cx_2-\frac{(x_{p1}+x_{p2})}{2}$ and $y_2(\theta_2)=a_2\,sin(\phi)\,cos(\theta_2)-b_2\,cos(\phi)\,sin(\theta_2)+cy_2-\frac{(y_{p1}+y_{p2})}{2}$.

Proof of Theorem 1 *(Shadow Fading Correlation Coefficient Between IEEE 802.15.4 Receivers)*

Figure 2 shows the elliptical scatterer regions S_1 and S_2 surrounding receivers R_1 and R_2 respectively. Let the number of obstacles in S_1 and S_2 at any communication instance between the transmitter and receiver is given by the Poisson distribution (2). If $\alpha_j^i; i\in\{1,2\}, j\in\{1,2,\cdots,M(S_i)\}$ represents the attenuation of a radio signal reaching receiver R_i due to jth obstacle in scatterer region S_i, then the net reduction in signal

strength (in dBm) due to $M(S_i)$ obstacles in region S_i is given by $Z_s^i = \sum_{j=1}^{M(S_i)} \alpha_j^i$ where Z_S^i is the signal strength attenuation due to shadow fading. For log-normally distributed shadow fading noise under stationary conditions, if $M(S_i)$ is given then Z_S^i is Normally distributed i.e. if μ_s and σ_s^2 corresponds to the mean and variance of α_j^i, then $f\left(Z_s^i|M(S_i)\right) = M(S_i)N(\mu_s, \sigma_s^2)$ where $N(\cdot)$ is the normal distribution PDF with conditional mean and variance given by $E\left[Z_s^i|M(S_i)\right] = \mu_s M(S_i)$ and $Var\left[Z_s^i|M(S_i)\right] = \sigma_s^2 M(S_i)$ respectively.

The correlation coefficient between shadow fading random variables Z_s^1 and Z_s^2 is given by

$$\rho = \frac{cov(Z_s^1, Z_s^2)}{\sqrt{Var(Z_s^1)Var(Z_s^2)}} \tag{A1}$$

which require the derivation of $Var\left(Z_s^i\right)$ and $cov(Z_s^1, Z_s^2)$. Since $E\{M(S_i)\} = Var\{M(S_i)\} = \omega|S_i|$, $Var\left(Z_s^i\right)$ can be derived from law of total of variance as

$$\begin{aligned} Var\left(Z_s^i\right) &= Var\left\{E\left[Z_s^i|M(S_i)\right]\right\} + E\left\{Var\left[Z_s^i|M(S_i)\right]\right\} \\ &= Var\{M(S_i)\mu_s\} + E\{M(S_i)\sigma_s^2\} = \omega(\mu_s^2 + \sigma_s^2)|S_i| \end{aligned} \tag{A2}$$

whereas, $cov(Z_s^1, Z_s^2)$ can be derived from the law of total covariance as

$$Cov(Z_s^1, Z_s^2) = cov\{E[Z_s^1|M(S_1)], E[Z_s^2|M(S_2)]\} + E\{cov[Z_s^1, X_s^2|M(S_1), M(S_2)]\}. \tag{A3}$$

Since conditional mean is given by $E\left[Z_s^i|M(S_i)\right] = \mu_s M(S_i)$, the covariance of the conditional mean in (A2), can be simplified as $cov\{E[Z_s^1|M(S_1)], E[Z_s^2|M(S_2)]\} = \mu_s^2 cov[M(S_1), M(S_2)]$. Since for a spatial Poisson processes, random variables corresponding to the Poisson count for disjoint areas are independent, the radio obstacle count for S_i can be written as the sum of two independent Poisson random variables by splitting the region S_i into two disjoint areas as $S_i = (S_i \cap S_{12}^c) \cup S_{12}$ resulting in

$M(S_i) = M\big((S_i \cap S_{12}^c) \cup S_{12}\big) = M(S_i \cap S_{12}^c) + M(S_{12})$. Let $A_i = M(S_i \cap S_{12}^c)$ and $B = M(S_{12})$ then, $A_i \sim Poisson(\omega |S_i \cap S_{12}^c|)$ and $B \sim Poisson(\omega |S_{12}|)$ resulting in $cov[M(S_1), M(S_2)] = cov(A_1 + B, A_2 + B) = Var(B) = \omega |S_{12}|$. Therefore, the covariance of conditional mean in (A3) is given by $cov\{E[Z_s^1 | M(S_1)], E[Z_s^2 | M(S_2)]\} = \mu_s^2 \omega |S_{12}|$.

To compute the expectation of conditional covariance $E\{cov[Z_s^1, Z_s^2 | M(S_1), M(S_2)]\}$ in (A3), we split the shadow fading noise at each receiver as $Z_s^i = \sum_{j=1}^{M(S_i)} \alpha_j^i = \sum_{j=1}^{A_i + B} \alpha_j^i = C_i + D$ where C_i is the shadow fading attenuation due to region $S_i \cap S_{12}^c$ and D is the shadow fading due to the overlapping region S_{12}. Therefore, the conditional mean is $E\{cov[Z_s^1, Z_s^2 | M(S_1), M(S_2)]\}$ $= E\{cov[C_1 + D, C_2 + D | M(S_1), M(S_2)]\} = E\{Var[D | M(S_{12})]\} = \sigma_s^2 \omega |S_{12}|$ resulting in (A3) being simplified as

$$cov(Z_s^1, Z_s^2) = \omega(\mu_s^2 + \sigma_s^2) |S_{12}|. \quad \text{(A4)}$$

Finally applying (A2) and (A4) on (A1) results in (9). ■

Proof of Theorem 2 *(Shadow Fading Cross-Correlation Likelihood Function)*

The cost function for the maximum likelihood estimate of a parameter is the joint distribution of the multiple observations of a random variable when the value of the parameter is assumed to be known. For our application the Cartesian coordinates of the transmitter is the parameter to be estimated while the random variables that are being observed are the shadow fading residuals at each receiver. Therefore, to derive the joint distribution of shadow fading residuals from semi-parametric marginal CDF given by (11) and pair-wise correlation coefficient given by (9) we will use the elliptical copula function since the dependency between the shadow fading residuals that is being modeled

is the correlation coefficient which is a linear dependency. In addition, t-copulas capture the linear dependency between extreme values of the random variable [17]. Hence for M receivers, the student-t copula density with ς degree of freedom (DoF) and $M \times M$ correlation coefficient matrix $\beth$ is given by [17] as

$$c_{\varsigma,\beth}(u_1, u_2, \dots, u_M) = \frac{f_{\varsigma,\beth}\left(t_\varsigma^{-1}(u_1), t_\varsigma^{-1}(u_2), \dots, t_\varsigma^{-1}(u_M)\right)}{\prod_{k=1}^{M} f_\varsigma\left(t_\varsigma^{-1}(u_k)\right)} \tag{A5}$$

where $u_i \in [0,1]$ is the standard uniform random variable, $f_{\varsigma,\beth}(x_1, x_2, \dots, x_M) = \frac{\Gamma\left(\frac{\varsigma+M}{2}\right)}{|P|^{\frac{1}{2}}(\varsigma\pi)^{\frac{M}{2}}\Gamma\left(\frac{\varsigma}{2}\right)}\left[1 + \frac{\mathbb{x}^T \beth^{-1} \mathbb{x}}{\varsigma}\right]^{-\frac{(\varsigma+M)}{2}}$, $\Gamma(\cdot)$ is the Gamma function and $\mathbb{x} = [x_1, x_2, \dots, x_M]^T$ $f_\varsigma(x) = \frac{\Gamma\left(\frac{\varsigma+1}{2}\right)}{\sqrt{\varsigma\pi}\Gamma\left(\frac{\nu}{2}\right)}\left[1 + \frac{x^2}{\varsigma}\right]^{-\frac{(\varsigma+1)}{2}}$. Finally, setting $u_i = \tilde{F}_i(z_{si})$ in (A5) gives the likelihood function for transmitter localization using shadow fading cross-correlation as (12) ■

Proof of Theorem 3 (*α-Divergence of Shadow Fading Residuals From An IEEE 802.15.4 Transmitter*)

Figure 13 shows the tracking of an IEEE 802.15.4 mobile transmitter by a stationary receiver. At each sampling instance, receiver collects a sequence of N RSSI values from the transmitter. Assume that at time instant $n-1$, the mobile transmitter is at position η_{n-1} and in the subsequent instance n, the receiver moved by radial distance Δr_n to reach location η_n. In addition, assume that during this time period, the heading of the mobile transmitter changed by $\Delta\phi_{n-1}$ while the bearing between the mobile transmitter and stationary receiver at the origin changed by $\Delta\psi_{n-1}$.

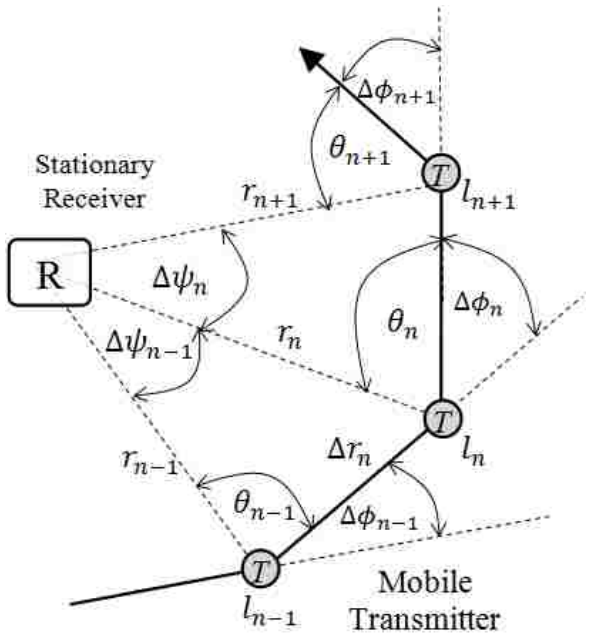

Fig 13. Continuous tracking of a mobile receiver

Shadow fading noise at positions η_{n-1} and η_n arise from the movement of pedestrians or machinery within elliptical fading region S_{n-1} and S_n respectively formed between the transmitter and receiver. Therefore, the α-divergence between N RSSI values collected at positions η_{n-1} and η_n can be derived by substituting the shadow fading PDF given by (1) at positions η_{n-1} and η_n in α-divergence equation (2) resulting in

$$\begin{aligned} D_\alpha(n-1 \parallel n) &= -log\left\{\int_{-\infty}^{\infty}\sum_{k=0}^{\infty}[f(x|k)f(k|S_{n-1})]^\alpha[f(x|k)f(k|S_n)]^{1-\alpha}\ dx\right\} \\ &= -log\left\{\int_{-\infty}^{\infty}\sum_{k=0}^{\infty}f(x|k)[f(k|S_{n-1})]^\alpha[f(k|S_n)]^{1-\alpha}\ dx\right\} \\ &= -log\left\{\sum_{k=0}^{\infty}[f(k|S_{n-1})]^\alpha[f(k|S_n)]^{1-\alpha}\int_{-\infty}^{\infty}f(x|k)dx\right\} \\ &= -log\{\sum_{k=0}^{\infty}[f(k|S_{n-1})]^\alpha[f(k|S_n)]^{1-\alpha}\} \\ &= \omega(1-\alpha)|S_{n-1}|\left(\frac{|S_n|}{|S_{n-1}|}-1\right) \\ &\quad -log\left\{\sum_{k=0}^{\infty}\frac{exp\{-\omega|S_{n-1}|\}(\omega|S_{n-1}|)^k}{k!}\left(\frac{|S_n|}{|S_{n-1}|}\right)^{(1-\alpha)k}\right\} \end{aligned} \qquad \text{(A6)}$$

where $|S_{n-1}|$ and $|S_n|$ are the area for elliptical regions S_{n-1} and S_n respectively and are given by $|S_{n-1}| = \frac{\pi(r_m+r_{n-1})\sqrt{r_m^2+2r_m r_{n-1}}}{4}$ and $|S_n| = \frac{\pi(r_m+r_n)\sqrt{r_m^2+2r_m r_n}}{4}$. Since $r_n = r_{n-1}\sqrt{1-\frac{2\Delta r_n \cos\theta_{n-1}}{r_{n-1}}+\left[\frac{\Delta r_n}{r_{n-1}}\right]^2}$ the area S_n can be written as $|S_n| = |S_{n-1}|\left(1-\frac{\beta_{n-1}r_{n-1}}{r_m+r_{n-1}}\right)\sqrt{1-\frac{2\beta_{n-1}r_{n-1}}{r_m+2r_{n-1}}}$ where $\beta_{n-1} = \sqrt{1-\frac{2\Delta r_n \cos\theta_{n-1}}{r_{n-1}}+\left[\frac{\Delta r_n}{r_{n-1}}\right]^2}-1$. Setting $\gamma_{n-1} = \left(1-\frac{\beta_{n-1}r_{n-1}}{r_m+r_{n-1}}\right)\sqrt{1-\frac{\beta_{n-1}r_{n-1}}{r_m+2r_{n-1}}}-1$ results in the elliptical area for S_n being represented by the area of S_{n-1} as $|S_n| = |S_{n-1}|(1+\gamma_{n-1})$. Therefore, (A6) can be written as $D_\alpha(n-1 \parallel n) = \omega|S_{n-1}|[(1-\alpha)\gamma_{n-1}+1] - \log\left\{\sum_{k=0}^{\infty}\frac{[\omega|S_{n-1}|(1+\gamma_{n-1})^{(1-\alpha)}]^k}{k!}\right\}$. Since $\sum_{k=0}^{\infty}\frac{1}{k!}[\omega|S_{n-1}|(1+\gamma_{n-1})^{(1-\alpha)}]^k = \exp\{\omega|S_{n-1}|(1+\gamma_{n-1})^{(1-\alpha)}\}$, resulting in $\log\left\{\sum_{k=0}^{\infty}\frac{[\omega|S_{n-1}|(1+\gamma_{n-1})^{(1-\alpha)}]^k}{k!}\right\} = \omega|S_{n-1}|(1+\gamma_{n-1})^{(1-\alpha)}$. Hence, the α-divergence between RSSI values collected at time instants $(n-1)$ and n is given by (13)

V. PLACEMENT OF RECEIVERS FOR SHADOW FADING CROSS-CORRELATION BASED LOCALIZATION[1]

M. R. Basheer and S. Jagannathan

Abstract— *In this paper, a wireless receiver placement algorithm for localizing a radio transmitter in a shadow fading rich environment such as a factory floor or indoor mall rife with pedestrian and machinery traffic is introduced. The objective of this placement algorithm is to identify a minimum number of wireless receivers, their placement within the workspace and the number of shadow fading residuals used to compute cross-correlation between shadow fading residuals measured by receivers such that no matter where the transmitter is located in this workspace, the error in estimating its position is less than a predefined threshold. To achieve this overall goal, this paper first derives a receiver placement algorithm that attains complete localization coverage for a given workspace with minimum number of receivers. Subsequently, the Cramer-Rao Lower Bound (CRLB) for the variance in transmitter location estimation using cross-correlation of shadow fading residuals is derived as a function of receiver position and the number of shadow fading samples used to compute cross-correlation between receivers. To achieve a localization error better than the predefined threshold, the shadow fading residual sample count is adjusted such that the square root of CRLB is less than this error threshold. The primary advantage of using CRLB as the metric for evaluating receiver placement is that CRLB ensures that the generated receiver positions are independent of the method used to compute shadow fading cross-correlation. Any unbiased efficient*

[1] Research Supported in part by GAANN Program through the Department of Education and Intelligent Systems Center. Authors are with the Department of Electrical and Computer Engineering, Missouri University of Science and Technology (formerly University of Missouri-Rolla), 1870 Miner Circle, Rolla, MO 65409. Contact author Email: mrbxcf@mail.mst.edu.

estimator for shadow fading cross-correlation will attain this lower bound in localization error. Finally, the efficacy of our receiver placement algorithm is demonstrated using simulations and experimental data involving IEEE 802.15.4 wireless transceivers.

***Keywords**: Shadow Fading, Cross-correlation, Optimal Placement, Spatial Correlation, Pseudo-Likelihood, Fisher Information, Cramer Rao Lower Bound.*

1. INTRODUCTION

Accurate estimation of an asset location under pedestrian and machinery traffic is an important requirement for monitoring and control applications in a manufacturing environment. Received signal strength indicator (RSSI) based localization provides a less costly while easily deployable alternative to other localization techniques that rely on wireless signal properties such as time of flight or angle of arrival [1]. However, providing consistent localization accuracy in an environment rife with pedestrian and machinery traffic such as factory floor or indoor mall presents serious challenges.

The primary cause for localization error in RSSI-based localization is channel fading [2]. Fading can be either fast changing due to constructive/destructive interference caused by multipath radio signals or slow changing due to relevant radio obstructions in the path of the incoming radio signals called shadowing. In [3], the authors have derived a novel localization scheme that measures similarity between shadow fading noises observed by adjacent stationary receivers to locate the position of a mobile transmitter. Similarity in shadow fading noise arises between adjacent receivers when movement of pedestrians, machinery or other radio obstacles near their vicinity cause partial or complete blockage of radio signals from the transmitter. In [3], the authors were able to achieve sub-meter accuracy by placing 8 wireless receivers along the periphery of the food court area in an indoor mall that measured approximately 1250 sq. m in area.

However, the dependency between transmitter localization accuracy and the number of receivers or their placement within this workspace that resulted in sub-meter localization accuracy is not addressed.

It is well known that the receiver placement geometry can significantly affect the localization accuracy of an algorithm [4]. Therefore, this paper, attempts to address this issue by providing a receiver placement algorithm that will attain a predefined Cramer-Rao Lower Bound (CRLB) for variance in localizing a transmitter. Employing CRLB as the metric for evaluating various receiver placements geometry for localization accuracy improvement ensures that the accuracy enhancements achieved for a particular receiver position is independent of the method used to compute cross-correlation. In addition, lowering the CRLB results in reducing the uncertainty in the transmitter location estimate, this has been the main line of reasoning in various optimal placement strategies [5-7].

In [8] a sub-optimal receiver placement algorithm using Delaunay refinement was presented for localization using range estimation from RSSI values measured at the receivers. This method utilized the Delaunay triangulation's property that maximizes the minimum angle of all triangles generated in this triangulation [9]. This results in receiver placement geometries that are as close to an equilateral triangular grid as possible except when constrained by the bounding walls of the workspace. However, at tight corners near the bounding walls Delaunay refinement results in receiver placements that are very close to each other. Consequently, this method yields large number of receivers for certain workspace geometries. In addition, this method [8] was developed for range based

localization which as pointed out in [3] has shown results with large localization error under pedestrian and machinery traffic.

In [10], Delaunay triangulation is used for solving the sensor coverage problem wherein the objective is to cover every point within the target area by the sensing region of a sensor. However, this method uses series of heuristic steps to handle coverage holes near the boundary of the workspace. In addition, the method penalizes overlapping of sensing area. By contrast for transmitter localization using wireless receivers, overlap of communication range is necessary. This indicates that work in [10] is not directly suitable for localization.

In [11], optimal sensor placement and motion coordination for target tracking problem is addressed while assuming a) Gaussian errors for radial distance estimation and b) the radial distance estimation variance is assumed to be independent of the actual distance between the transmitter and receiver which is a stringent assumption. Fisher information determinant of the transmitter location estimator was used as the cost function in [11]. However, range based localization performs poorly in environment such as factory floor or indoor malls which is rife with shadow fading noises arising due to pedestrian and machinery traffic. In addition, Gaussian distribution of range measurement arises only under very high signal (LoS) to noise (NLoS) ratio thereby limiting the adaptability of this method in real environment. Further, our experiments [3] have shown a strong relationship between radial distance estimation variance to the actual distance between the transmitter and receiver which clearly shows that the applicability of this method [11] is limited.

On the other hand, in [12], a sub optimal count algorithm for placing cameras on a workspace to localize mobile robots was presented. Angle of orientation measurements from two cameras was used to estimate the Cartesian coordinates of the robot. However, this method cannot ensure all points on the workspace to have localization error less than a user specified error threshold. By contrast, in [13], the nonlinear Euclidean distance between N receivers and the transmitter is first linearized and then the unknown position of the transmitter is solved using linear least squares estimation technique. Receiver locations are selected such that the condition number, which is the ratio of the maximum to the minimum eigenvalue, of certain receiver position matrix is minimized. However, the linearizing method used in [13] results in N linear equations with dependent errors rendering biased position estimates that fails to minimize the localization error.

In contrast, the adaptive beacon placement methodology in [14] addresses the problem of placing additional receivers (beacons) using an empirical approach to further improve localization accuracy given an initial set of receiver placement. Since the entire target area is not searched, this method does not yield a uniform location error while this solution can only generate new receiver positions that improve upon an initial receiver layout which itself is a major issue.

The proposed receiver placement algorithm proceeds in two stages. In stage 1, our algorithm addresses complete localization coverage within a workspace. For uniquely estimating the location of a transmitter within a workspace from cross-correlation of shadow fading residuals at the receivers require a minimum of three receivers in communication range to this transmitter. So in this stage a minimum receiver placement coverage algorithm is envisioned such that no matter where the transmitter is positioned

within the workspace, there will be at least three wireless receivers in communication range to this transmitter. Since the communication range of a wireless transmitter is non deterministic, probabilistic communication range model is assumed whereby a receiver can accurately decode data from a transmitter with certain probability if it is within a circular disc of radius R centered at the location of transmitter.

In stage 2 of our algorithm, the dynamics of cross-correlation based localization is introduced through CRLB of transmitter localization variance. CRLB which is the inverse of fisher information matrix measures the effect of parameters such as receiver position, number of shadow fading residuals used to compute cross-correlation and so on in accurately estimating the location of a transmitter. In this stage, to achieve localization accuracy better than a predetermined threshold, the algorithm uses the CRLB and the receiver position generated from stage 1 to compute the number of shadow fading residuals that each receiver has to measure for computing cross-correlation in fading noise between its neighbors.

Therefore, this paper begins in Section 2.1 with a brief background on Cramer-Rao Lower Bound while Section 2.2 introduces the wireless shadow fading model. In Section 2.3, the composite likelihood is introduced that simplifies the creation of likelihood function when complex interdependency occurs between measured RSSI samples. Section 3.1 presents the optimal receiver placement grid from complete localization coverage while Section 3.2 handles optimal receiver placement around boundaries of a workspace. Section 3.3 derives the CRLB for shadow fading cross-correlation based transmitter localization. Section 4 list the step by step algorithm for receiver placement for tracking the position of transmitter using cross-correlation of

shadow fading residuals with accuracy better than a predetermined threshold. In Section 5, results and analysis of the proposed approach is demonstrated in simulation and with hardware experiments. Subsequently, some concluding remarks are given.

2. BACKGROUND

A brief background on CRLB and indoor shadowing model is introduced.

2.1 CRAMER-RAO LOWER BOUND

CRLB specifies the theoretical lower bound in variance that is achievable when estimating a deterministic parameter from a series of observations of the random variable using an unbiased estimator [15]. For transmitter localization using shadow fading cross-correlation, the Cartesian coordinate of the transmitter, given by $(\eta = \{\eta_1, \eta_2, \eta_3\}^T)$ where η_1, η_2 and η_3 represents the perpendicular projections onto x, y and z axis, is the parameter that is being estimated from pair-wise correlation coefficient values measured between adjacent receivers. Any unbiased estimator for the parameter of interest that achieves CRLB is said to be a statistically efficient estimator [15]. CRLB is related to the Fisher information matrix as $CRLB(\eta) = I^{-1}(\eta)$ where

$$I(\eta) = \begin{bmatrix} E\left[\left(\frac{\partial}{\partial\eta_1}\ln L(X|\eta)\right)^2\right] & E\left[\frac{\partial}{\partial\eta_1}\ln L(X|\eta)\frac{\partial}{\partial\eta_2}\ln L(X|\eta)\right] & E\left[\frac{\partial}{\partial\eta_1}\ln L(X|\eta)\frac{\partial}{\partial\eta_3}\ln L(X|\eta)\right] \\ E\left[\frac{\partial}{\partial\eta_2}\ln L(X|\eta)\frac{\partial}{\partial\eta_1}\ln L(X|\eta)\right] & E\left[\left(\frac{\partial}{\partial\eta_2}\ln L(X|\eta)\right)^2\right] & E\left[\frac{\partial}{\partial\eta_2}\ln L(X|\eta)\frac{\partial}{\partial\eta_3}\ln L(X|\eta)\right] \\ E\left[\frac{\partial}{\partial\eta_3}\ln L(X|\eta)\frac{\partial}{\partial\eta_1}\ln L(X|\eta)\right] & E\left[\frac{\partial}{\partial\eta_3}\ln L(X|\eta)\frac{\partial}{\partial\eta_2}\ln L(X|\eta)\right] & E\left[\left(\frac{\partial}{\partial\eta_3}\ln L(X|\eta)\right)^2\right] \end{bmatrix}$$ is

the 3×3 fisher information matrix for estimating η from shadow fading correlation coefficient vector $X = \{\rho_{ij}\}; i, j \in \{1,2,\cdots,M\}$, $L(X|\eta)$ is the likelihood function for η from X and $E[\cdot]$ is the expectation function over η. If we assume that the transmitter is not moving in some predictable pattern then *x*, *y* and *z* axis projections of the transmitter coordinates are independent of each other and consequently all off-diagonal elements in the Fisher information matrix are zeros resulting in

$$I(\eta) = \begin{bmatrix} I(\eta_1) & 0 & 0 \\ 0 & I(\eta_2) & 0 \\ 0 & 0 & I(\eta_3) \end{bmatrix} \quad (1)$$

where $I(\eta_k) = E\left[\left(\frac{\partial}{\partial \eta_k} \ln L(X|\eta)\right)^2\right]$.

2.2 INDOOR SHADOW FADING CORRELATION MODEL

For modeling shadow fading in a wireless environment, this paper relies on a wireless propagation model called the Geometrically Based Single Bounce Elliptical Model (GBSBEM) [16]. Though GBSBEM was originally developed to model the Angle of Arrival (AoA) and Time of Arrival (ToA) of incoming signals, it was extended in [3] to model a shadow fading correlation observed between adjacent IEEE 802.15.4 receivers in a dynamic environment such as factory floors, restaurants etc. with pedestrian and machinery traffic.

In this model, any radio signal that reaches the receiver after bouncing off of a scatterer (or radio obstacle) in the localization region can affect signal fading if and only if its ToA satisfies $t \leq \frac{r}{c} + \tau_m$ where r is the radial separation between the transmitter and receiver, c is the speed of radio waves, $\frac{r}{c}$ is the ToA of LoS signal and τ_m is the receiver specific maximum path delay for scattered signals. This upper bound in ToA for signals reaching the receiver defines an elliptical scattering region surrounding the transmitter and receiver, as shown in Figure 1, with the transmitter and receiver forming the foci and the major and minor axis of this ellipse are given by $r + r_m$ and $\sqrt{r_m^2 + 2r_m r}$ respectively where $r_m = c\tau_m$. Any movement of pedestrians or machinery within this elliptical region could potentially influence the RSSI measured at the receiver.

GBSBM can model RSSI values measured by an IEEE 802.15.4 receiver since the IEEE 802.15.4 receivers computes the RSSI as the squared sum of incoming signal

amplitude arriving within an integration time window [17]. Hence τ_m defines the integration time window for an IEEE 802.15.4 receiver. For two adjacent IEEE 802.15.4 receivers $(R_1 \& R_2)$ as in Figure 2, the elliptical scattering regions $(S_1 \& S_2)$ with a common transmitter (T) has an overlapping region (S_{12}) where the presence of any radio obstacle can result in correlated variation in RSSI at both receivers.

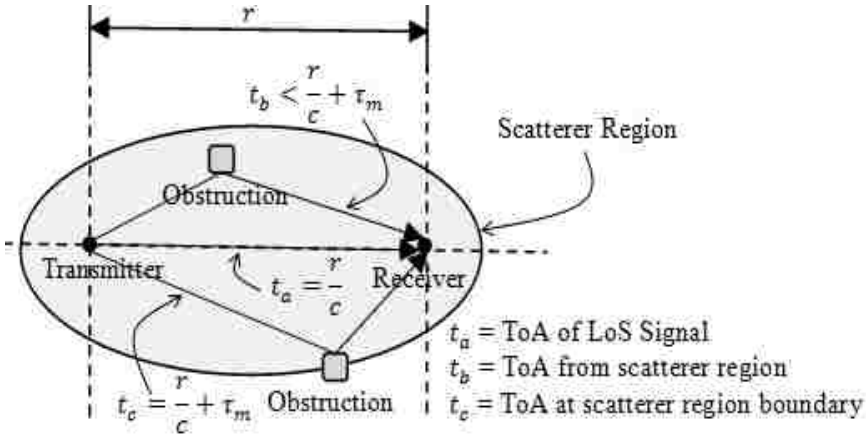

Fig 1. GBSBEM wireless channel model

To account for a dynamic environment with pedestrian and machinery traffic, author in [3] assumed a Poisson traffic rate resulting in the correlation (ρ) between shadow fading residuals observed at receivers R_1 and R_2 for signals arising from a common transmitter T given by

$$\rho = \frac{|S_{12}|}{\sqrt{|S_1||S_2|}}. \quad (2)$$

where S_1 and S_2 are the elliptical scatterer regions surrounding receivers R_1 and R_2 respectively, S_{12} is overlapping region between scattering regions S_1 and S_2 and $|\cdot|$ is the area operator.

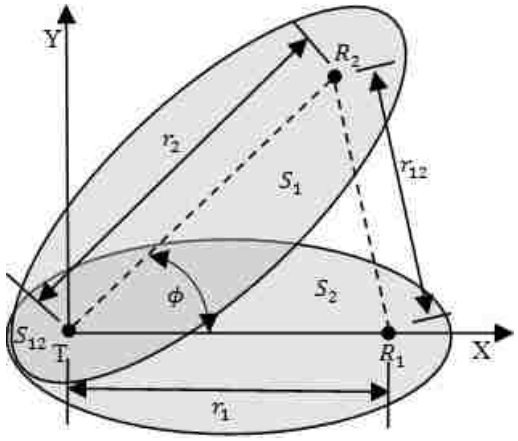

Fig 2. Overlapping of scattering regions causing correlation in shadow fading residuals

To estimate the location of the transmitter from correlation coefficient the distribution of the correlation coefficient has to be derived. In [18, 19], a normalization transformation called the Fisher transformation given by

$$ז = \frac{1}{2}\log\frac{1+\rho}{1-\rho} = \tanh^{-1}(\rho). \quad (3)$$

was applied to approximate the distribution of correlation coefficient by a normal distribution with variance $\frac{1}{M-3}$ where M is the number of data samples used to compute the correlation coefficient.

2.3 COMPOSITE LIKELIHOOD

Estimating parameters for a complicated system with intricate dependency between observations involve the derivation of a full likelihood function that encapsulates all its complexities. For a large number of interdependent observations, full likelihood derivation may be infeasible or computationally burdensome. However, the full likelihood function may be approximated by a weighted product of pair-wise

likelihood function forming a pseudo-likelihood function as in Composite Likelihood (CL) method [20] given by

$$L_c(\eta) = \prod_{i=1}^{M} \prod_{\substack{j=1 \\ i<j}}^{M} L_{ij}\left(\eta \middle| x_i, x_j\right)^{w_{ij}} \tag{4}$$

where $L_c(\eta)$ is the composite likelihood function that is used to approximate the full likelihood, η is the parameter vector that is being estimated from M observations of random variable X whose realization are given by $x_i; i \in \{1,2,\cdots,M\}$, $L_{ij}\left(\eta \middle| x_i, x_j\right)$ is the pair-wise likelihood function between samples $x_i; i \in \{1,2,\cdots,M\}$ and $x_j; j \in \{1,2,\cdots,M\}$ and w_{ij} is the weight function that determines the influence of the pair-wise likelihood $L_{ij}(\cdot\,|\cdots)$ on the overall likelihood function. It was shown in [20] that CL based estimators can be consistent, asymptotic normal and provide a valid compromise between computational burdens and robustness in estimating high dimensional parameters.

For radial distance estimation from shadow fading measurements, the likelihood function has to encapsulate the complicated interdependency arising between RSSI values measured by receivers. Derivation of this likelihood function in a workspace with large number of wireless receivers is a non-trivial problem. In this paper, the actual likelihood function for estimating transmitter location is approximated by a pair-wise pseudo likelihood function obtained from correlation measurement between shadow fading residuals from adjacent receivers using CL method as

$$L_c(\eta) = \prod_{i=1}^{M} \prod_{\substack{j=1 \\ i<j}}^{M} f\left(\text{ר}_{ij} \middle| \eta_{ri}, \eta_{rj}, \eta\right) \tag{5}$$

where ר_{ij} is the Fisher transformed shadow fading correlation coefficient between receivers R_i & R_j positioned at Cartesian coordinates η_{ri} and η_{rj}, η represents the Cartesian coordinate of the transmitter and $f\left(\text{ר}_{ij} \middle| \eta_{ri}, \eta_{rj}, \eta\right)$ respresents the PDF of fisher

transformed shadow fading correlation coefficient when the Cartesian coordinates of the receivers and transmitter are available.

3. RECEIVER PLACEMENT UNDER CROSS-CORRELATION OF SHADOW FADING

It is assumed that a set of M receivers, $S = \{s_1, s_2, \cdots, S_M\}$, are available within workspace A to track the position of a transmitter by measuring cross-correlation of shadow fading residuals between receiver pairs. A probabilistic communication range model is assumed where a receiver $s_i; i \in \{1,2, \cdots, M\}$ located at Cartesian coordinate η_i can successfully detect and decode signals from a transmitter located at Cartesian coordinate η_T with a probability p if and only if $\|\eta_T - \eta_i\| \leq R$ where $\|\cdot\|$ is the Euclidean distance between Cartesian coordinates η_T and η_i.

Now we will define some fundamental properties of receiver placement within A for localization using cross-correlation of shadow fading residuals.

Definition 1: (*Neighbors of a receiver*) For a set of M receivers $S = \{s_1, s_2, \cdots, S_M\}$ deployed in workspace A, a subset of receivers $\mathbb{N}_i \subset S$ is said to be the neighbors of a receiver $s_i \in S$ located at η_i if and only if $\|\eta_i - \eta_j\| \leq R$ where η_j is the location of receiver $s_j \in \mathbb{N}_i$.

Definition 2: (Cross-correlation coverage) A location η in a workspace A is said to be under cross-correlation coverage if and only if there are at least two receivers within communication range of a transmitter if it is located at η i.e.

$$C(\eta) \triangleq \sum_{i=1}^{M} I_{\{0,R\}}(\|\eta - \eta_i\|) \geq 2; s_i \in S \tag{6}$$

where $S = \{s_1, s_2, \cdots, S_M\}$ is the set of M receivers deployed in workspace A, η_i represents the location of receiver $s_i \in S$ and $I_{\{0,R\}}(\|\eta - \eta_i\|) = \begin{cases} 1, & 0 \le \|\eta - \eta_i\| \le R \\ 0, & elsewhere \end{cases}$ is the indicator function.

Since the cross-correlation of shadow fading residuals given by (2) depends only upon the radial separation between a pair of receivers and the transmitter, it is invariant to the reflection in the position of receivers and transmitter. In other words two transmitters that are positioned at mirror locations to the plane joining the receivers will have the same correlation coefficient. Therefore, to uniquely localize a transmitter at every point within the localization workspace requires at least three receivers to be in communication range with the transmitter. Therefore localization coverage is defined as follows.

Definition 3: (Localization coverage) A location η in a workspace A with M receivers, $S = \{s_1, s_2, \cdots, S_M\}$, is said to be under localization coverage if and only if there are at least three receivers within communication range of η i.e.

$$C(\eta) \ge 3; s_i \in S. \tag{7}$$

Definition 4: (*Direct Neighbors*) In a workspace A with M receivers, $S = \{s_1, s_2, \cdots, S_M\}$, receivers $s_j \in S$ and $s_k \in S$ are said to be direct neighbors of receiver $s_i \in S$ if

$$j \triangleq arg \min_{\substack{l \in \{1,2,\cdots,M\} \\ l \ne i}} (\|\eta_i - \eta_l\|) \tag{8}$$

and

$$k \triangleq arg \min_{\substack{l \in \{1,2,\cdots,M\} \\ l \ne i,j}} (\|\eta_i - \eta_l\|). \tag{9}$$

Now we will derive some basic properties for the radial distance between direct neighbors. Subsequently, these properties will be used to derive an optimal geometry for

receiver placement that will span the largest area under cross-correlation coverage within its perimeter with least number of receivers.

Lemma 1: For a receiver s_i that is part of a 2D receiver placement for localization coverage in a workspace A with M receivers, the radial distance to its direct neighbors s_j and s_k should satisfy the following conditions

$$\|\eta_i - \eta_j\| \leq R \tag{10}$$

and

$$\|\eta_i - \eta_k\| \leq R. \tag{11}$$

Proof: Assume that a transmitter is placed next to the receiver s_i then by (7) for this location $(\eta = \eta_i)$ to be under localization coverage, $\sum_{l=1}^{M} I_{\{0,R\}}(\|\eta_i - \eta_l\|) \geq 3$ resulting in $\sum_{\substack{l=1 \\ l\neq i}}^{M} I_{\{0,R\}}(\|\eta_i - \eta_l\|) + I_{\{0,R\}}(\|\eta_i - \eta_i\|) \geq 3$ or

$$\sum_{\substack{l=1 \\ l\neq i}}^{M} I_{\{0,R\}}(\|\eta_i - \eta_l\|) \geq 2 \tag{12}$$

Since by (8) and (9) receivers s_j and s_k are the closest to receivers to s_i and consequently, if these receivers are farther than the communication range R, (12) can never be satisfied. Therefore, the radial distance between receiver s_i and s_j is constrained as in (10) and (11).

3.1 OPTIMAL UNCONSTRAINED RECEIVER PLACEMENT FOR COMPLETE LOCALIZATION COVERAGE

Direct neighbors provide localization coverage for a receiver; consequently, a placement algorithm that attempts to span the workspace with localization coverage with least number of receivers would attempt to maximize this localization coverage area for each receiver while minimizing the overlap of coverage regions provided by other receivers. Now we will derive a receiver placement grid geometry that will maximize the

area spanned by a receiver under localization coverage while minimizing the overlap of coverage regions.

Theorem 1: (*Equilateral Triangular Grid for Receiver Placement*) A receiver placement strategy whose objective is to span the largest area under localization coverage with least number of receiver while ensuring no coverage holes exists within the grid will have all its receivers placed in an equilateral triangular grid.

Proof: Let $\mathrm{H}_i = \{\eta_{i1}, \eta_{i2}, \cdots, \eta_{iN}\}$ represents the position of N receivers that are neighbors of a receiver s_i in this optimal placement algorithm. Under the assumption that the placement of a receiver is not restricted to be within the boundaries of a workspace, this placement algorithm will place receivers maximally separated from each other while maintaining complete localization coverage. From Definition 1, the maximum distance between a receiver s_i to its neighbors is R i.e. $\|\eta_i - \eta_{il}\| = R; \eta_{il} \in \mathrm{H}_i$. In addition, this algorithm should span the entire communication range of s_i under localization coverage using s_i's neighbors without any coverage holes. Figure 3 shows the localization coverage formed around receiver s_i by its two neighbors s_j and s_k that are separated by radial length R from s_i and spanning an interior angle θ. The total localization coverage region due to receivers s_i, s_j and s_k , represented as A_L depends on θ and for $0 < \theta \leq \frac{2\pi}{3}$ it is the region of overlap of three circles as in Figure 3.1 and 3.2 whereas for $\frac{2\pi}{3} < \theta \leq \pi$ A_L is the region of overlap of two circles as in Figure 3.3. The area of region A_L is given by

$$|A_L| = \begin{cases} [\pi - \theta - \sin\theta]R^2 & , \frac{2\pi}{3} < \theta \leq \pi \\ \left[\frac{4\pi}{3} - \sqrt{3} - \theta\right]\frac{R^2}{2} & , 0 < \theta \leq \frac{2\pi}{3} \end{cases}. \tag{13}$$

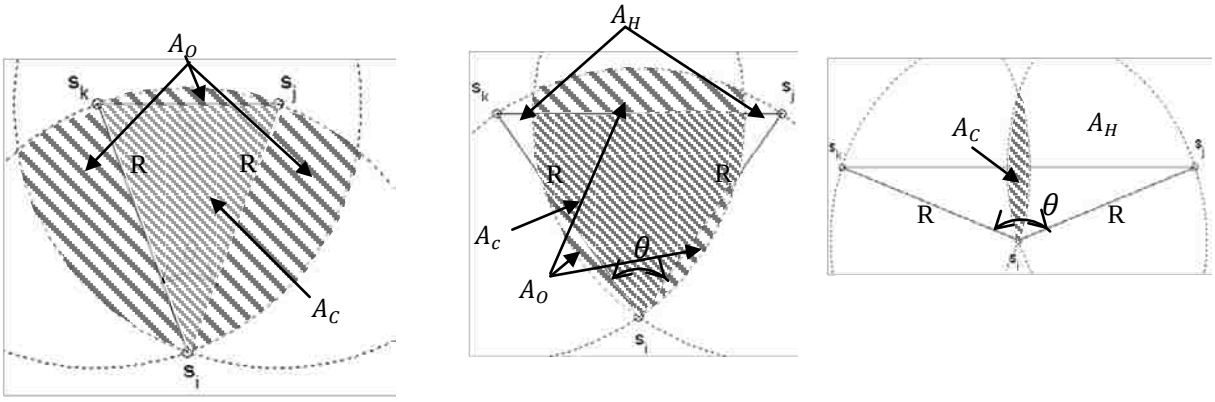

(a) $0 < \theta \leq \frac{\pi}{3}$ (b) $\frac{\pi}{3} < \theta \leq \frac{2\pi}{3}$ (c) $\frac{2\pi}{3} < \theta \leq \pi$

Fig 3. Location coverage by a receiver and its direct neighbors

To span the entire communication range of s_i under localization coverage, other neighbors of s_i will be placed around it leading to overlap in localization coverage which is undesirable. However, the region that falls within a triangle defined by the edges connecting receivers s_i, s_j and s_k has the potential for being only covered by receivers s_i, s_j and s_k. Therefore, the localization coverage region A_L can be divided into two distinct regions depending on whether it falls within or outside this triangular region. Region A_O that overflows this triangular region has the potential for overlapping with the localization coverage provided by other receivers in workspace A whereas, region A_C is uniquely covered by s_i, s_j and s_k provided the area of overlapping region is zero ($|A_O| = 0$). From Figure 3.2 and 3.3, when $\theta > \frac{\pi}{3}$, the communication range of s_i now includes a coverage hole represented by A_H. Therefore, to span the communication range of s_i under localization coverage without any coverage holes, the range of θ is restricted between $0 < \theta \leq \frac{\pi}{3}$. Therefore, to have least number of receivers needed to span the

communication range of s_i under localization coverage for $0 < \theta \leq \frac{\pi}{3}$ the area of triangular region ($|A_C|$) has to be maximized while the area of localization coverage overlapping region ($|A_O|$) has to be minimized. In other words the ratio $\frac{|A_C|}{|A_O|} = \frac{|A_C|}{|A_L| - |A_C|} = \frac{1}{\frac{|A_L|}{|A_C|} - 1}$ has to be maximized or maximize the ratio $\frac{|A_C|}{|A_L|}$. For $0 < \theta \leq \frac{\pi}{3}$, $|A_C| = \frac{1}{2} R^2 \sin\theta$ and $|A_L| = \left[\frac{4\pi}{3} - \sqrt{3} - \theta\right] \frac{R^2}{2}$ resulting in $\frac{|A_C|}{|A_L|}$ given by

$$\frac{|A_C|}{|A_L|} = \frac{\sin\theta}{\frac{4\pi}{3} - \sqrt{3} - \theta}; 0 < \theta \leq \frac{\pi}{3} \tag{14}$$

which attains maximum when $\theta = 60$ degrees.

3.2 RECEIVER PLACEMENT NEAR WORKSPACE BOUNDARY

When receiver placement are restricted to be within a perimeter wall, as is typically in several localization applications, an equilateral grid placement of receivers cannot completely span the workspace under localization coverage. Figure 4 shows localization coverage holes arising due to the constraints on receiver placement imposed by the boundaries of a workspace. However, the objective of receiver placement under boundary constraints remains the same as in unconstrained receiver placement i.e. to maximize the area under localization coverage while minimizing the overlap of coverage regions. Since the perimeter walls restricts possible locations where direct neighbors of a receiver, any location within the workspace that is chosen for its direct neighbors will be at radial distance less than the communication range R. Therefore, if a location $\eta_i \in A$ which is at radial distance $r_j \leq R$ and $r_k \leq R$ to receivers s_j and s_k respectively in A, then if this location η_i is a potential candidate for placing a new receiver s_i if it maximizes the ratio $\frac{|A_C|}{|A_L|}$ given by

$$\frac{|A_C|}{|A_L|} = \begin{cases} \frac{|A_T|}{|A_L|}, & r_{jk} \le R \\ \frac{|A_P|}{|A_L|}, & r_{jk} > R \end{cases} \tag{15}$$

where $r_{jk} = \|\eta_j - \eta_k\|$, $|A_T| = \sqrt{s(s-r_j)(s-r_k)(s-r_{jk})}$ is the area of the triangle formed by joining the edges from η_i to η_j and η_k, $s = \frac{(r_j + r_k + r_{jk})}{2}$, $|A_P|$is the localization region within this triangle shown by shaded region in Figure 5 and $|A_L|$ is the total localization area formed by the overlap in communication range of receivers s_j, s_k and the new receiver s_i at η_i.

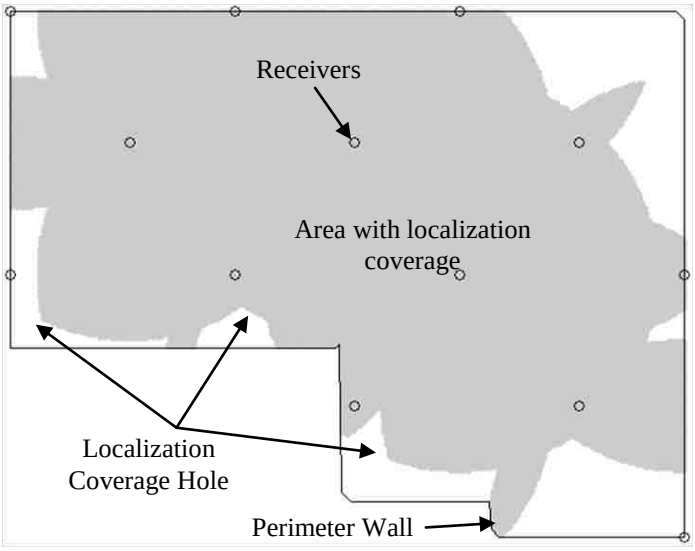

Fig 4. Location coverage holes near the boundary of a perimeter wall

The equation for the area of overlap of three circles to find $|A_L|$ is given in [21]. The area $|A_P|$ is the sum of the area of a pentagon formed by points A, B, C, D and η_i as listed in Figure 5 and two circular sectors of radius R around AB and CD with centers at

η_j and η_k respectively. To find the coordinates of A, B, C and D set the location of receiver s_j as the origin, the intersection points are $A = (-R, 0)$, $\eta_i = \left(-r_j \cos\theta_j\,, -r_j \sin\theta_j\right)$ and $D = \left(-\left(r_{jk} - R\right), 0\right)$ are readily found. However, to find B and C, first find the point of intersections of line $y = -\tan\theta_j\left(x + r_{jk}\right)$ with circle $x^2 + y^2 = R^2$ and line $y = -\tan\theta_k\, x$ with circle $\left(x - r_{jk}\right)^2 + y^2 = R^2$. For the first set of points, location $B = (x_b, y_b)$ is the one that is closer to $\left(-r_{jk}, 0\right)$ while for the later choose the location $C = (x_c, y_c)$ that is closer to $(0,0)$. Therefore the area of region A_L is given by $|A_L| = \frac{1}{2}R^2\left(\theta_j' - \sin\theta_j'\right) + \frac{1}{2}R^2(\theta_k' - \sin\theta_k') - \frac{Ry_b}{2} - \frac{(x_b + x_c)}{2}r_j\cos\theta_j + \frac{(y_b + y_c)}{2}r_j\sin\theta_j - \frac{y_b(r_{jk} - R)}{2}$ where $\theta_k' = 2\sin^{-1}\left(\frac{(x_c - r_{jk} + R)^2 + y_c^2}{2R}\right)$ and $\theta_j' = 2\sin^{-1}\left(\frac{(x_b + R)^2 + y_b^2}{2R}\right)$.

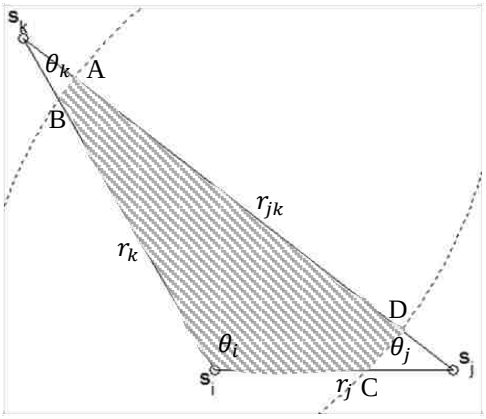

Fig 5. Localization coverage within the triangle defined by joining η_i, η_j and η_k

In the previous section we derived a placement strategy to achieve complete localization coverage. Now we will derive a metric to evaluate this receiver placement in locating the position of a wireless transmitter using cross-correlation of shadow fading residuals measured by the receivers.

3.3 METRIC FOR EVALUATING RECEIVER PLACEMENT UNDER TRANSMITTER LOCALIZATION USING CROSS-CORRELATION OF SHADOW FADING RESIDUALS

In this section, the CRLB of transmitter location estimation variance at a location within the workspace will be derived as function of the Cartesian coordinates of the receivers and the number of RSSI samples used to compute shadow fading cross-correlation. CRLB, which is the inverse of fisher information, provide an insight into the extent to which parameters such as the position of a particular receiver within the workspace or the number of RSSI samples used to measure cross-correlation can be adjusted to attain specific transmitter localization accuracy.

Since the objective of this paper is find a receiver placement that will attain transmitter localization accuracy better than a pre-specified threshold (ϵ_u), our primary parameter of interest is the maximum CRLB within a workspace. If $\mathrm{J}(\eta_\mathrm{T}|\mathrm{H}_s, \mathrm{W})$ represents the CRLB for a location η_T within the workspace A as a function of the receiver position H_s and W the number of RSSI samples from which the cross-correlation between shadow fading residuals were measured, then

$$\Gamma(\mathrm{H}_s, W) = \max_{\eta_T \in A} J(\eta_T|\mathrm{H}_s, W) \tag{16}$$

is the metric that will be used to compare receiver placement strategies. The point η_{max} where this maximum CRLB was observed is given by

$$\eta_{\max} = arg\max_{\eta_T \in A} J(\eta_T|\mathrm{H}_s, W). \tag{17}$$

Now we will derive the CRLB for a particular location within the workspace.

Theorem 2: (*CRLB for shadow fading cross-correlation*) Cramer-Rao Lower Bound for the variance in estimating the transmitter at Cartesian coordinate η_T within a workspace A from $N \geq 3$ receivers that are under localization coverage with a transmitter using cross-correlation of shadow fading residuals between receiver pairs is given by

$$J(\eta_T|H_s, W) = \frac{1}{4(W-3)} \sum_{k=1}^{3} \left[\frac{1}{\sum_{i=1}^{N} \sum_{\substack{j=1 \\ i<j}}^{N} \frac{1}{\left(1-\rho_{ij}^2\right)^2} \left[\frac{\partial \rho_{ij}}{\partial \eta_{Tk}}\right]^2} \right] \tag{18}$$

where $\mathrm{H}_s = \{\eta_1, \eta_2, \cdots, \eta_N\}$ are the Cartesian coordinates of receivers $S = \{s_1, s_2, \cdots, s_N\}$, W is the number of RSSI samples used by receiver pairs s_i & $s_j; i, j \in S, i \neq j$ to compute cross-correlation ρ_{ij} and η_{T1}, η_{T2} and η_{T3} are the x, y and z orthogonal Cartesian components of η_T.

Proof: If the estimated position of the transmitter is at $\eta_T = \{x, y, z\}$ while the transmitter was actually at $\eta_{T0} = \{x_0, y_0, z_0\}$ then the square of the localization estimation error is given by $\|\eta_T - \eta_{T0}\|^2 \triangleq (x - x_0)^2 + (y - y_0)^2 + (z - z_0)^2$. The average value of this localization error, called the Mean Square Error (MSE), for transmitter localization when the receivers are at H_s and cross-correlation was computed from W RSSI samples is given by $MSE(\eta_T|\mathrm{H}_s, W) \triangleq E[\|\eta_T - \eta_{T0}\|^2|\mathrm{H}_s, W] = E[(x - x_0)^2 + (y - y_0)^2 + (z - z_0)^2|\mathrm{H}_s, W]$. Under the assumption that the x, y and z coordinates of a transmitter are independent of each other then $MSE(\eta_T|\mathrm{H}_s, W) = E[(x - x_0)^2|\mathrm{H}_s, W] + E[(y - y_0)^2|\mathrm{H}_s, W] + E[(z - z_0)^2|\mathrm{H}_s, W] = Var(x|\mathrm{H}_s, W) + Var(y|\mathrm{H}_s, W) + Var(z|\mathrm{H}_s, W)$ where $Var(\cdot)$ represents the variance function over random variable. The lower bound for MSE of localization error is given by the CRLB as

$Var(x|\mathrm{H}_s, W) \geq \frac{1}{I(x|\mathrm{H}_s,W)}$, $Var(y|\mathrm{H}_s, W) \geq \frac{1}{I(y|\mathrm{H}_s,W)}$ and $Var(z|\mathrm{H}_s, W) \geq \frac{1}{I(z|\mathrm{H}_s,W)}$ resulting in $MSE(\eta_T|\mathrm{H}_s, W) \geq \frac{1}{I(x|\mathrm{H}_s,W)} + \frac{1}{I(y|\mathrm{H}_s,W)} + \frac{1}{I(z|\mathrm{H}_s,W)} = \sum_{k=1}^{3} \frac{1}{I(\eta_{Tk}|\mathrm{H}_s,W)}$ where the orthogonal x, y and z components of the Cartesian coordinates of the transmitter are represented by η_{T1}, η_{T2} and η_{T3} respectively and $I(\eta_{Tk}|\mathrm{H}_s, W); k \in \{1,2,3\}$ represents the Fisher information matrix for the orthogonal Cartesian coordinate component $\eta_{Tk}; k \in \{1,2,3\}$ of transmitter when H_s and W are available. Therefore, the lower bound for MSE in locating a transmitter at position x, y and z within the workspace using N receivers positioned at $\mathrm{H_s} = \{\eta_{\mathrm{s1}}, \eta_{\mathrm{s2}}, \cdots, \eta_{\mathrm{sN}}\}$ is given by

$$J(\eta_T|\mathrm{H}_s, W) = \min[MSE(\eta_T|\mathrm{H}_s, W)] = \sum_{k=1}^{3} \frac{1}{I(\eta_{Tk}|\mathrm{H}_s,W)} = Tr\left(\frac{1}{I(\eta_T|\mathrm{H}_s,W)}\right). \quad (19)$$

Since the derivation of the exact likelihood function for a set of N receivers used for cross-correlation based localization is quite difficult, we will approximate the actual likelihood with the composite likelihood as explained in section 2.3. The composite likelihood of observing a sequence of fisher transformed shadow fading correlation coefficients from N receivers that are in communication range with the transmitter and each computing cross-correlation from W RSSI samples from the transmitter is given by

$$L(\eta_T|\mathrm{H}_s, W) \propto \prod_{i=1}^{N} \prod_{\substack{j=1 \\ i<j}}^{N} \exp\left\{-\frac{\left(\hat{\mathrm{ϒ}}_{ij} - \mathrm{ϒ}_{ij}\right)^2}{\frac{1}{(\mathrm{W}-3)}}\right\} \quad (20)$$

where $\hat{\mathrm{ϒ}}_{\mathrm{ij}} = \tanh^{-1}\left(\hat{\rho}_{\mathrm{ij}}\right)$ is the fisher transformation applied to the measured correlation coefficient $\left(\hat{\rho}_{\mathrm{ij}}\right)$ between receivers $\mathrm{R_i}$&$\mathrm{R_j}$ while $\mathrm{ϒ}_{\mathrm{ij}} = \tanh^{-1}\left(\rho_{\mathrm{ij}}\right)$ is the shadow fading correlation between receiver $\mathrm{R_i}$&$\mathrm{R_j}$ arising from GSBEM as in (2). The log-likelihood is given by

$$l(\eta_T|\mathrm{H}_s, W) = \log L(\eta_T|\mathrm{H}_s, W) = C + -(W-3) \sum_{i=1}^{N} \sum_{\substack{j=1 \\ i<j}}^{N} \left(\hat{\mathrm{ϒ}}_{ij} - \mathrm{ϒ}_{ij}\right)^2. \quad (21)$$

where C is a constant that is used to normalize $L(\eta_T|\mathrm{H}_s, W)$.

Therefore, the Fisher information for estimating the Cartesian coordinate projections $\eta_{Tk}; k \in \{1,2,3\}$ along x, y and z axis is given by

$$I(\eta_{Tk}|\mathrm{H}_s, W) = E\left[\left(\frac{\partial}{\partial \eta_{Tk}} l(\eta_T|\mathrm{H}_s, W)\right)^2\right]$$
$$= 4(W-3)^2 E\left\{\left[\sum_{i=1}^{N}\sum_{\substack{j=1 \\ i<j}}^{N}\left(\hat{\mathfrak{1}}_{ij} - \mathfrak{1}_{ij}\right)\frac{\partial \mathfrak{1}_{ij}}{\partial \eta_{Tk}}\right]^2\right\}. \quad (22)$$

Assuming that the cross-correlation measurement errors are assumed to be independent, (22) can be simplified as

$$I(\eta_{Tk}|\mathrm{H}_s, W) = 4(W-3)^2 E\left\{\left[\sum_{i=1}^{N}\sum_{\substack{j=1 \\ i<j}}^{N}\left(\hat{\mathfrak{1}}_{ij} - \mathfrak{1}_{ij}\right)\frac{\partial \mathfrak{1}_{ij}}{\partial \eta_{Tk}}\right]^2\right\}$$
$$= 4(W-3)^2 \sum_{i=1}^{N}\sum_{\substack{j=1 \\ i<j}}^{N} E\left[\left(\hat{\mathfrak{1}}_{ij} - \mathfrak{1}_{ij}\right)^2\right]\left[\frac{\partial \mathfrak{1}_{ij}}{\partial \eta_{Tk}}\right]^2$$
$$= 4(W-3)\sum_{i=1}^{N}\sum_{\substack{j=1 \\ i<j}}^{N}\left[\frac{\partial \mathfrak{1}_{ij}}{\partial \eta_{Tk}}\right]^2. \quad (23)$$

Since $E\left[\left(\hat{\mathfrak{1}}_{ij} - \mathfrak{1}_{ij}\right)^2\right] = \frac{1}{W-3}$ and $\frac{\partial \mathfrak{1}_{ij}}{\partial \eta_k} = \frac{1}{\left(1-\rho_{ij}^2\right)}\frac{\partial \rho_{ij}}{\partial \eta_{Tk}}$ resulting in (23) being written as

$$I(\eta_{Tk}|\mathrm{H}_s, W) = 4(W-3)\sum_{i=1}^{N}\sum_{\substack{j=1 \\ i<j}}^{N}\frac{1}{\left(1-\rho_{ij}^2\right)^2}\left[\frac{\partial \rho_{ij}}{\partial \eta_{Tk}}\right]^2. \quad (24)$$

Now applying (19) on (23) gives the CRLB for transmitter location estimation variance from measuring cross-correlation in shadow fading residuals between N receivers located at H_s as in (18).

Therefore, the CRLB for a location in the workspace can be reduced by increasing the number of RSSI samples (W) used to compute cross-correlation (2) or by adjusting the position of the receivers such that the new position of the receivers will result in less noise in measuring the correlation coefficient of shadow fading for radio signals from the common transmitter. In addition, we will now show that just by adding a new receiver to

the list of receivers that are already in communication range with a transmitter the CRLB can be further reduced.

Corollary 1: (*CRLB and receiver count*) Increasing the number of receivers under localization coverage at a location η within the workspace reduces the CRLB for transmitter location estimation variance using cross-correlation of shadow fading residuals at that location.

Proof: Let $\mathrm{H}_s = \{\eta_1, \eta_2, \cdots, \eta_N\}$ and $\mathrm{H}'_s = \{\eta_1, \eta_2, \cdots, \eta_N, \eta_{N+1}\}$ then $\mathrm{I}(\eta_{\mathrm{Tk}}|\mathrm{H_s}, \mathrm{W}) = \sum_{\mathrm{i}=1}^{\mathrm{N}} \sum_{\substack{\mathrm{j}=1 \\ \mathrm{i}<j}}^{\mathrm{N}} \frac{1}{\left(1-\rho_{\mathrm{ij}}^2\right)^2} \left[\frac{\partial \rho_{\mathrm{ij}}}{\partial \eta_{\mathrm{Tk}}}\right]^2$ and $\mathrm{I}(\eta_{\mathrm{Tk}}|\mathrm{H}'_{\mathrm{s}}) = \sum_{\mathrm{i}=1}^{\mathrm{N}+1} \sum_{\substack{\mathrm{j}=1 \\ \mathrm{i}<j}}^{\mathrm{N}+1} \frac{1}{\left(1-\rho_{\mathrm{ij}}^2\right)^2} \left[\frac{\partial \rho_{\mathrm{ij}}}{\partial \eta_{\mathrm{Tk}}}\right]^2$ or by rearranging $\mathrm{I}(\eta_{\mathrm{Tk}}|\mathrm{H}'_{\mathrm{s}}) = \sum_{\mathrm{i}=1}^{\mathrm{N}} \sum_{\substack{\mathrm{j}=1 \\ \mathrm{i}<j}}^{\mathrm{N}} \frac{1}{\left(1-\rho_{\mathrm{ij}}^2\right)^2} \left[\frac{\partial \rho_{\mathrm{ij}}}{\partial \eta_{\mathrm{Tk}}}\right]^2 + \sum_{\mathrm{i}=1}^{\mathrm{N}+1} \frac{1}{\left(1-\rho_{\mathrm{i(N+1)}}^2\right)^2} \left[\frac{\partial \rho_{\mathrm{i(N+1)}}}{\partial \eta_{\mathrm{Tk}}}\right]^2 = \mathrm{I}(\eta_{\mathrm{Tk}}|\mathrm{H_s}) + \sum_{\mathrm{i}=1}^{\mathrm{N}+1} \frac{1}{\left(1-\rho_{\mathrm{i(N+1)}}^2\right)^2} \left[\frac{\partial \rho_{\mathrm{i(N+1)}}}{\partial \eta_{\mathrm{Tk}}}\right]^2$.

Since $\sum_{\mathrm{i}=1}^{\mathrm{N}+1} \frac{1}{\left(1-\rho_{\mathrm{i(N+1)}}^2\right)^2} \left[\frac{\partial \rho_{\mathrm{i(N+1)}}}{\partial \eta_{\mathrm{Tk}}}\right]^2 \geq 0 \Rightarrow \mathrm{I}(\eta_{\mathrm{Tk}}|\mathrm{H}'_{\mathrm{s}}) \geq \mathrm{I}(\eta_{\mathrm{Tk}}|\mathrm{H_s})$ resulting in $\frac{1}{\mathrm{I}(\eta_{\mathrm{Tk}}|\mathrm{H_s})} \geq \frac{1}{\mathrm{I}(\eta_{\mathrm{Tk}}|\mathrm{H}'_{\mathrm{s}})} \Rightarrow J(\eta_T|H_s, W) \geq J(\eta_T|H'_s, W)$

4. RECEIVER PLACEMENT ALGORITHM

The receiver placement algorithm for a workspace A measuring 387 units x 369 units using receivers that have a 99 percentile communication range of 80 units, i.e. $R = 80$, and a maximum path delay of $r_m = 20$ units can be described as

1. Let x_{offset} and y_{offset} represents the offsets from bottom left corner of the workspace A from which the equilateral grid placement starts. In addition let ϕ represents the orientation of the grid with respect to the x axis, then using brute force

search through $x_{offset} \in \{0, R\}$, $y_{offset} \in \left\{0, \frac{\sqrt{3}}{2}R\right\}$ and orientation $\phi \in \{0,120\}$ for an equilateral grid with least number of receivers that will fit inside the workspace A such that the shortest distance between the receivers in this grid to the nearest boundary wall is as large as possible and is less than R. This will ensure the maximum coverage of the workspace with an equilateral grid while ensuring that the coverage holes at the boundary of the workspace are as large as possible. Figure 6.1 shows the equilateral grid placement while Figure 6.2 shows the localization coverage in dark gray within this workspace.

2. For each coverage hole, search through possible points in its vicinity that maximizes (9). Repeat this step till the entire workspace falls under localization coverage. Figure 7.1 shows the receivers placements and the resulting localization coverage within the workspace. The intensity of the shading represents $C(\eta)$ give by (6) at a location $\eta \in A$.

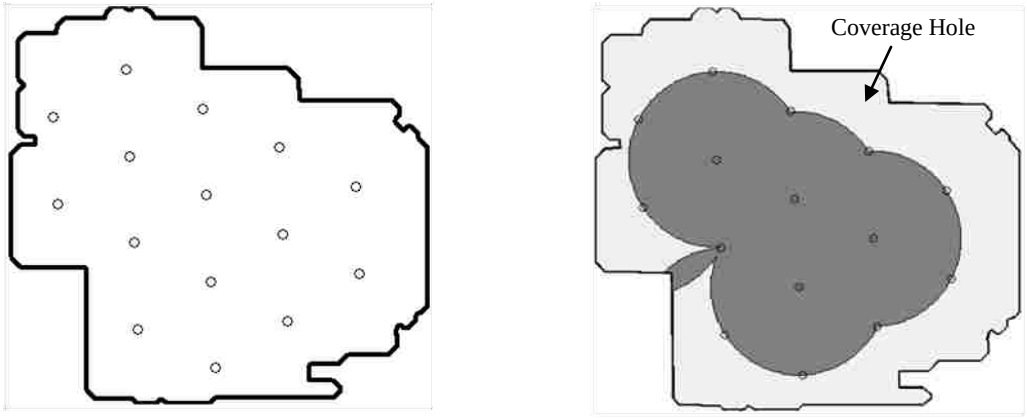

(1) Equilateral grid placement

(2) Localization coverage due to equilateral grid placement

Fig 6. Initial stages of receiver placement algorithm within a workspace

3. The receiver placement H_s generated in previous step forms the input to (16). $J(\eta_T|\mathrm{H}_s, W)$ is computed for various position of transmitter (η_T) within the workspace A and is plotted in Figure 7.2. $\Gamma(\mathrm{H}_s, W)$, which the maximum of $J(\eta_T|\mathrm{H}_s, W)$ for the entire workspace, is computed for various values of W till $\sqrt{\Gamma(\mathrm{H}_s, W)} \leq \varepsilon_{\mathrm{u}}$. For the layout under consideration for this demonstration, the number of shadow fading residuals to be measured by the receiver to achieve $\epsilon_u = 10$ was found to be at $W = 83$.

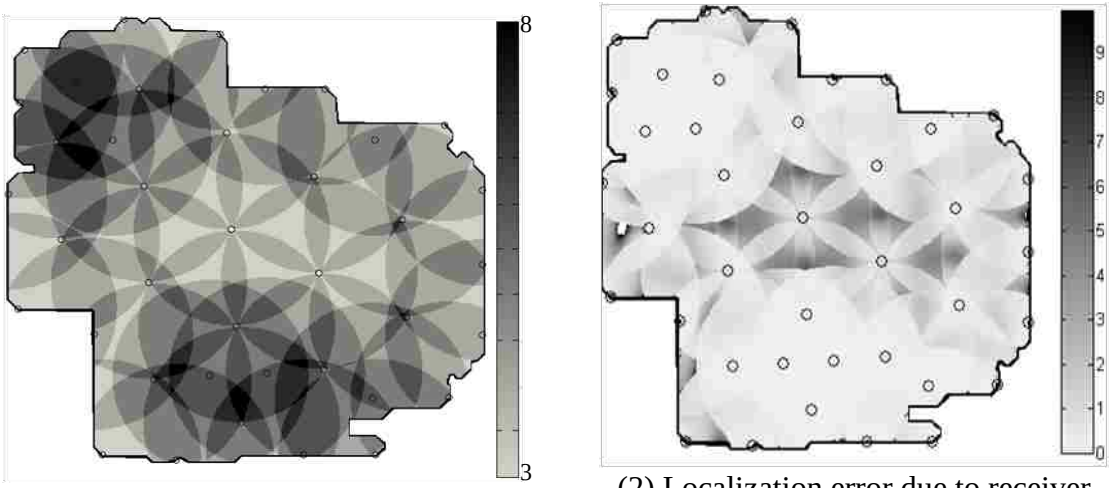

(1) Localization coverage due to receiver placement

(2) Localization error due to receiver placement

Fig 7. Receiver placement localization coverage and error analysis within a workspace

5. RESULTS AND ANALYSIS

In this section we analyze the performance of our receiver placement algorithm in comparison to receiver placement algorithms using Delaunay refinement triangulation [8]. The receiver placement strategy in [8] was developed for transmitter localization

using RSSI ranging. However, the central idea behind this method is to use Delaunay refinement algorithm to search through the localization workspace for receiver positions that would minimize the transmitter localization error. Hence this method can be easily adapted to work for our cross-correlation based localization by using (16) as the quality metric for Delaunay refinement in [8].

5.1 RECEIVER COUNT VS. COMMUNICATION RANGE

In this simulation the communication range of wireless transceivers used for localization was varied from 1.7m to 5.3m and the number of receivers needed to cover ERL 114 lab that measured 12m x 13m in dimension was plotted in Figure 8 for both the proposed placement strategy and Delaunay Refinement placement strategy [8]. The pre-specified localization error threshold ϵ_u was set at 1m. This required 135 shadow fading samples to be used to compute correlation coefficient for the proposed placement strategy. For [8], the number of samples W used to compute the quality metric (16) is determined by the value W for a 3 receiver equilateral triangular placement with edges equal to the communication range that would result in (16) less than or equal to ϵ_u^2.

From the Figure 8, Delaunay refinement method resulted in slightly large number of receivers than the coverage method proposed in this paper. The primary reason for this higher count for the number of receivers in Delaunay refinement placement algorithm in comparison to our placement algorithm stems from adapting a computation geometry method such as Delaunay refinement for receiver placement. Delaunay triangulation was originally developed to build equilateral triangular meshes for solving finite element method simulations [9]. Hence regions that are close to the boundary conditions typically need more sample points to create accurate meshes to represent the variation of the field that is being simulated as they have to satisfy the twin requirement of equilateral mesh

and satisfying the quality criterion (pre-specified error threshold). In adapting the DR method for receiver placement, the authors in [8] used the receiver position in the workspace as the sample points to simulate the variation of transmitter localization error over the workspace. Therefore, for workspace with not so smooth bounding wall, the necessity to satisfy the twin requirement of equilateral mesh pattern while satisfying the pre-specified error threshold can result in more receivers being placed near the bounding walls. On the contrary our method works by finding receiver locations near the coverage hole that maximizes (15) and consequently has more freedom in exploring possible location.

5.2 LOCALIZATION ACCURACY VS. RECEIVER PLACEMENT

Figure 9 shows the placement of receivers for the proposed scheme for maximum wireless communication range of 5.5m.

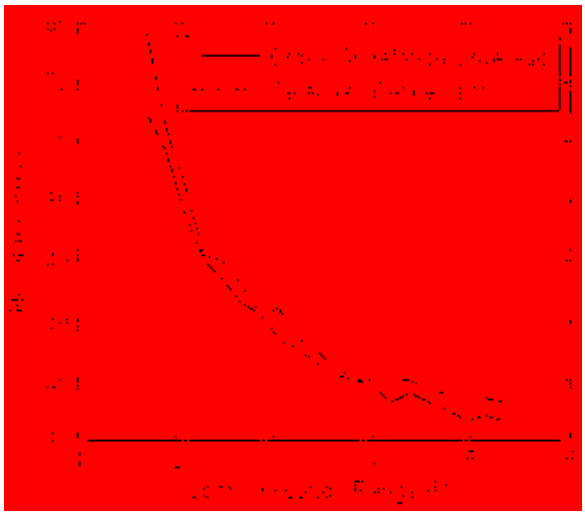

Fig 8. Receiver count vs. communication range

The proposed solution yielded 11 receivers to provide complete localization coverage. In this simulation, the receivers will localize the position of a transmitter that is placed at 10 random test points marked T_1 through T_{10} in workspace as shown in Figure 9 with a pre-specified error threshold of $\epsilon_u = 1m$.

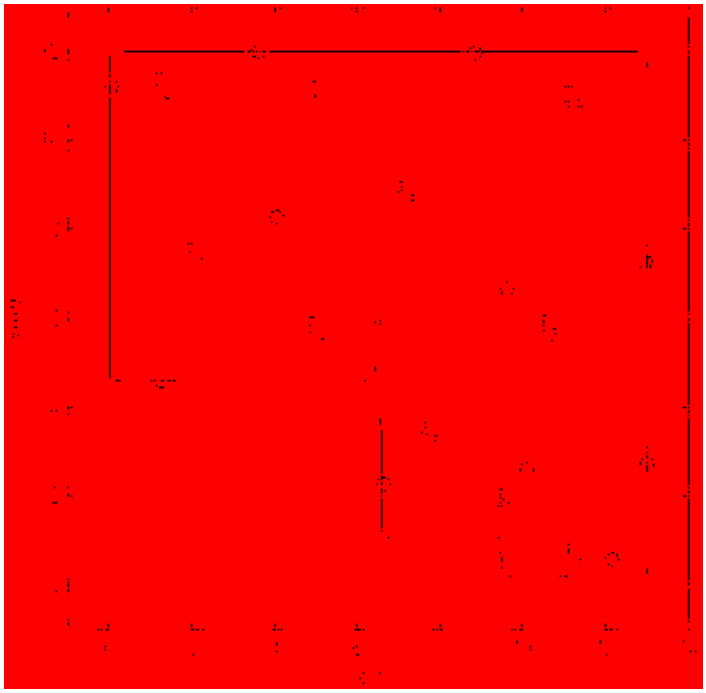

Fig 9. Receiver placement over sample workspace

Correlated shadow fading at the receivers was simulated by first generating Poisson distributed pedestrian interferers with an average pedestrian density of $\omega = 1$ pedestrian/sq.m that are uniformly distributed around the localization workspace. Subsequently, standard normal random variable corresponding to the attenuation factor in dB of each pedestrian interferer is generated. The net shadow fading loss in dB at each receiver is the sum total of all attenuation factors for each interferer within the elliptical

scattering region surrounding the receiver and the common transmitter at a test point $T_i; i \in \{1,2,\cdots,10\}$. In the previous simulation it was derived that to achieve $\epsilon_u = 1m$ for ERL 114, 135 shadow fading samples have to be collected. Hence the process of generating Poisson interferers followed by summing the standard normal attenuation factors were repeated 135 times to generate the required shadow fading samples at each receiver for a single localization simulation run. Statistical data from 40 such runs are tabulated in Table 1.

TABLE 1. LOCALIZATION ERROR LEVELS AT VARIOUS LOCATIONS

Transmitter Location	**No. of receivers in range**	**Localization Error (m)**			
		Mean	**Median**	**90th Perc.**	**Std. Dev**
T_1	4	0.894	0.792	1.579	0.466
T_2	3	0.926	0.883	1.526	0.472
T_3	4	0.792	0.828	1.377	0.418
T_4	4	0.779	0.698	1.534	0.481
T_5	4	0.879	0.927	1.445	0.407
T_6	3	0.955	1.100	1.693	0.562
T_7	5	0.652	0.690	1.076	0.325
T_8	6	0.677	0.550	1.401	0.484
T_9	3	0.907	0.943	1.484	0.475
T_{10}	4	0.712	0.762	1.167	0.360

The average error at all the test points were within the pre-specified upper threshold of $\epsilon_u = 1m$. Localization accuracy at test point T_6 was the highest of all the 10 test points and would be attributed to (a) the presence of the bounding wall that restricts the number of interferers that can contribute to the correlation coefficient at receivers and (b) only 3 receivers are in range of that test point. The localization accuracy at other test point followed the number of receivers that are in communication range of that test point

as expected from (16). The median error was also well within ϵ_u except for test point T_6 which as explained earlier has only 3 receivers in range and is close to the bounding walls.

6. CONCLUSIONS

In this paper, a novel placement algorithm for transmitter localization using cross-correlation of shadow fading residuals was presented. The feasibility of the proposed receiver placement algorithm was demonstrated using simulations. The receiver count generated by our algorithm was shown to be better than Delaunay refinement based algorithm [8]. Localization accuracy simulations have shown that the receivers were able to localize the transmitters with average accuracy better than the pre-specified error threshold.

REFERENCES

[1] A. Ramachandran, and S. Jagannathan, "Spatial diversity in signal strength based WLAN location determination systems," *Proc. of the 32nd IEEE Conf. on Local Comp. Networks* , pp. 10-17, Oct. 2007.

[2] N. R. Yousef, A. Sayed, and L. Jalloul, "Robust wireless location over fading channels," *IEEE Trans. Veh. Technol.*, vol. 52, no. 1, pp. 117–126, 2003.

[3] M. R. Basheer, and S. Jagannathan, "Localization of objects using cross-correlation of shadow fading noise and copulas," *Global Telecommunications Conference (GLOBECOM 2011), 2011 IEEE* , pp.1-5, 5-9 Dec. 2011.

[4] F. Gustafsson and F. Gunnarsson. "Mobile positioning using wireless networks: Possibilities and fundamental limitations based on available wireless network measurements," *IEEE Signal Proc. Magazine*, vol. 22, no. 4, pp. 41–53, Jul. 2005.

[5] S. Martínez, and F. Bullo, "Optimal sensor placement and motion coordination for target tracking," *Proc. of the inter. Conf. on Robotics and Automation*, Barcelona, Spain, pp. 4544-4549, April 2005.

[6] R. Rajagopalan, N. Ruixin, C.K. Mohan, P.K. Varshney, and A.L. Drozd, “Sensor placement algorithms for target localization in sensor networks,” Radar Conference, 2008. RADAR '08. IEEE , vol., no., pp.1-6, 26-30 May 2008

[7] A. Bishop, B. Fidan, B. Anderson, K. Dogancay, and P. Pathirana, “Optimality analysis of sensor-target localization geometries,” Automatica, vol. 46, no. 3, pp. 479–492, 2010.

[8] M.R. Basheer, and S. Jagannathan, “A new receiver placement scheme using Delaunay refinement-based triangulation,” *Wireless Comm. and Netw. Conf. (WCNC), 2010 IEEE* , vol., no., pp.1-6, 18-21 April 2010

[9] J.R. Shewchuk, “Delaunay Refinement Algorithms for Triangular Mesh Generation,” *Comp. Geometry: Theory and Appl.*, vol. 22, no. 1-3, pp. 21-74, May 2002.

[10] C. Wu, K. Lee, and Y. Chung, “A Delaunay Triangulation based method for wireless sensor network deployment,” *Comp. Comm.*, vol. 30, no. 14-15, pp. 2744-2752, Oct 2007.

[11] S. Martínez, and F. Bullo, “Optimal sensor placement and motion coordination for target tracking,” *Proc. of the inter. Conf. on Robotics and Automation*, Barcelona, Spain, pp. 4544-4549, April 2005.

[12] V. Isler, “Placement and distributed deployment of sensor teams for triangulation based localization,” In *Proc. IEEE ICRA*, pp. 3095-3100, May, 2006.

[13] Yousi Zheng, Han Wang, Lei Wan, Xiaofeng Zhong, “A placement strategy for accurate TOA localization algorithm,” *Annual Conference on Communication Networks and Services Research*, pp. 166-170, 2009.

[14] N. Bulusu, J. Heidemann, D. Estrin, “Adaptive beacon placement,” *Distributed Computing Systems, 2001. 21st Intl. Conf. on.* , pp. 489-498, Apr 2001.

[15] H. L. Van Trees, Detection, Estimation, and Modulation Theory, Part I, *New York: Wiley*, 1968.

[16] J.C. Liberti, and T.S. Rappaport, “A geometrically based model for line-of-sight multipath radio channels,” *Vehicular Tech. Conf., 1996. Mobile Tech. for the Human Race., IEEE 46th* , vol.2, pp.844-848, May 1996.

[17] Hyeon-Jin Jeon, T. Demeechai, Woo-Geun Lee, Dong-Hwan Kim and Tae-Gyu Chang, "IEEE 802.15.4 BPSK receiver architecture based on a new efficient detection scheme," *IEEE Trans. on Signal Proc.*, vol.58, no.9, pp.4711-4719, Sept. 2010.

[18] H. Hotelling, "New Light on the Correlation Coefficient and its Transforms," *Journal of the Royal Statistical Society. Series B (Methodological)*, vol. 15, no. 2, pp. 193-232, 1953.

[19] R.A. Fisher, "Frequency distribution of the values of the correlation coefficient in samples of an indefnitely large population," Biometrika, vol. 10, no. 4, pp. 507-521, 1915.

[20] C. Varin, N. Reid, and D. Firth, "An overview on composite likelihood methods," Statistica Sinica, 21, in press., 2011.

[21] M.P. Fewell, "Area of common overlap of three circles," *Tech. Rep. DSTO-TN-0722, Australian Government, Department of Defence, Defence Science and Technology Organization*, Oct. 2006.

SECTION

2. CONCLUSIONS AND FUTURE WORK

In this dissertation localization of a mobile transmitter in an indoor environment using radio signal strength indicator was undertaken while addressing many of the common limitations of the existing approaches. Signal fading arising in multipath rich environment such as factory floors, indoor malls and so on provide considerable challenge to accurately localizing transmitters for existing received signal strength indicator (RSSI) based localization algorithm was the primary focus of the research. Our localization strategy takes advantage of radio fading by measuring the spatial correlation in RSSI that arise between co-located receivers when movement of people or machinery occurs in its vicinity. Additionally, velocity estimation using α-divergence of RSSI is particularly suited for tracking slow moving targets such as pedestrians which showed considerable measurement noise in velocity estimation using accelerometers in an Inertial Navigation Systems. Finally, combining cross-correlation based localization with α-divergence based tracking using Bayesian particle filters was shown to achieve sub-meter accuracy.

In the first paper, localization errors for a range-based localization algorithm under line of sight (LoS) and non LoS (NLoS) conditions between a transmitter and receiver were considered to develop a localization quality metric called *R-factor*. Application of *R-factor* to existing range-based localization algorithm called Proximity in Signal Space (PSS) was shown to improve the robustness of its transmitter location estimates by avoiding radial distance estimates from receivers that has large mean square error. Additionally, *R-factor* has the potential to reduce energy consumption at the

receivers and base station by forwarding only those RSSI values to the base station that has an *R-factor* below a threshold set by the base station.

This paper also shows that using spatial diversity and combining RSSI values from them by taking the root mean square (RMS) can reduce the R-factor at a receiver thereby improving the accuracy of locating a transmitter. The efficacy of the proposed localization quality metric was demonstrated on IEEE 802.15.4 transceivers running PSS where the mean localization accuracy improved by 22%. Adding antenna diversity to the receivers and combining the individual RSSI from each diversity channel through RMS improved the mean localization accuracy by 27%. Therefore, existing localization algorithms that use time, angle or RSSI for position can take advantage of the R-factor to improve localization estimates.

The second paper looked into a receiver placement strategy that would limit the error in locating a transmitter using range-based localization algorithm below a user specified threshold with least number of receivers. The presented sub-optimal placement solution employs Constrained Delaunay Triangulation with refinement to tessellate the localization area into independent triangular sections. Receivers placed at the vertices of these triangular sections are guaranteed to locate a transmitter with accuracy better than the user specified threshold. Application of our placement strategy on an existing range-based localization algorithm called Constrained Weighted Least Square (CWLS) resulted in 75 percentile of localization estimates with an error less than the threshold of 1m. Further, in comparison to a placement algorithm based on heuristics, our placement strategy improved the localization accuracy by 21% primarily by eliminating receiver

placement geometries that could potentially result in large dilution of precision for range-based localization methods.

The third paper introduced a cross-correlation based localization strategy called *LOCUST* for passive RFID tag localization. LOCUST relies on the functional relationship between cross-correlation in backscattered multipath noise and the radial distance between RFID tags to relatively localization them in a target area. Pair-wise cross-correlation information from a cluster of RFID tags was combined using a composite likelihood method to form the localization optimization function which was then solved to obtain their Cartesian coordinates using a stochastic optimization technique called simulated annealing with tunneling.

Simulation results from localizing 16 RFID tags under LoS and NLoS conditions in a localization area that measures 20m x 20m x 20m has shown consistently that LOCUST performs better than manifold learning algorithms such as multi-dimensional scaling (MDS) and locally linear embedding (LLE) for various operating frequency up to 100MHz. However, the multipath fading cross-correlation falls rapidly to zero for radial separations above a wavelength distance between the RFID tags. Consequently, this technique is relegated to localize RFID tags that operate under 15MHz for practical purposes.

Fourth paper extended the operating frequency of cross-correlation based localization to 2.4GHz by exploiting the cross-correlation in shadow fading instead of the cross-correlation in multipath fading. An Ornstein-Uhlenbeck stochastic filter was presented to extract shadow fading residuals from the measured RSSI values. Subsequently, these residuals are combined using a Student-t copula likelihood function

that was solved using simulated annealing with tunneling optimization algorithm. In addition, a dead-reckoning based mobile tracking algorithm where the relationship between a mobile transmitter's velocity and the α-divergence of RSSI signals measured by receivers was introduced.

To prevent the localization error from accumulating over time in the dead-reckoning based tracking scheme, a Bayesian particle filter was presented where position estimates from dead-reckoning based tracking scheme forms the initial condition for solving the student-t copula based cross-correlation likelihood function. The reasons for faster convergence and accuracy of our Bayesian particle filter based tracking are due to (a) the initial conditions for the student-t copula likelihood function optimization is very close to the global maxima and (b) the distribution of transmitter's mobility model provides a prior condition that additionally constraints the possible search space for optimizing the student-t copula function. Experimental run in a laboratory environment was able to achieve sub-meter accuracy for a mobile transmitter moving at speeds less than 1 m/s.

The final chapter of this dissertation explored the placement strategy for cross-correlation based localization method. This paper addressed the limited range of wireless transceivers and derived a placement algorithm than will provide complete localization coverage within a workspace. In addition, the Cramer Rao Lower Bound (CRLB) for the estimation of transmitter location from shadow fading cross-correlation was derived. By combining complete localization coverage with CRLB based receiver quality metric, the proposed method was able to achieve transmitter localization accuracy better than a pre-specified error threshold. In addition, experimental and simulation results has shown that

the proposed placement strategy was found to result in less number of receivers than Delaunay Refinement based placement strategy proposed in Paper 2.

Future applications of cross-correlation based localization method should focus on improving the convergence speed of student-t copula function for tracking mobile transmitters that are faster than 1m/s. In addition, future work should explore RSSI based heading estimation to replace the current requirement for a compass or gyroscope to estimate heading. This could be possibly achieved by exploiting the asymmetry in transmitter antenna radiation pattern or antenna arrays to estimate the absolute orientation of the transmitter in the localization area. Extending the placement algorithm to a three dimensional workspace would be a challenge as it would increase the dimensionality of the receiver placement problem and consequently slowing the convergence to a placement solution that will result in the accuracy of locating a transmitter better than a pre-specified error threshold.

VITA

Mohammed Rana Basheer was born in Trivandrum, India. In August 1998, he received his B.Tech. in Applied Electronics and Instrumentation from the College of Engineering of University of Kerala, India. Subsequently he worked with Tata Consultancy Services and Hughes Software Systems from 1998 to 2001. In Dec 2003, he received his M.S. degree in Computer Engineering from the University of Missouri-Rolla, Rolla, Missouri, USA. From 2003 to 2007 he worked with Garmin International at Olathe, Kansas. In July 2012, he received his Ph.D. in Computer Engineering from the Missouri University of Science and Technology, Rolla, Missouri, USA. He started working for Broadcom Corporation from July 2010.

He has published several conference and journal papers, some of which are listed with the references of this research. Mohammed Rana Basheer has been a member of the Institute of Electrical and Electronics Engineers (IEEE). He was inducted into Tau Beta Pi Honor Society in 2008.